SEISMIC REHABILITATION OF RC STRUCTURAL WALLS

By

Mohamed Mohamed Ebrahim Elnady

B.Sc., M.Sc. (Mansoura University)

A Thesis

Submitted to the School of Graduate Studies

In Partial Fulfillment of the Requirements

for the Degree

Doctor of Philosophy

McMaster University

DOCTOR OF PHILOSOPHY (2008) McMaster University

(Civil Engineering) Hamilton, Ontario

Title: Seismic Rehabilitation of RC Structural Walls

AUTHOR: Mohamed Mohamed Ebrahim Elnady,

B.Sc. in Civil Engineering, Mansoura University

M.Sc. in Structural Engineering, Mansoura University

SUPERVISOR: Professor Ahmed Ghobarah

NUMBER OF PAGES: xxviii, 302

ABSTRACT

Structural walls in existing buildings designed to pre 1970s codes may have deficient shear reinforcement and lap splice detailing. Lap splices at the bottom of the walls were designed in compression with anchorage length of 24-bar diameter. When the structural wall is subjected to lateral loads during a major seismic event, the lap splice is in the zone of maximum moment and shear and may be subjected to tension. Such design may cause non-ductile behaviour and sudden failure of the wall due to shear or bond slip of the lap splice reinforcing bars. The effect of shear and ductility rehabilitation on the behaviour of reinforced concrete structural walls, without lap splice, have shown improvement in the structural wall shear resistance and ductility and hence overall structural ductility and seismic loads resistance. Research on rehabilitation of reinforced concrete (RC) structural walls with both deficient shear reinforcement and lap splice detailing is still needed.

The principal objectives of this study were to evaluate the seismic behaviour of non-ductile reinforced concrete structural walls before and after rehabilitation using carbon fibre reinforced polymers (CFRP). These objectives were achieved through experimental and analytical investigations.

The experimental phase of this research involved testing large scale models of RC structural walls with deficient shear strength and lap splice detailing to reproduce failure modes observed following major seismic events and to evaluate the rehabilitation schemes. Ten RC structural walls were built and tested under cyclic loading. Three control walls were tested as-built with non-ductile detailing and seven walls were rehabilitated before testing. The purpose of the rehabilitation techniques was to prevent brittle failure in shear or bond slip and to improve the ductility and energy dissipation of RC structural walls.

The analytical phase of this study involved evaluation of the inelastic dynamic response of RC residential building with nonductile structural walls as well as retrofitted walls. An

efficient macroscopic model to represent the behaviour of RC structural walls when subjected to pushover, cyclic and dynamic seismic loads was developed. The proposed model was intended to adequately describe the hysteretic behaviour of walls and to be capable of accurately predicting both flexural and shear components of inelastic deformation. The model predictions were compared with the experimental results. The comparisons showed that the developed analytical model predicted the inelastic walls response with a good accuracy. The analytical model was capable to evaluate the nonlinear dynamic behaviour of an existing building under seismic excitation before and after rehabilitation.

ACKNOWLEDGEMENTS

I thank God the Most Merciful, the Most Gracious, and the only Cherisher and Sustainer.

I wish to express my deep gratitude to my supervisor Dr. Ahmed Ghobarah for his firm support scientifically, technically and morally during all the stages of this research program. I thank the members of my supervisory committee Dr. Peijun Guo and Dr. Mohamed Hamed for their valuable advices and suggestions that definitely enhanced the quality of this research. The support of the technicians of the Department of Civil Engineering Mr. Perrett, and Mr. Forget is deeply appreciated. Thanks are also due to the Department of Civil Engineering Chair, Faculty, Graduate Students, and Staff who assisted me in every way they could during the past four years.

I thank my family members, and my wife for their patience, and sincere prayers that made this work possible.

Financial support from Egyptian Government, Ministry of Higher Education, Department of Cultural Relationships, and Missions is gratefully appreciated.

TABLE OF CONTENTS

LIST OF FIGURES

LIST OF TABLES

LIST OF SYMBOLS

A_{frp}	Cross sectional area of FRP sheet
A_g	Gross cross sectional area of concrete element
A_s	Cross sectional area of steel reinforcement
A_{sx}	Longitudinal reinforcement
A_v	Cross sectional area of shear reinforcement
b_v	Effective width of wall
b_x	Width of wall
b_y	Length of concrete confined end zone element of wall
c	Concrete cover of the concrete section
C_c	Compressive force in the compression zone of the section
C_s	Compressive force in the compression steel
d_v	Effective depth of wall section
d_b	Diameter of longitudinal steel bar of the concrete section
E_c	Initial concrete stiffness
E_{frp}	Modulus of elasticity of FRP sheets
E_g	Tangent stiffness of the FRP-confined concrete stress-strain relationship
E_j	Modulus of elasticity of FRP jacket
E_s	Modulus of elasticity of steel reinforcement
E_{sec}	Secant concrete stiffness

EA	Axial stiffness
f_1	Principal tensile concrete stress
f_{1max}	Maximum concrete tensile stress across a crack
f_2	Principal compressive concrete stress
f_{2max}	Maximum concrete strength in compression that corresponds to tensile strain ε_1
f_c	Concrete compressive stress
f_{cr}	Concrete cracking strength
f_{ct}	Concrete tensile stress
f_c'	Concrete compressive strength
f_{cc}'	Concrete confined strength
f_{frp}	Tensile stress in shear strengthening jacket
f_l'	Lateral confining pressure produced by steel ties
f_{sx}	Axial stress of longitudinal reinforcement in shear element
f_v	Stress in shear reinforcement
F_{v1}, F_{v2}	Forces in the two vertical actuators
F_H	Forces in the horizontal actuator
f_y	Steel yield strength
f_{yh}	Yield strength of confining hoops
k_e	Confinement effectiveness coefficient
GA	Effective shear rigidity

h	Wall height
l_w	Wall length
L_d	Development length of the steel bar as required by Code Provisions
L_e	Length of the steel bar at which average bond stress u_e exists
L_p	Length of plastic hinge
M	Bending moment
N	Axial load capacity of the shear element
P	Axial load applied on wall
P_1	Ultimate strength of bar hook
P_1	Residual strength of bar hook
P_h	Force developed in the bar hook
r_c	Chamfer radius of concrete section
s	Slip of steel bar
S	Spacing of shear reinforcement
s_1	Steel bar slip corresponding to bond of τ_1
s_3	Steel bar slip corresponding to bond of τ_3
s_h	Slip of the bar hook
s_{h1}	Slip of the bar hook corresponding to the ultimate kook force
s_{h3}	Slip of the bar hook corresponding to the residual kook force
S_{mx}	Crack spacing in x-direction
S_{my}	Crack spacing in y-direction

S_x	Spacing of the reinforcement in x-direction
S_y	Spacing of the reinforcement in y-direction
T	Tensile force in the tension steel bars
t_j	FRP jacket thickness
u_e	Average bond stress along the embedded length of the steel bar
u_{xf}	Unrestrained displacement of concrete section in x-direction
u_{xj}	Lateral deformation of the FRP jacket in x-direction
u_{xr}	Lateral displacement of concrete section in x-direction due to lateral confining pressure
u_{yf}	Unrestrained displacement of concrete section in y-direction
u_{yr}	Lateral displacement of concrete section in y-direction due to lateral confining pressure
v	Shear stress that could be resisted by the shear element
v_c	Concrete Poisson's ratio
v_{ci}	Shear stress that could be transmitted across a crack
V	Shear strength of concrete shear element
V_c	Shear strength from concrete mechanism
V_i	Initial (Nominal) shear strength
V_f	Final shear strength
V_n	Nominal shear strength
V_s	Shear strength from steel mechanism

V_f	The shear resistance due to one layer of FRP on each side
w	Crack width of concrete element
w_i	The i^{th} length of unconfined concrete region in a concrete section
γ	Shear strain
θ	Crack inclination to the horizontal and inclination of the principal axes
θ_{top}	The rotation at the top level of the wall
ρ_s	Transverse reinforcement ratio
ρ_x	Reinforcement ratio of longitudinal reinforcement
σ_x	Lateral confining pressure in x-direction imposed by FRP jacket on concrete section
σ_y	Lateral confining pressure in y-direction imposed by FRP jacket on concrete section
σ_j	FRP jacket tensile stress
σ_r	Lateral confining pressure in radial direction imposed by FRP jacket on concrete section
ε_1	Principal tensile concrete strain
ε_2	Principal compressive concrete strain
ε_j	Tensile strain in FRP jacket
ε_c	Concrete strain
ε_{cc}	Compressive concrete strain corresponding to f_{cc}'

ε_{cr}	Concrete cracking strain
ε_o	Compressive concrete strain corresponding to f_c'
ε_x	Strain in x-direction of the concrete element
ε_v	Strain in y-direction of the shear element
α_t	Factor that defines the residual concrete tensile strength
α_{tx}	Factor that defines the residual concrete tensile strength in x-direction
α_{ty}	Factor that defines the residual concrete tensile strength in y-direction
τ	Steel-to-concrete bond strength
τ_1	Ultimate steel-to-concrete bond strength
τ_3	Residual steel-to-concrete bond strength
λ_t	Factor defines the decay rate of concrete post cracking tensile strength
β	Post-yield slope of steel stress-strain relationship
Δ	Lateral displacement at the top of the wall
Δ_y	Lateral yield displacement at the top of the wall
μ	Displacement ductility

CHAPTER 1

INTRODUCTION

1.1 PREAMBLE

Moment resisting frame was the common structural system used for multistory buildings in the 1950's and remained until the 1970's when ductile detailing of moment resisting frame was introduced for seismic resistance. Observed behaviour following severe earthquakes in 1988 Armenia, 1985 Chile, 1985 Mexico, 1977 Romania, 1971 San Fernando (California, USA), 1967 Caracas (Venezuela), 1963 Skopje (Macedonia), 1960 Chile, 1963 Yugoslavia, 1972 Nicaragua, 1989 Loma Prieta, 1994 Northridge (USA), 1995 Kobe (Japan), 1990 Philippine, 1986 Kalamata (Greece), and the 1999 Kocaeli (Turkey), revealed that existing frames suffered extensive damage. Reinforced concrete frames suffered failure of columns and beam-column joint, which in many cases caused the collapse of the building.

Reported observations following severe earthquakes during the past four decades indicated that well designed and detailed reinforced concrete (RC) structural wall systems structures showed an excellent behaviour compared to frame-type concrete structures. In addition, RC structural walls contributed significantly to the survival of reinforced concrete structures compared to framed structures. The use of structural walls resulted in less distortion and less damage to non-structural components. For example, following the 1988 Armenia, the 1985 Chile, 1985 Mexico, the 1977 Romania, the 1971 San Fernando (USA), the 1967 Caracas (Venezuela), the 1963 Skopje (Macedonia), the 1960 Chile earthquakes, minor damage was observed in structures featuring RC structural walls. The superior performance of structural wall system and efficiency in controlling structural and non-structural damage, and because of limited interstorey drifts was observed from post-earthquakes as reported by Fintel (1995).

1.2 MOTIVATION

Building codes are frequently updated as a result of the advances in engineering knowledge and experience. Over the past forty years, major changes in the zoning maps and design philosophies occurred. Changes in seismic zoning maps may move buildings to more vulnerable seismic zones. Changes in the function of the building may increase the seismic loads due to increased importance factor or gravity loads. Therefore, many of the existing RC structural walls may not comply with the recent code provisions, and therefore these walls represent significant hazard to the life of occupants and their investment. Current design practices recognize RC structural wall as one of the most efficient systems in resisting lateral seismic loads in structures.

Numerous multistorey buildings were built before the 1970's and before the introduction of seismic codes. They were mainly designed for gravity loads. These buildings are featuring RC walls as a part of the gravity load resisting system. Recent earthquakes such as the 1989 Loma Prieta, 1994 Northridge (USA), 1995 Kobe (Japan), 1990 Philippine, 1986 Kalamata (Greece), and the 1999 Kocaeli (Turkey) tested the vulnerability of existing reinforced concrete structures to severe seismic events.

Brittle failure modes in RC structural walls would significantly reduce the overall ductility of the structure. Structural walls with nonductile detailing such as inadequate lap splice of structural wall bars, absence or inadequate shear reinforcement did not perform well during past seismic events and suffered from shear or bond slip brittle failures. Walls suffered form failure of construction joints, and buckling of flexural rebars at the boundaries. Spalling and degradation of concrete were observed following the 1985 Chile, and the 1971 San Fernando earthquakes, (Wyllie et al. 1986, Jennings 1971). Therefore, rehabilitation of the structural walls represents a feasible approach to reduce the hazard in existing structures and to provide safety to occupants and their investments. In addition, rehabilitation of RC structural walls with both deficient shear reinforcement and lap splice detailing is an improvement area that needs to be investigated.

1.3 OBJECTIVES

The main objectives of this research program are to:

1. Experimentally evaluate the seismic behaviour of reinforced concrete structural walls with deficient shear reinforcement and lap splice detailing.
2. Investigate rehabilitation schemes for RC structural walls with deficient lap splice detailing, shear reinforcement, and propose repair systems for damaged walls following an earthquake event.

1.4 SCOPE

The aim of the present research program is on the seismic rehabilitation of RC structural walls with deficient shear reinforcement and overlap splice detailing and repair of damaged walls using carbon fiber reinforced polymers (CFRP) wrapping. The approach of this study included investigation of the behaviour and rehabilitation of structural walls by means of experimental and analytical research. The experimental program involved testing models of the walls to reproduce observed failures following earthquakes and evaluate the proposed rehabilitation schemes. The rehabilitation schemes included the use of unidirectional and bi-directional CFRP for strengthening and repair of the test walls. Proposed rehabilitation systems, if successful, can be applied to the repair of damaged walls following earthquakes. The analytical work involved modeling of RC structural walls to predict their inelastic response under pushover, cyclic, and dynamic loadings.

To achieve the research objectives, the scope of this research includes:

1. Development of an experimental program to examine the behaviour of as-built RC structural walls plastic hinge zone with deficient shear reinforcement and lap splice detailing. The experimental program included testing of ten structural walls.
2. Application of rehabilitation techniques to enhance the shear resistance of non-ductile RC structural walls and to account for the bond slip failure of the non-ductile RC

structural walls reinforcement detailing, and hence to improve the ductility of existing walls when subjected to seismic loads.

3. Evaluation of the rehabilitation techniques by examining and comparing the recorded behaviour of walls with different rehabilitation schemes.
4. Analytical modeling of RC structural walls to predict their inelastic response under pushover, cyclic, and dynamic loadings.

1.5 THESIS ORGANIZATION

The thesis is divided into eight chapters. Chapter 1 is an introduction describing the objective and scope of the research. Chapter 2 is a literature review of the available experimental research on rehabilitation of walls and the analytical research on modeling of walls. Chapter 3 describes details of the experimental program, the test setup, and the wall specimen design and construction as well the details of the repair/ rehabilitation schemes. The results of the cyclic tests are presented in Chapter 4. Analysis and comparison between tested walls results are presented in Chapter 5. In Chapter 6 an analytical model was proposed and comparisons between test results and the analytical results are discussed. The inelastic dynamic analysis of results of a standard building is described in Chapter 7. In Chapter 8, a summary of the research contribution, the main conclusions and recommendations for future research are presented.

CHAPTER 2

LITERATURE REVIEW

2.1 GENERAL

The impact and cost of the consequences of damage caused by earthquakes worldwide during the past three decades raised the question of how to protect the public and reduce the economic losses in the case of a severe earthquake. Most seismic design standards are based on a life safety approach where structural damage is accepted providing that collapse is avoided. With an increasing demand for structural systems with improved seismic performance, there is renewed interest in reinforced concrete (RC) structural wall systems, (Ghobarah 2000). Structural walls when properly designed and detailed represents an effective lateral load resisting system.

Structural walls in existing buildings designed to pre 1970s codes may have deficient shear reinforcement and lap splice detailing. Lap splices near the bottom of the wall were designed in compression with anchorage length of 24 bar diameter (ACI 318, 1968). When the structural wall is subjected to the lateral load during a major seismic event, the lap splice is in the zone of maximum moment and shear with possible tension in the extreme fibres. Such design may cause nonductile behaviour and sudden failure of the wall due to shear or bond slip of the lap splice reinforcement bars. Figures 2.1 and 2.2 show common RC structural wall failures due to deficient shear detailing. Figures 2.3 and 2.4 show failure due to deficient lap splice detailing of structural walls during the 1971 San Fernando and the 1985 Chile earthquakes, respectively.

2.2 RC STRUCTURAL WALLS

Buildings designed with RC structural walls were able to withstand, with less damage compared to the framed-type structures, the effects of these seismic excitations.

For example, a rare opportunity was provided after the 1985 Chile earthquake to investigate the performance of structural walls during seismic events. The seismic response of the buildings with reinforced concrete structural walls provided clear evidence that RC structural walls possess sufficient lateral stiffness to limit the drift and the earthquake damage. Reinforced concrete structural walls performance during the 1985 Chile earthquake was clear evidence about their benefits as a good lateral load resisting system. A survey followed the 1985 Chile earthquake indicated that majority of reinforced concrete buildings relied on reinforced concrete walls as a vertical and lateral load resistant system, Wood (1991). However, the 1985 Chile earthquake shaking was strong and lasted more than 60 seconds and the peak ground acceleration was greater than 0.35g. Reinforced concrete buildings with RC structural walls performance was based on the damage survey after the earthquake excitation. Surveys indicated that only less than 10% of the buildings suffered from moderate to severe structural damage, (Wood 1991). In the following, discussions will focus on the characteristics of the RC structural walls.

2.2.1 Definition and loads on walls

Reinforced concrete structural walls are a vertical diaphragm, which are commonly used to resist in-plane seismic lateral loads. They carry also the vertical axial loads from floors tributary areas. They can subject to out-of-plane forces when the earthquake direction under consideration is perpendicular to the wall. Designers often neglect the out-of-plan effects and design the walls for in-plane lateral load resistance only in addition to the axial load (Paulay and Priestly 1992).

2.2.2 Classifications of RC structural walls

Paulay and Priestly (1992) classified RC structural walls according to their aspect ratio (H/l_w, where H is the wall height and l_w is the wall length). The walls with aspect ratio greater than 4 are classified as a high rise wall (flexural wall) and the walls with aspect ratio less than 4 are classified as low rise (squat walls). Elnashai et al. (1990) used the moment to shear ratio M/VL, where M is the moment at wall base, V is the shear force

and L is the wall length, to classify walls as a high rise walls (flexure walls) if M/VL ratio was greater than 1.5, and the walls with M/VL ratio less than 1.5 were classified as low rise (squat walls).

Squat structural walls typically demonstrate little energy dissipation through their hysteretic behaviour under seismic events and they are out of scope of this study. Under seismic loading, more energy dissipation is usually required to ensure the structures perform satisfactorily. Paulay and Priestley (1992) investigated the possibilities of achieving acceptable levels of energy dissipation in squat shear walls, mainly by flexural yielding of the reinforcement. Shear failures originating from diagonal tension or compression failure show limited ductility and dramatic degradation in strength and stiffness.

2.2.3 Potential failure modes

In the design of new RC structural walls and strengthening of existing ones, it is important to recognize the potential modes of failure. Diagonal tension shear failure mode may occur when the web reinforcement is insufficient to resist high shear stresses. On the other hand, diagonal compression failure mode may occur when large amount of shear reinforcement is needed to resist these high shear stresses. Moreover, due to cyclic loading reversals during seismic events, the compression strength of the web concrete is reduced.

Lap splice detailing may present a potential weakness as shown in Figure 2.3. Near horizontal failure planes may develop in plastic hinge zones along intersecting cracks. This may lead to sliding shear failure. Figure 2.5 shows the development of sliding shear failure mechanism of RC structural walls. In the following sections discussion of failure modes of walls are presented.

2.2.3.1 Flexural failure

Flexural failure with yielding of the tension steel occurs mainly in high-rise walls. In addition, under cyclic loading when the cover spalls off, the compression steel may buckle. Lefas et al. (1990) and Iso et al. (2000) reported on this type of failure.

2.2.3.2 Shear failure

There are two modes of shear failure. They are diagonal tension and diagonal compression. Concrete failure starts with inclined cracks that take the X shape in case of cyclic loading. Several studies have been investigated and reported on this type of failure (Lombard 1999, Fiorato et al. 1983, Oesterle et al. 1984, Taghdi et al. 2000, and Iso et al. 2000, Khalil and Ghobarah 2005).

2.2.3.3 Instability of wall section

The danger of premature failure by instability of the section occurs due to out-of-plane local bucking when parts of a thin-wall section are subjected to compression strains. Vallenas et al. (1979) reported on this type of failure for slender walls with rectangular cross-section. To prevent this mode of failure,, Paulay and Priestley (1992) recommended that wall thickness should be greater than 1/16 of the first floor height. In addition, they concluded that properties of inelastic buckling are more affected by the wall length than by unsupported height and provided several formulae for the minimum thickness as a function of the wall length, aspect ratio, steel arrangement, and the level of ductility required of the wall. A thickness to length ratio of 1/10 offer reasonable protection against section instability per CSA A23.3 (2004) Code provisions.

2.2.3.4 Sliding shear failure

Sliding shear failure mode is characterized by sliding of the wall along its base. Construction joints are potential weaknesses planes that are susceptible sliding shear failure. Sliding shear is the largest single cause for both stiffness and strength degradation in plastic zones. Effective control of sliding can be conveniently achieved by use of diagonal reinforcement (Paulay and Priestley 1992). Riva et al. (2003) reported that this type of failure increases with decreasing axial load. They observed a sliding shear failure of a well-detailed full-scale structural wall with no axial load applied. Sliding shear failure is more expected to walls with low height-to-length ratio (Wiradinata et al. 1986).

2.2.3.5 Rocking failure

When the overturning moment is larger than the stabilizing moment the wall rocks back and forth with its foundation under cyclic load. In addition, the wall may rock on its foundation if the connection with the foundation was lost. This type of failure is common in precast concrete shear walls (Caccese and Harris 1986).

2.2.3.6 Anchorage failure of lap splices

Failure of a structural wall construction joint during the 1971 San Fernando earthquake was reported by Jennings (1971) as shown in Figure 2.3. The insufficient lap splice length was the main reason for this type of failure. It worth to be noted that this type of failure was observed at the fourth floor of the ten-storey building, which indicates that the lap splice failure is not restricted to the base of the wall or at the connection of the wall with the foundation and the lap splice detailing requires attention at any location they are introduced through the height of the structural walls.

2.3 ANALYTICAL MODELS

Experimental investigations are limited, time and effort consuming. Therefore, efficient, reliable and accurate analytical models are of interest as an alternative to experimental work. Well developed analytical models can be used to supplement and extend the experimental research.

Several procedures for analytical modelling of RC structural walls have been proposed. They can be divided into two major groups, microscopic and macroscopic models. Microscopic models are derived from solid mechanics considerations to obtain a solution through the finite element approach, whereas macroscopic models are phenomenological in nature and are based on observed test results.

2.3.1 Microscopic models

Microscopic modeling using finite element analysis of walls is an effective approach for linear elastic analysis, but their implementation is limited in the case of inelastic dynamic analysis of multi-storey buildings with RC walls. These analyses require highly detailed and complex models to describe the cyclic dynamic behaviour. They require a costly finite element program and a large amount of time for input of the structural model, computing the response, and interpretation of the results. They can be useful for determining localized damage to structural components; however, more practical approaches that emphasis on predictions of global behaviour rather than local behaviour are needed for practical design (Kim et. al. 2005).

Khatri et al. (1995) and Navidapour (2000) used finite element package (ADINA) to perform nonlinear analysis of concrete walls and assumed a plane stress condition. They used concrete plane stress elements to model the conrete and 2-node truss elements for modeling the reinforcement steel. This approach was associated with a substantial computational effort to achieve reasonable accuracy.

2.3.2 Macroscopic Models

Macro-models are easier to apply, but they do have limitations, the main one being that the analytical results are usually valid only for the specific conditions upon which the derivation of the model is based (Vulcano and Bertero, 1987). Several researchers reported on this type of walls models (Vulcano and Bertero 1987, Linde and Bachmann 1994, Ghobarah and Youssef 1999, Orakcal et al. 2004, Kim et. al. 2005,.

Linde and Bachmann (1994) developed a model used for the simulation of the dynamic behaviour of earthquake-resistant multi-storey walls. The model consists of non-linear springs connected by rigid beams. The model properties were derived based on elastic theory for cantilever walls as well as non-linear physical behaviour of wall cross-sections supplemented by empirical data. The developed model consisted of four non-linear springs connected by rigid beams. The non-linear flexural behaviour was governed

by the two outer vertical springs. The non-linearity of the model was made up of a simplified multi-linear behaviour of the springs. They assumed in the model that full cracking has already taken place prior to the application of the loads. The stiffness in the post-yielding range was taken as a fraction of the stiffness in the uncracked elastic range. The shear behaviour of the model was modelled by the horizontal spring at around 1/3 of the wall height from the bottom of the model. The macro elements were coded as user-elements and implemented in the general finite element code ABAQUS. The macro element is shown in Figure 2.6. The model performance was found to be satisfactory compared to test results for the flexural dominated walls, however, it was not compared to shear dominated test results.

The macro model developed by Ghobarah and Youssef (1999) represented the inelastic behaviour of RC structural walls as shown in Figure 2.7. The model consisted of nonlinear springs connected by linear beam elements. The effects of the axial load and the bending moment on the shear behaviour of the structural wall were taken into account. The model was shown to be suitable for representing the static and dynamic responses of reinforced concrete structural walls of different sizes. Although the model was calibrated with experimental work and the results were in a good agreement, the model is still not yet calibrated with experimental results from walls that exhibited different failure modes.

Orakcal et al. (2004) proposed a wall macro model and compared the model results with experimental data for slender reinforced concrete walls with rectangular cross sections. A horizontal spring placed at 0.4 of the wall height. The flexural response was simulated by a series of macrofibers uniaxial elements connected to infinitely rigid beams at floor levels. The primary simplifications of the model involves applying the plane sections-remain-plane assumption in calculating the strain level in each uniaxial element and uncoupling of flexural and shear modes of deformation of the wall element.

2.3.3 Limitations of the available models

The available macroscopic models represented the wall as a set of nonlinear translation and/or rotational springs connected by rigid beams. The hysteretic representations of the nonlinear springs were selected as simple as possible to avoid complicating the analysis. For this reason, these models were not capable of correctly representing the hysteretic behaviour, especially in the case of the shear springs. Therefore, available models are not suitable for representing the behaviour of walls when shear effects are significant. In addition, some models are not capable of correctly representing the strength deterioration past peak capacity under cyclic loading. These deficiencies in available models cause severe limitations on their application to represent the behaviour of reinforced concrete structural walls subjected to seismic or cyclic loading (Ghobarah and Youssef 1999). For example, the model developed by Orakcal et al. (2004) significantly underestimates the compressive strains and thus may not be accurate in simulating strength degradation and failure of walls due to crushing of concrete. In addition, its modeling methodology was intended to simulate only flexural response and effects of shear-flexure interaction on possible shear failure mechanism were not considered.

2.4 SCALE MODEL TESTING

Testing full scale models needs large testing facilities, therefore, most researchers conduct scale model tests. Small-scale modeling reduces the size of a structural model without losing important characteristics in the behavior of the prototype. The model scale must be sufficiently reduced so that the tests can be conducted with laboratory equipment limitation.

Models of reinforced concrete structures must accurately reproduce the behaviour of the prototype through all the stages of loading up to the point of failure including the type of failure. It is extremely difficult for reinforced concrete structures models to satisfy all the material similarity constraints. When using steel as reinforcement in the wall, the

scale for Young's modulus is equal to one. Since the scale for Young's modulus of concrete would also have to be one. Difficulties arise when smaller size aggregates are used. In this case it is difficult to obtain a Young's modulus of the same magnitude as with reinforced concrete structures. This obstacle can be overcome by reducing the area of the model reinforcement correspondingly, so that the force in the model reinforcement is reduced. By making this adjustment, it is then possible to arrive at an equal scale for the stiffness of the reinforcement and for the concrete in the test model. The disadvantage of this procedure is that the change in area of model reinforcement will influence bond, which is also affected by the properties of model concrete. The similarity of bond behaviour of reinforced concrete models is, important, since bond failure modes to be studied in this investigation.

2.5 WALLS TESTING RESEARCH

Due to the complex nature of wall testing, limited experimental research has been conducted. Experimental testing is commonly used for evaluating the inelastic seismic performance of structures and structural components. There are several experimental methods available for evaluating the inelastic seismic performance of a particular structure or elements. The most realistic simulations of seismic response are shake table tests. However, shake tables are of limited size and capacity. Because of these limitations, static cyclic tests are used to impose prescribed histories of load (or displacement) on a specimen (Williams et al. 2001). To combine the realism of shake table tests and the simplicity of the quasi-static test, the pseudo-dynamic test method was introduced. The pseudodynamic test method combines well-established structural dynamics analytical techniques with experimental testing. In this test method, a computer is used on-line to determine the displacement or load history to be imposed on a test specimen using the same cyclic test equipments. The inertia and damping characteristics of the test structure as well as the ground acceleration are numerically prescribed. The restoring forces are measured experimentally from the deformed specimen at each step in the test. Thus, the quasi-

statically imposed displacements of the test structure will resemble those that would have developed if the structure were tested dynamically (Williams et al. 2001).

Lopes (2001), studied the seismic performance of RC walls under extreme conditions leading to shear failure. Four small-scale reinforced concrete walls under cyclic loading and low shear ratio (M/VL=1.1) were tested. Special emphasis was given to the parameters that were failure mode dependent.

Khalil and Ghobarah (2005), presented an experimental program for identifying the causes of structural walls failures and investigating potential rehabilitation schemes of 1/3 scale RC structural walls. Scale models of the plastic hinge region of the wall were tested. The tests focused on modeling the plastic hinge region and imposing the effect of the rest of the wall on the top of this plastic hinge region using the test setup. The wall was shown to fail prematurely in shear reproducing the failures observed in walls following recent major earthquakes. They used CFRP sheets to wrap the walls and to prevent the shear failure and enhance the wall ductility. The CFRP sheets wrapping was successful to improve the wall lateral stiffness and enhance its ductility and the shear failure mode was prevented as well.

2.6 REHABILITATION OF WALLS

Some of the proposed and applied techniques for rehabilitation of RC structural walls using traditional materials and using fiber reinforced polymers are discussed in following sections.

2.6.1 Rehabilitation using traditional materials

Fiorato et al. (1983) and Palermo (2002) proposed rehabilitation techniques that involved removing damaged concrete and casting new concrete after straightening and adjusting the existing reinforcement. They concluded that the original strength of the wall cannot be completely restored and the stiffness and ductility are significantly reduced. Lefas et al. (1990) proposed another technique that involved replacing damaged concrete

in the end zones of the walls and filling cracks using epoxy injection. They reported that the strength, stiffness, and ductility of the retrofitted walls were less than the original walls. It was observed that the use of epoxy-injection improved the stiffness at the serviceability limit state but it did not have considerable effect on the strength of the repaired walls.

Another rehabilitation technique, which is widely used in practice, involves increasing the thickness of wall through concrete jacketing by casting new concrete and adding reinforcement. This method may interrupt the function and the operation of the building and may need modification of the foundation. It was reported by Vallenas et al (1979) and Fiorato et al. (1983) that this type of rehabilitation is effective in increasing the strength and stiffness of the walls. On the other hand, the overall behaviour of the structure will be altered because of the increased stiffness of the wall. This stiffness increase can significantly alter the fundamental period of the structure and attracts higher forces during earthquakes. Moreover, it was reported that shear failure occurred at the second floor when jacketing technique involved the first floor wall only (Vallenas et al. 1979).

Taghdi et al. (2000) used steel plates or rods for rehabilitation of structural walls. They used diagonal steel strips externally bonded to the wall by epoxy to prevent diagonal tension and diagonal compression failures. In addition, they used vertical strips attached along wall end zones to improve the ductile behaviour of the wall. The method was reported to be successful in increasing the stiffness and ductility of the tested low-rise structural walls but was not tried on high-rise structural walls. This rehabilitation technique is expected to increase the stiffness of the wall thus altering the dynamic characteristics of the structure.

Elnashai and Pinho (1997) suggested based on the new performance-based design that the rehabilitation of the wall does not only involve restoring or increasing strength but also providing the required performance. They investigated four aspects of walls' rehabilitation. First, increase of stiffness to meet required performance and control deformations under lateral loads. Second, improving of flexural strength to provide the required strength to resist loads due to earthquakes. Third, increasing shear strength to

prevent brittle shear failure during major seismic events. Last aspect was ductility improvement to dissipate energy during earthquakes and ensure that sudden and complete collapse does not occur. These suggested selective rehabilitation techniques were proposed to improve only the desired property of the structural wall without affecting the other properties. The techniques seem to be effective though some of them may not be practical.

2.6.2 Rehabilitation Using Fibre Reinforced Polymers

Limited research were reported on using fibre-reinforced polymers (FRP) in the rehabilitation of walls. The available research is reviewed in this section.

In 1999, Lombard performed general rehabilitation of structural walls using carbon fibre reinforced polymers externally bonded to the two faces of the wall. The aspect ratio of the walls was 1.8. Four walls were constructed. One as a control specimen, which was repaired then retested, and two tests on strengthened walls. No axial load was applied during the lateral loading tests. The repair technique involved using applying fibres in the vertical direction, and mix of vertically and horizontally oriented fibres. Failure of the walls was reported to be ductile in some cases and in some cases non-ductile modes of failure occurred such as loss of anchorage or tearing of the fibres.

Antoniades et al. (2003) tested five squat structural walls up to failure under lateral cyclic loading and then repaired them using high strength mortar and lap-welding of fractured reinforcement. Only one of test walls was subjected to axial loading. The walls were subsequently retrofitted using FRP jackets as well as adding FRP strips to the wall edges. Test results indicated that the FRP increased the shear strength of the repaired walls by approximately 30% with respect to the traditionally repaired walls but the energy dissipation capacity of the original walls was not restored.

Paterson and Mitchell (2003), tested four structural walls. Specimens' length to thickness ratio was four, which would fall under the category of columns rather than walls. The specimens had lap splices of the longitudinal reinforcement in potential plastic hinging region, inadequate confinement of boundary regions, and inadequate anchorage of the

transverse reinforcement. The test results indicated that the retrofit schemes were successful in improving the ductility and energy dissipation of the tested walls. The retrofit schemes included combination of the headed reinforcement and the carbon fiber wrap.

Khalil and Ghobarah (2005), tested three 1/3 scale RC structural walls to evaluate the seismic rehabilitation of the walls. Two rehabilitated walls and one as-built specimen were tested. The specimens had nonductile reinforcing details, including inadequate shear reinforcement in potential plastic hinging regions, inadequate confinement of boundary regions, and inadequate anchorage of the transverse reinforcement. The rehabilitation schemes involved shear strengthening, end zones confinement and ductility improvement. They used bi-directional carbon fibre polymers for shear strengthening and unidirectional carbon fibre polymers for confinement and ductility enhancement. Two anchoring techniques were used, in-house made carbon fibre strands and steel rods. The test results showed that the rehabilitation schemes were successful in improving the ductility and energy dissipation of the tested specimens. They found also that the steel anchoring technique was more effective in increasing the confinement of the specimens' boundary element regions than the carbon fibre strands. Deterioration of strength was observed past the loading cycles at ductility level of 2. This was attributed to the debonding of CFRP wrapping and the failure of anchoring system. The measured deformations were significantly large compared to the expected deformations of RC structural walls.

2.7 SUMMARY

Many multi-story RC structures were built prior to 1970 and located in seismic zones have been designed only for gravity loads without proper considerations of lateral loads. The lack of seismic considerations in gravity loads designed structures resulted in insufficient lateral load resistance of these buildings under effect of earthquakes. When assessing these buildings, deficiencies such as absence or inadequate shear reinforcement of structural wall and insufficient lap splice length of structural walls steel reinforcement

were observed. The longitudinal and transverse reinforcement distribution and lap splice details in structural walls govern the ductility and control the failure mode in existing structures. Therefore, many of the existing concrete buildings may not comply with the recent code provisions, and therefore these buildings represent significant hazard to the life of occupants and their investment.

Structures, during their lifetime, may be subjected to change of loading, substantial damage due to impact or seismic events, deterioration due to cracking, loss of section or corrosion, and even change of use. All of these reasons lead to the need for rehabilitation of structures and structural components such as RC structural walls. Rehabilitation of structural walls did not received much attention by researchers due to the difficulty and high cost of experimental research. To eliminate the potential failure of structural walls, there is current interest in their rehabilitation. However, research and applications of the new advanced composite materials (FRP) in the rehabilitations of structural walls are still behind other alternative systems.

Rehabilitation of structural elements using FRP had been successfully applied to beams, columns, joints, slabs and other structural elements but work on rehabilitation of existing RC structural walls is still far behind. Limited previous test results on walls' rehabilitation indicated that using externally bonded carbon fibre sheets is an effective seismic strengthening and repair schemes for walls (Khalil and Ghobarah 2005). Available results showed that the use of FRP in rehabilitation of walls is promising. However, discrepancies and inconsistencies were observed in some of the reviewed tests that would be attributed to experimental difficulties and problems related to abrupt failure of anchorage between the fibres and the foundation of the wall. The use of vertical fibres and horizontal fibres improves flexural and shear resistance but hardly increases ductility or energy dissipation capacity. To increase ductility the compressed concrete should be confined. In addition, the brittle modes of failure by debonding of the fibres and loss of anchorage reported by both Lombard (1999), Iso (2000) and Khalil (2005) need to be avoided by providing efficient anchorage between the fibres and the wall at the end zones.

To extend the experimental work, there is a need for a representative analytical model that contains the main characteristics of RC structural wall and completely describe the hysteretic behaviour. These characteristics include stiffness degradation, strength deterioration, and pinching behaviour. Moreover, to include the nonlinear shear behaviour of walls, a suitable shear model should be used (Ghobarah and Youssef 1999). Available RC structural wall macro-models had generally shown good agreement for flexural dominant response. With axial springs representing the boundary elements, they can follow the moment curvature envelope well if the structural walls were controlled by flexure; however, they were less accurate for simulating inelastic shear response. Several shear models had been introduced, but they had often not given satisfactory results.

2.8 RESEARCH SIGNIFICANCE AND CONTRIBUTION

Lack of seismic detailing in the pre 1970's RC structural walls is a source for hazard to the society and investments. The aim of this research is to evaluate the inelastic response of the pre-seismic designed walls and to propose repair and rehabilitation schemes of such walls. By achieving the research objectives by means of the scope of this research, the research contributions are:

1. Providing simple and effective FRP seismic rehabilitations schemes for rehabilitations of RC structural walls with deficient lap splice and shear reinforcement detailing.
2. Development of an analytical macro model to observe the inelastic response of RC structural walls under seismic excitations.

The expected contributions have the merit of being based on the experimental results of RC structural walls.

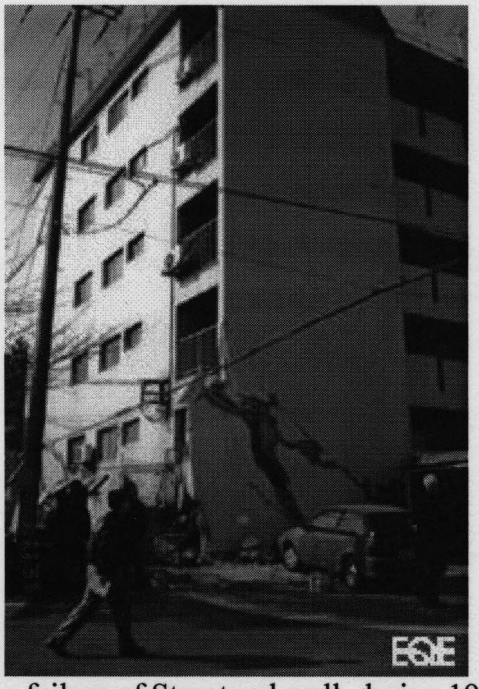

Figure 2. 1 Premature shear failure of Structural wall, during 1995 Kope, earthquake.
(http://www.hewett.norfolk.sch.uk/curric/NEWGEOG/Tectonic/Earth/Building.htm (accessed March 2006))

Figure 2. 2 Failure of a structural wall during the 1986 Kalamata earthquake (Lopes 2001).

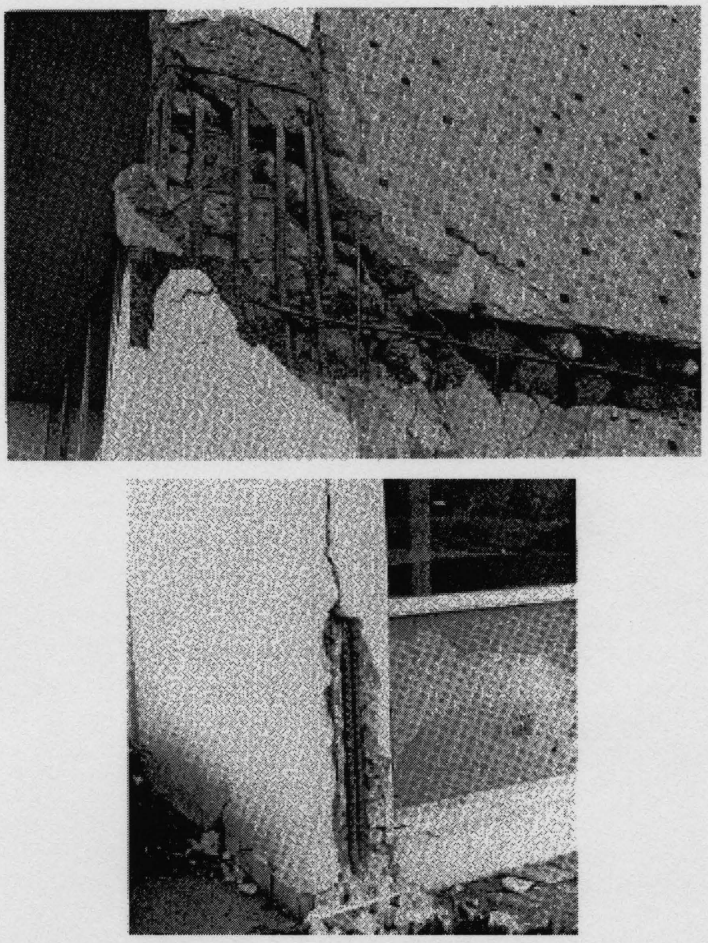

Figure 2. 3 Failure of a structural wall construction joint during the 1971 San Fernando EQ. (Jennings 1971).

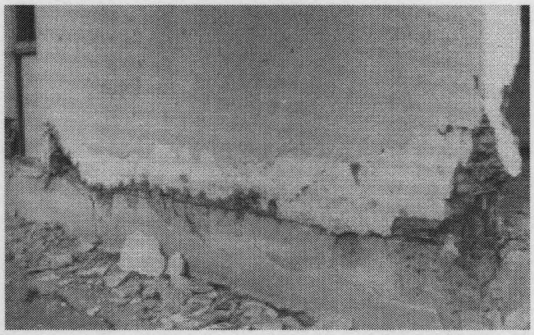

Figure 2. 4 Failure of shear wall observed after the 1985 Chile EQ. (Wyllie et al. 1986).

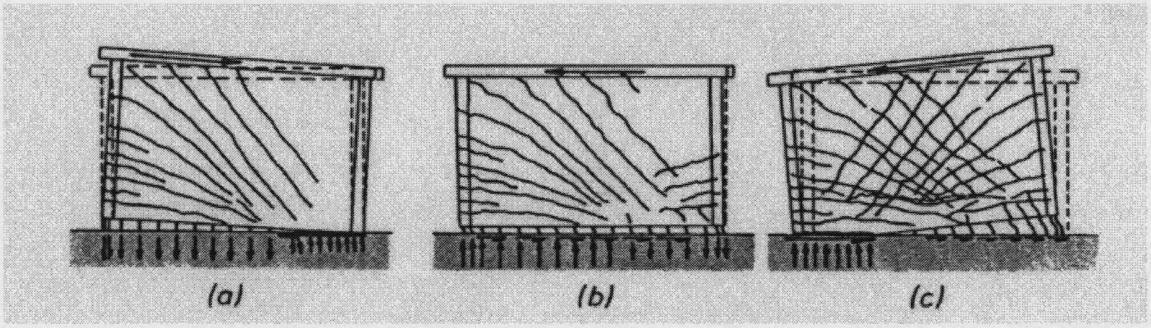

Figure 2. 5 Development of sliding shear mechanism (Paulay and Priestley 1992).

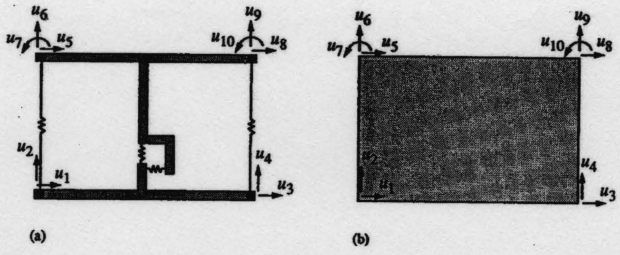

Figure 2. 6 Part of multi-storey wall (a) macromodel element with degrees of freedom: element displayed physically with springs and beams, (b) a user RC wall element.

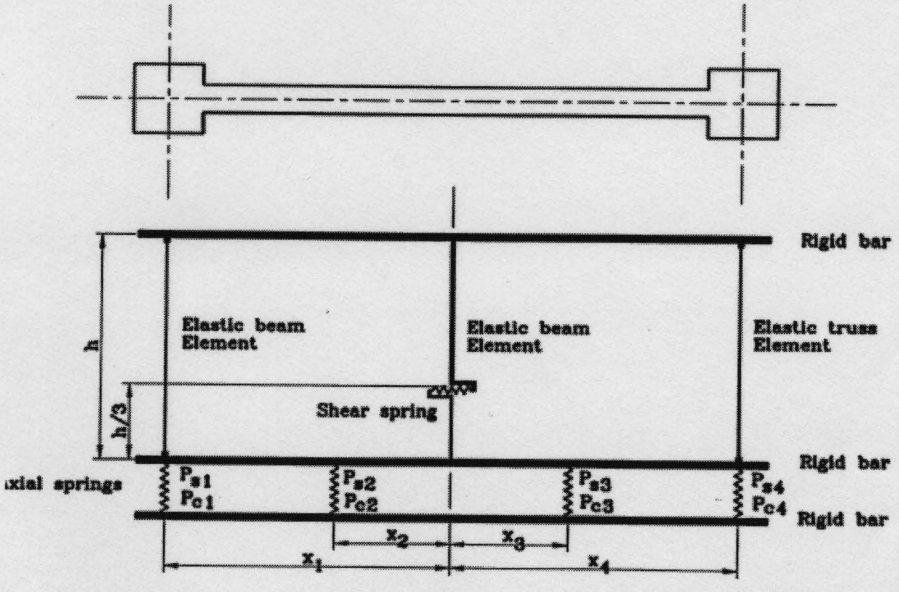

Figure 2. 7 Reinforced concrete wall member model (Ghobarah and Youssef 1999).

CHAPTER 3

EXPERIMENTAL PROGRAM

3.1 INTRODUCTION

The research objective is to simulate existing RC structural walls, which were designed according to the pre-seismic codes, i.e. pre 1970 with deficient shear reinforcement, lap splice, and non-ductile detailing. The experimental program involved testing scaled models of the RC structural walls with deficient shear strength and lap splice detailing to reproduce failure modes observed after major earthquakes and evaluate the proposed rehabilitation schemes. Ten reinforced concrete structural walls were built and tested using online cyclic testing procedure. Three control walls were tested as-built with nonductile detailing, CW1 to CW3. In addition, seven rehabilitated walls, i.e. RW3 to RW9, were tested. The purpose of the wall rehabilitation is to prevent brittle failure in shear or bond slip and to improve the ductility of the RC structural walls. In this chapter, the experimental program and the rehabilitation schemes are described in detail.

3.2 WALL DESIGN AND CONSTRUCTION

3.2.1 Test wall modeling

There are two different types of models: elastic models which represent the behaviour in the elastic range and strength models which represent the behaviour of the prototype up to failure, (Sabnis and Harris 1983). Strength models are classified into three categories: (i) true models where all the variables are modeled according to similitude law requirements, (ii) adequate models where some of the second order variables are not modeled according to similitude law requirements, and (iii) distorted models where some of the first order variables are not modeled according to similitude law requirements. For cyclic loading the shear strength and ductility of the control walls can be determined and

compared with that of the rehabilitated walls. The mass of the wall is ignored because it is small, approximately 2 % of the story mass, compared to the mass of the structure which is the main component of the inertia force during the earthquake event. Similarly, in the case of pseudodynamic testing the loading is applied statically. In this case, the same similitude law requirements were applied for both of the cyclic and the pseudodynamic tests.

3.2.2 Similitude law requirements

1. The true model, which maintains complete similarity. A model that satisfies each and every stipulation set forth by a proper dimensional analysis would be said to have complete similarity.

2. The adequate model, which maintains "first-order" similarity. With special insight into a problem, it may be possible to reason that some of the stipulations set forth by proper dimensional analysis are of "second-order" importance. For example, in rigid-frame problems it is known that axial and shearing forces are of second-order importance relative to bending moments insofar as deformations are concerned. Thus it may be adequate to model the moment of inertia but not the cross- sectional areas of members. Thus, a model which satisfies each and every first-order stipulation which is set forth by a proper dimensional analysis but which may not satisfy certain second-order stipulations would be said to have first-order similarity.

3. The distorted model, which fails to satisfy one or more of the first-order stipulations as set forth by proper dimensional analysis.

For the static model used two dimensions were included: Force (F) and length (L) while the time was excluded. The force scale is S_F and the length scale is S_L. The first selected scale is the length scale (S_L) which governs the height of the specimen, $S_L = H_m / H_p$ where H_m and H_p represents the height of model and the height of the prototype, respectively. The model height was selected to be 1/3 that of the prototype. The second model scale is the Young's modulus of elasticity, E, ($S_E = S_F S_L^{-2}$) which is selected to be 1 because the same reinforced concrete material and FRP composites were used in the model

and in the prototype. This gives the force scale S_F to be 1/9. Formulas and values of the selected parameters are shown in Tables 3.1 and 3.2.

3.2.3 Modeling of the plastic hinge zone

The maximum, axial load, bending moment and shear force of a cantilever wall are at the base. For this reason, the plastic hinge zone and most of the damage occur near the bottom of the wall. Therefore, instead of testing the whole wall height, only the plastic hinge zone will be modeled and tested. The rest of the wall height is assumed to behave elastically during earthquakes. To take the effect of the top part of the wall into consideration during cyclic tests, constant axial load, variable shear force, and bending moment were applied to the top of test wall. It worth to be noted that axial load varies during real earthquakes. For ten-story structure of 33 m height and wall length l_w = 3 m, the height of the plastic hinge zone is estimated to be equal to l_w according to CSA A23.3 (2004). Therefore, for a scale of 1:3 the height of the plastic hinge zone was assumed to be 1100 mm high and 1000 mm wide. For prototype wall thickness of 360 mm, the thickness of the test wall at the plastic hinge zone is taken as 120 mm. With length to thickness ratio less than 10 the possibility of out of plane buckling is reduced. In addition, four strong I-shaped vertical steel columns along with four steel guide channels were used to guide the specimen and keep the deformations inplane only during the tests.

3.2.4 Design of test walls

The tested walls represented the plastic hinge zone of a structural wall as shown in Figure 3.1. The test walls were designed to the ACI-318 (1968) guidelines to model existing walls with nonductile detailing. Three control RC structural walls were built to represent walls with lap splice length of 24 bar diameter. This length of lap splice is for steel in compression. Current lateral load levels subject the walls to moments that cause tension in the steel reinforcement. In addition, construction practices located the lap splice at the wall's expected plastic region. Such lap splice length was not sufficient to develop enough bond force to yield the flexural reinforcement steel. Control walls CW1 to CW3

reinforcement details are shown in Figures 3.2 to 3.5. Seven rehabilitated walls RW3 to RW9 were tested using cyclic loading to simulate lateral earthquake effects.

3.2.5 Construction of the test walls

Plywood forms were assembled for the top block, bottom foundation block and the test wall. The steel reinforcement cages for both the top block and the bottom foundation block were assembled outside the wooden forms with spacers to maintain the concrete cover for the reinforcement then they are fitted into the wooden forms. The top block and bottom foundation reinforcements were fitted in position. The test wall specimen steel reinforcement was assembled in place. The bars are extended into the top block and the bottom foundation block with sufficient anchorage length and with 180 degrees end hooks according to CSA A23.3 (2004) specifications. The gaps between the plywood sheets were sealed with tape to prevent bleeding of the concrete that may occur during casting. Prior to assembling the reinforcement cage, some of the steel bars were instrumented with strain gauges. The ribs on the bars were removed by grinding and the bars were smoothed at the strain gauge locations. The walls were constructed in a horizontal position to eliminate the possibility of aggregate segregation and honeycombing. To prevent undesirable deformation of the wall specimen before it reaches its full strength, supporting posts were placed under the wall specimen during casting and left in place for 28 days.

The sides of the forms were tied together using threaded steel tie rods to prevent bulging of the form under the lateral pressure of wet concrete. The concrete was delivered to the laboratory by concrete truck. The concrete mix consisted 176 kg/m^3 of Portland cement (#10); coarse aggregates of maximum size 10 mm, fine aggregate (sand) and water. The target slump was 75 mm. The concrete was mechanically vibrated to eliminate voids. Several hours after casting, the RC walls were covered with wet burlap to provide a moist curing environment. Polyethylene sheets were used over the burlap sheets to retain the moisture.

3.3 MATERIAL PROPERTIES

3.3.1 Concrete

All the specimens were cast at the same time in controlled environment inside the laboratory using the same concrete design mix. The design of the mix is given in Table 3.3. The specified concrete compressive strength f'_c was selected to be 25 MPa. Three cylinders were tested after 7 days, 28 days and on the day the wall was tested, to determine the concrete compressive strength. Three cylinders were tested after 28 days, to determine the concrete splitting tensile strength. The average splitting tensile strength of the tested concrete cylinders were 3.2 MPa. Concrete cylinders compression test results at 28 days as well as on the wall test day are shown in Table 3.4. The modulus of elasticity is assumed equal to the secant modulus at stress of 40% of the ultimate strength. Measured modulus of elasticity E was 2.80×10^4 MPa, while calculated value according to CSA A23.3 (2004) Clause 8.6.2 was 2.61×10^4 MPa. The measured modulus of elasticity was marginally higher than that given by the CSA A23.3 (2004) by 6.6%.

3.3.2 Reinforcement steel

Grade 400 MPa steel reinforcement deformed bars were used as main and transverse reinforcement. Deformed steel bars M10, M15 and M20 were used for the vertical reinforcement of the wall. For the horizontal reinforcement, M10 deformed bars and 6.35 mm diameter plain bars were used. To determine the yield stress and the ultimate tensile strength, several coupons from different steel bar diameters were tested. The yield and ultimate tensile strengths of these bars are summarized in Table 3.5.

3.3.3 Fibre reinforced polymer

Carbon fibre reinforced polymer (CFRP) sheets were used for rehabilitation of the test walls. Tyfo fibre wrap composite strengthening system was used with uni-directional CFRP and bi-directional CFRP sheets, Fyfeco (2005). Tyfo BCC composites and Tyfo SCH-35 Composite fabrics were used in the rehabilitation. The Tyfo BCC is a bi-

directional carbon fabric where the primary fibres are oriented in the ±45° directions. The Tyfo SCH-35 Composite is a unidirectional carbon fabric where the primary fibres are oriented in the 0° directions. The resin material Tyfo S epoxy was used as recommended by the manufacturers. Tyfo S epoxy is composed of two parts, Part A which is a resin and Part B which is a hardener. The two parts were combined at a ratio of 100: 42 by volume and thoroughly mixed for five minutes with 400-600 RPM mixer until uniformly blended. A paint roller was used to cover the concrete surface with a thin layer of the epoxy. The composite sheets were saturated with the Tyfo S epoxy before being applied to the concrete surface. A summary of the average values for the mechanical properties of the composite fibres as suggested by the supplier and as tested are given in Table 3.6. The discrepancies between the ultimate measured ultimate tensile strength and supplier's suggested values may be due the misalignment in the testing machine and the exact orientation of the test coupons' fibres. A small misalignment in fibre direction during the preparation of the test coupon may lead to a different failure location and strength.

3.3.4 Steel anchors

In the rehabilitated walls RW3 to RW9 steel anchors were used. The anchors were installed through the walls to anchor the wrapped FRP sheets on both sides of the walls. The anchors were 12.5 mm diameter high strength grade 5 steel bolts. The length of the anchors was 8 inches and the average yield strength was 830 MPa as provided by the supplier.

3.4 TEST SETUP

The wall specimens were constructed with a rigid RC block at the top and a stiff RC foundation block at the bottom of the specimen. The purpose of the top rigid beam is to ensure that the axial load, shear force, and bending moment are transferred uniformly to the top of the specimen. The stiff foundation block will carry the reaction forces to the laboratory strong floor. The loading setup used to impose moment, shear, and axial forces

on the wall specimen is shown in Figure 3.6 to 3.8. Three hydraulic actuators were used. The vertical actuators were used to apply axial loads and moments during the test. A rigid steel beam was connected to the top reinforced concrete block using ten 25 mm high strength bolts. The top ends of the two vertical actuators were connected to the two ends of the top steel beam using four 25 mm high strength bolts at each end. The horizontal actuator was connected at one end to a stiff reaction frame. The other end was connected to the end of an L-shaped steel rigid I-beam. Details of the actuator specifications and capacities are given in Table 3.7. The actuators were controlled using a Flex Test^{TM} GT digital controller with supervisor computer, which was connected to the digital control through an Ethernet network cable. The software used for control was Model 793.1 Multipurpose Testware^{TM}. Two online computers were used simultaneously to control the test. These were the digital controller supervisor's computer and the external data acquisition computer for collecting the instrumentation readings

3.5 INSTRUMENTATIONS

The actuators and test walls were heavily instrumented to measure applied loads, strains and displacements. A variety of instruments were used in measuring and recording data during the tests. The applied forces were measured using the load cells built into the actuators. Forty strain gauges were installed in each specimen at the locations shown in Figure 3.9. The displacement measuring devices were 6 string potentiometers, 11 linear variable differential transformers (LVDTs), 3 MTS Temposonics as shown in Figure 3.10. The data acquisition recording system included 12 MTS analog inputs, load cells, and two online computers one for actuators and test control and the other for computation and data logger. A data acquisition system which consisted of an analog to digital board with a maximum capacity of 81 channels was used. Data acquisition readings were recorded every 1 second. Some of the important instrumentations were recorded by both the external

data logger and the MTS data-acquisition to minimize the risk of data loss and to provide a check for verification between the measurements recorded by different systems.

3.5.1 Strains in steel reinforcement

The strain gauges were glued to the steel and covered with a protective rubber layer to prevent damage to the gauges during concrete casting. The strain gauges were placed at the top, at the end of the lap splice and at the bottom of the wall to enable comparison of top and bottom moments in the wall as well as at the end of the lap splice. Strain gauges were placed on the two layers of steel in the wall to record information on how the strain varied on both faces of the wall. Strain gauges were also placed on the transverse bars.

3.5.2 FRP strains

The strains in the FRP sheets were measured using linear 10 mm long strain gauges. The surface of the sheets was covered with a thin layer of epoxy at the locations where the strains were to be measured in order to obtain a smooth surface. The strain gauges were subsequently glued to the hardened epoxy. At two locations for each specimen the strain gauges were placed in the form of a Rosette to obtain the complete state of strain at the point. At other locations the strain gauges were either placed in the horizontal direction to measure lateral confinement strain or at 45° to the axis of the member to measure the maximum strain in the ±45° bi-directional CFRP sheets. The strain gauges were installed at approximately the same locations for all rehabilitated walls.

3.5.3 Displacements

Lateral displacements of the wall, relative rotation of the two end blocks, curvature of the wall, and shear deformation in the wall were measured using LVDTs. The full stroke of the LVDTs varied from 250 mm to 50 mm depending on the expected deformation at the location monitored. Besides, six string potentiometers are used. The full stroke of the string potentiometers is from 125 mm or 250 mm. In addition, three 24 bit resolution digital Temposonics displacement transducers were used in measuring the horizontal and vertical displacements and hence the wall top rotation. The lateral displacements along the

height of the wall were measured with respect to an independent rigid frame attached to the reinforced concrete foundation block. Therefore, errors in experimental measurements due to the pedestal movement were excluded. The instrumentations were calibrated using micrometer to establish the proportionality constant between the displacement and voltage before and after the test.

3.5.4 Shear deformation

From the measurements of the displacements along the test wall diagonal, the shear deformation γ was calculated using the formula:

$$\gamma = \frac{\sqrt{a^2 + b^2}}{2ab}(d_3 - d_4) \tag{3-1}$$

where γ is the shear deformation, d_3 and d_4 are the displacements for the first diagonal and the second diagonal as measured by LVDT 3 and LVDT 4, respectively, a = 900 mm is the height of the rectangle, and b = 900 mm is the length of the base of the rectangle, as shown in Figure 3.10.

3.6 LOADING

Static cyclic and pseudodynamic testing procedures were used to study the behaviour of structural walls with deficient lap splice detailing and deficient shear strength under seismic loads before and after rehabilitation using CFRP. The two vertical actuators, as shown in Figures 3.6 to 3.8, were used to apply an axial compression load and a moment while the horizontal actuator applied a shear force and a moment. Figure 3.1 shows the cyclic sub-structured model.

3.6.1 Loading sequence

To perform cyclic tests, the force or displacement control modes were used according the state of specimen. Elastic small cycles under force control were applied to check the instrumentations. Two cycles at each loading level of elastic and past yield were imposed on the test wall. The tests were conducted under force control to yield then

displacement control. The vertical axial compression load was applied first with the horizontal force held at zero. After the constant axial load was applied to the wall, the horizontal force was increased slowly at a rate of 25 kN/min. For cyclic tests, the loading was paused at intervals to mark the cracks in the walls and to inspect the specimens.

3.6.2 Shear to moment ratio

In the static cyclic tests, the actuators were controlled so that the moment to shear ratio was held constant at 1.1, 5 and 2.25 for walls CW1, CW2 and CW3, respectively. Rehabilitated walls RW3 to RW9 were tested under moment to shear ratio 2.25. This was achieved by controlling the vertical actuators to have a constant axial compression force of 340 kN and an additional force which is directly proportional to the horizontal force. The forces in the two vertical actuators F_{v1} and F_{v2} were related to the horizontal force F_H by the formulae as shown in Table 3.8. These ratios classify the wall as a flexural wall according to Elnashai et al. (1990). This relatively low value is shown to occur in many high rise walls when subjected to earthquake ground motion due to the effect of higher modes of vibration and wall-frame interaction in buildings where both a moment resisting frame and a structural wall resist the lateral load. Feedback from the load cell in the horizontal actuator was used to drive the vertical actuators. The equations are valid whether the horizontal actuator is under force or displacement control.

3.7 REHABILITATION SCHEMES

The aim of the rehabilitation procedures is to eliminate brittle failure modes and to ensure ductile behaviour by increasing the shear strength of the wall and preventing the lap splice failure. The seismic retrofit involved the use of steel anchors bolts, carbon fiber wrap, and fillet weld of the lap spliced reinforcement at the base of the wall. The rehabilitation schemes included adding shear and confinement reinforcement as well as wrapping the concrete with CFRP sheets. The sheets were not connected to the foundation to avoid increasing the flexural strength and thus promoting a ductile flexural failure.

Details of the strengthening scheme of each wall is described in the following sections. Schematic plots for the rehabilitation processes and photographic images for the rehabilitated walls are shown in Figures 3.11 to 3.22.

After testing, some walls were repaired and retested. The walls were laid horizontally and the disintegrated and spalled off concrete was removed using electrical jackhammer. New strain gauges were installed on the reinforcement bars then the walls were placed into the wooden forms again and cleaned using air pressure before casting new concrete. The same concrete mix as the new walls was delivered to the laboratory by concrete truck. The repaired walls were cured in the same manner as the original walls.

Adequately confined concrete can reach high levels of strains before crushing. However, the end zones of the test walls were confined using smooth steel bar ties. This confinement was not enough to enhance the compression strength of concrete. Therefore, it was necessary to wrap the end zones with uni-directional CFRP to improve the ductile behaviour of the walls.

3.7.1 Application of CFRP sheets

Special care was given to the application process of composite sheets to the concrete surface, as the quality of the bond between the sheets and the concrete surface is crucial to the efficiency of the strengthening technique. The concrete surface was smoothed and cleaned from protrusions using grinder, as recommended by several specifications such as ICBO, AC 125 (2001). The corners of the walls were rounded to a radius of 25 mm using a grinder. Application of the different types of CFRP sheets on the concrete surface was similar regardless of the type of the sheet. The two parts of the Tyfo S epoxy were mixed using a heavy duty-low speed electric mixer. A primer coat was used to cover the concrete surface with a thin layer. The FRP sheets were impregnated with the Tyfo S epoxy. The FRP sheets were wrapped around the concrete surface, adjusted and pressed against the surface using a steel roller to remove the excess adhesive and the entrapped air between the sheets. The sheets were allowed to cure at least 7 days at room

temperature before testing. The wall was painted with an initial coat of the Tyfo S Epoxy and then each layer was soaked with the epoxy prior to wrapping the wall.

3.7.2 Shear strengthening

The aim of this rehabilitation procedure is to increase the shear strength of the wall in order to prevent the brittle shear failure and to allow ductile flexural hinging to occur. Proper and careful detailing of earthquake resisting structural wall is crucial particularly when the end column zones were subjected to large compressive strains. Detailing should consider the full structural interaction of the boundary elements with the web wall, the principal vertical reinforcement should not buckle, and sufficient area of compression concrete should be adequately confined against expansion due to large compressive strains. The use of confining reinforcement is effective in enhancing both the compression strain capacity and compression strength of the concrete core.

A bi-directional fabric with the fibres aligned in ±45° directions was most effective to arrest the 45 degree cracks that develop in the wall. Tyfo BCC is a composite material woven in the ±45° directions.

3.7.3 Ductility enhancement

The aim of this rehabilitation procedure is to enhance the ductility of the wall. A unidirectional fabric with the fibres aligned in the horizontal direction is most effective to confine the end zones of the walls. Confinement of the concrete improves the compressive strength and the wall ductility. Tyfo SCH-35 unidirectional Composite material was used to confine the end columns. Mechanical anchors through the thickness of the wall were used to complete the confinement hoop.

3.7.4 Lap splice retrofit

The aim of this rehabilitation procedure is to prevent the failure of the wall due to lap splice bond slip. The presence of the lap splice at the critical section of the RC structural wall plastic hinge zone is not recommended for the seismic design. The bars in a welded lap splice may yield before the lap splice failure and provide the necessary ductility

and energy dissipation during earthquake event. Successful external lap splice retrofit system is difficult. Therefore, a fillet weld of the lap-spliced rebars was unavoidable.

3.7.5 Rehabilitation techniques

Seven rehabilitated walls were constructed and testes. Table 3.9 summarizes the reinforcement details of the walls. In the following sections the details of the rehabilitation schemes are presented.

3.7.5.1 Rehabilitation scheme for RW3

This wall was tested as control wall and then it was rehabilitated as described herein. In this wall, the lap spliced rebars were welded first using fillet weld. The weld size was designed so that yield and rupture of the spliced rebars would occure outside the spliced length. The length of the weld was 200 mm.

The shear rehabilitation scheme involved wrapping the wall with two layers of Tyfo BCC ±45° fabric. Two through holes were drilled at the top and two others at the bottom in the web of the wall. Four high strength steel bolts were inserted through the holes. Circular washer plates of 60 mm diameter and 8 mm thick washer plates were used to clamp on the outsides of the CFRP layers. The objective of those bolts was to improve end anchorage for the fibres and prevent delamination from starting at the top and at the bottom regions of the wall.

The ductility improvement scheme involved the confinement of two end column zones of the wall with five U-shaped layers of Tyfo SCH-35, after installing the shear strengthening CFRP layers. The five layers were necessary to prevent buckling of reinforcement under compression and to provide end columns confinement to concrete. Steel anchors through the wall acted as the fourth side that closed the U-shaped hoops. The U-shaped sheet covered approximately 300 mm on both sides of the wall. Twenty holes were drilled through the wall at a spacing of 100 mm, i.e. 10 holes per each end zone column. High strength 12.5 mm (0.5 inch) diameter high strength bolts were inserted through the holes. The holes were spaced so that they comply with the spacing

requirements for steel confinement hoops in the CSA A23.3 (2004) code provisions. Circular washer plates, 60 mm in diameter and 8 mm thickness, were used. All the anchors were tightened to a torque of 250 N.m. Details of walls CW1 to CW3 are shown in Figure 3.11, and the rehabilitation process of RW3 is shown in Figures 3.12 to 3.16.

3.7.5.2 Rehabilitation scheme for RW4

This wall was tested as control wall, i.e. CW2, and then was rehabilitated for retesting as described in this section. The lap spliced rebars were welded using fillet weld, after the damaged old concrete was removed. New strain gauges were installed, and new fresh concrete was cast.

The shear rehabilitation scheme involved using smooth steel bars of 6.35 mm diameter. The typical spacing between the shear reinforcement as well as the confinement stirrups was 50 mm. The added shear reinforcement was assembled in the horizontal direction perpendicular to the wall height.

The ductility improvement scheme involved the confinement of the two end column zones of the wall with closely spaced closed ties of 6.35 mm diameter. Details of CW2 are shown in Figure 3.11, and the rehabilitation process for RW4 is shown in Figure 3.17.

3.7.5.3 Rehabilitation scheme for RW5

This wall was tested as control wall, i.e. CW1, and then was rehabilitated as described in this section. The lap spliced rebars were welded using fillet weld, after the damaged old concrete was removed. New strain gauges were installed, and new fresh concrete was cast.

The shear rehabilitation scheme involved wrapping the wall with two layers of Tyfo BCC as described in RW3, but without the top and bottom anchor bolts. Plain steel bars 6.35 mm diameter were used as shear reinforcement. The typical spacing between the shear reinforcement was 50 mm. The added shear reinforcement was assembled at ±45° to the base of the wall. The contribution of the two Tyfo BCC layers in resisting shear forces

was necessary so that the total shear capacity of RW5 will be greater than the maximum expected base shear associated with the ultimate flexural capacity. This was necessary to ensure the ductile beaviour of the wall.

The ductility improvement scheme involved the confinement of two end column zones of the wall with two U-shaped layers of CFRP sheets, and closely spaced closed ties of 6.35 mm diameter. The CFRP sheets confinement was identical as describer in Section 3.7.5.1, except for the number of the layers. The same type of the anchor bolts was used, but without the four anchor bolts for clamping the web CFRP top and bottom edges. The holes were spaced so that they comply with the spacing requirements for steel confinement hoops in the CSA A23.3 (2004) code provisions. Details of the rehabilitated test wall is shown in Figure 3.18.

3.7.5.4 Rehabilitation scheme for RW6

The shear rehabilitation scheme involved wrapping the wall with four layers of Tyfo BCC as described in RW3, but without the top and bottom anchor bolts, instead, a clamping 75 mm width plate was installed at the bottom of the wall to prevent web crushing. This number of CFRP layers was needed to increase the shear resistance of the wall. In addition, plain steel bars 6.35 mm diameter were used as shear reinforcement. The typical spacing between the shear reinforcement was 50 mm. The shear reinforcement was assembled in the horizontal direction perpendicular to the wall height.

The ductility improvement scheme involved the confinement of two end column zones of the wall with four U-shaped layers of FRP sheets, and closely-spaced closed-ties of 6.35 mm diameter. The same confinement process as described in Section 3.7.5.1 was used. The rehabilitation details are shown in Figure 3.19.

3.7.5.5 Rehabilitation scheme for RW7

The rehabilitation process for RW7 was identical to RW6 except for two items. First, the shear reinforcement was assembled at ±45° directions to the base of the wall.

Second, there was no clamping plate at the base of wall. The rehabilitation process is shown in Figure 3.20.

3.7.5.6 Rehabilitation scheme for RW8

The shear rehabilitation scheme involved using steel reinforcement. Shear reinforcement of M10 (11.3 mm diameter) steel rebars were used at spacing of 100 mm and for the confinement ties were spaced @ 50 mm. The added shear reinforcement was assembled in a ±45°, X-configuration, to the base of the wall. There was no FRP wrapping for shear strengthening.

The ductility improvement scheme involved the confinement of two end columns' zones of the wall. Three U-shaped layers of FRP sheets, and closely spaced closed ties of 6.35 mm diameter were required to provide the end columns with concrete confinement and to prevent rebar buckling. The same confinement process as described in Section 3.7.5.1 was used. Twenty holes were drilled through the wall at a spacing of 100 mm. High strength 10 mm (3/8 inch)-diameter bolts were inserted through the holes. Square washer plates, 75 mm length, and 10 mm thickness, were used. The rehabilitation process is shown in Figure 3.21.

3.7.5.7 Rehabilitation scheme for RW9

The rehabilitation procedure for RW9 was identical to RW8 except for one item. The shear reinforcement was assembled in the horizontal direction, i.e. perpendicular to the wall height. The rehabilitation details are is shown in Figure 3.22.

3.8 CALCULATED FLEXURAL AND SHEAR CAPACITIES

To guide the loading during test, the expected flexural and shear capacities of the tested walls were calculated using section analysis. The concrete cylinder compression strength, the reinforcement steel tensile yield strength, and the ultimate strength of the rebars were used in the calculation of the wall capacities. In addition, manufacturer supplied strength and strain of the used CFRPs as well as the coupons results for CFRPs

were used for the calculations. The actual and the nominal capacities were calculated. Table 3.10 presents the walls details and expected nominal flexural and shear capacities.

Table 3.1 Similitude Ratio (S) of the 1/3 Scale Test Model

Parameter	Similitude formula	Scale	Comments
Linear Dimension	S_L	1/3	Independent variable
Young's Modulus (E)	$S_E = S_F S_L^{-2}$	1.00	Independent variable
Poisson's ratio (ν)	none	1.00	Material related variable
Stress	$S_F S_L^{-2}$	1.00	Material related variable
Strain	none	1.00	Material related variable
Displacement	S_L	1/3	Geometric related variable
Rotation	none	1.00	Geometric related variable
Area of reinforcement	S_L^2	1/9	Geometric related variable
Force	$S_F = S_L^2$	1/9	Load related variable
Moment	$S_M = S_F S_L = S_L^3$	1/27	Load related variable
Energy (work)	$S_W = S_F S_L = S_L^3$	1/27	Load related variable
Time	S_T	1.00	Excluded
Peak ground acceleration (PGA)	S_{PGA}	1/3	
Frequency of prototype	S_f	1.00	
Frequency of model	$1/(S_f)^{0.5}$	1.00	

Table 3.2 Prototype Structural Wall/ Model Dimensions and properties

Parameter		Prototype	Similitude Ratio	Test Model
Length, L_w (m)		3.00	1/3	1.00
Height, h_w (m)		3.30	1/3	1.10
Thickness, t_w (m)		0.36	1/3	0.12
Elastic Modulus (E), MPa		2.6045×10^4	1.00	2.6045×10^4
Translational Mass M_T, $kN.s^2/m$		15.00	1/3	5.00
Rotational Inertia M_{rot}, $kN.s^2.m$		$0.10 \times M_T$		$0.10 \times M_T$
Damping Ratio	1st Mode	0.03	1.00	0.03
	2nd Mode	0.03	1.00	0.03
Rayleigh Proportional Damping	Mass (a_1)	0.324	1.00	0.324
	Stiff. (a_2)	0.0135	1.00	0.0135
Fundamental Period (s)	1st Mode	1.00	1.00	1.00
	2nd Mode	0.162	1.00	0.162
Peak ground acceleration (PGA) g (m/s^2)		0.348	1/3	0.348/ 3.00 = 0.116

Table 3.3 Concrete mix design (quantities constitute one cubic meter only)

Mix component	Component Weight kg/m^3 (kN/m^3)
Cement type 10	176 (1.73)
Slag cement	59 (0.58)
Gravel size 10 mm	1060 (10.4)
Sand	980 (9.6)
Water	100 (0.98)

Table 3.4 Cylinders Compression Test Results

Age of concrete	Compressive Strength f'_c (MPa)
7 days	20.30
28 days	33.50
Day of CW2 test	37.30
Day of CW3 test	37.50
Day of RW3 test	35.60
Day of RW4 test	38.00
Day of RW5 test	39.00
Day of RW6 test	38.00
Day of RW7 test	39.00
Day of RW8 test	36.60
Day of RW9 test	34.90

Table 3.5 Reinforcement properties (Yield strength at 0.2 % offset)

Nominal bar diameter	bar diameter (mm)	Area (mm^2)	Yield strength (MPa)	Ultimate Strength (MPa)
M20	20.0	300.0	496.0	718
M15	16.0	201.1	450.0	760
M10	11.3	100.0	489.0	589
Ties (6.35 mm)	6.35	31.70	570.0	616

Table 3.6 Mechanical properties of the fibre composites from suppliers data (Fyfeco, 2005) and (as tested, Khalil 2005)

Material	Tensile Modulus, (GPa)	Ultimate Tensile strength, (MPa)	Ultimate tensile strain
Tyfo BCC (on the 0° direction)	65 (38)	717 (437)	1.1% (1.1 %)
SCH-35	78 (79.8)	991 (1008)	1.26% (1.5 %)

Table 3.7 MTS hydraulic actuators specifications

Actuator model	Length at mid Stroke (m)	Stroke (mm)	Capacity in Tension (kN)	Capacity in compression (kN)	Position/ direction
243.45	2.35	±250	500	500	East/ Vertical
243.70	2.98	±250	960	1460	East/ Horizontal
244.41	2.74	±250	500	500	West/ Vertical

Table 3.8 MTS hydraulic actuators forces relationships

Actuator model	M/VL = 5	M/VL = 2.25	Position/ direction
243.45	$F_{v1} = -176 + 1.09\,F_H$	$F_{v1} = -176 + 0.323\,F_H$	East/ Vertical
243.70	F_H = independent	F_H = independent	East/ Horizontal
244.41	$F_{v2} = -164 - 1.09\,F_H$	$F_{v2} = -164 - 0.323\,F_H$	West/ Vertical

Table 3.9 Walls details

Parameter	CW2	CW3	RW3	RW4	RW5	RW6	RW7	RW8	RW9
M / VL	5.0	2.25	2.25	2.25	2.25	2.25	2.25	2.25	2.25
Axial load, kN	340	340	340	340	340	340	340	340	340
Flexural reinforcement	6M15	6M15	6M15	6M15	6M15	8M20	8M20	6M20	6M20
Shear reinforcement	6mm @180 mm	6mm @180 mm	6mm @180 mm	6mm @50 mm	6mm @100 mm*	6mm @50 mm	6mm @100 mm*	M10 @100 mm*	M10 @100 mm
Confinement reinforcement	---	---	---	6mm @50 mm	6mm @50 mm	6mm @50 mm	6mm @50 mm	6mm @50 mm	6mm @50 mm
Confinement CFRP layers (t = 0.89 mm)	---	---	5	2	2	4	4	3	3
Shear CFRP layers (t = 0.86 mm)	---	---	2	2	2	4	4	---	---
Steel anchors	---	---	12.5 @100 mm	12.5 @100 mm	12.5 @100 mm	12.5 @100 mm	12.5 @100 mm	10.0 @100 mm	10.0 @100 mm

* Reinforcement at ± 45°

Table 3.10 Summary of walls expected approximate nominal moment and shear capacities

Parameter	CW2	CW3	RW3	RW4	RW5	RW6	RW7	RW8	RW9
M / VL	5.0	2.25	2.25	2.25	2.25	2.25	2.25	2.25	2.25
Axial load, kN	340	340	340	340	340	340	340	340	340
V_c, kN	228	228	228	228	228	228	228	228	228
V_s, kN, ties with f_y = 400 MPa	138	138	138	495	495	495	495	782	782
$V_c + V_s$, kN	366	336	336	723	723	723	723	1010	1010
N FRP layers × V_{FRP} per layer, kN	---	---	2× 138	---	2× 138	4× 138	4× 138	---	---
$V_{FRP} + V_s$	138	138	414	495	771	1047	1047	782	782
$V = V_c + V_s + V_{FRP}$	366	336	642	723	999	1275	1275	1010	1010
M_{cr}, kN.m	92.4	92.4	92.4	92.4	92.4	92.4	92.4	92.4	92.4
M_y, kN.m	Fail	Fail	540	540	540	960	960	750	750
M_u, kN.m	---	---	970	970	970	1480	1480	1250	1250

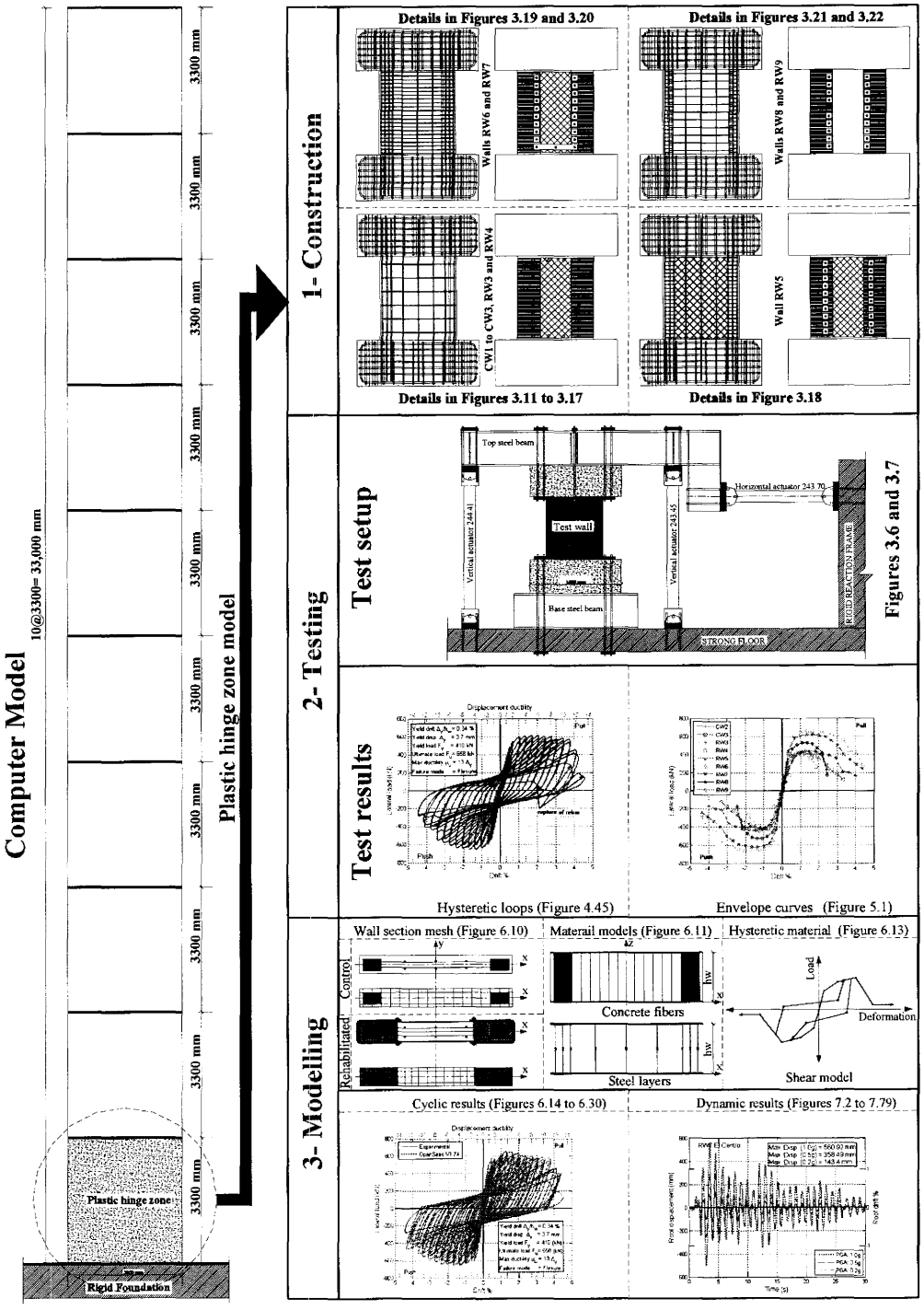

Figure 3. 1 Model-based simulation of overall structural response (left) with laboratory testing of the plastic hinge region of 10 storey RC structural wall (right)

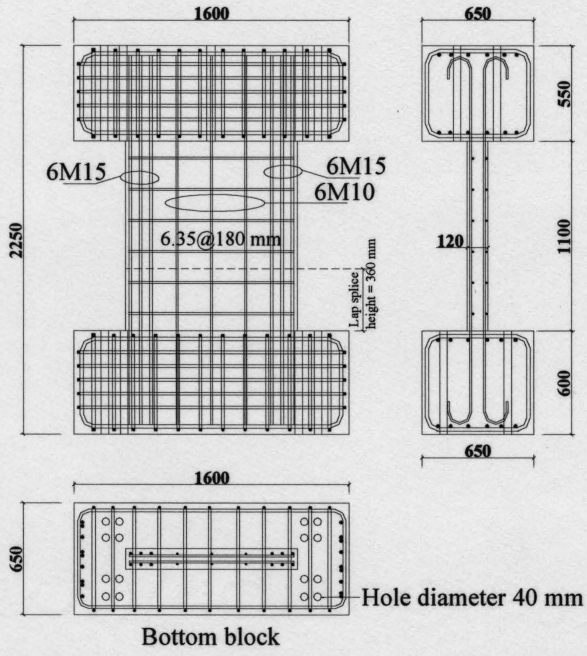

Figure 3. 2 Reinforcement details for test walls CW1 and CW2

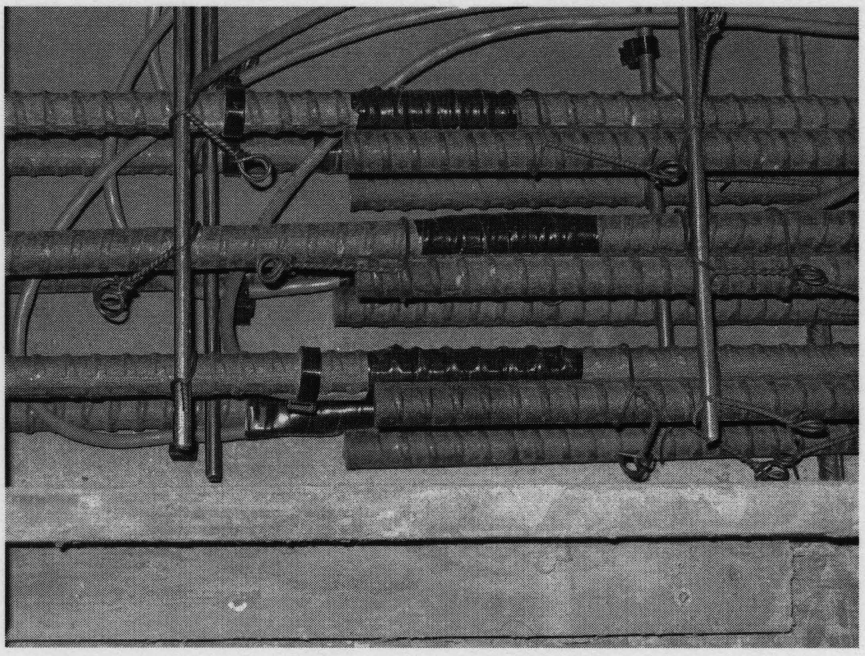

Figure 3. 3 Lap splice

Figure 3. 4 Wall reinforcement details

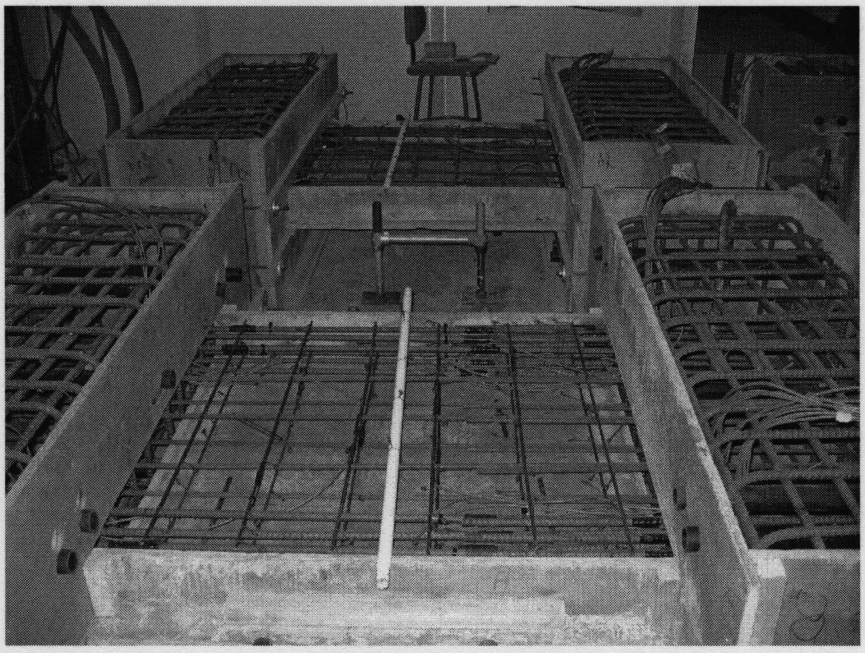

Figure 3. 5 Specimens Construction

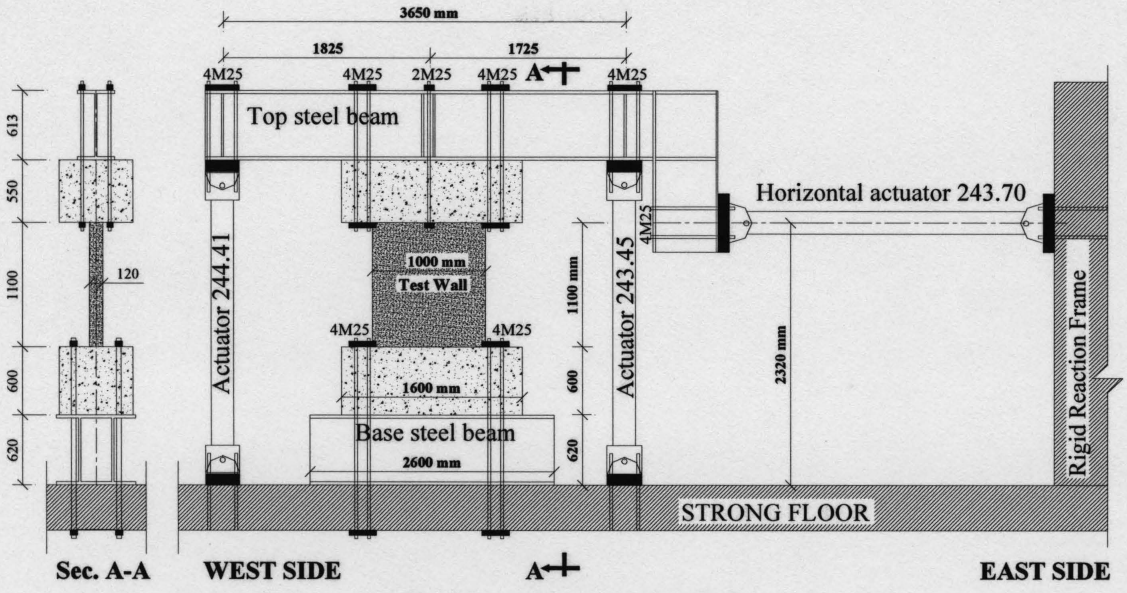

Figure 3. 6 Test setup details

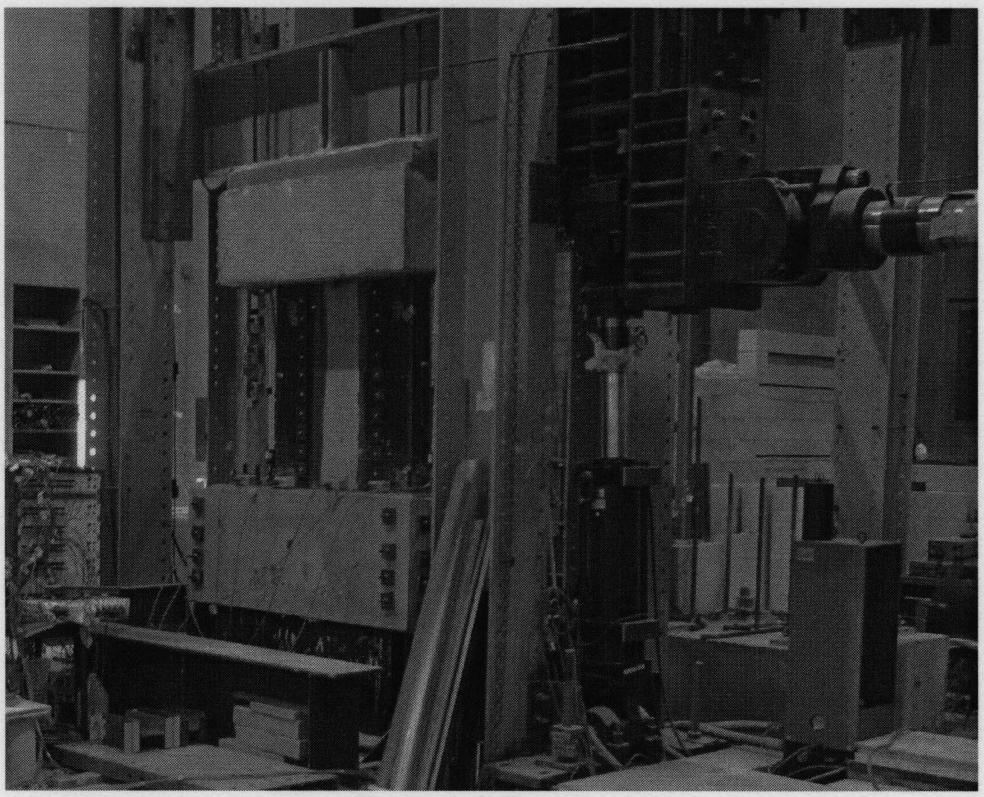

Figure 3. 7 Test setup

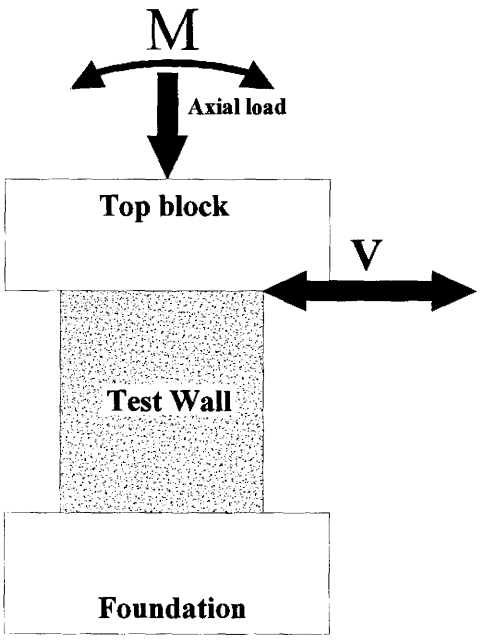

Figure 3. 8 Applied loads to the test walls.

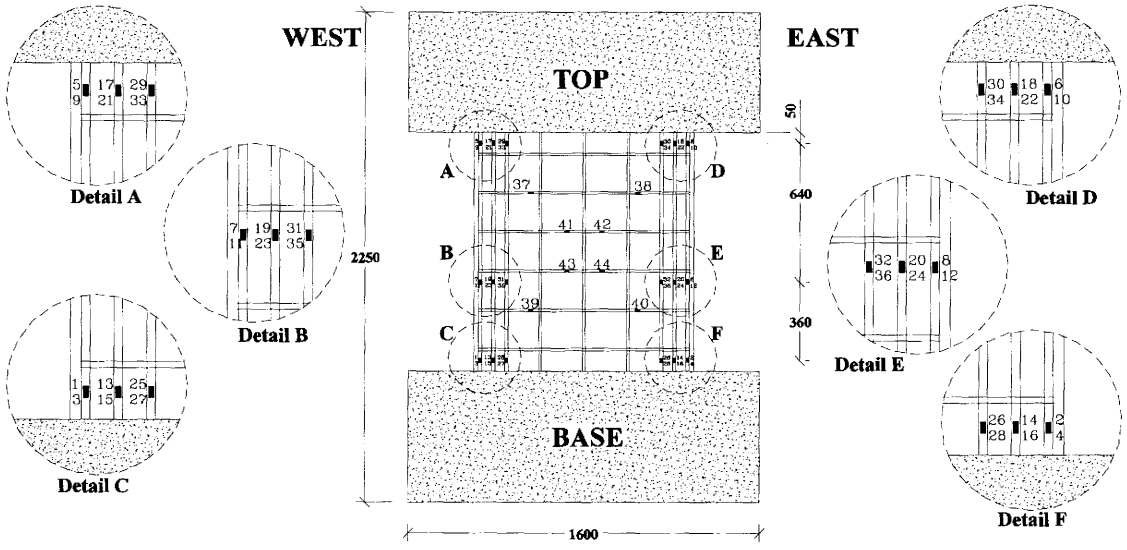

Figure 3. 9 Strain gauge locations

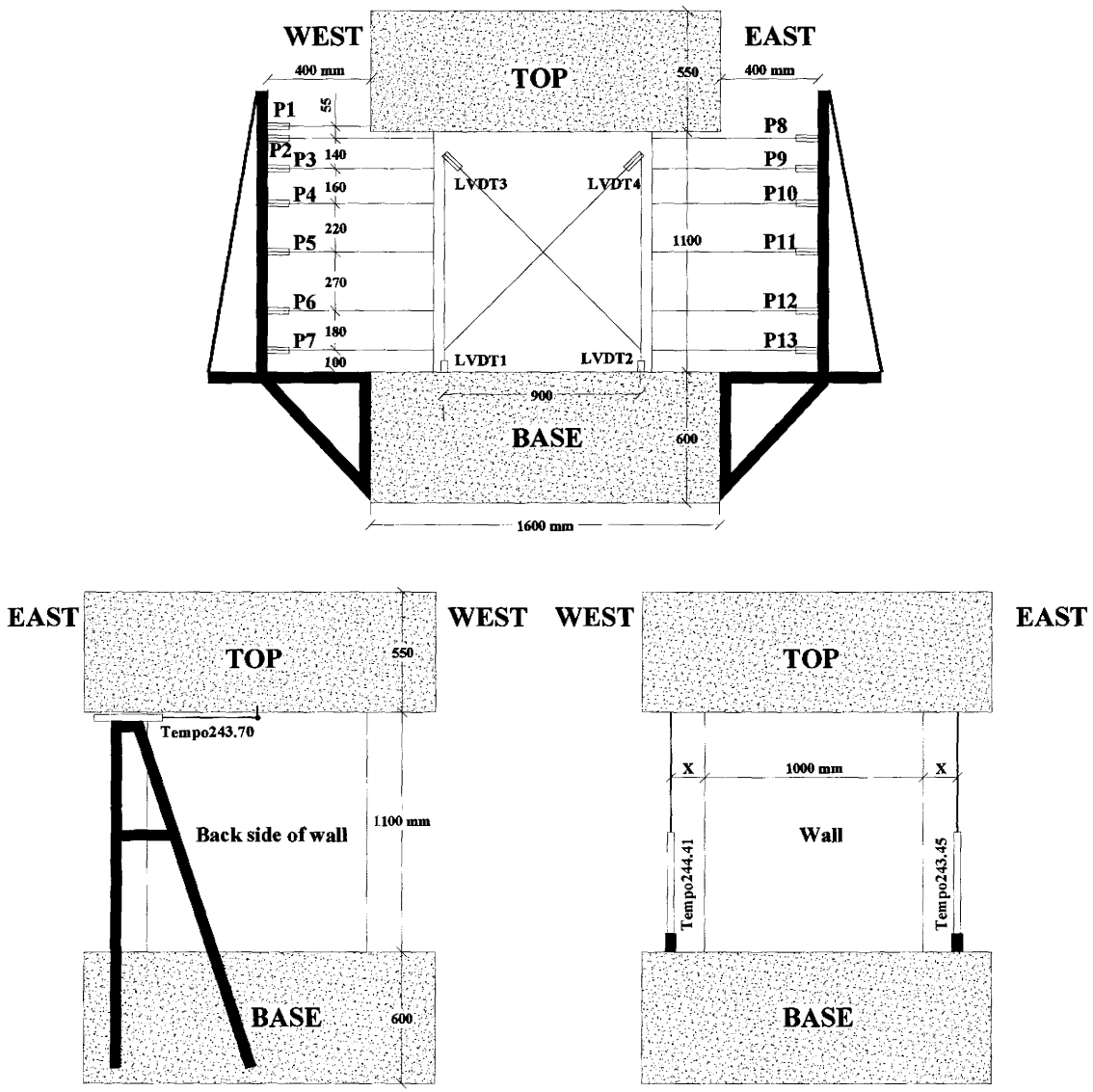

Figure 3. 10 Displacement transducers positions

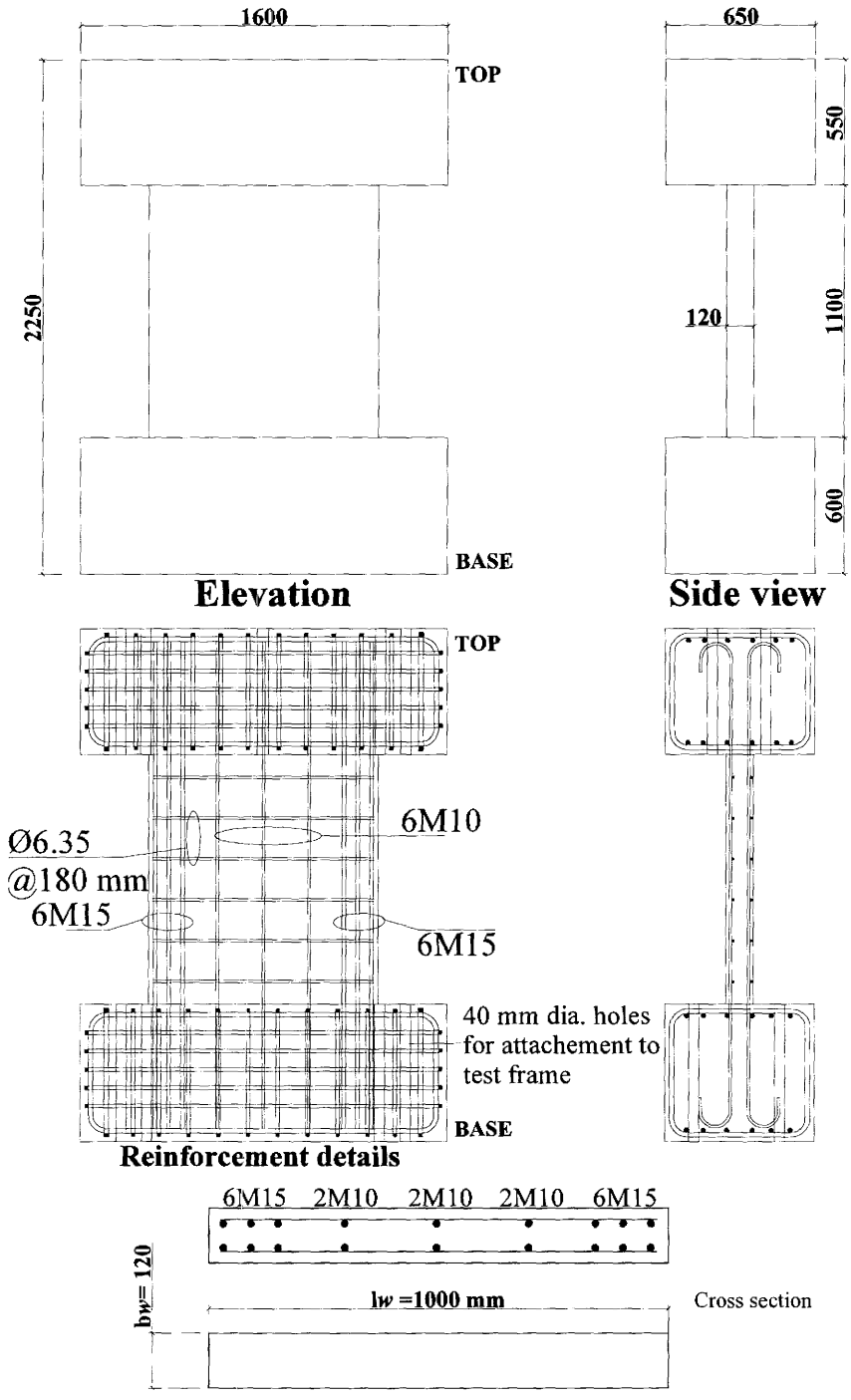

Figure 3. 11 Details of walls: CW1 to CW3

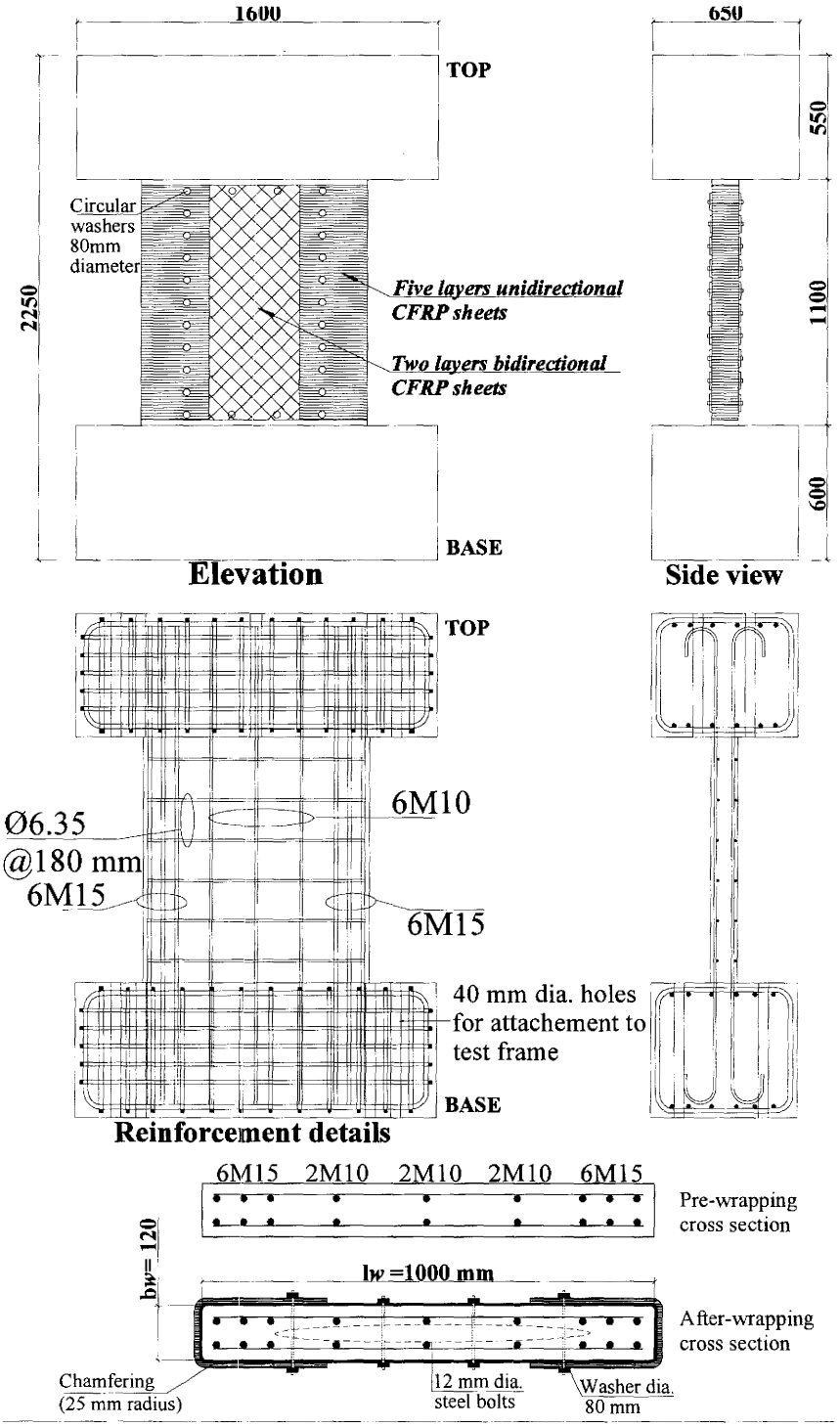

Figure 3. 12 Rehabilitation scheme for wall: RW3

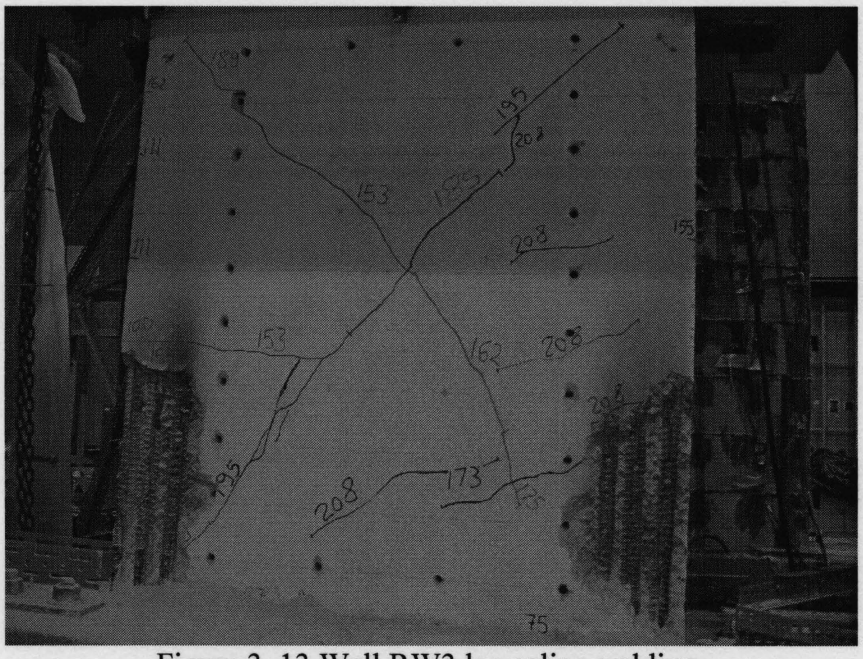

Figure 3. 13 Wall RW3 lap splice welding.

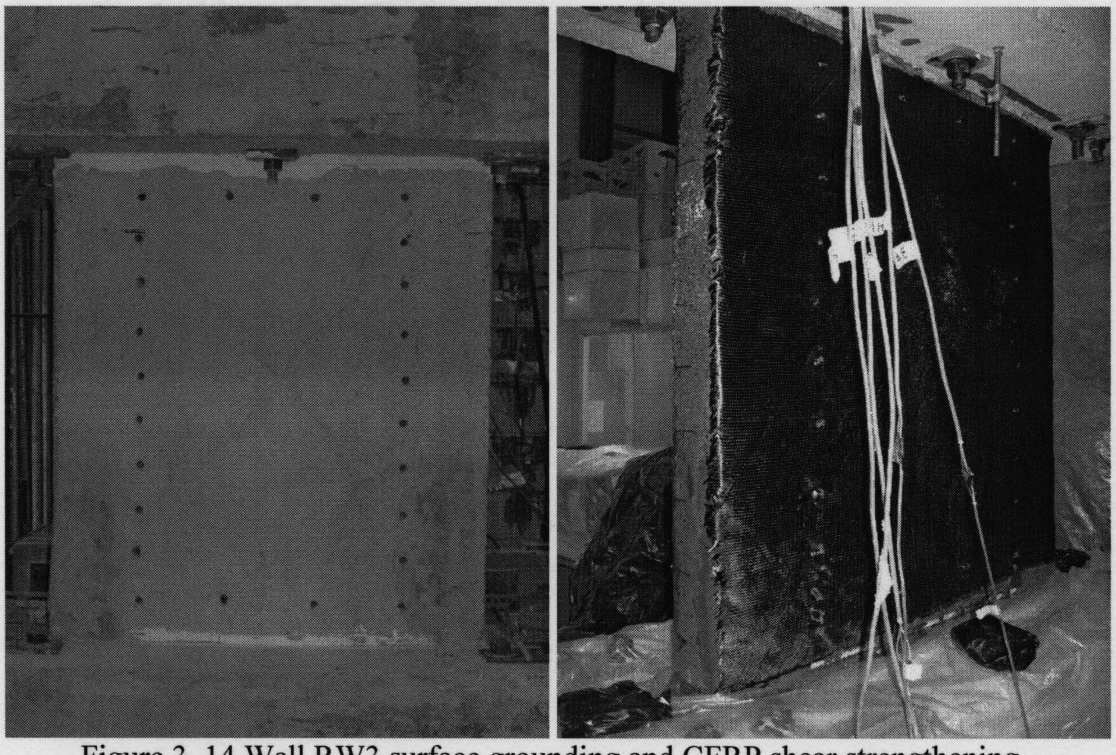

Figure 3. 14 Wall RW3 surface grounding and CFRP shear strengthening.

Figure 3. 15 Wall RW3 CFRP end column confinement.

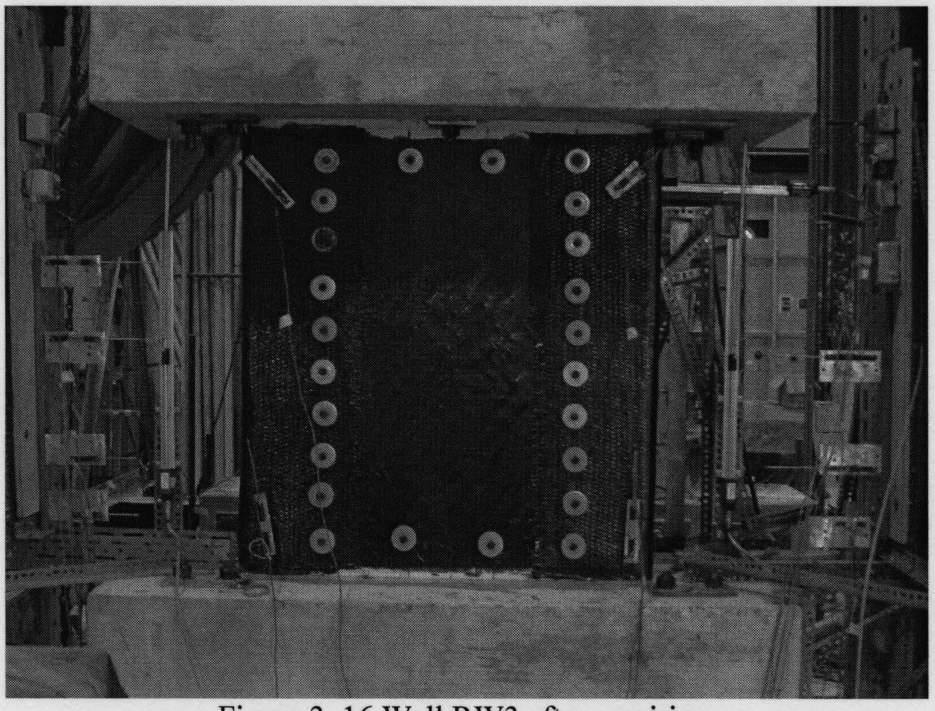

Figure 3. 16 Wall RW3 after repairing.

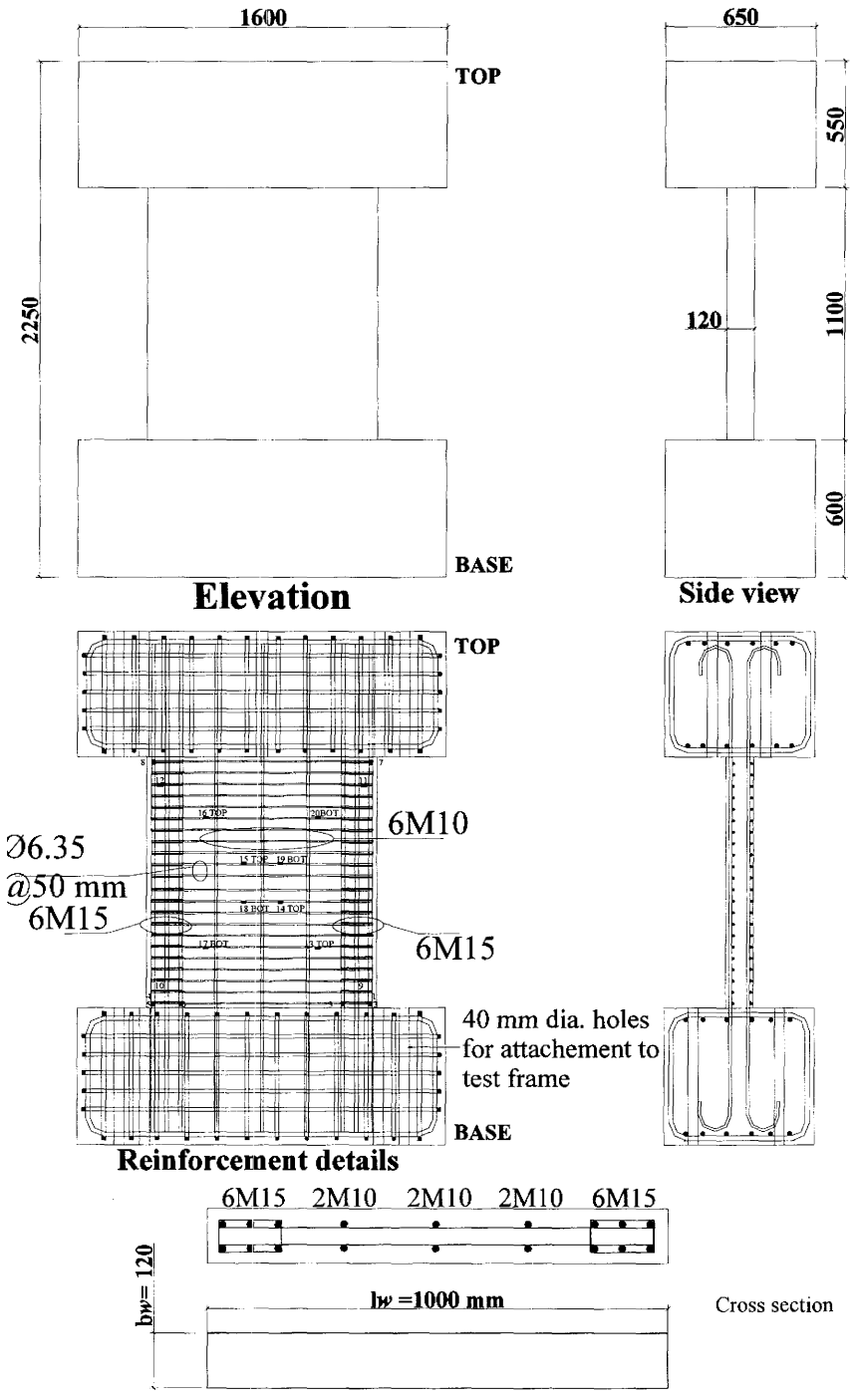

Figure 3. 17 Rehabilitation scheme for wall: RW4

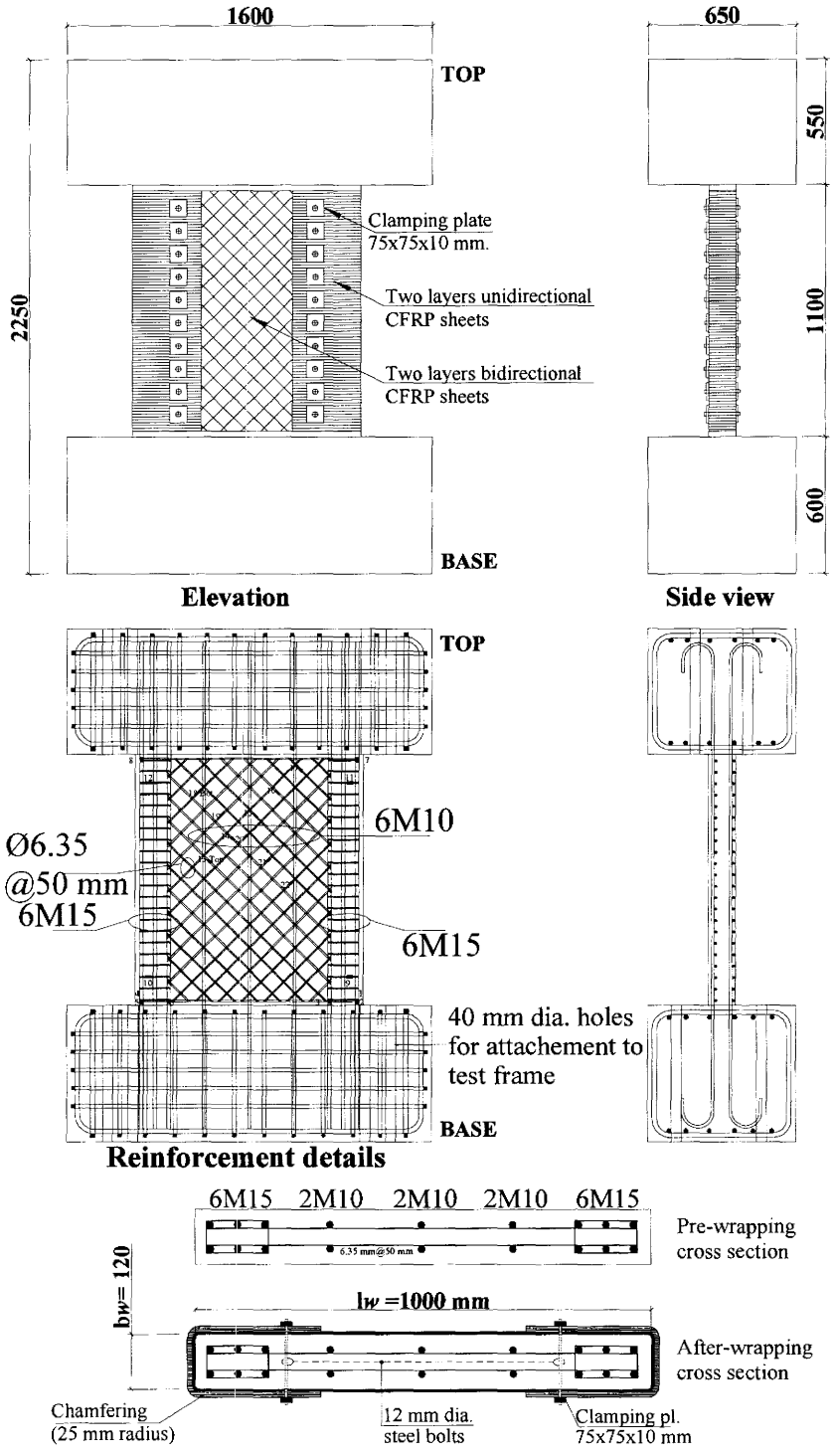

Figure 3. 18 Rehabilitation scheme for wall: RW5

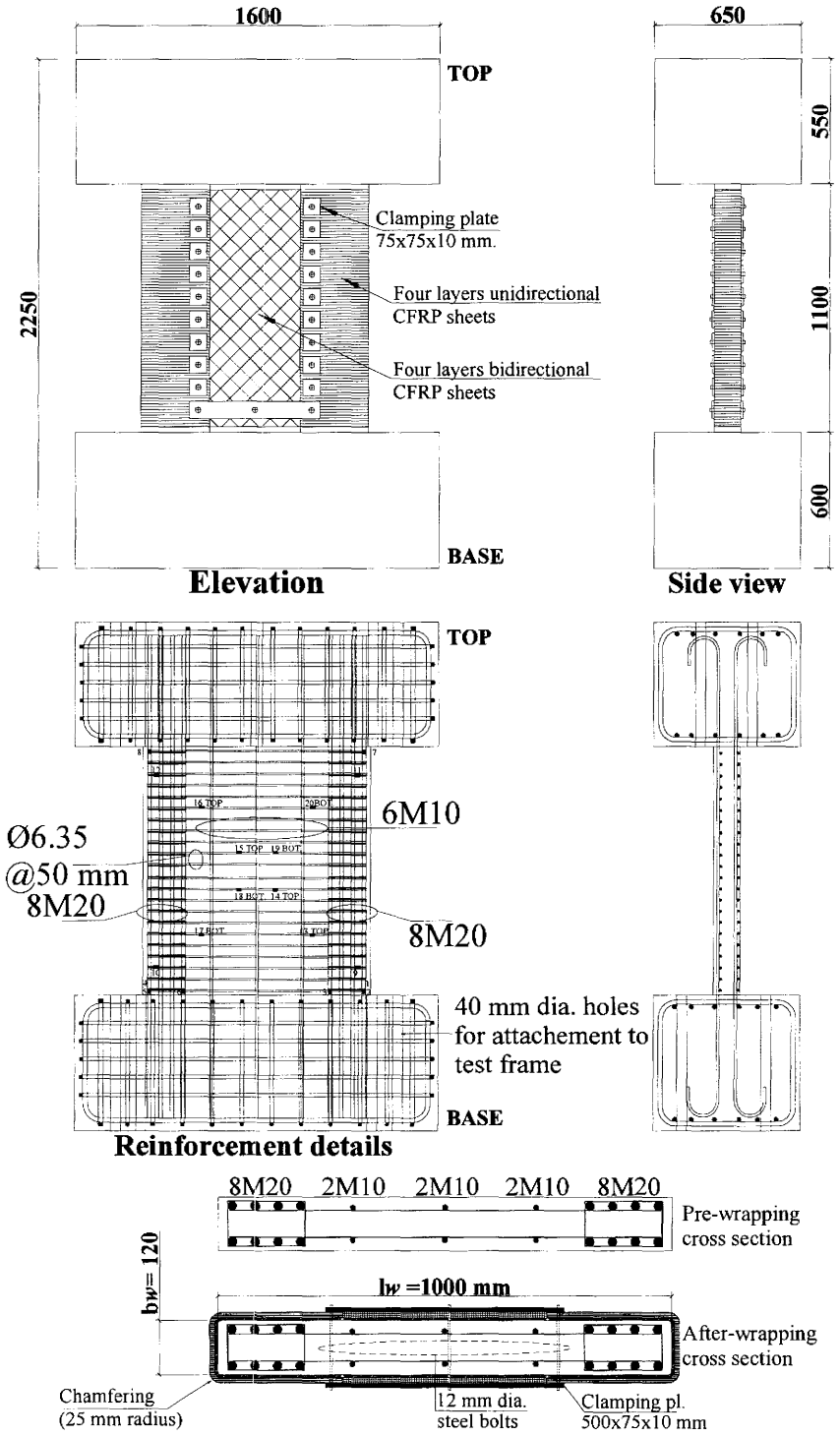

Figure 3. 19 Rehabilitation scheme for wall: RW6

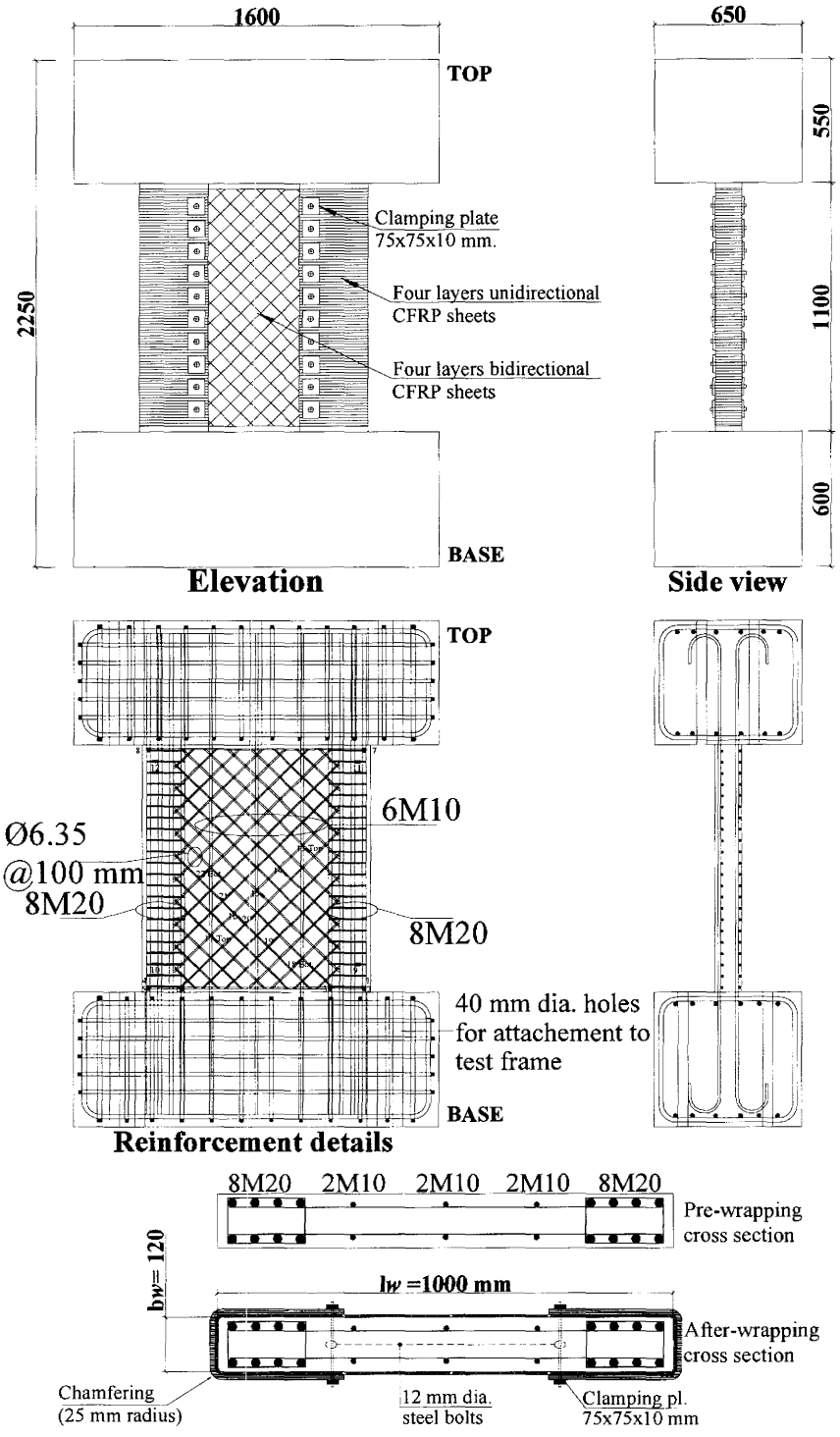

Figure 3. 20 Rehabilitation scheme for wall: RW7

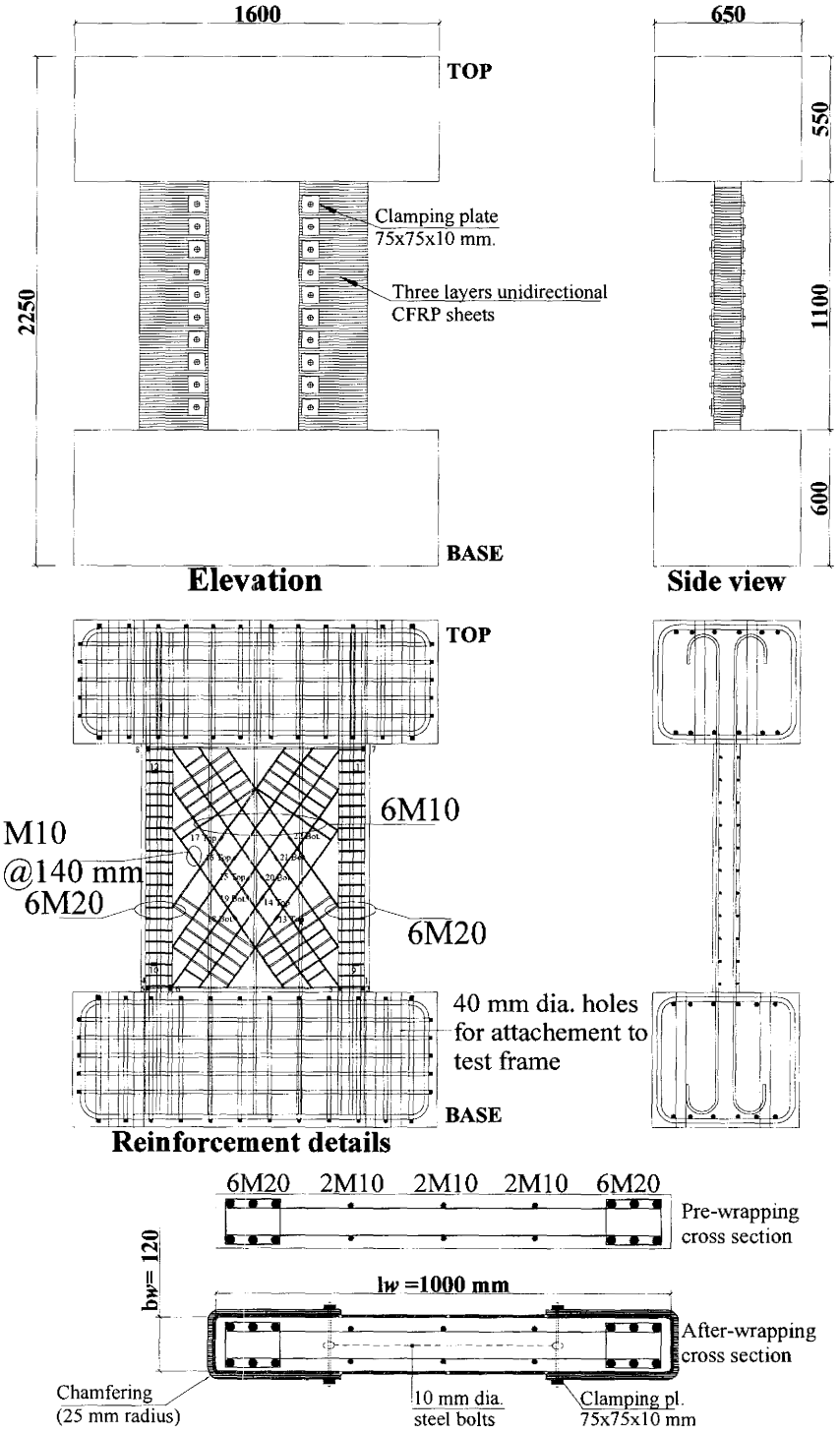

Figure 3. 21 Rehabilitation scheme for wall: RW8

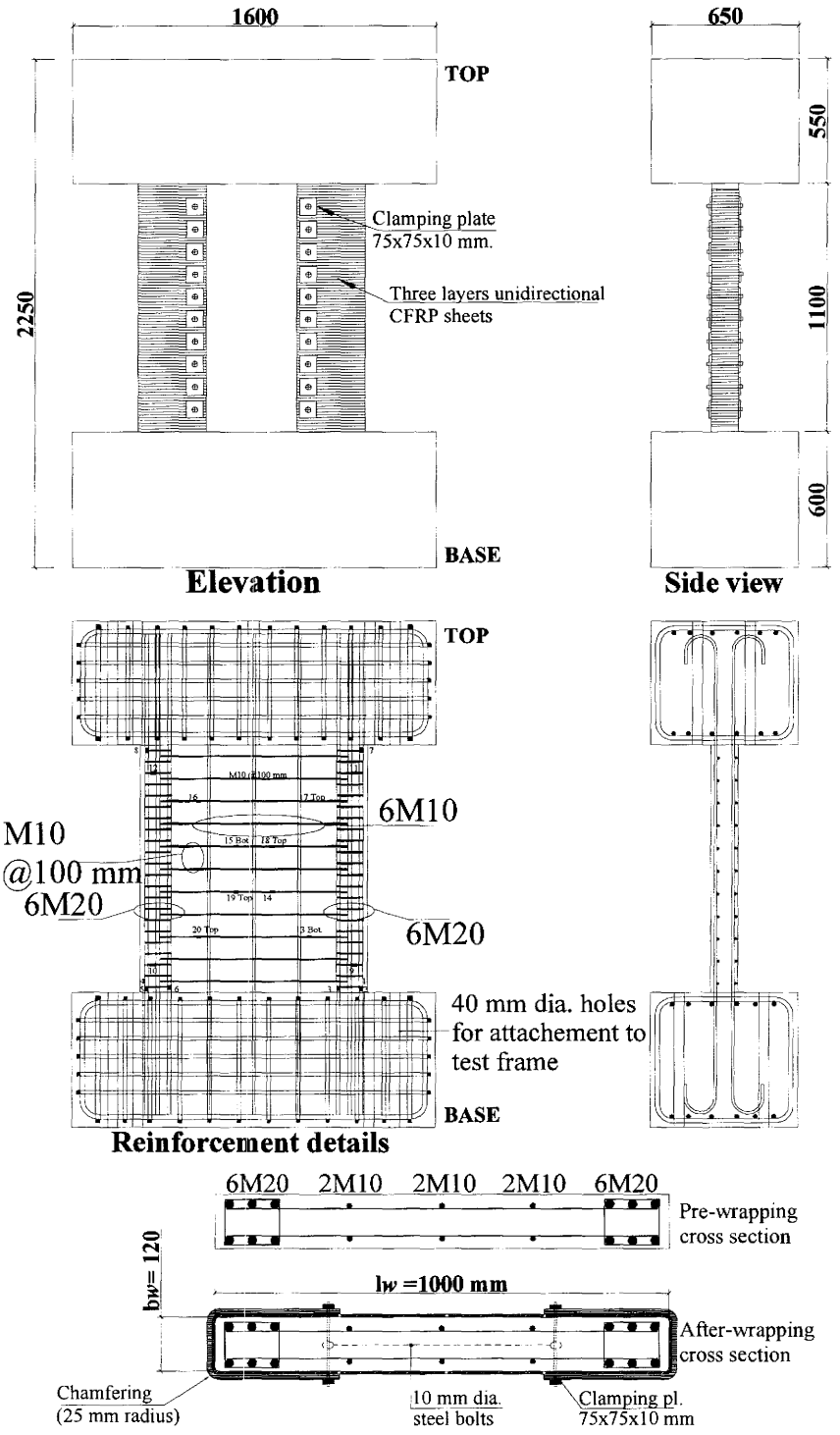

Figure 3. 22 Rehabilitation scheme for wall: RW9

CHAPTER 4

CYCLIC LOAD TEST RESULTS

4.1 INTRODUCTION

The results of static cyclic loading tests are presented and discussed in this chapter. Three control walls were tested and identified as CW1 to CW3 with moment to shear ratios (M/VL) of 1.1, 5 and 2.25, respectively. Seven walls, RW3 to RW9, were rehabilitated and tested. Wall CW1 was used to test the system performance, the instrumentation and was used to estimate the range of the force control and the yield displacement. In addition, the wall was used to estimate the initial lateral and rotational stiffnesses of the test walls for conducting the pseudodynamic test. Wall CW1 was used successfully to check the reference frame to which all the lateral displacements are referred. The reference frame was fixed onto the test wall foundation to avoid the rigid body motion of the test wall. Several loading cycles with maximum horizontal load of ±60 kN were applied and the corresponding top lateral displacement was 0.20 mm. The wall behaved satisfactory as it was expected during all these elastic loading cycles until it failed in shear unexpectedly. In this chapter, the behaviour of the walls during the tests are described and the experimental data are presented. During the tests, the walls were monitored, and inspected closely to spot the first crack as well as to monitor the crack development and finally to identify the failure mode. Data measurements included the loads, displacements, and strains. Comparisons between the behaviour of the rehabilitated walls and the control walls are presented in Chapter 5.

4.2 CONTROL WALLS

Two control walls CW2 and CW3 were tested and the test results are presented in this section. The walls were identical but were subjected to loads that imposed different moment to shear ratios on the walls.

4.2.1 Control wall CW2

This as-built wall was tested as a control specimen without rehabilitation. The loads were applied by the two vertical and one horizontal actuators to produce moment to shear ratio (M/VL) of 5. This high ratio classified the wall behaviour as a flexural wall and the wall was expected to show flexural dominated behaviour.

To simulate observed failure modes of walls following recent earthquakes, it was proposed to conduct the test by applying a horizontal load at the top of the wall of ±15 kN, ±45 kN, and finally ±100 kN cycles. If the first yield of the longitudinal flexural reinforcement was determined then the test will continue by displacement control. During the test progress, the wall was monitored closely to spot the first crack as well as to monitor the crack development and to identify the failure mode. The first visible crack developed at the toe of the wall at a horizontal load of approximately ±45 kN. The first cracks that developed were tension cracks at the bottom of the wall and spread to near mid-height. For the third loading cycle of ±100 kN, the existing cracks started to open up and new horizontal crack developed just at the top end of the lap splice zone at load of 75 kN. The horizontal crack developed at 75 kN and extended in the horizontal direction as the load increased to 85 kN. No shear cracks were observed at this loading level. With increasing load in the same direction up to 100 kN, the wall failed prematurely due bond slip of the lap splice. The applied loads were low enough not to cause yielding of the longitudinal reinforcement. Figure 4.1 shows the tested wall after failure.

Lateral Displacement

Six string potentiometers, one horizontal Temposonic and 7 LVDT displacement transducers were used to measure lateral displacements at different heights of the wall. The lateral displacements were measured at 10%, 25%, 50%, 75%, and 85% of the wall height as well as at the top of the wall. The relationship between the top horizontal force and drift is shown in Figure 4.2. The figure shows that there was no significant loss of stiffness after the first cracking and before the final failure. The maximum displacement was 2.4 mm which represents 0.22 % lateral drift.

Rotations

The rotation was calculated using two sensitive high resolution (24 bit resolution, Temposonics). The Temposonics bases were fixed directly to the foundation block and the top of the temposonic was attached to the bottom of the top rigid concrete block. The rotations in radians were calculated as follows:

$$\theta_{Tempo} = (Tempo_{243.45} - Tempo_{244.41})/X_{Tempo} \quad (4.1)$$

where θ_{Tempo} is the top rotation, $Tempo_{243.45}$ is the vertical displacement at the east side of the wall, $Tempo_{244.41}$ is the vertical displacement at the west side of the wall, X_{Tempo} is the horizontal distance between the two vertical Temposonics in the same units of the Temposonics readings, i.e. mm. The maximum rotation the wall reached before failure was approximately 4×10^{-3} rad. The rotation at the top of the wall is shown in Figure 4.3.

In addition, the rotation was calculated using two 100 mm stroke vertical LVDTs attached to the web of the wall. The results show that the measurements from different instrumentation were consistent.

Shear Deformation

The shear deformation γ was calculated for wall using LVDTs 3 and 4 installed at ±45° to a horizontal reference as shown in Figure 3.10. The shear deformation was calculated using the simple formula:

$$\gamma = \frac{(d_3 - d_4)}{900\sqrt{2}} \tag{4.2}$$

where d_3 to d_4 are the displacements for LVDT 3 and LVDT 4 respectively. The shear deformation for the whole wall is shown in Figure 4.4.

Strains

The maximum recorded strains were from strain gauge No. 11 and strain gauge No. 23. These strain gauges were attached to the longitudinal reinforcement in the end element of the wall near the bottom. Those results are shown in Figures 4.5 and 4.6. The strain readings indicate that the longitudinal steel bars did not yield. The yield strain determined from coupon tests of the steel reinforcement was 0.002 mm/mm. The longitudinal reinforcement did not yield due to the premature failure of the wall by bond slip.

The recorded strains in the horizontal reinforcement bars were always in tension regardless whether the horizontal actuator was pushing or pulling. The maximum measured strains at failure were at strain gauge No. 44. The location of this strain gauge was the middle of the horizontal bar at mid height of the wall. The high strain readings were because the strain gauge was bridging a crack. It was observed that because there were no significant shear cracks up to failure, the maximum strains in the horizontal bars were small compared to the measured strain. Figure 4.7 shows the strain reading from strain gauge 44.

4.2.2 Control wall CW3

Wall CW3 was tested as-built without rehabilitation. The loads applied by the two vertical and one horizontal actuators were synchronized to produce moment to shear ratio of 2.25.

The wall was inspected closely after each loading step to detect the first crack and determine the failure mode. The loading cycles of maximum horizontal load of ±10 kN, ±20 kN, ±30 kN, ±40 kN, ±50 kN under force control were applied. Each cycle was repeated twice. It was observed that the wall was still in the elastic range until the end of

the ±50 kN load cycle. The maximum horizontal displacement during the second cycle at this load level was approximately 0.25 mm in both directions. After this cycle, the horizontal force was returned to zero to switch the horizontal actuator control to displacement control using the actuator internal displacement transducer control. The difference between the displacement at the point of attachment of the actuator and the displacement of the top of the wall was taken into account in plotting the data. At horizontal displacement of ±0.4 mm the force reached ±67 kN and two horizontal cracks were observed at the base of the wall. At horizontal displacement of ±1.1 mm the force reached ±155 kN and first diagonal cracks were observed in both inclined ±45° directions. At a horizontal displacement of ±2.6 mm the force was ±195 kN and the two diagonal cracks opened up again and extended from corner-to-corner of the wall in both diagonal directions. At horizontal displacement of approximately 3.3 mm the force was approximately 198 kN in pull direction and the wall failed due to bond slip of the lap splice. At this point the test was terminated. Figure 4.8 shows shear cracking and the failure mode of the wall due to bond slip.

Lateral Displacement

The relationship between the top horizontal force and drift is plotted in Figure 4.9. The figure shows that there was no significant loss of stiffness after the first cracking and before the final failure. The maximum recorded displacement near failure was 3.1 mm which represented drift of approximately 0.3 %. The measured drift of 0.3 % was small compared to 2.5% interstory drift ratio of the National Building Code of Canada (NBCC 2005 clause 4.18.13.3).

Rotations

The rotation was calculated using two sensitive high resolution Temposonics fixed directly to the foundation block and attached to the bottom of the top rigid concrete block. The rotation at the top of the wall is shown in Figure 4.10. The maximum rotation of the wall before failure reached 3.2×10^{-3} rad.

Shear Deformation

The shear deformation γ was calculated for the test wall using LVDTs 3 and 4. These two LVDTs measured the diagonal displacement. The shear deformation of the wall with applied load is shown in Figure 4.11. The shear forces and deformations were small enough to cause shear failure of the test wall.

Strains

The maximum recorded strains were from strain gauge No. 26 and strain gauge No. 28. These two gauges were installed on the flexural vertical reinforcement near the bottom of the end columns. Those results are shown in Figures 4.12 and 4.13. The strain readings indicated that the longitudinal steel bars did not yield because the wall failed prematurely by bond slip.

The strains in the horizontal reinforcement bars were always in tension whether the horizontal actuator was pushing or pulling. The maximum measured strain at failure was from strain gauge No. 39 mounted on a horizontal bar in the middle third of the height. The gauge was bridging a diagonal crack. It is observed that because there were no significant shear cracks up to failure, the maximum strains in the horizontal bars were less than 60 % of the yield strain. Figure 4.14 shows the strain readings from strain gauge 39.

4.3 REPAIRED/ REHABILITATED WALLS

Seven walls RW3 to RW9 were tested. The results of the seven repaired/ rehabilitated walls are presented and discussed in this section.

4.3.1 Rehabilitated wall RW3

The wall previously tested as control wall CW3 was repaired by removing the cracked concrete, welding the lap splice and casting new concrete. The wall was wrapped with CFRP as described in Section 3.7.5.1. The loads from the three actuators were synchronized to subject the wall to moment to shear ratio of 2.25.

The horizontal cyclic load was applied up to ±100 kN under force control then the control was switched to displacement control. The selected load level of ±100 kN was still

well below the elastic limits as confirmed by strain measurements. At each load level, two loading cycles were conducted. Using force control at the start of the test was necessary because the displacements were small and more difficult to control. In addition, small variations in displacements corresponded to large changes in load. The horizontal displacement at the second cycle at load level ±100 kN was approximately 1.85 mm in both directions. After this cycle, the load application of the horizontal actuator was changed to displacement control.

The yield displacement was determined to be 4.00 mm corresponding to drift ratio of 0.36 %, and the associated yield load was 225 kN. A horizontal crack was observed at the bottom of the two end zones of the wall due to flexural yielding of the end zone longitudinal reinforcements. The displacement was increased to ductility levels 1.5 then 2 up to ductility 8. There were no noticeable debonding or delamination of the FRP observed in the web or the confined end elements. For the next four cycles at ductility levels of 3 and 4 the specimen was still gaining strength due to strain hardening of the steel reinforcement and the confinement effect of the FRP on the compression strength of the concrete at the end zones. The applied horizontal load reached 435 kN at ductility level 4. The horizontal flexural cracks from each side at the base of the wall joined with the wider cracks opening at the base of the end zones. The FRP was still functioning and confining the end zones as well as sharing in the shear force resistance. In the next cycle of loading at ductility level 5 and drift ratio 1.82 %, there was no more gain in the specimen strength. Because of the many cyclic load reversals the unwrapped bottom 50 mm of the wall suffered extensive flexural and shear cracking and the strength of the specimen started to deteriorate. The maximum load of approximately 395 kN was reached at ductility level of 6.

The specimen sustained a full cycle at ductility level 7, and the load dropped slightly to 385 kN. During the first cycle at ductility level 8, a longitudinal rebar in the end column ruptured and the load dropped significantly from 340 kN to 260 kN in the pull direction. During the pull half of the next loading cycle at ductility level 9 another rebar

ruptured and the load dropped to 105 kN. The test was stopped at ductility level 11 corresponding to drift ratio of 4.00 %. Figure 4.15 shows the wall before the test and Figure 4.16 shows the failure of the wall. The figure shows concrete crushing in the bottom 50 mm of the wall.

Lateral Displacement

The lateral displacements were measured at 25%, 50%, 75% of the wall height as well as at the top of the wall. The relationship between the top horizontal force and drift is shown in Figure 4.17. The figure shows that there was no significant loss of strength up to ductility level 5, i.e. at lateral drift of 1.82 %. The specimen strength started to deteriorate slowly during the loading cycles at ductility levels of 6 and 7. During the next loading cycles at ductility levels 8 to 11, the strength deteriorated to about 1/3 of the maximum strength of the wall. The maximum lateral displacement that the wall reached at that level was approximately 44 mm in the push cycle.

Rotations

The rotation was calculated from the reading of two high resolution Temposonics fixed directly to the foundation block and attached to the bottom of the top rigid concrete beam. The variation of the rotation at the top of the wall with the applied horizontal load is shown in Figure 4.18. The test results showed that the top rotation at yield was approximately 0.005 rad. The maximum rotation that the wall reached before failure was approximately 0.02 rad. This indicated that the specimen achieved a rotational ductility of 4, and more than 6 times the rotation at failure for control wall CW3.

Shear Deformation

The shear deformation γ is plotted against the applied horizontal load in Figure 4.19. The total shear deformation of the rehabilitated wall at load level of 200 kN was approximately 0.001 rad. This was almost equal to the total shear deformation of control wall at the same level of load. The average shear stiffness was 200,000 kN/ rad, which was

the same for both the control and rehabilitated walls. The reason for this was the premature failure of the control walls due to bond slip, which occurred before any significant shear deformation occurred.

Strains in steel reinforcement

The maximum recorded strains were from strain gauge SG2 installed on the outermost rebars at the base of the wall. Typical results are shown in Figure 4.20. The strain readings indicated that the longitudinal steel rebars sustained high strains past yield strain of 0.2% during the test. However, the operational range of the used strain gauges is 2%, at many positions the recorded strains were more than 2%. Past this level the gauge readings continued to indicate what was happening but the actual numbers may not be reliable.

The maximum measured strains at failure of the horizontal reinforcing bars were from strain gauge No. 40 located near the middle third of the wall height. It was observed that the maximum strains in the horizontal bars were less than 1/3 the strain in the case of the control wall. The reason was that the CFRP shared in the shear force resistance. Figure 4.21 shows the strain reading from strain gauge 40.

Strains in FRP

The readings from strain gauges SG2 and SG8 installed on the CFRP indicated that the CFRP was fully utilized. The maximum strain recorded on the confinement CFRP near the bottom of the column zones was 0.005 mm/mm. In addition, the maximum strain recorded at the middle of wall height of the bidirectional CFRP was also 0.005 mm/mm. Figure 4.22 shows the strains in the confinement CFRP as recorded from SG2. Figure 4.23 and 4.24 show the strains in the CFRP sheets on the wall web as recorded from SG8 and SG11, respectively.

4.3.2 Rehabilitated wall RW4

The loads applied by three actuators were synchronized to subject the rehabilitated wall RW4 to moment to shear ratio 2.25. The test wall was subjected to cyclic loads of ±50

kN, ±100 kN, ±150 kN under force control. Each cycle at a new load was repeated twice. It was observed that, the wall was still in the elastic range to the end of ±150 kN cycle. The maximum horizontal displacement at this last cycle was approximately 1.00 mm in both directions. After this cycle, the horizontal actuator control was switched to displacement control using the internal actuator displacement transducer. At horizontal displacement of ±1.4 mm the horizontal actuator force was ±185 kN. At this load level several flexural horizontal cracks were observed at the end zone columns of the wall. During the subsequent loading steps before yielding numerous horizontal cracks were observed at both end zones. The yield displacement was determined to be approximately 3.4 mm and the corresponding force was 300 kN. At ductility level 1.5 the force reached 365 kN on average between the push and pull loading and the previously opened cracks widened. No additional cracks were detected. At ductility level 2 the horizontal force increased to 390 kN. At ductility level 3 the force increased to 410 kN. The previously opened diagonal cracks widened and extended from corner-to-corner of the wall. Due to cyclic load reversal and under high strains at the wall toes, the concrete cover spalled off with signs of concrete crushing. Figure 4.25 shows the crack pattern of the wall at ductility level 4, which shows the horizontal and diagonal cracks in both directions. The maximum lateral load was 436 kN. At ductility level 5 the wall strength started to deteriorate due to crushed concrete and widened cracks. The maximum load at that ductility level was 370 kN. The strength deteriorated significantly during the loading cycles at ductility level 6 due to crushed concrete and fracture of longitudinal rebars. The maximum load at this ductility level was approximately 200 kN.

Lateral Displacement

The lateral displacements at the top of the wall were measured and plotted in the form of drift against the top horizontal force as shown in Figure 4.26. The yield displacement was 3.40 mm. The figure shows that there was no significant loss of strength up to ductility level 4, which corresponded to lateral drift of 1.25 %. The specimen

strength started to deteriorate slowly during the second cycle at ductility level 5. During the subsequent two cycles at ductility level 6, the strength deteriorated to about 40 % of the maximum strength of the wall. The maximum lateral drift that the wall reached at that level was 1.85 %.

Rotations

The rotation at the top of the wall is shown in Figure 4.27. The test results showed that the top rotation at yield was 0.005 rad which indicated that the specimen achieved a rotational ductility of 3, and more than 5 times the rotation at failure for control wall CW3. The maximum rotation that the wall reached before failure was approximately 0.015 rad.

Shear Deformation

The lateral load plotted against the shear deformation is shown in Figure 4.28. The total shear deformation of the rehabilitated wall at load level of 200 kN was 0.0005 rad and was almost equal to half the total shear deformation of the control wall at the same level of load. The average shear stiffness was 400,000 kN/ rad for the rehabilitated wall as compared to 200,000 kN/ rad for the control wall. The lack of symmetry in the shear response was because the developed diagonal shear corner-to-corner shear in push direction was not completely developed in pull direction. The strength deterioration as a result of the concrete crushing in pull direction and flexural rebars ruptures was another reason for the unsymmetrical response during the last two loading cycles.

Strains in steel reinforcement

The maximum recorded strains were from the strain gauge SG1 installed on the outermost rebars near the base of the wall. The strain measurements are shown in Figure 4.29. The strain readings indicated that the longitudinal steel rebars yielded and sustained high strains during the test. Strains in the order of 4% were measured. However, past the operational range of the gauges of 2%, the accuracy of the readings is questionable. Strain gauge readings along the height of the bars indicated that most of the bar length yielded.

The maximum recorded strains in the horizontal bars near the middle of the wall height were from strain gauge No. 18 as shown in Figure 4.30. It was observed that the maximum strains in the horizontal bars were close to yield at the end of the test.

Strains in Confinement Ties

Readings from strain gauge SG9 installed on the confinement ties indicated that the confined concrete was under high strains. Figure 4.31 shows that the strain in the confinement ties at the toes of the wall was more than 0.003 mm/mm, which indicated that concrete confinement was effective at high loads. On the other hand, the confining ties at the top of the wall were still in the elastic range as shown by the strain gauge SG12 located near the top of the wall and plotted in Figure 4.32.

4.3.3 Rehabilitated wall RW5

Figure 4.33 shows a front view of the wall before testing. The wall RW5 was strengthened using bi-directional CFRP to upgrade the shear resistance, and with unidirectional CFRP for confinement enhancement of the end columns. In addition, the shear reinforcement installed in the wall was configured at ±45°. The shear reinforcement consisted of 6.35 mm steel bars. The steel was selected such that the horizontal projection of this shear reinforcement was equal to the horizontal shear reinforcement that was installed in wall RW4. The load was applied during the test to subject the wall to moment to shear ratio of 2.25. Due to expected high yield load, the wall was tested under force control to ±50 kN, ±100 kN, ±150 kN. After that the actuators control was changed to displacement control. At each load level the wall was subjected to two loading cycles. The maximum horizontal displacement at the second cycle of the ±150 kN load was approximately 1.00 mm in both directions. At horizontal displacement of ±1.6 mm, the force was approximately 195 kN and horizontal cracks were observed at the base of the wall. The yield of the flexural reinforcement was recorded at wall top displacement of 2.75 mm with corresponding horizontal force of 270 kN. At ductility level 1.5 the force reached an average of 350 kN between the push and pull forces. The previously opened horizontal

cracks at the base widened and extended to finally join. At ductility level 2 the force increased to 390 kN. At ductility level 3 the force reached 410 kN. At the end of the second cycle of loading at ductility level 3, the bottom ends of the CFRP started to debond. The horizontal load at ductility level 4 was 420 kN, without significant debonding of the FRP sheets. The maximum strength of the wall was observed at ductility levels of 5 and 6 loading cycles, which was approximately 430 kN. There was no additional strength gain after ductility level 6. Strength deterioration started after the rupture of one of the main flexural rebars, which led to drop in the strength from 430 kN to 350 kN. During the pull half of the loading cycle at ductility level 7, two main reinforcement flexural rebars ruptured and the wall strength dropped from 370 kN to 250 kN. The test wall continued to lose strength with subsequent loading cycles at ductility levels of 8 to 10 due to web CFRP debonding as well as main longitudinal reinforcement rupture. The horizontal load at the end of the test was almost 30% of the maximum horizontal load that the wall resisted.

Lateral Displacement

The relationship between the top horizontal force and drift of the wall is shown in Figure 4.34. The displacement at the first yield of the longitudinal reinforcement was determined to be 2.75 mm. The figure shows that there was no significant loss of strength up to ductility level 6, which corresponded to lateral drift of 1.5 %. With further loading cycles, specimen strength continued to deteriorate to 25 % of the maximum strength of the wall. The maximum lateral drift that the wall reached at that level was approximately 2.25 %.

Rotations

Relationship between the applied lateral force and the rotation at the top of the wall is shown in Figure 4.35. The test results showed that the top rotation at yield was approximately 0.0025 rad, which indicated that the specimen achieved a rotational ductility of 8. This is more than 5 times the rotation at failure for control wall CW3. The maximum rotation that the wall reached before failure was approximately 0.02 rad.

Shear Deformation

The relationship between the horizontal top load and the shear deformation γ is shown in Figure 4.36. The unsymmetrical response in shear was because the cracks developed during the loading history affected the shear response during the next loading cycles. The total shear deformation of the rehabilitated wall at load level 200 kN was approximately 0.0003 rad and was almost equal to 30% of the total shear deformation of control wall at the same level load. The average shear stiffness is 400,000 kN/ rad for the rehabilitated wall, and 200,000 kN/ rad for the control wall.

Strains in steel reinforcement

The maximum-recorded strains were from strain gauge SG11 installed on the outermost rebars and at the base of the wall. The strains measured at the bottom of the wall are shown in Figure 4.37 while the strains measured at the top of the wall SG17 were plotted in Figure 4.38. The strain readings indicated that the longitudinal steel rebars sustained high strains during the test. The strain readings from 3 strain gauges installed along the longitudinal bar indicated that the yielding spread to most of the wall's height.

The maximum recorded strains in the shear reinforcement were from strain gauge No. 29. The strains were close to yield at the end of the test as shown in Figure 4.39.

Strains in Confinement Ties

The reading from strain gauges installed on the confinement 6.35 mm ties at the wall's end column elements are shown in Figure 4.40. The location of the measured strains was a tie near the bottom toes of the wall at 100 mm above the base of the wall. The maximum reading reached was 0.0009 mm/mm, which indicated that the contribution of the CFRP confinement wrapping kept the strain in the ties at lower levels than yield.

Strains in FRP

Figure 4.41 shows the strain measurements in the confinement CFRP around the end column element of the wall. Readings from strain gauges installed on the CFRP indicated that the CFRP was fully utilized. For example, the maximum strain recorded on the

confinement CFRP was 0.00013 mm/mm. Figure 4.42 shows the strains in the CFRP for shear strengthening. The maximum strain recorded by SG 9 at the middle height of the bidirectional CFRP was close to 0.003 mm/mm. The strains were measured along the fibre direction of ±45°.

4.3.4 Rehabilitated wall RW6

The wall was strengthened using four layers of uni-directional CFRP for confinement and four layers of bidirectional CFRP for shear strengthening. Figure 4.43 shows the front view of the wall before testing. Two clamping steel plates 10 mm thick, 75 mm wide, and 500 mm long were used to prevent web CFRP sheets from debonding near the bottom edge of the wall. Sikadur epoxy mortar was used as a filler and strong adhesive between the plates and the CFRP sheets. Double shear force transfer mechanism was developed by applying these two plates. The loads applied by three actuators were synchronized to subject the rehabilitated wall RW6 to moment to shear ratio 2.25.

It was expected that the lateral load at first yield of flexural reinforcement to be approximately 400 kN. Therefore, the test was conducted under load control for the loading cycles of ±50 kN, ±100 kN, ±200 kN. Each loading cycle was repeated twice throughout the whole test. The maximum horizontal displacement at the second cycle at the load level of ±200 kN was approximately 1.30 mm in both directions. At horizontal displacement of ±3.00 mm, the force was ±350 kN. The first yield of the longitudinal flexural reinforcement steel in the end columns was recorded at displacement 3.70 mm with associated force of 410 kN. At ductility level 1.5 with force level of 530 kN on average, horizontal cracks were observed at the base of the wall. The previously opened horizontal cracks at the base of the wall widened and extended from the wall ends towards the middle. During loading cycle at ductility level 2 the horizontal force increased to 575 kN. The top middle part of the web CFRP sheets started to debond at the ductility level 2 and extended to 150 mm downward from the top edge. The CFRP wrap for the rest of wall did not debond. At ductility level 3 the measured horizontal force increased to 630 kN. It

was observed that the bottom horizontal cracks from both wall ends were joined at the middle at the end of the loading cycle at ductility level 3. The horizontal load reached at ductility level 4 was 640 kN. The bottom edges of the web bidirectional CFRP fourth layer started to debond during this cycle. The CFRP debonding was not significant with the maximum drop in the load of less than 5% from the maximum resisted horizontal force by the wall during this cycle. The maximum strength of the wall was observed at ductility levels of 4 to 6, which was approximately 660 kN. There was no additional strength gain after ductility level 6. As the area of debonding increased, the wall's strength started to deteriorate at loading cycle of ductility level 7. The maximum lateral force reached was 620 kN. During the loading cycle of ductility level 8, the maximum force decreased to 600 kN. At ductility levels 9 and 10 the maximum measured horizontal forces were 590 kN and 570 kN, respectively. The test wall strength dropped to 510 kN at ductility level 11. The bottom 25% of the CFRP debonded by the end of ductility level 12, which led to a significant loss of specimen's strength. The maximum horizontal sustained force at ductility level 12 was 430 kN. At ductility level 13, there were two consecutive ruptures of main flexural rebars which led to significant loss of the wall strength. The wall strength dropped from 430 kN to 275 kN in push and 135 in pull directions. Crushing failure of the concrete at the bottom of the end column and the bottom steel plate are shown in Figure 4.44. It was observed that the bottom steel plate played a significant role in preventing early CFRP debonding, and hence, prevented early strength deterioration.

Lateral Displacement

The lateral drift plotted against the top horizontal force is shown in Figure 4.45. The displacement at the first yield of the reinforcement steel was 3.70 mm. The figure showed that there was no significant loss of strength up to ductility level 7 which corresponds to lateral drift of 2.35 %. The specimen strength started to deteriorate significantly during the loading cycles at ductility level 11 and the subsequent ductility levels. During the ductility level 12 loading cycle, the strength deteriorated to about 67 %

of the maximum strength of the wall. The maximum lateral drift that the wall reached at that level ductility was 4.37 %.

Rotations

The rotation at the top of the wall is shown in Figure 4.46. The test results showed that the top rotation at yield was approximately 0.003 rad, which indicated that the test wall achieved a rotational ductility of 10. The maximum rotation that the wall reached before failure was approximately 0.03 rad.

Shear Deformation

The shear deformation is shown in Figure 4.47. The maximum shear the wall sustained was 660 kN. The average shear stiffness was 400,000 kN/ rad for the rehabilitated wall.

Strains in steel reinforcement

The maximum recorded strains were from strain gauge SG16 installed on the outermost rebars and located near the base of the wall. These measurements were plotted in Figure 4.48 for a strain gauge located at the bottom of the wall and in Figure 4.49 for the strain gauge SG21 installed at the top of the wall. The strain readings indicated that the longitudinal steel rebars sustained high strains during the test. The readings from several strain gauges indicated that yielding extended to most of the rebar length.

The maximum recorded strains in the transverse reinforcement were from strain gauge SG33 located near the middle height of the wall web as shown in Figure 4.50. From this figure it was observed that the maximum strains in the horizontal bars were close to yield at the end of the test.

Strains in Confinement Ties

Reading from strain gauges SG23 and SG24 installed on the confinement ties near the bottom of the end columns indicated that the confined concrete was under high strains

as shown in Figures 4.51 and 4.52, respectively. The strain records indicated that the confined concrete was under high stress at failure, which caused concrete disintegration.

Strains in FRP

The readings from strain gauges SG4 and SG5 installed on the CFRP as plotted in Figures 4.53 to 4.54 indicated that the CFRP was fully utilized. The strain gauges were located at the bottom of the end column elements. The maximum strain recorded on the confinement CFRP was 0.006 mm/mm. Figure 4.55 showed that the recorded strains from a strain gauge SG13 located at the mid height of the wall and installed in the direction of fibre at ±45° of the bidirectional CFRP for shear strengthening. The maximum strain recorded at the mid height of the bidirectional CFRP was close to 0.004 mm/mm.

4.3.5 Rehabilitated wall RW7

The wall repair was identical to wall RW6. Bi-directional CFRP was used for shear strengthening. Unidirectional CFRP was used for confinement of end columns. There were two differences between wall RW6 and RW7. The shear reinforcement was configured at ±45°, and no clamping steel plate was used to confine the bottom edge of the web CFRP sheets. The wall rehabilitation with CFRP was described in Section 3.7.5.4. The loads were synchronized to subject the test wall to moment to shear ratio of 2.25. Figure 4.56 shows the wall's front view during the test.

The loading protocol was identical to test wall RW6. The first four load control cycles were up ±200 kN applied in ±50 kN increments. The maximum horizontal displacement at the loading cycle of ±200 kN was 1.30 mm in both directions, and the bottom edge of the fourth top bi-directional CFRP layer started to debond from the previously wrapped three CFRP layers. The use of the steel anchors to tie the ends of the U shaped CFRP confining the end columns was effective in preventing debonding from extending towards the end columns. At horizontal displacement of ±2.10 mm, the horizontal force reached 300 kN, and the previously debonded edges of the last CFRP layer extended toward the top of the wall. This CFRP debonding was not travelling

horizontally towards the web of the wall because of the effect of the steel anchors. The displacement at first yield of the flexural reinforcement was 3.70 mm, and the corresponding horizontal force was approximately 410 kN. It was observed that the top 80 mm of the CFRP debonded during the loading cycle of yield displacement. At ductility level 1.5 the applied horizontal force increased to 540 kN and horizontal cracks were observed at the base of the wall. In addition, the previously debonded web CFRP extended downward to 250 mm from the top edge of the wall. The previously opened horizontal cracks widened. At loading cycle of ductility level 2 the force increased to 570 kN and the top middle 1/3 height of the web CFRP sheets debonded. At ductility level 3 the horizontal actuator force increased to 610 kN. It was observed that at the bottom of the wall the horizontal cracks from each side of the wall joined each other at the middle. The horizontal load at ductility level 4 was 610 kN.

The maximum lateral load of 630 kN was observed at ductility level 5. At ductility level 6, the load dropped to 600 kN, and the bottom 200 mm of the web CFRP for shear strengthening debonded. During the loading cycles of ductility levels of 7 and 8, the strength of the wall deteriorated to 580 kN and 540 kN, respectively. By the end of the of ductility level 8, the bottom middle third of the web CFRP was debonded from the already cracked concrete. The wall strength was decreasing during the subsequent loading cycles. For example, at ductility levels 9 and 10 the maximum horizontal forces were 510 kN and 400 kN, respectively. The first ruptured main flexural rebar occurred at ductility level 9. Another main flexural rebar ruptured at ductility level 10, which led to a significant drop in the load from 510 kN to 400 kN. The specimen's strength dropped to 360 kN at ductility level 11, due to crushing of the concrete at the bottom third of the wall as shown in Figure 4.57. The maximum lateral force at ductility level 12 was 280 kN. At ductility levels of 12, there were more ruptures of main flexural rebars which led to significant loss of wall lateral resistance. Lateral load resistance of the wall dropped from 280 kN to 250 kN at ductility levels of 12 and 13, respectively. Figure 4.58 shows the wall at failure.

Lateral Displacement

The relationship between the top horizontal force and the drift of the wall is shown in Figure 4.59. The measured displacement at first yield of the longitudinal flexural reinforcement was 3.70 mm. The figure shows that there was no significant loss of strength up to ductility level 6 which corresponds to top lateral drift of 2.02 %. The specimen strength started to deteriorate rapidly during the ductility level 9 and the subsequent ductility levels. During the loading cycle at ductility level 12, the lateral load deteriorated to about 44 % of the maximum lateral load resistance of the wall. The maximum top lateral drift that the wall reached was approximately 4.37 %.

Rotations

The test results showed that the top rotation at yield was approximately 0.005 rad, which indicated that the specimen achieved a rotational ductility of 6. The rotation at the top of the wall is shown in Figure 4.60. The maximum rotation that the wall reached before failure was 0.03 rad.

Shear Deformation

The shear deformation is shown in Figure 4.61. The maximum shear force was 630 kN and the average shear stiffness is 400,000 kN/ rad for the rehabilitated wall.

Strains in steel reinforcement

The maximum-recorded strains were from strain gauge SG15 installed on the outermost longitudinal rebars in the end columns and at the base of the wall. The strain records from strain gauges installed near the bottom SG15 and top SG22 of the outermost bars are shown in Figures 4.62 and 4.63. These readings indicated that all bars yielded and a plastic hinge formed at the bottom of the wall. Strain recorded from strain gauge SG22 located at the top of the main flexural bars indicated that they also yielded.

The maximum recorded strains in the horizontal bars were from strain gauge No. 29 located near the mid height of the wall. It was observed that the maximum strains in the

horizontal bars were at steel yielding level before the end of the test. The strain measurements from strain gauge 29 were plotted in Figure 4.64.

Strains in Confinement Ties

Readings from strain gauge SG24 installed on the confinement tie near the bottom of the wall indicated that the confined concrete was under high strains at failure. Figure 4.65 shows that the strains in the confinement ties at the bottom toes of the wall were larger than 3100 microstrain, which indicated that confined concrete was under high stresses at failure.

Strains in FRP

The maximum strain recorded on the confinement CFRP from strain gauge SG10 was 0.0035 mm/mm which indicated that the fibres were highly stressed as shown in Figure 4.66. The maximum strain recorded by SG13 at the mid-height of the bidirectional CFRP was close to 0.004 mm/mm as shown Figure 4.67. The measured strain was along the direction of the ±45° fibre orientation.

4.3.6 Rehabilitated wall RW8

Rehabilitated walls RW8 and RW9 were identical except for the use of ±45° shear reinforcement for RW8 and horizontal shear reinforcement for RW9. For both walls the end column elements were confined using three layers of uni-directional CFRP wrap. The wall was subjected to a moment to shear ratio of 2.25.

Similar to test wall RW7 the load control was used for the loading cycles of ±50 kN, ±100 kN, ±150 kN and ±200 kN before switching to actuator displacement control for the rest of the test. The maximum horizontal displacement at loading cycle of ±200 kN was 1.40 mm in both the pull and push directions. The wall response remained in the elastic range. Some diagonal cracks in the web of the wall as well as a horizontal crack at the bottom of the wall were observed. The displacement corresponding to the first yield of the flexural steel bars was 3.00 mm and the force reached 320 kN. At loading cycle of

ductility level 1.5 the force was 400 kN and the previously opened horizontal cracks widened and extended. It was observed that the edges of the confinement CFRP started to debond at the top 200 mm of wall. At ductility level 2 the horizontal force increased to 460 kN. There were numerous diagonal cracks on the web part of the wall, but they were not significant to cause strength deterioration of the wall. At loading cycle of ductility level 3 the lateral force increased to 500 kN. It was observed that the bottom edges of the U shaped confining CFRP sheets were debonded at the end of this loading cycle. The anchoring system prevented the debonding from extending horizontally towards the end columns. The debonded height was aproximately 25% of the wall height measuring from base. The debonded width was 75 mm measured from the ends of the U shaped confining CFRP.

The horizontal load at the cycle of ductility level 4 increased to 520 kN. There were no new cracks, but the previously opened ones widened. The maximum strength of the wall observed at ductility level 5 was 534 kN. During the loading cycle of ductility level 6 and with continuous widening of the web diagonal cracks, the strength of the specimen started to deteriorate slowly. The maximum lateral load decreased to 510 kN at the ductility level 6. At the ductility level 7 the maximum horizontal force was 470 kN. The bottom 300 mm of the CFRP sheet spalled off during the second cycle of ductility level 7 as shown in Figure 4.68. In addition, the bottom 300 mm of the wall was significantly cracked. It was observed that the web concrete part of the wall's bottom started to crush by the end of this ductility level. A horizontal separation of the confining CFRP was observed at 200 mm from the bottom of the wall. At ductility level 8 the middle bottom 300 mm of the web concrete crushed and the maximum load dropped to 430 kN. At ductility level 9 a plastic hinge developed at the bottom 300 mm of the wall as shown in Figure 4.69, which led to drop in the lateral load resistance from 430 to 200 kN.

Lateral Displacement

The lateral drift of the wall is plotted against the top lateral horizontal load as shown Figure 4.70. The yield displacement was 3.00 mm. The figure shows that there was no significant loss of strength up to ductility level 6 which corresponded to lateral drift of 1.65 %. The specimen's strength started to deteriorate during the loading cycles of ductility level 7. The wall lateral load resistance deteriorated to about 88%, 81%, and 38% of the maximum strength of the wall at ductility levels of 7, 8, and 9, respectively. The maximum lateral drift the wall reached at the end of the test was approximately 2.5 %.

Rotations

The rotation at the top of the wall is plotted against the lateral load as shown in Figure 4.71. The test results show that the top rotation at yield was approximately 0.004 rad, which indicated that the specimen achieved a rotational ductility of 4. The maximum rotation the wall reached before failure was approximately 0.016 rad.

Shear Deformation

The relationship between the lateral load and the shear deformation is shown in Figure 4.72. The total shear deformation of the rehabilitated wall at load level 200 kN was approximately 0.0005 rad, and the average shear stiffness was 400,000 kN/ rad for the rehabilitated wall RW8.

Strains in steel reinforcement

Strain records from strain gauges SG12 and SG15 installed at the bottom and top of outermost bars of the wall are shown in Figures 4.73 and 4.74. The strain readings indicated that the longitudinal steel bars reached high strains during the test. Those readings indicated that the rebars yielded along their entire height.

The maximum recorded strains in the ±45° shear reinforcement steel were from strain gauge SG29 located near the mid height of the wall. The maximum strains in the horizontal bars were close to yield at the end of the test. Figure 4.75 shows the strain reading from strain gauge 29.

Strains in Confinement Ties

ReadingS from strain gauge SG19 installed on the confinement tie near the bottom of the column element indicated that the confined concrete was under high strains. Figure 4.76 shows that the strain in a confinement tie 100 mm above the base block was more than 3200 microstrain, which indicated that the tie yielded.

Strains in CFRP

Readings from strain gauge SG2 installed on the CFRP and located at the bottom of the wall indicated that the CFRP sheet was subjected to high strains as shown in Figure 4.77. For example, the maximum strain recorded on the confinement CFRP was 0.003 mm/mm. this was expected given that the steel ties yielded and reached a similar level of strain.

4.3.7 Rehabilitated wall RW9

The wall was repaired in a similar manner to test wall RW8 except for the shear reinforcement which was horizontal. The three actuators were used to apply a moment to shear ratio of 2.25.

During loading cycles of ±50 kN, ±100 kN, ±150 kN the test was conducted under load control. The maximum horizontal displacement at loading cycle of ±150 kN was approximately 1.50 mm in both the pull and push directions. There were few diagonal cracks in the web of the wall as well as a horizontal crack at the bottom of the wall starting at the end columns. The measured displacement at the onset of the first yield of the flexural reinforcement was approximately 3.30 mm and the lateral resisting force was approximately 258 kN. During loading cycle of ductility level 1.5 the horizontal load increased to 320 kN. During this cycle the edges of the confining CFRP started to debond in the top 200 mm of wall. At ductility level 2 the lateral force reached 370 kN. The horizontal force increased to 413 kN at the loading cycle of ductility level 3. At the end of the second loading cycle at ductility level 3 the bottom ends of the confining CFRP sheets were debonded. The debonded height was approximately 20% of the wall height starting

from the wall bottom. The lateral load at ductility level 4 was 415 kN. There were no new cracks, but the already opened ones widened. A horizontal separation of the confining CFRP material was observed at 200 mm above the bottom block of the wall. Numerous diagonal cracks on the web part of the wall were traced and marked. The cracks were not significant enough to cause strength deterioration of the wall during the second loading cycle at ductility level 4. There was no more strength gain after ductility level 4.

The maximum strength of the wall at ductility level 5 was 400 kN. The maximum horizontal load at the ductility level 6 was 400 kN. At ductility level 7 and with continuous widening of the web diagonal cracks, the strength of the specimen started to deteriorate moderately. At the ductility level 7 the horizontal maximum load reached was 350 kN. The bottom 300 mm of the CFRP sheets spalled off during this cycle. The bottom 300 mm of the wall was significantly cracked by the end of the second loading cycle at ductility level 7. At ductility level 8 the middle bottom 300 mm of the web concrete was crushed and the maximum load dropped to 250 kN. At ductility level 9 a drop in the strength from 250 kN to 200 kN was recorded. At ductility levels of 10 and 11 the maximum forces were 170 kN and 140 kN, respectively. There were no rupture of the flexural reinforcement, however, the bottom 300 mm wall's concrete was crushed by the end of ductility level 11. The vertical reinforcement were found to remain in compression during both the pull or push of the horizontal actuator. Figure 4.78 shows the developed plastic hinge at the wall's lower third of the height.

Lateral Displacement

The relationship between the top horizontal force and lateral drift of the wall is shown in Figure 4.79. The yield displacement was 3.30 mm. The figure shows that there was no significant loss of strength up to ductility level 5 which corresponded to lateral drift of 1.50 %. The test wall's strength started to deteriorate during the loading cycle at ductility level 6 and the subsequent loading cycles. During the loading cycle at ductility level 6, the strength deteriorated to about 80% of the wall maximum lateral load capacity.

The maximum lateral drift that the wall reached at the end of the test was approximately 3.3 %.

Rotations

The relationship between the rotation at the top of the wall and the lateral load is shown in Figure 4.80. The test results show that the top rotation at yield was approximately 0.0035 rad, which indicated that the specimen achieved a rotational ductility of 5.7. The maximum rotation that the wall reached before failure was approximately 0.02 rad.

Shear Deformation

The shear deformation is shown in Figure 4.81. The average shear stiffness was 400,000 kN/ rad for the rehabilitated wall. The maximum lateral load was 415 kN.

Strains in steel reinforcement

The maximum recorded strains were from strain gauge SG17 located near the bottom of the wall and installed on the outermost bars as shown in Figure 4.82. The strain readings indicated that the longitudinal flexural steel reinforcement rebars yielded and sustained high strains during the test. In addition, after the concrete cracked the steel bars buckled and were under compression either in pull or push half cycles towards the end of the test.

The maximum recorded strains in the horizontal shear reinforcement were from strain gauge No. 26 which was located near the mid-height of the wall. It was observed that the maximum strains in the horizontal bars were close to yield at the end of the test as shown in Figure 4.83.

Strains in Confinement Ties

Readings from strain gauge SG22 installed on the confinement ties at the bottom of the wall's end confined columns indicated that the ties yielded. Figure 4.84 showed that the strains in the confinement ties at the bottom toes of the wall was close to 3500 microstrain, which indicated that confined concrete reached the crushing stress.

Strains in FRP

The maximum strain recorded on the confinement CFRP was 0.011 mm/mm. Figure 4.85 showed the strains records from strain gauge SG2 located near the bottom edge on the confinement CFRP. It indicated that the CFRP was effective in confining the end columns of the wall.

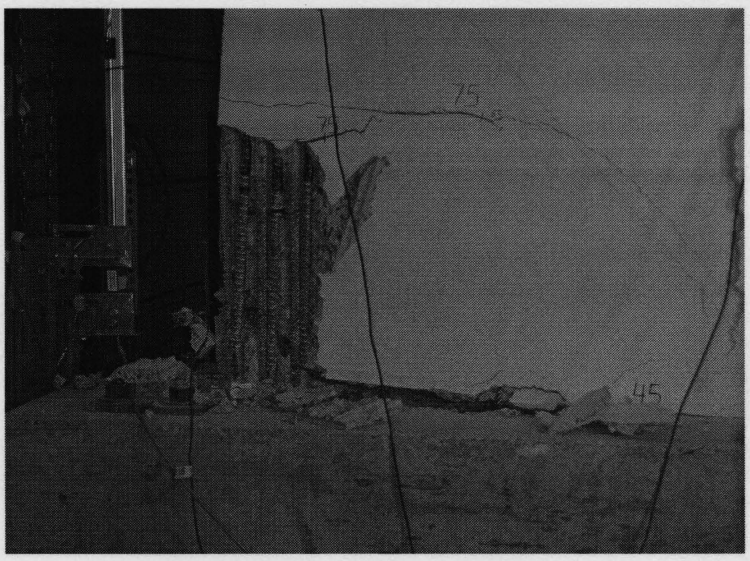

Figure 4- 1 CW2 Premature bond slip failure at wall bottom.

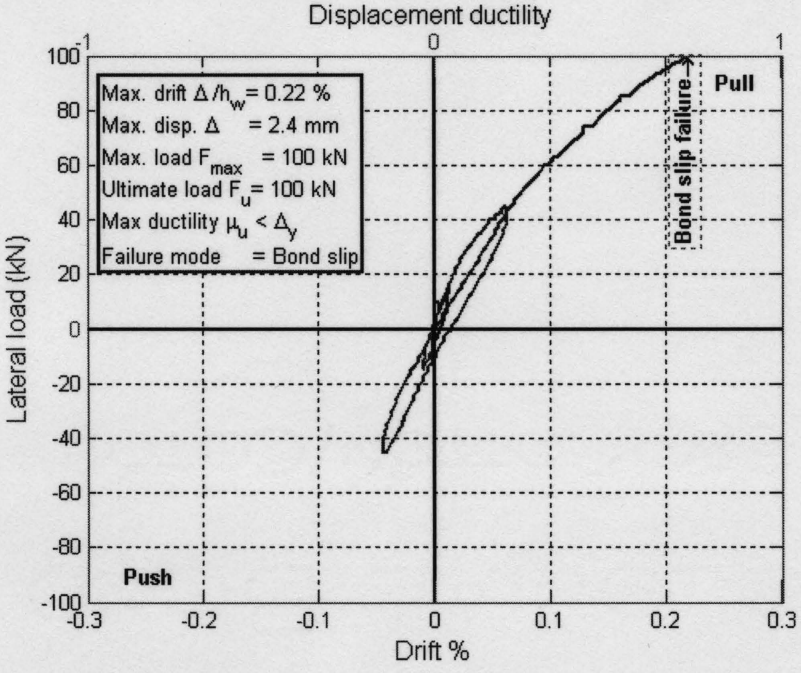

Figure 4- 2 CW2 Drift ratio-Lateral load relationship.

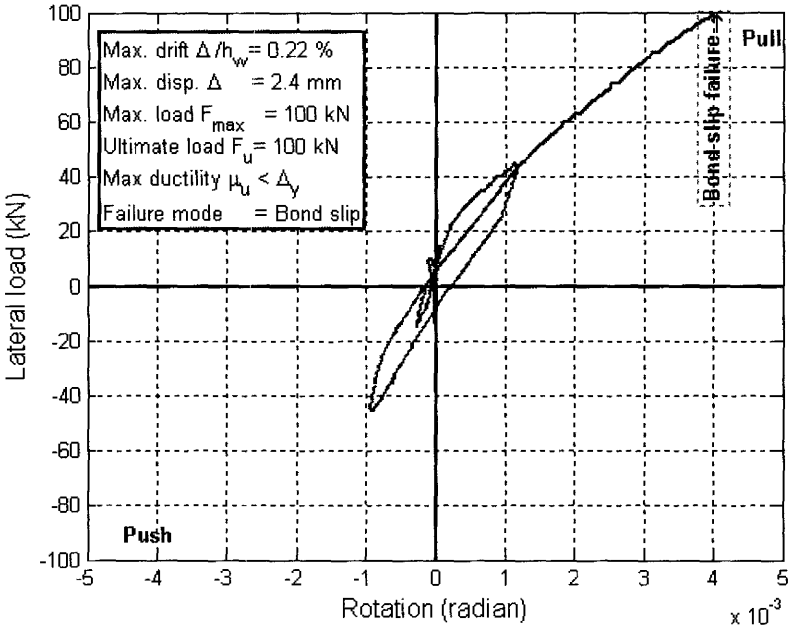

Figure 4- 3 CW2 Top rotation-Lateral load relationship.

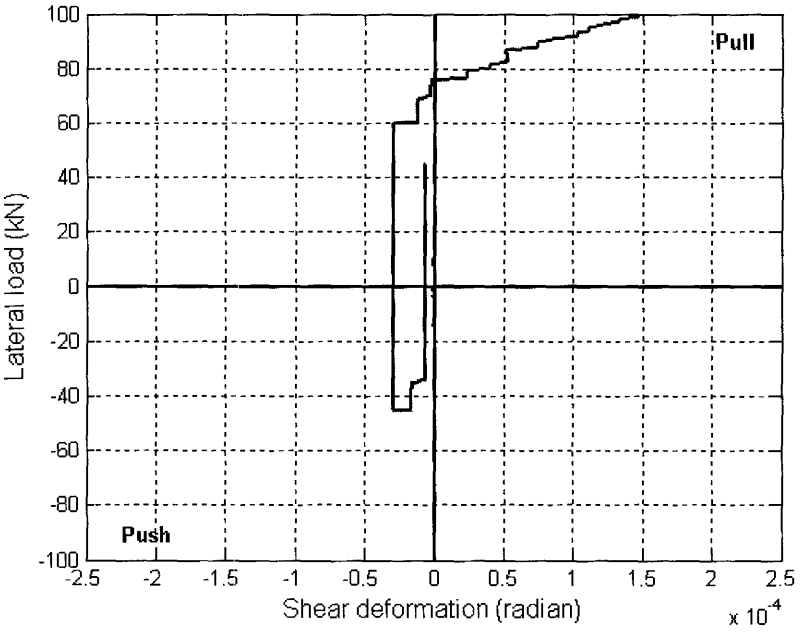

Figure 4- 4 CW2 Shear deformation- Lateral load relationship.

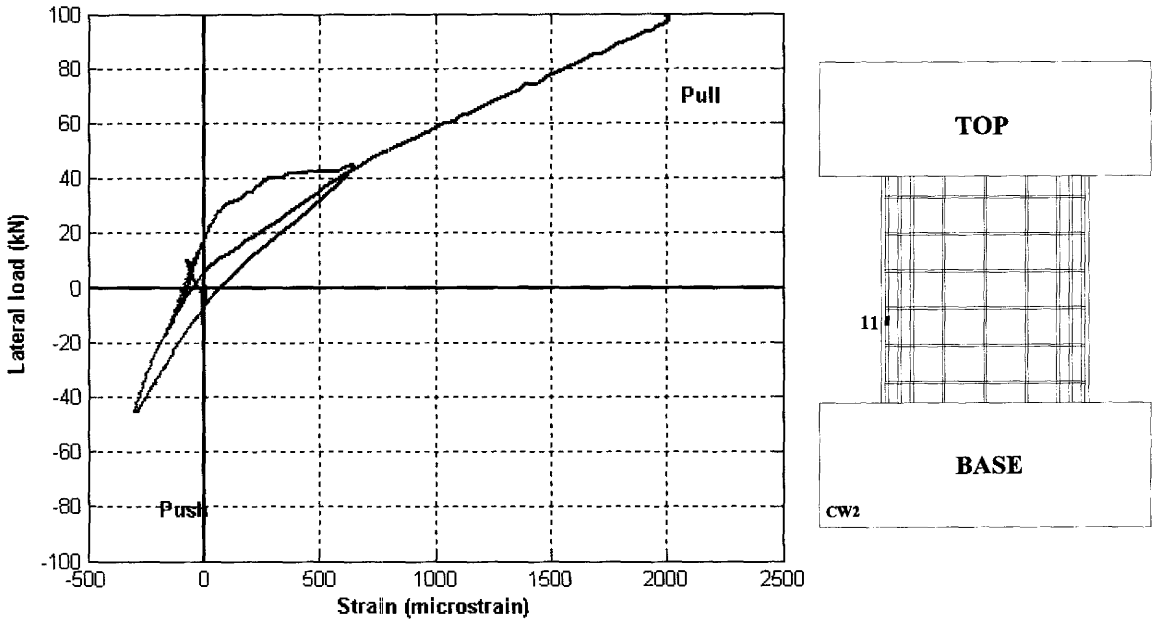

Figure 4- 5 CW2 Strain in gauge No. 11 Strain-Lateral load relationship.

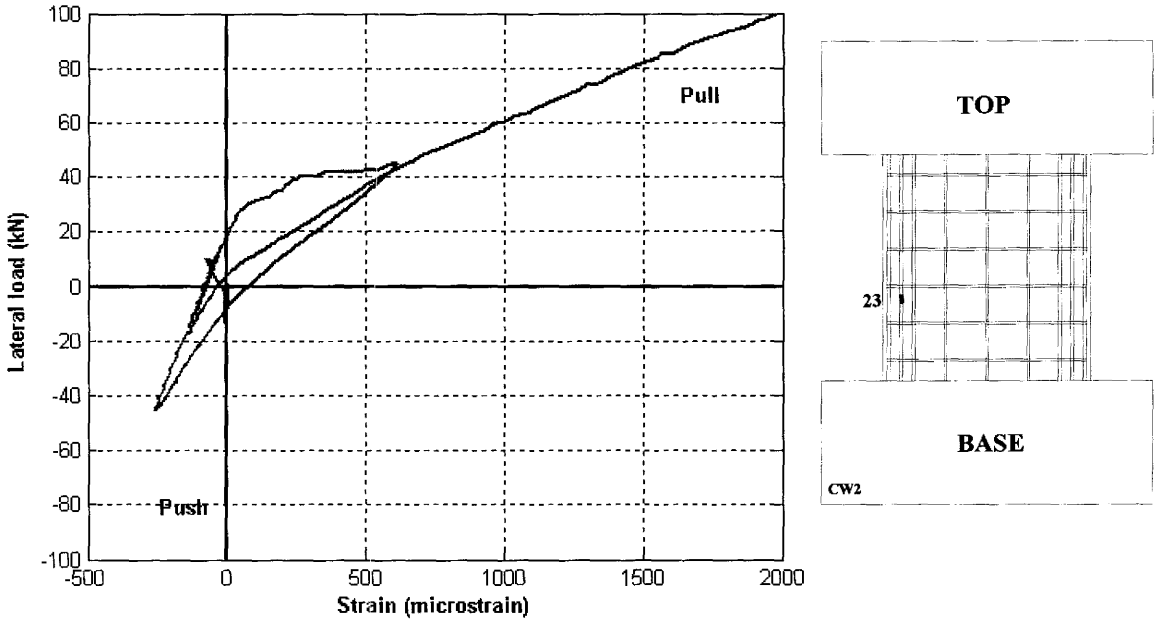

Figure 4- 6 CW2 Strain in gauge No. 23 -Lateral load relationship.

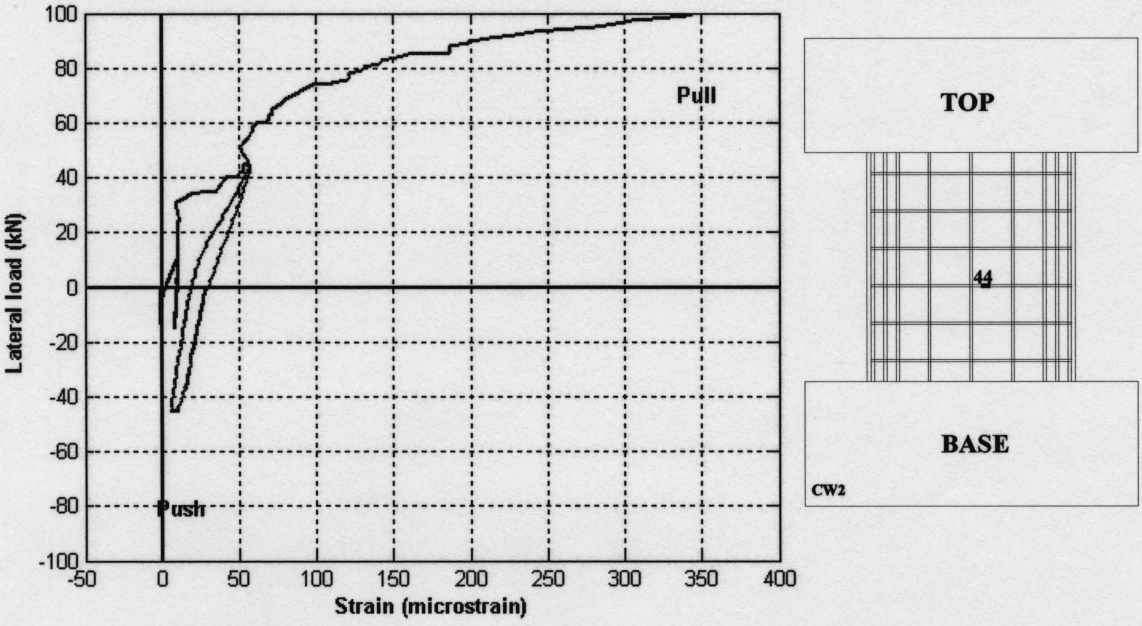

Figure 4- 7 CW2 Strain in gauge No. 44 -Lateral load relationship.

Figure 4- 8 CW3 cracks patterns and bond slip failure at wall bottom

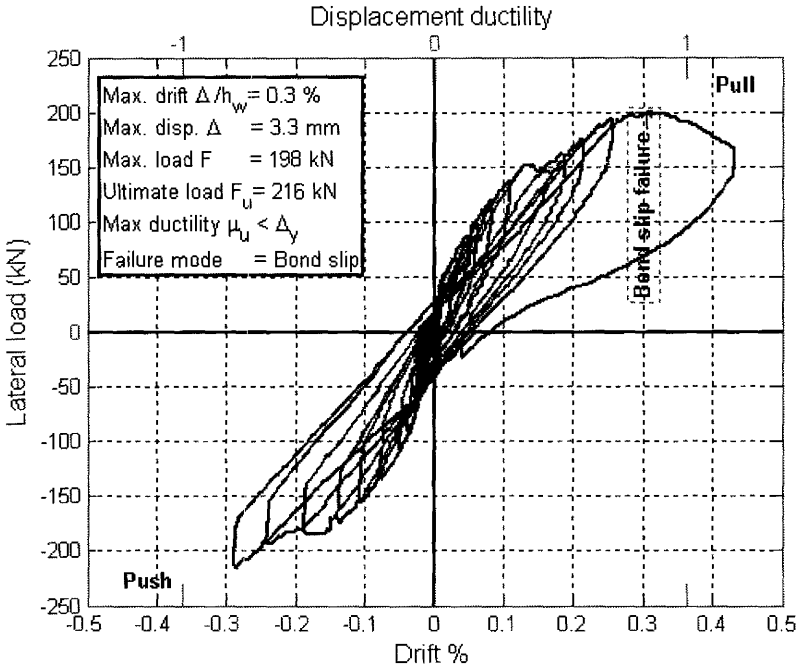

Figure 4- 9 CW3 Drift ratio-Lateral load relationship.

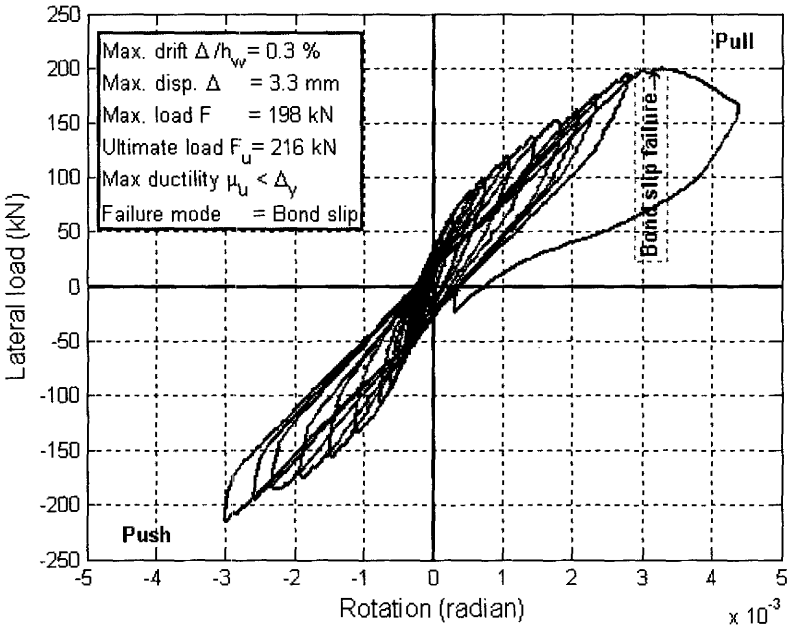

Figure 4- 10 CW3 Top rotation-Lateral load relationship.

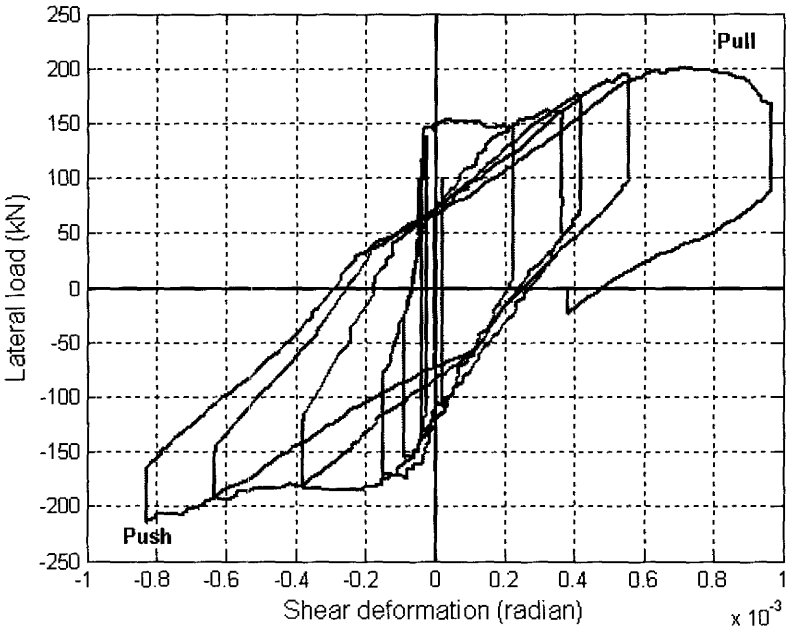

Figure 4- 11 CW3 Shear deformation -Lateral load relationship.

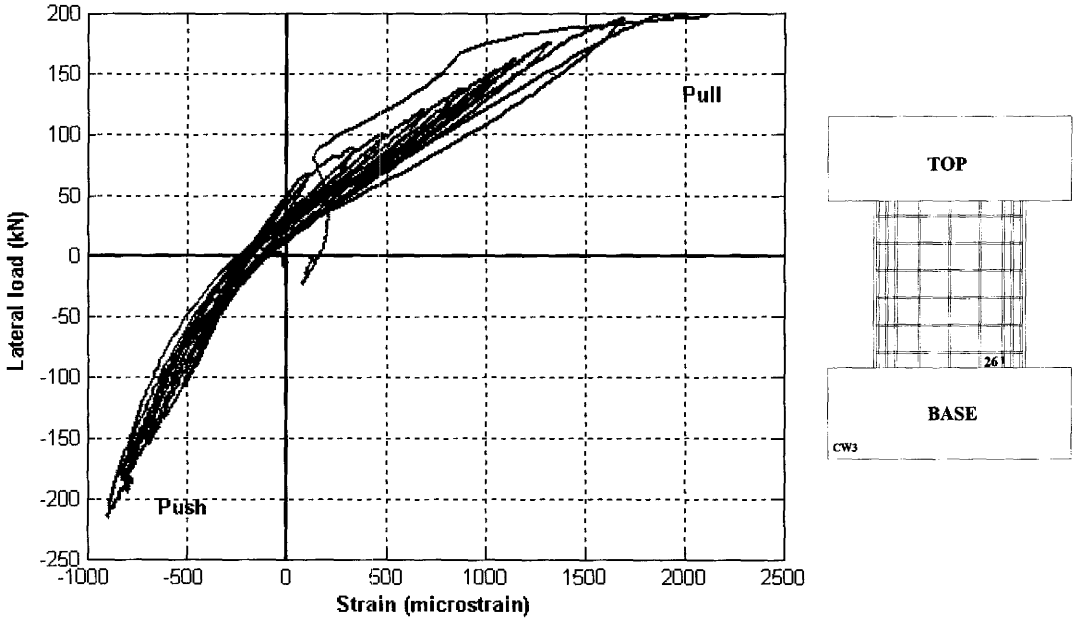

Figure 4- 12 CW3 Strain in gauge No. 26 -Lateral load relationship.

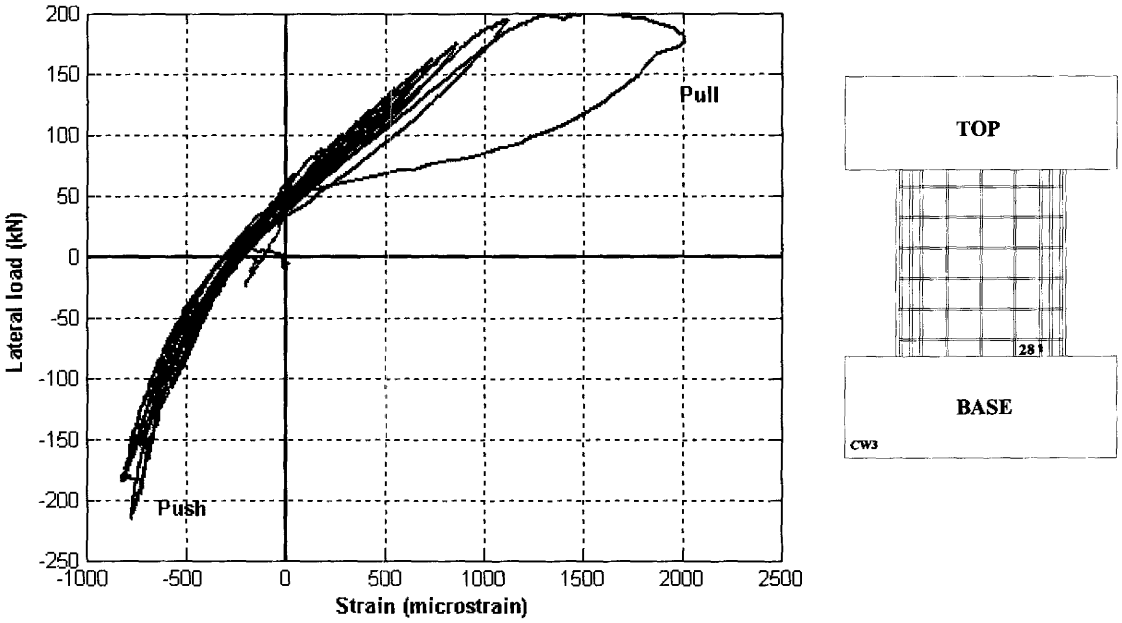

Figure 4- 13 CW3 Strain in gauge No. 28 -Lateral load relationship.

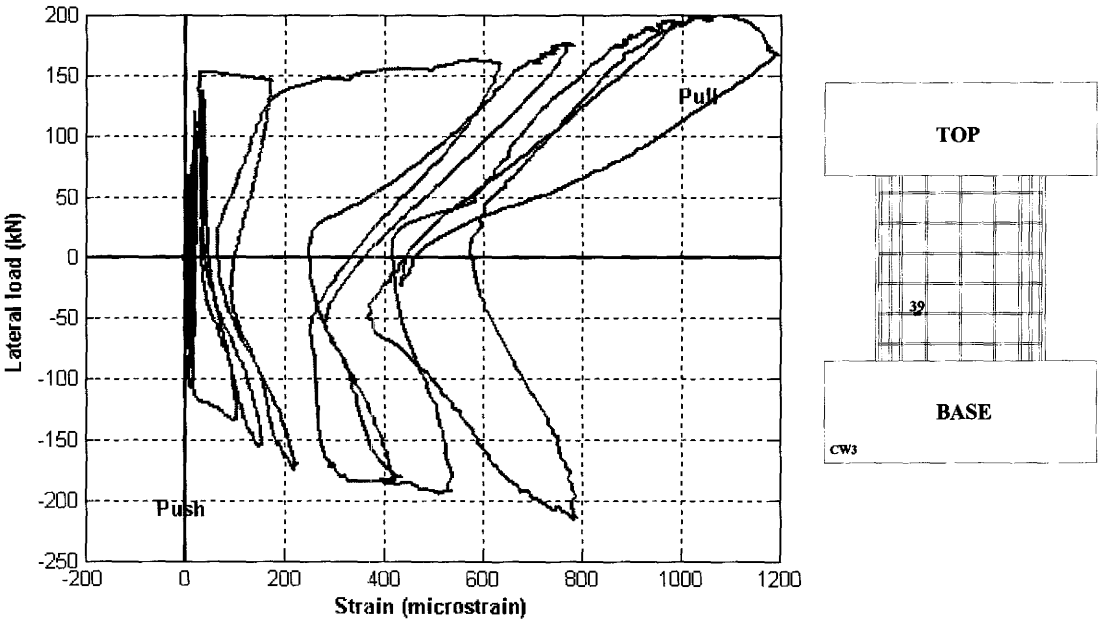

Figure 4- 14 CW3 Strain in gauge No. 39 -Lateral load relationship.

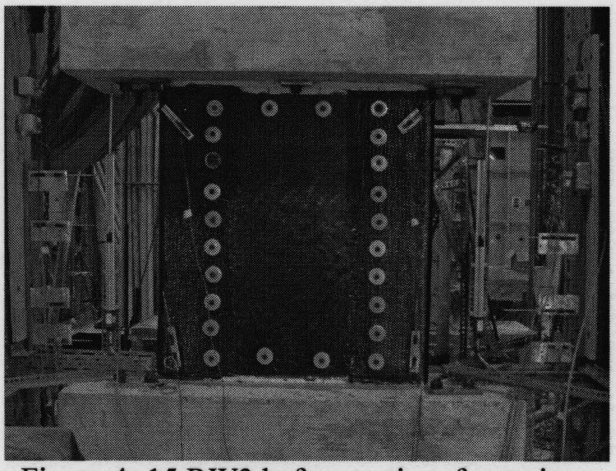

Figure 4- 15 RW3 before testing, front view.

Figure 4- 16 RW3 at failure.

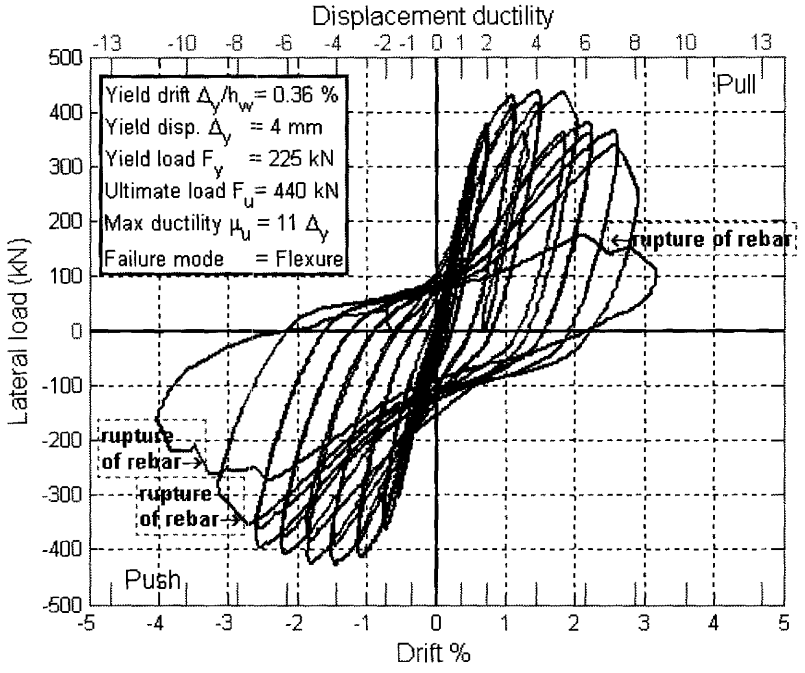

Figure 4- 17 RW3 Drift ratio-Lateral load relationship.

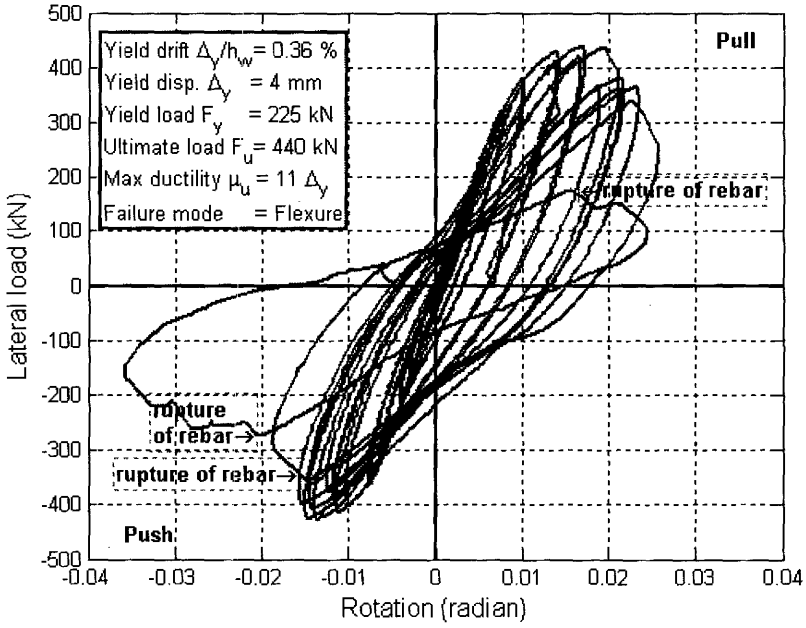

Figure 4- 18 RW3 top rotation-Lateral load relationship.

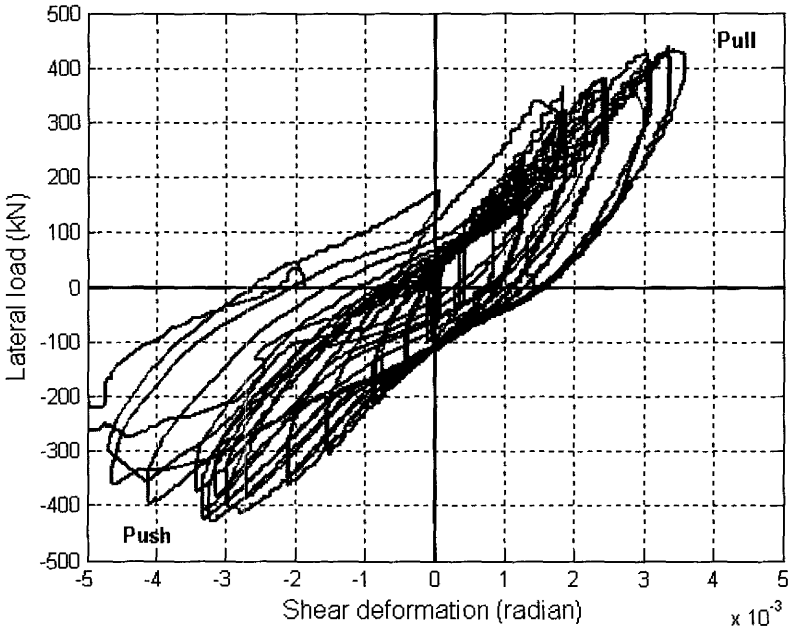

Figure 4- 19 RW3 Shear deformation -Lateral load relationship.

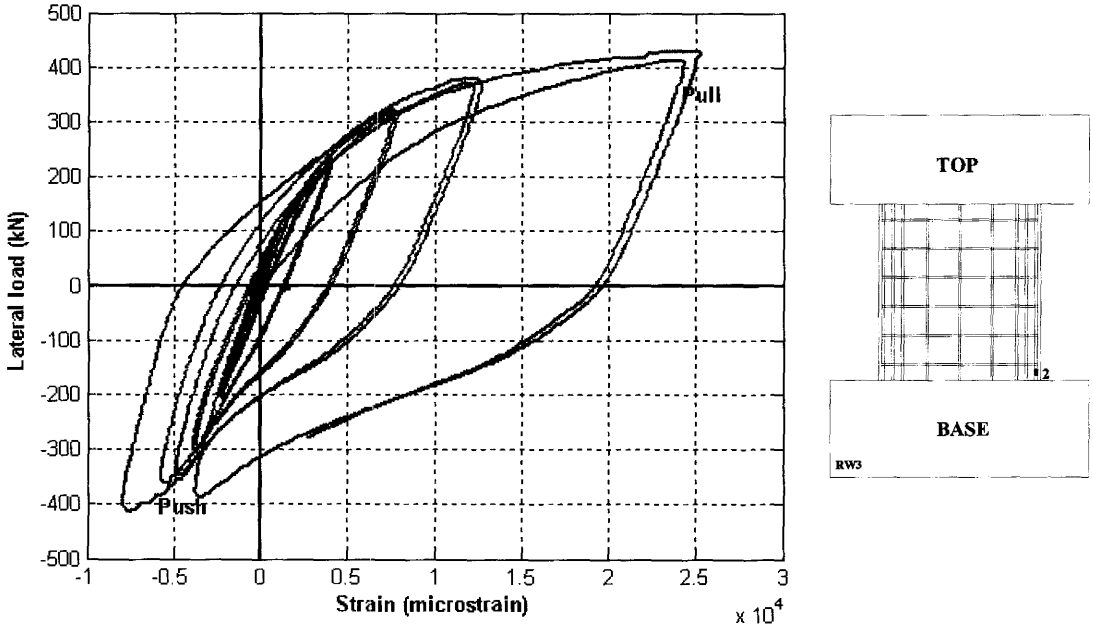

Figure 4- 20 RW3 Strain in gauge SG 2 -Lateral load relationship.

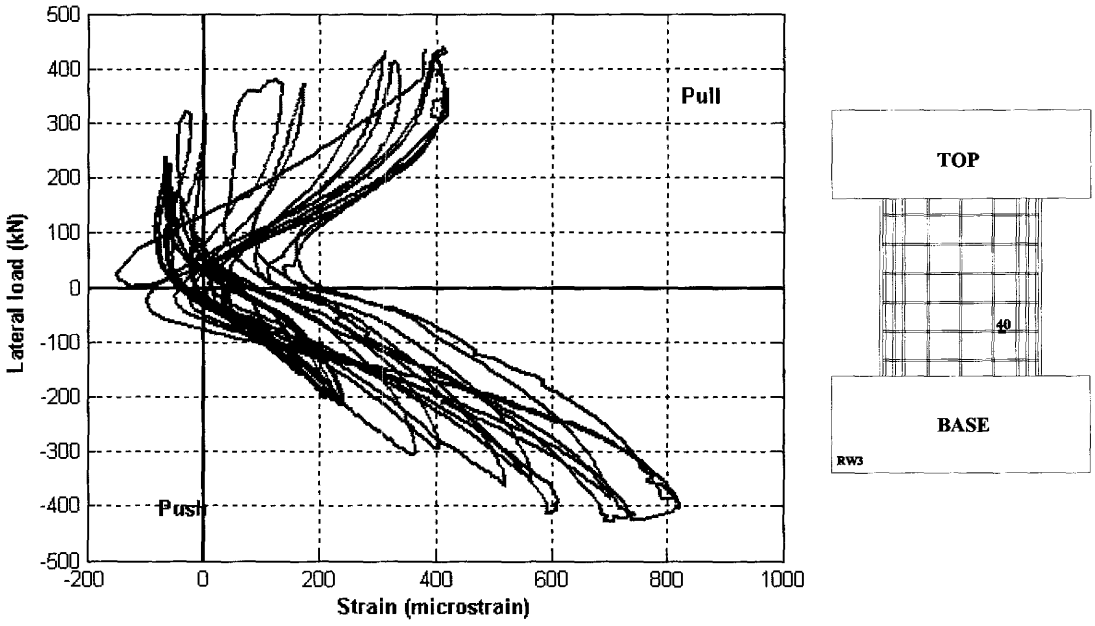

Figure 4- 21 RW3 Strain in gauge SG 40 -Lateral load relationship.

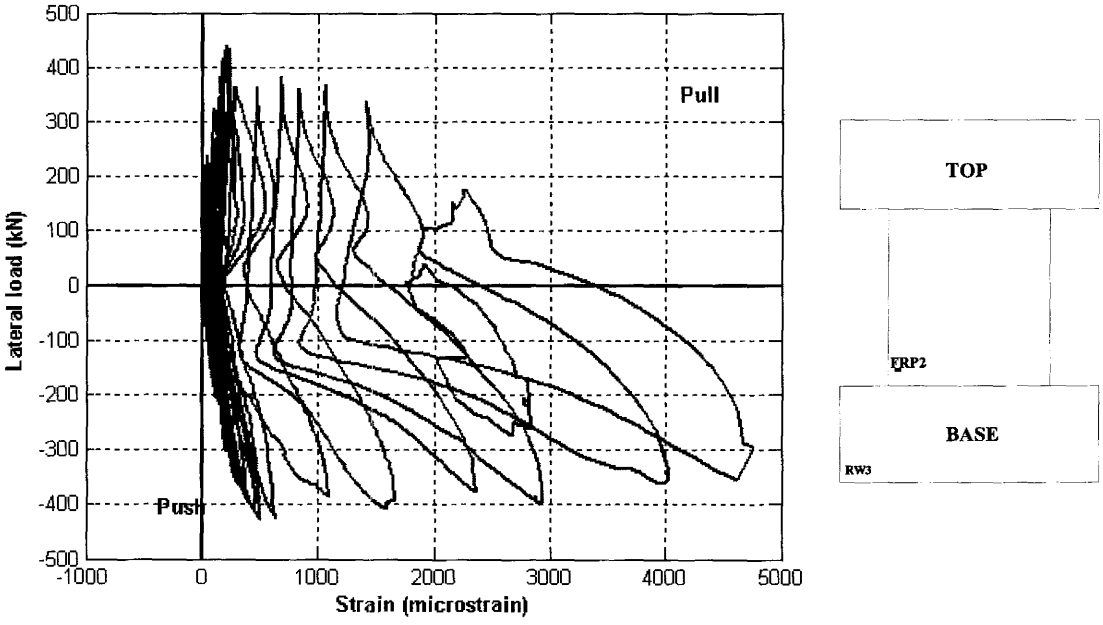

Figure 4- 22 RW3 Strain in CFRP gauge SG 2 -Lateral load relationship.

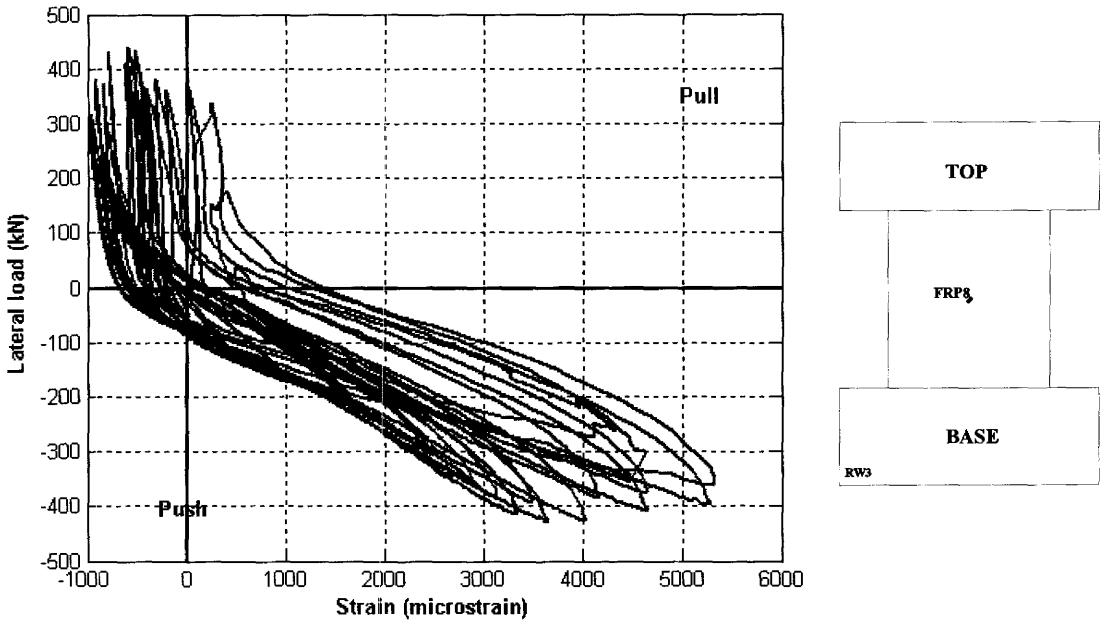

Figure 4- 23 RW3 Strain in CFRP gauge SG 8 -Lateral load relationship.

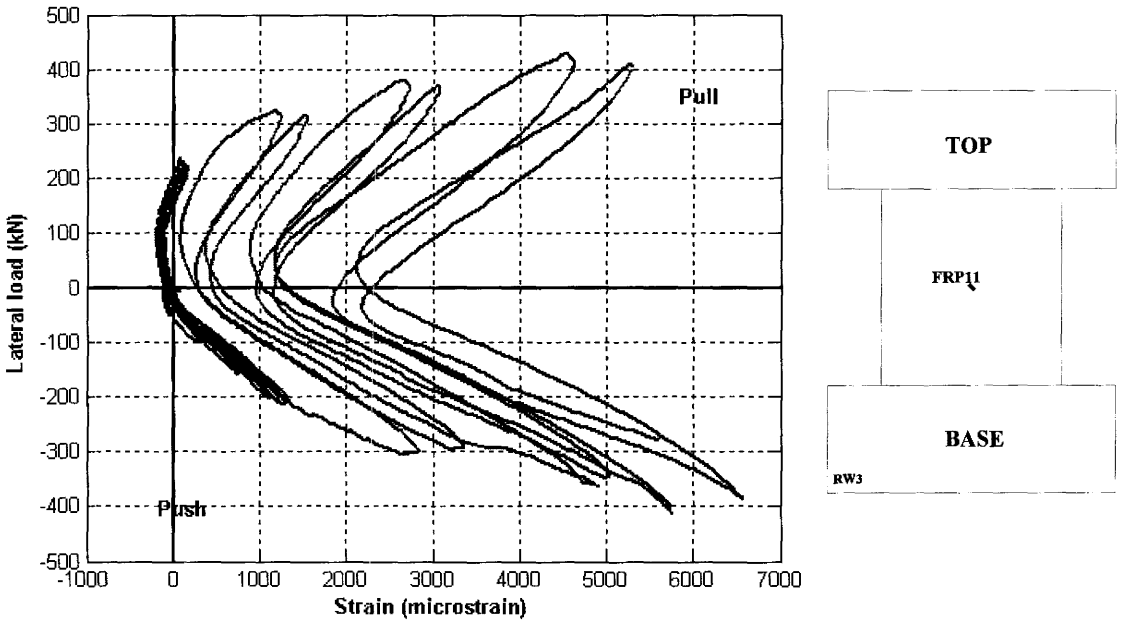

Figure 4- 24 RW3 Strain in CFRP gauge SG 11 -Lateral load relationship.

Figure 4- 25 RW4 crack pattern at ductility level 4.

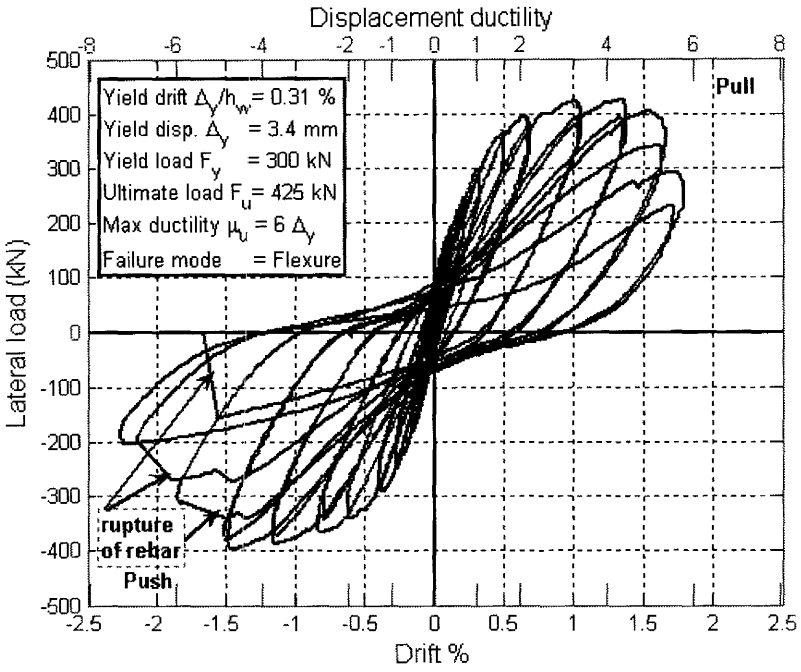

Figure 4- 26 RW4 Drift ratio-Lateral load relationship.

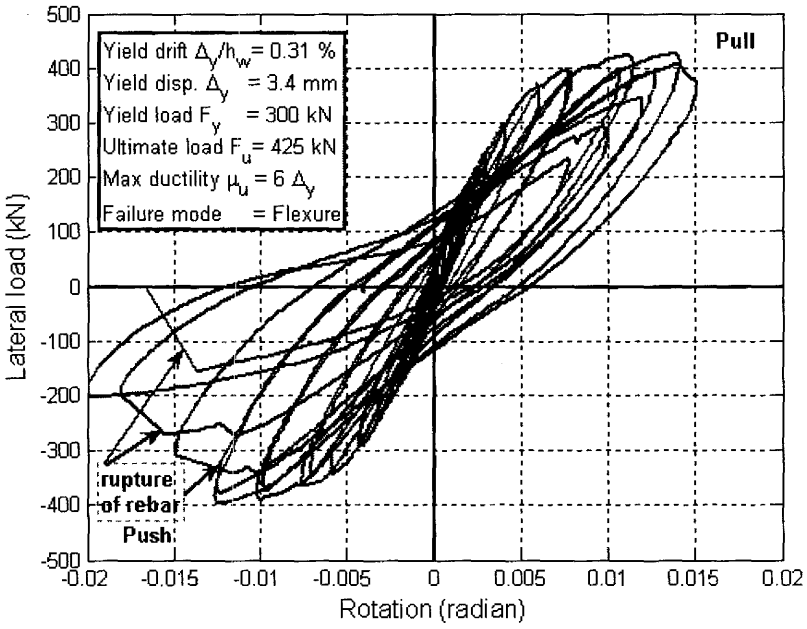

Figure 4- 27 RW4 top rotation-Lateral load relationship.

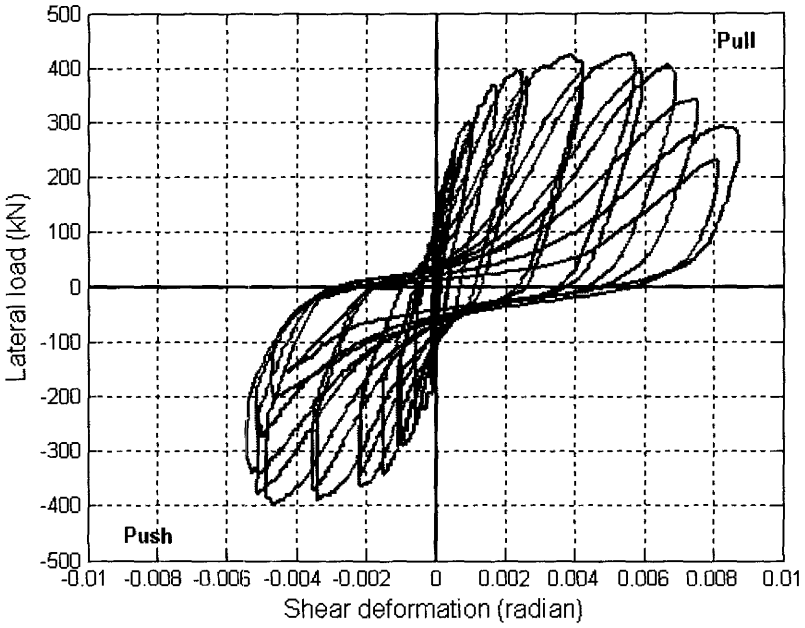

Figure 4- 28 RW4 Shear deformation -Lateral load relationship.

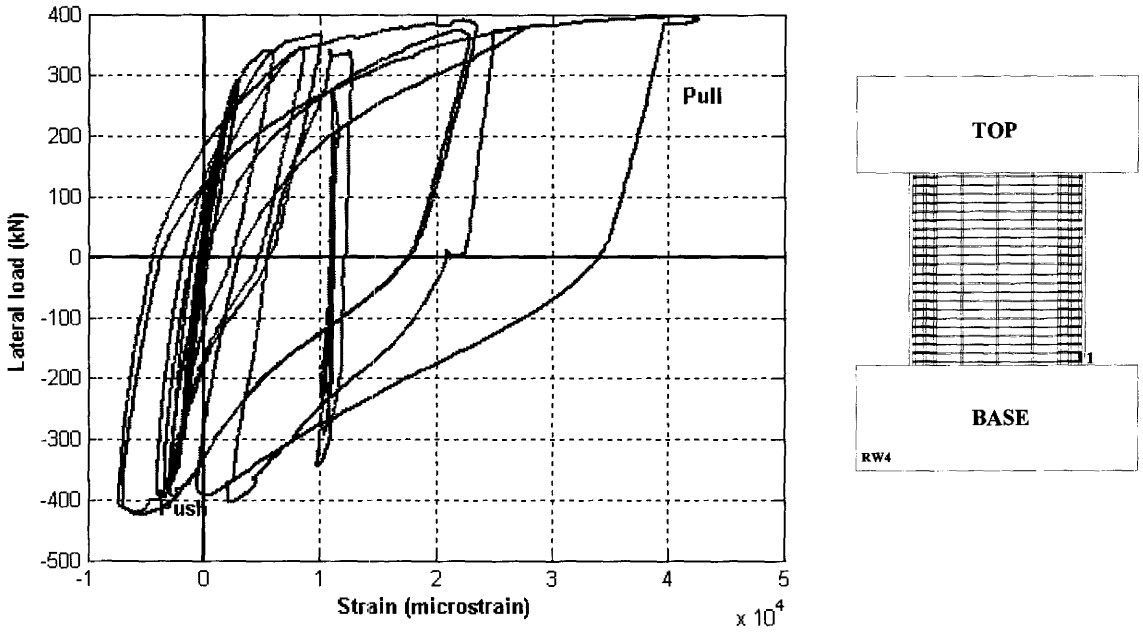

Figure 4- 29 RW4 Strain in gauge SG 1 -Lateral load relationship.

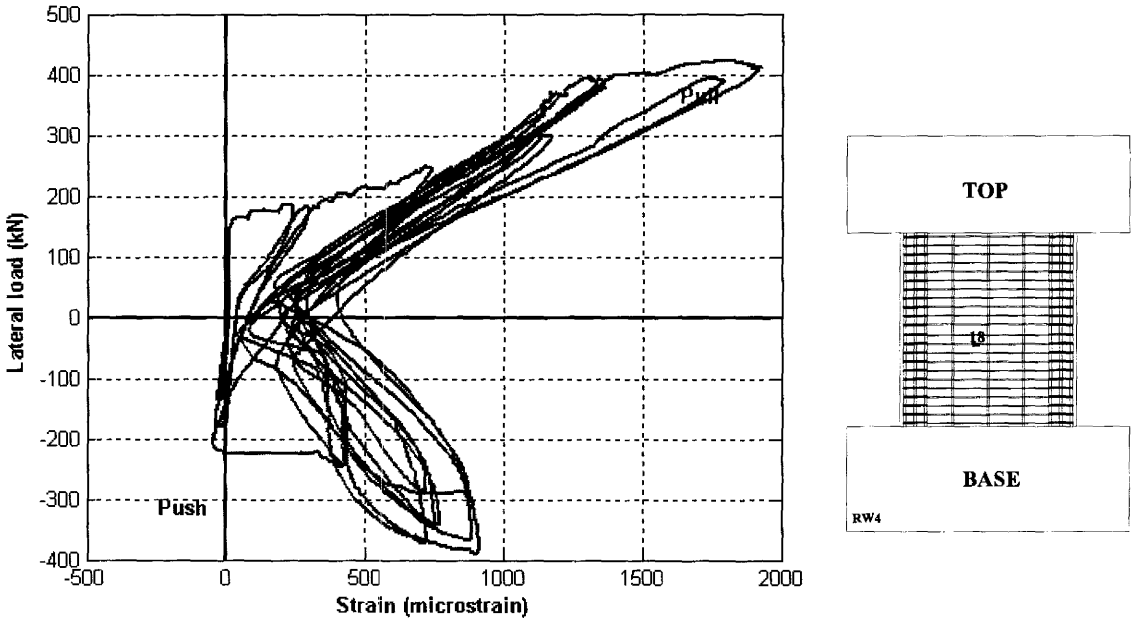

Figure 4- 30 RW4 Strain in gauge SG 18 -Lateral load relationship.

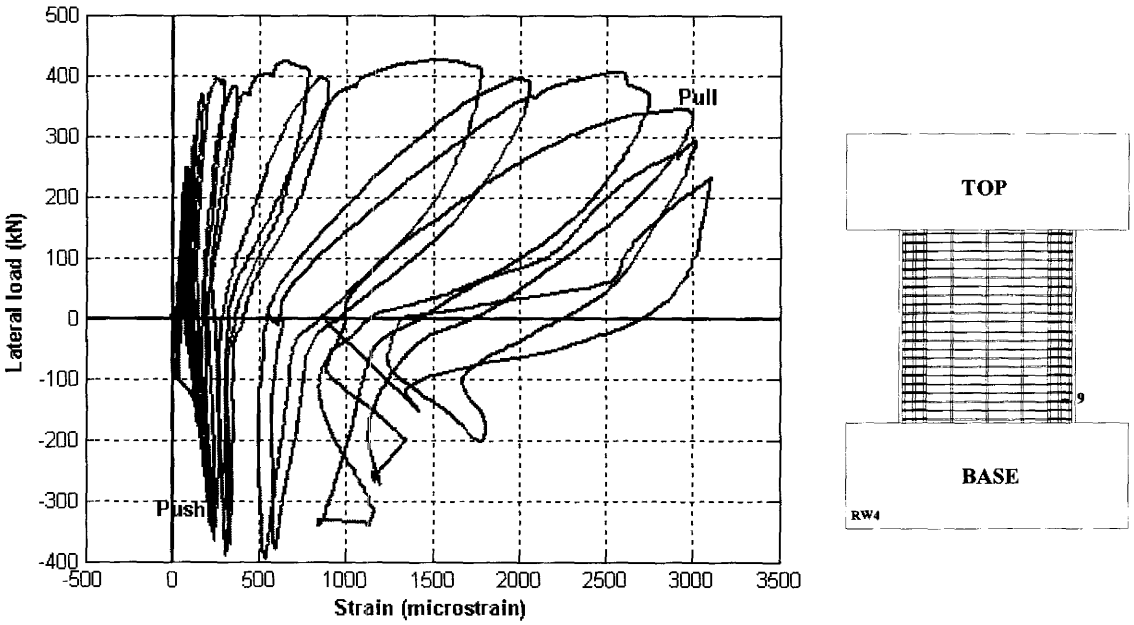

Figure 4- 31 RW4 Strain in confinement ties gauge SG 9 -Lateral load relationship.

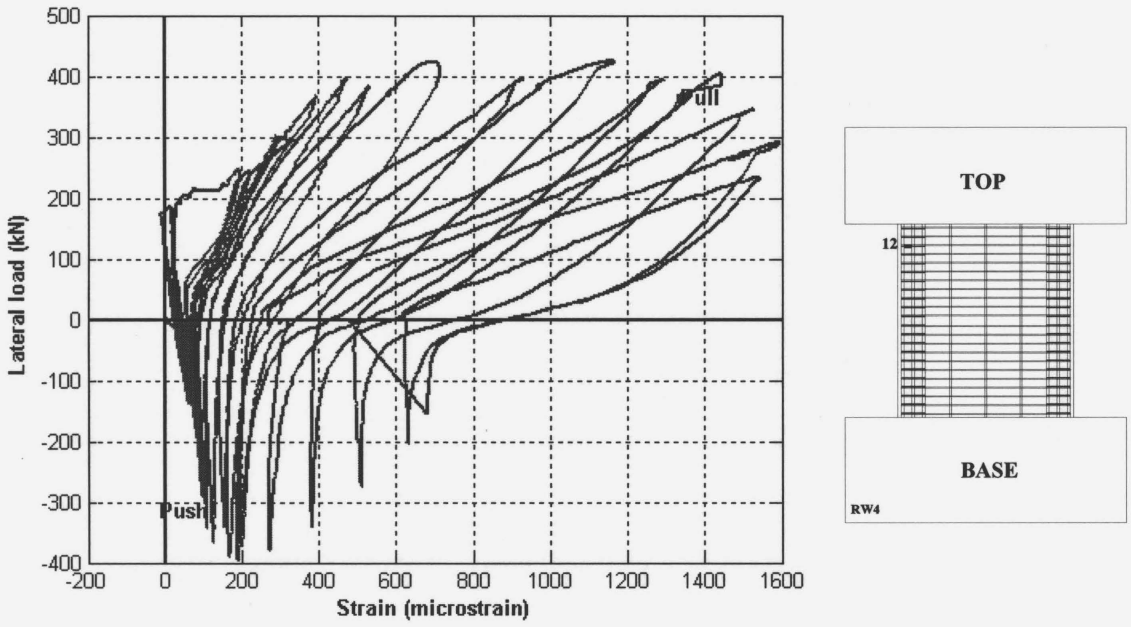

Figure 4- 32 RW4 Strain in confinement ties gauge SG 12 -Lateral load relationship.

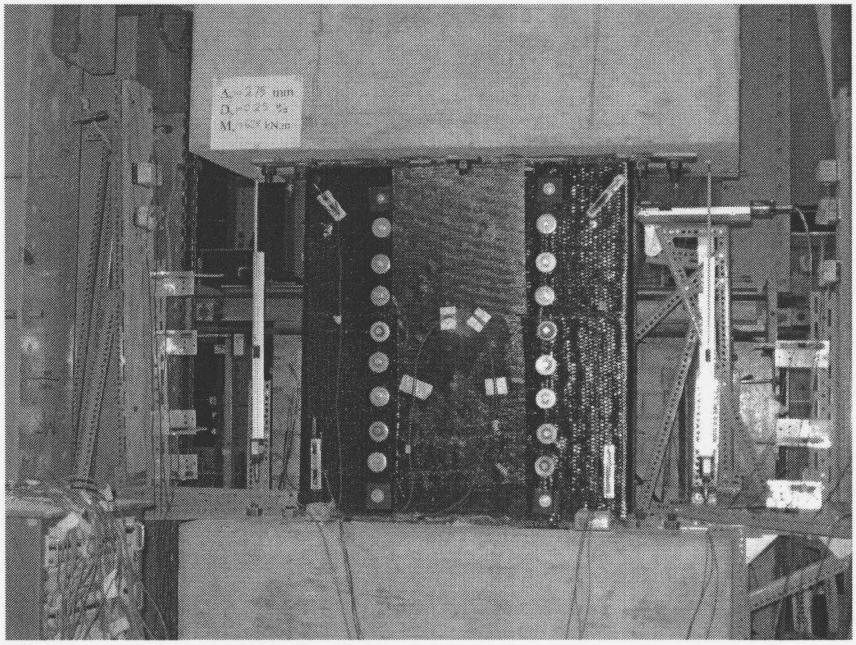

Figure 4- 33 RW5 at the first yield of flexural rebar, front view.

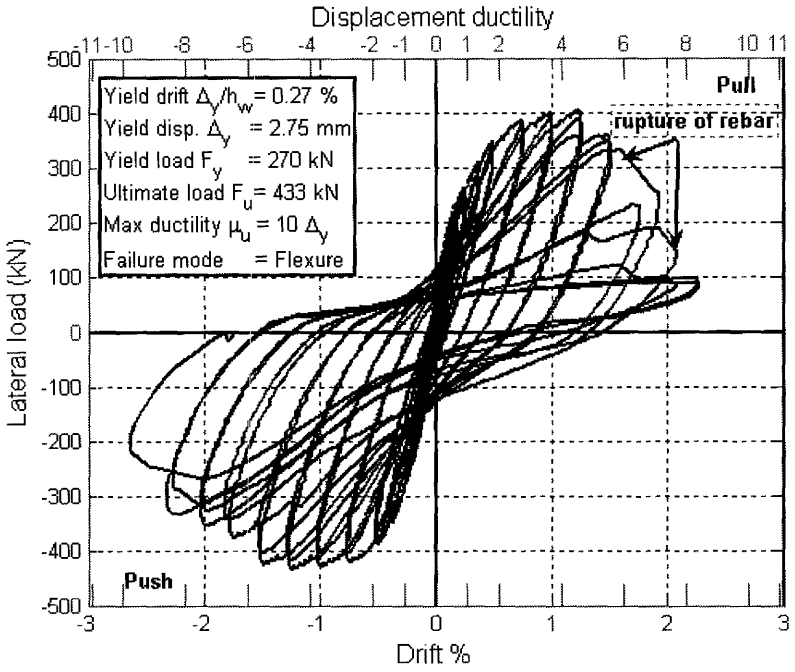

Figure 4- 34 RW5 Drift ratio-Lateral load relationship.

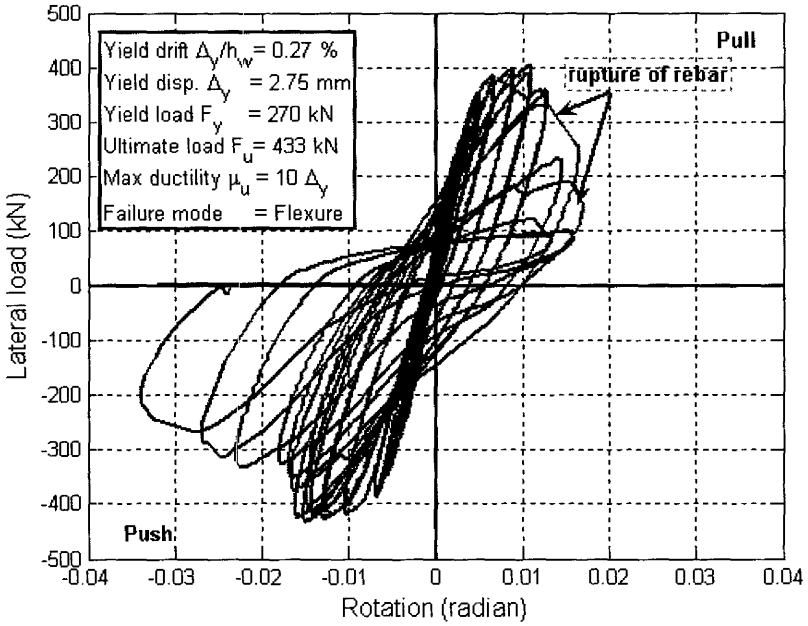

Figure 4- 35 RW5 top rotation-Lateral load relationship.

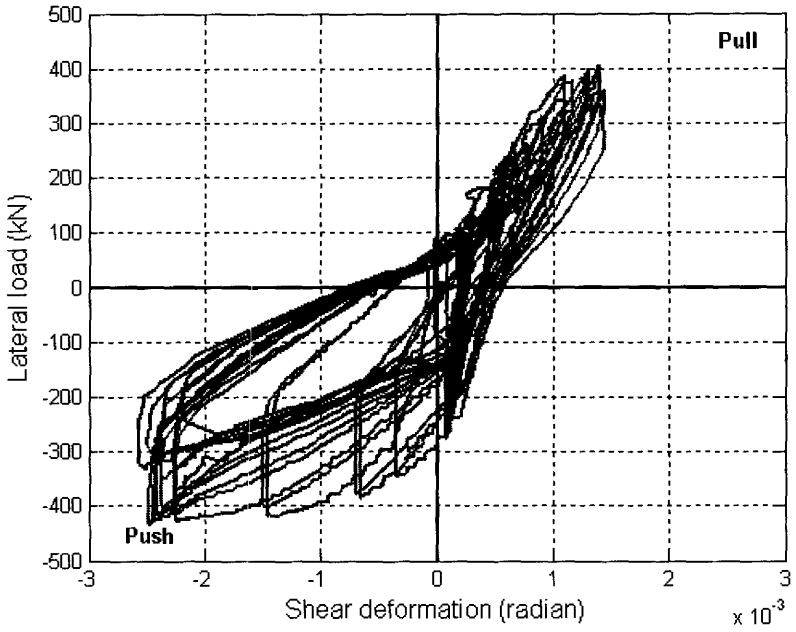

Figure 4- 36 RW5 Shear deformation -Lateral load relationship.

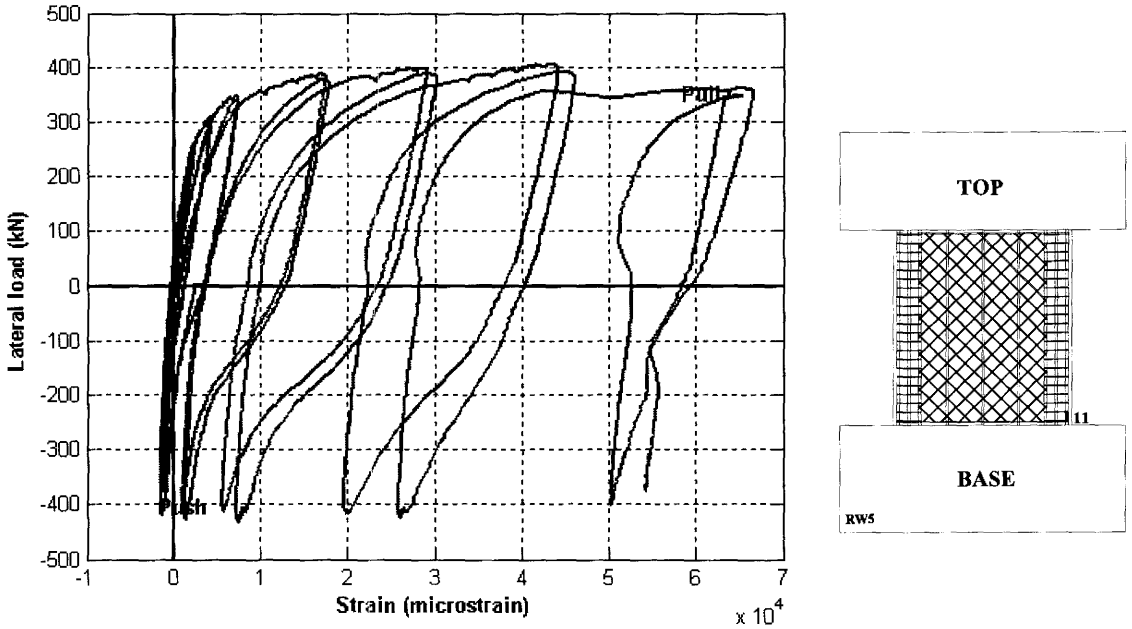

Figure 4- 37 RW5 Strain in gauge SG 11 -Lateral load relationship.

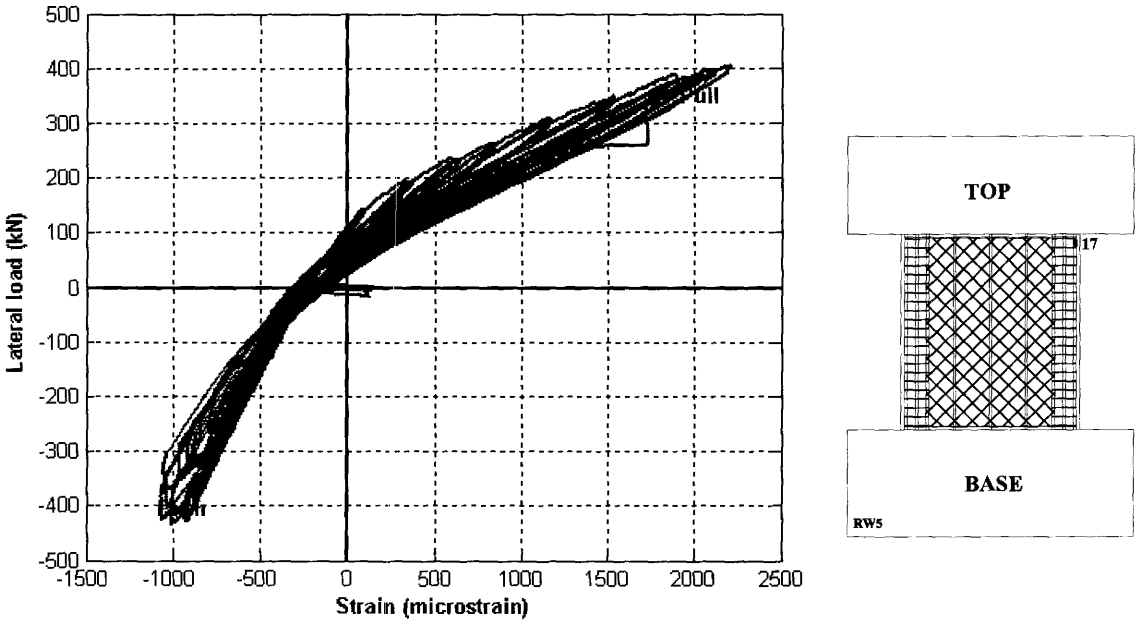

Figure 4- 38 RW5 Strain in gauge SG 17 -Lateral load relationship.

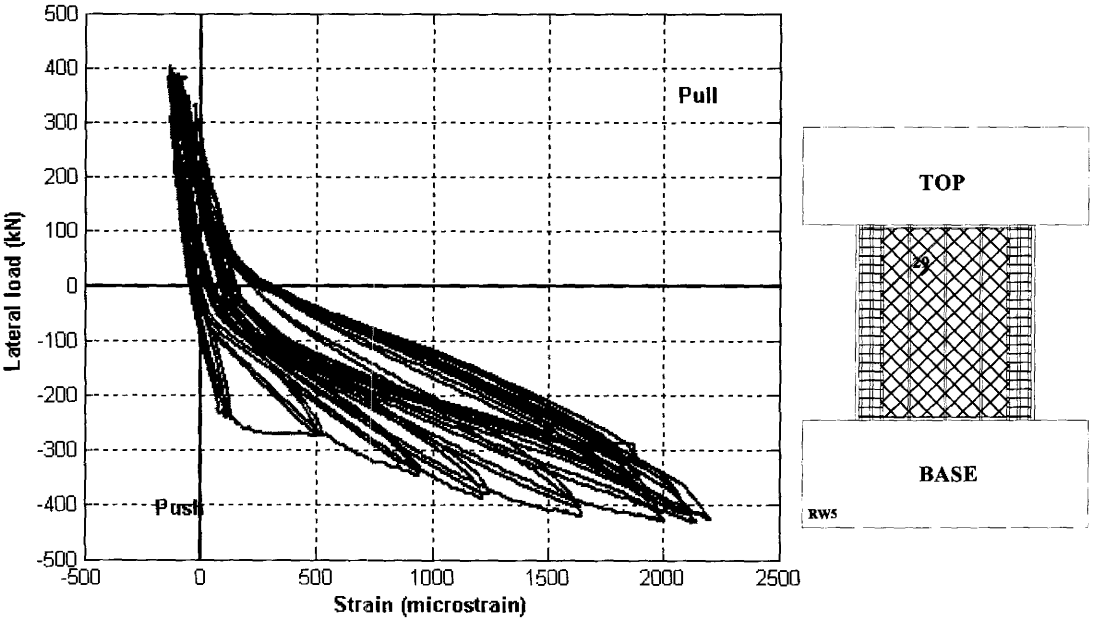

Figure 4- 39 RW5 Strain in gauge SG 29 -Lateral load relationship.

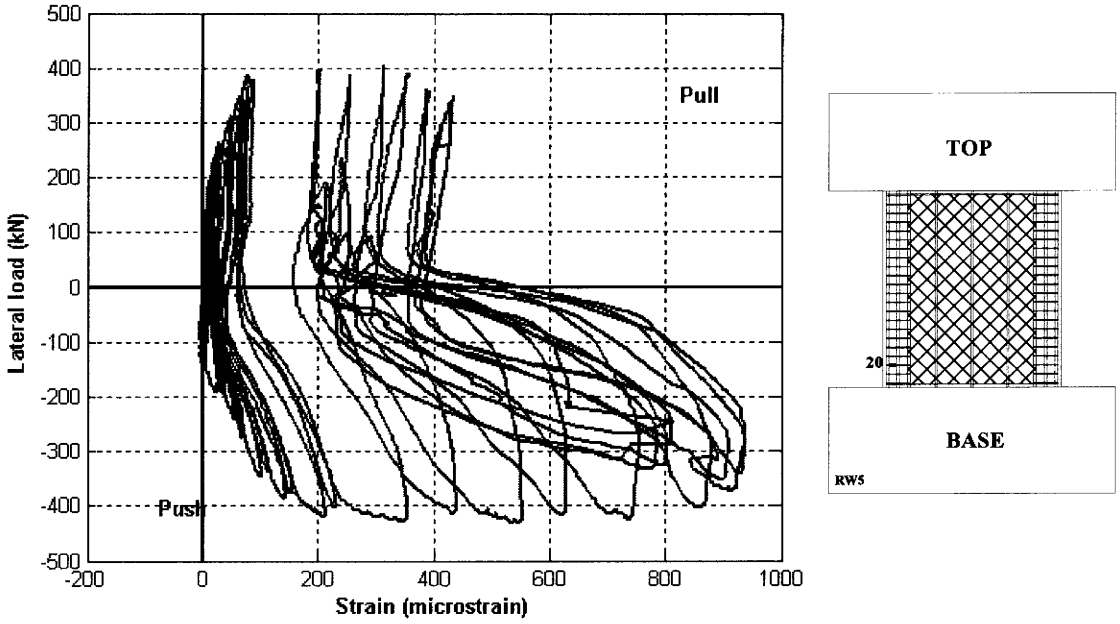

Figure 4- 40 RW5 Strain in confinement ties gauge SG 20 -Lateral load relationship.

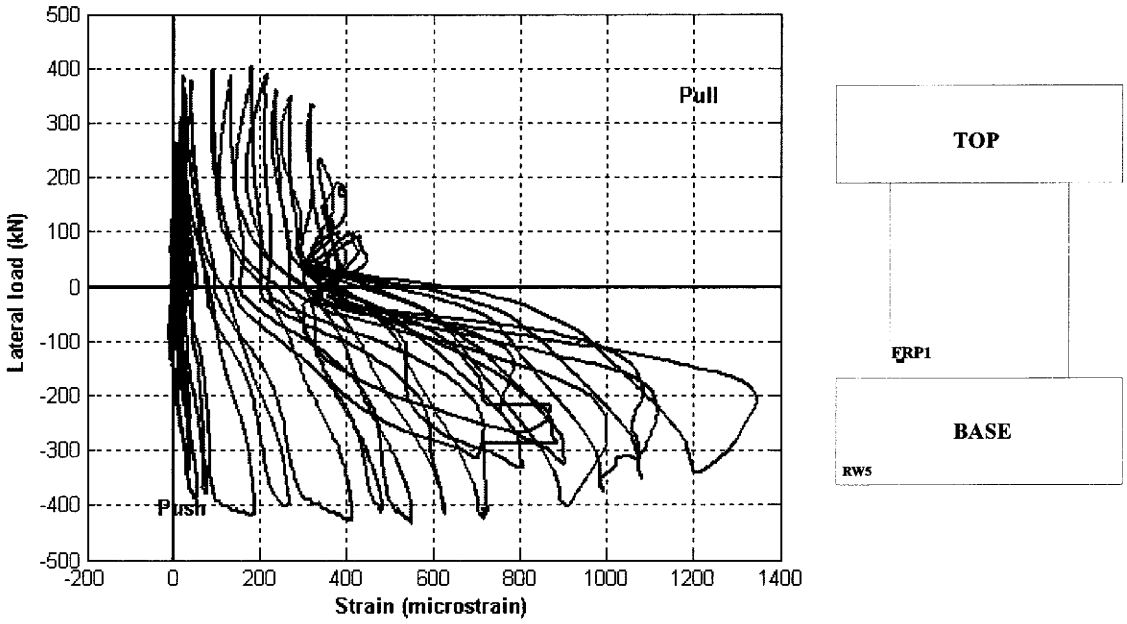

Figure 4- 41 RW5 Strain in CFRP gauge SG 1 -Lateral load relationship.

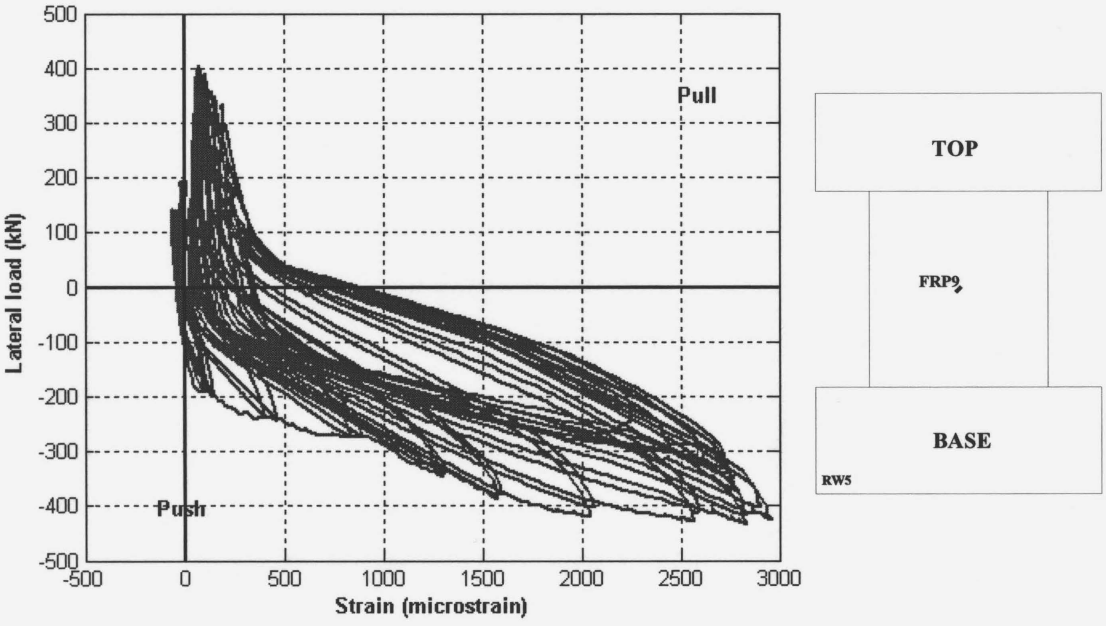

Figure 4- 42 RW5 Shear CFRP: Strain in gauge SG 9 -Lateral load relationship.

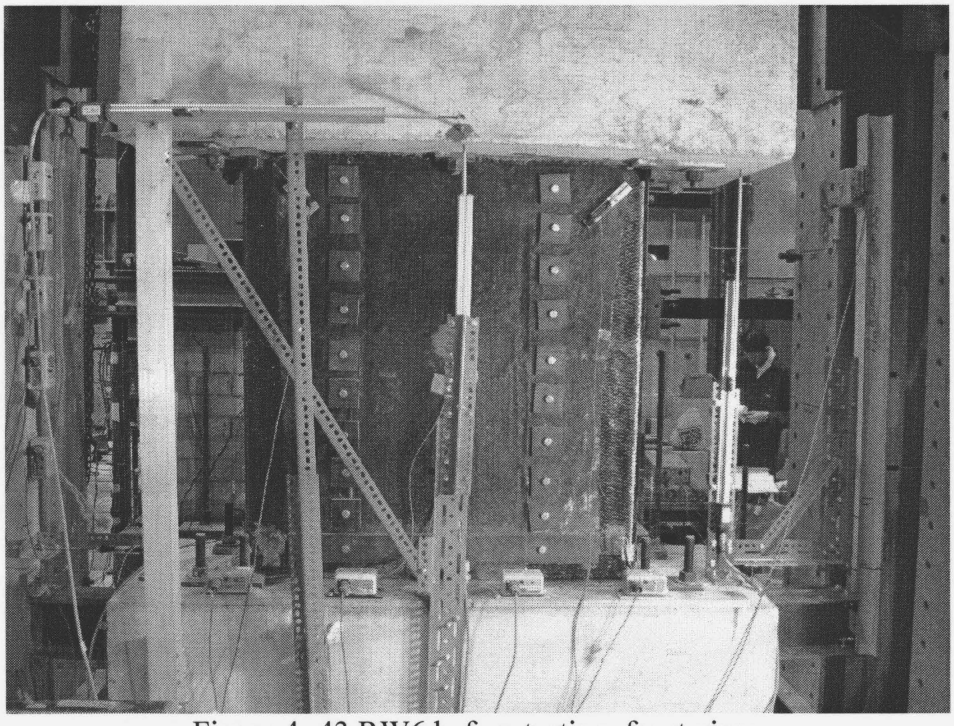

Figure 4- 43 RW6 before testing, front view.

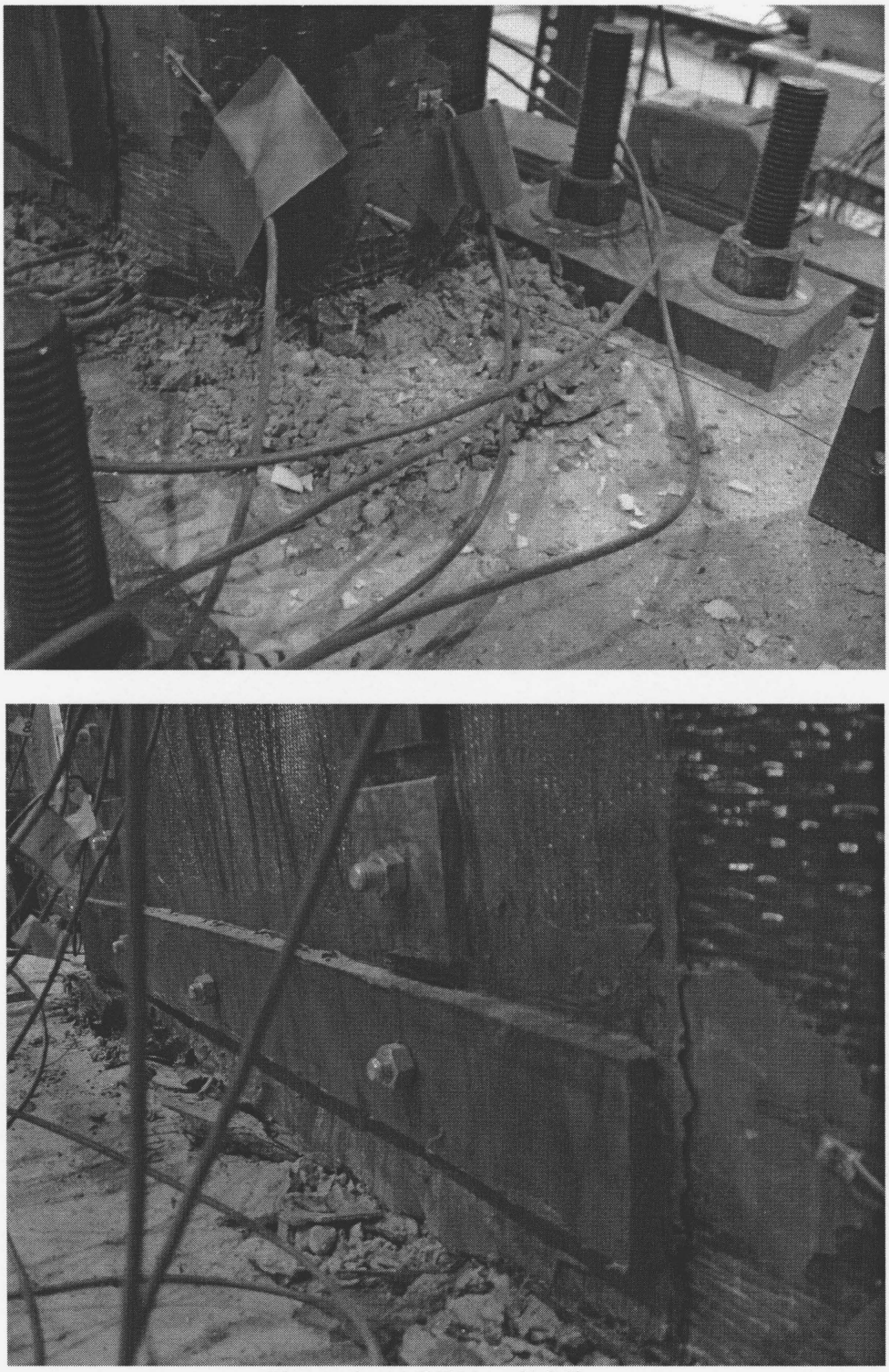

Figure 4- 44 RW6 wall failure.

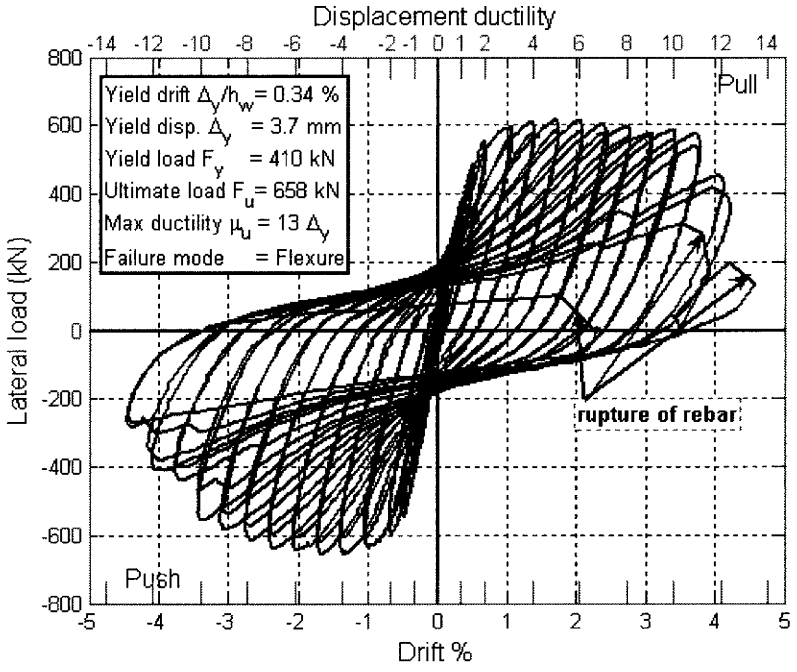

Figure 4- 45 RW6 Drift ratio-Lateral load relationship.

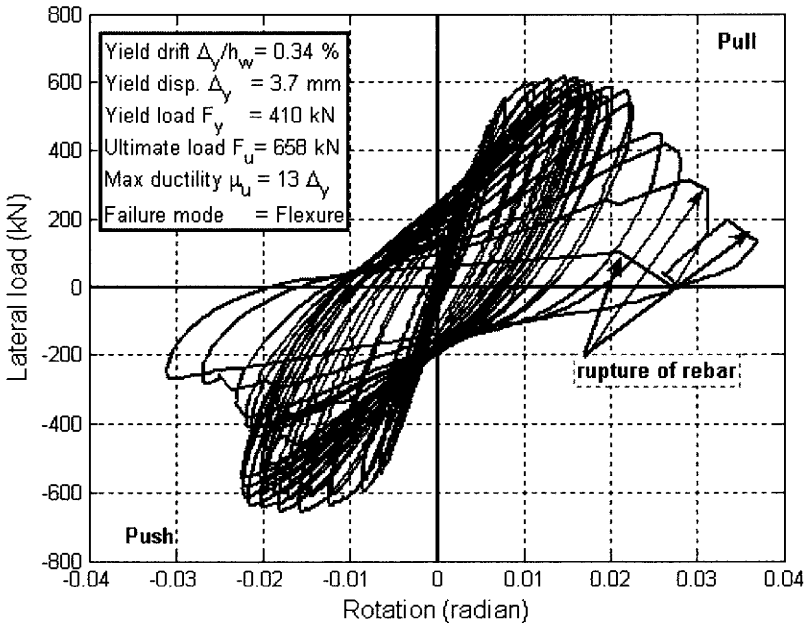

Figure 4- 46 RW6 top rotation-Lateral load relationship.

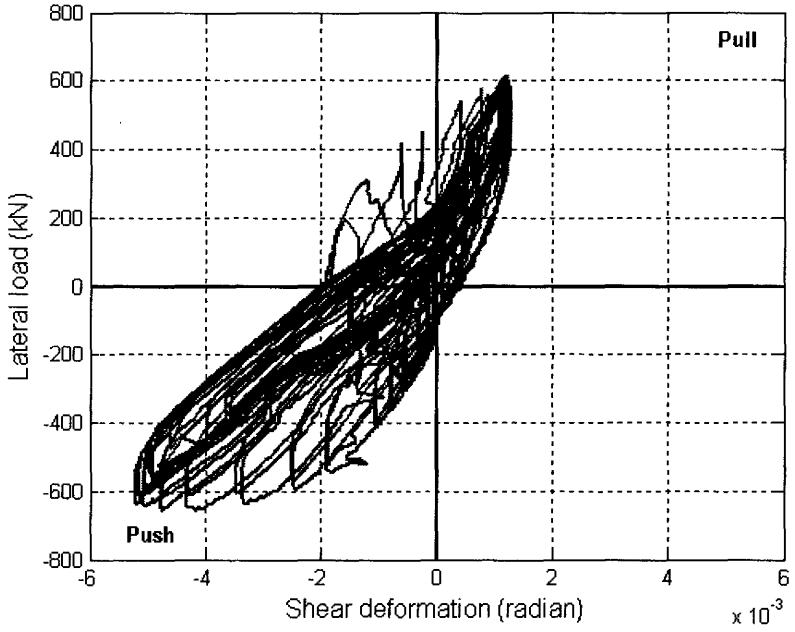

Figure 4- 47 RW6 Shear deformation -Lateral load relationship.

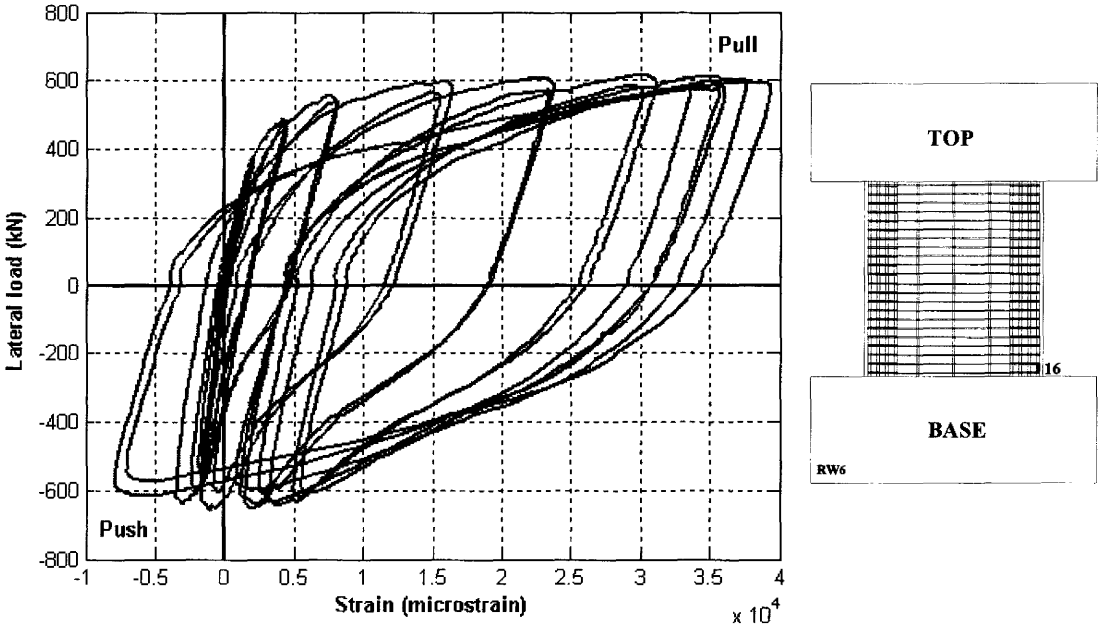

Figure 4- 48 RW6 Strain in gauge SG 16 -Lateral load relationship.

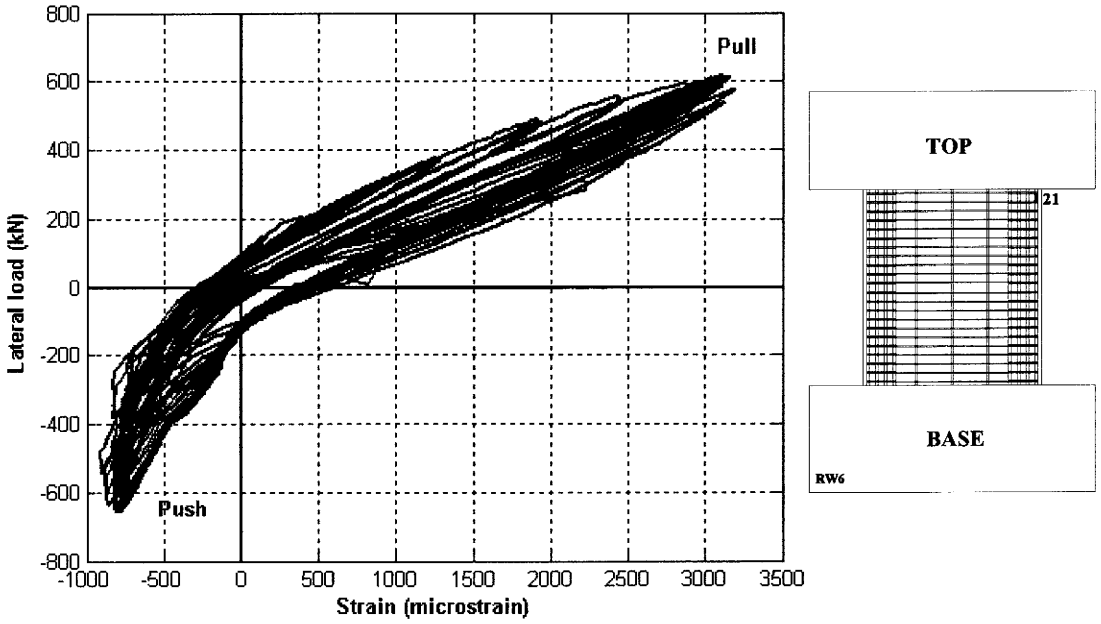

Figure 4- 49 RW6 Strain in gauge SG 21 -Lateral load relationship.

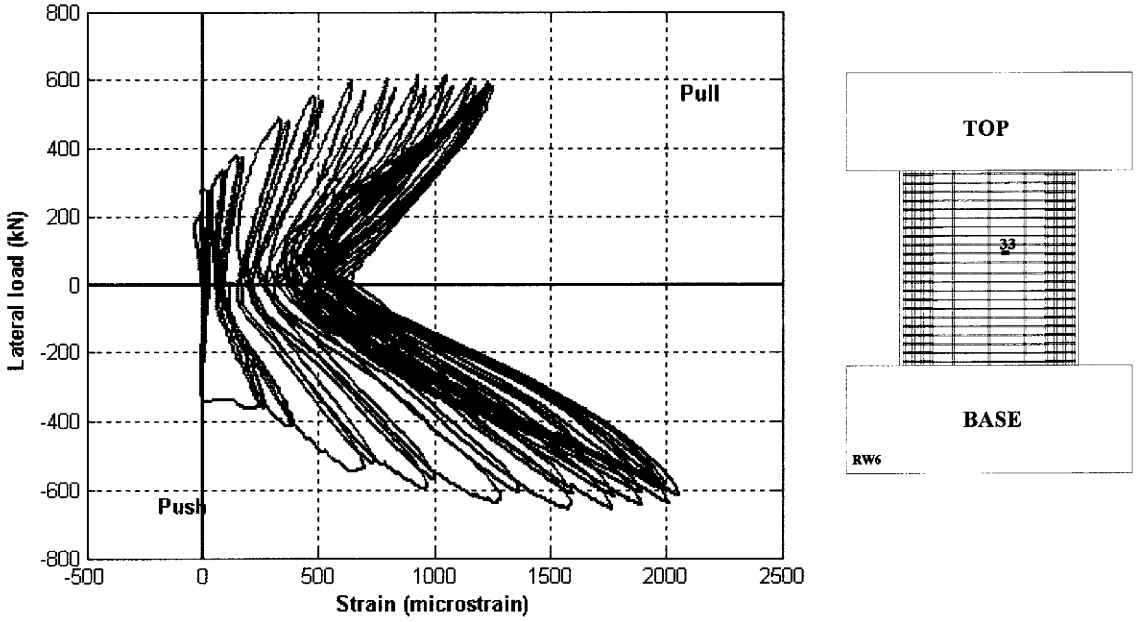

Figure 4- 50 RW6 Strain in gauge SG 33 -Lateral load relationship.

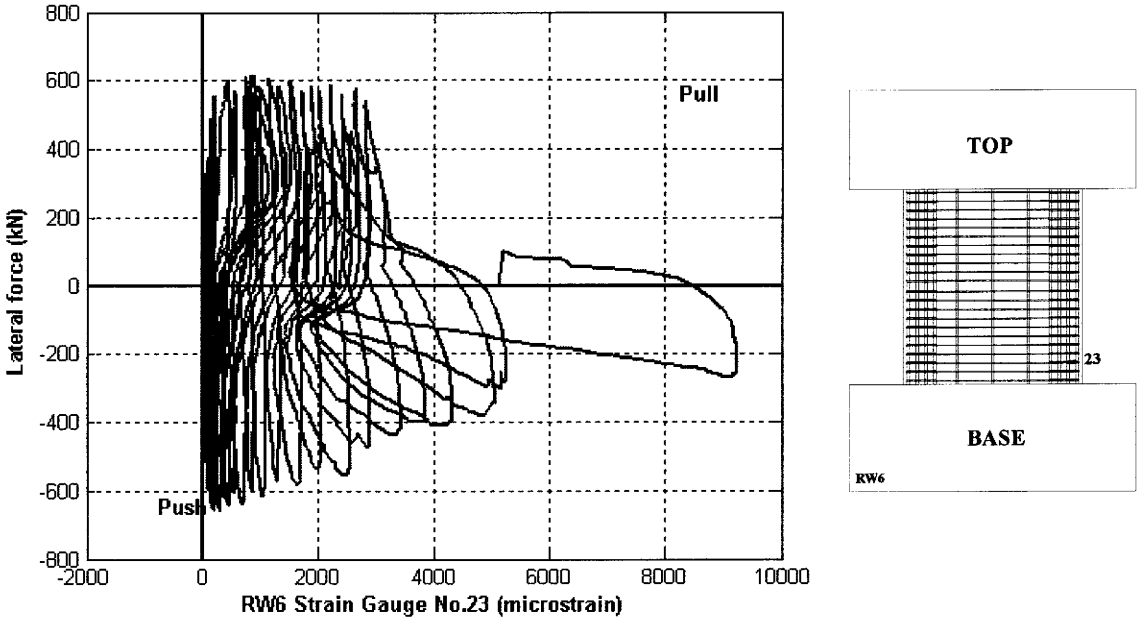

Figure 4- 51 RW6 Strain in confinement ties gauge SG 23 -Lateral load relationship.

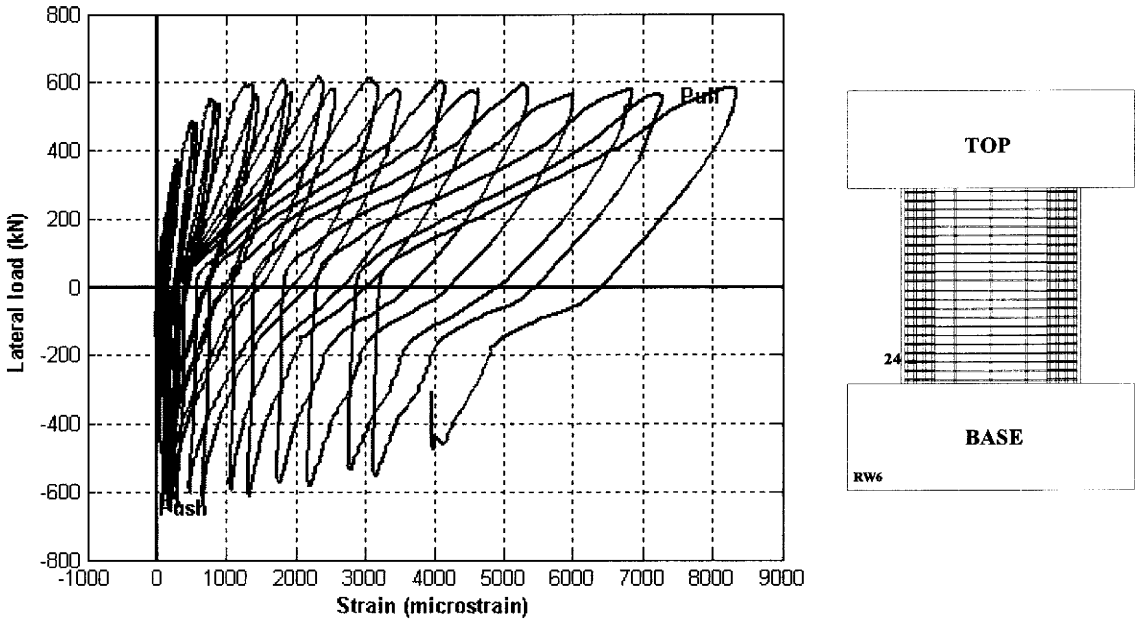

Figure 4- 52 RW6 Strain in confinement ties gauge Strain in gauge SG 24 -Lateral load relationship.

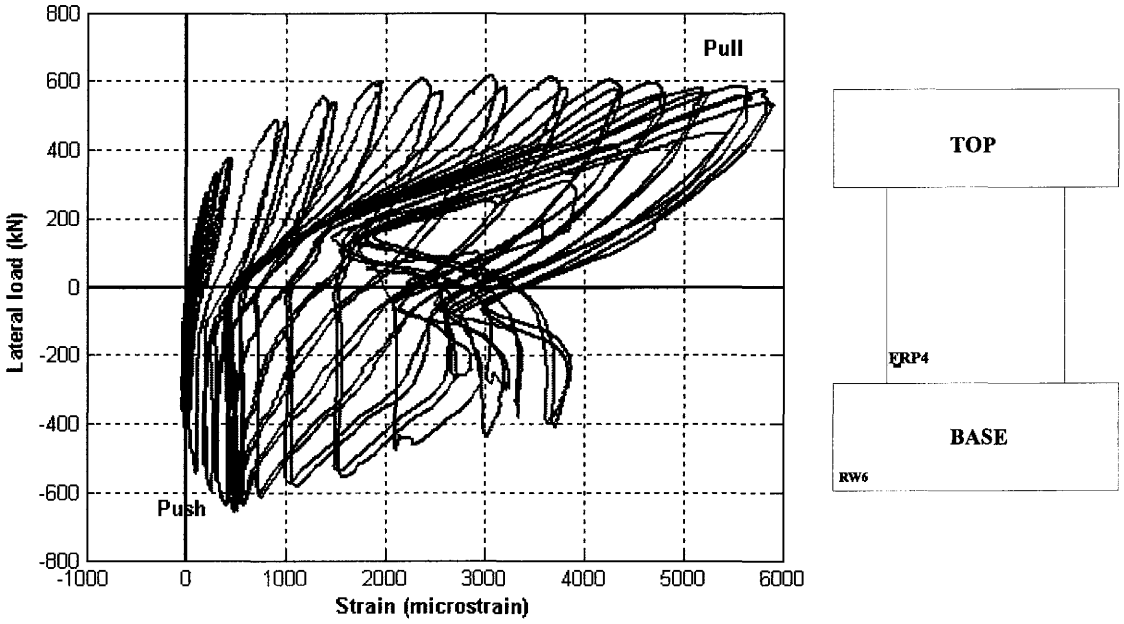

Figure 4- 53 RW6 Strain in CFRP gauge SG 4 -Lateral load relationship.

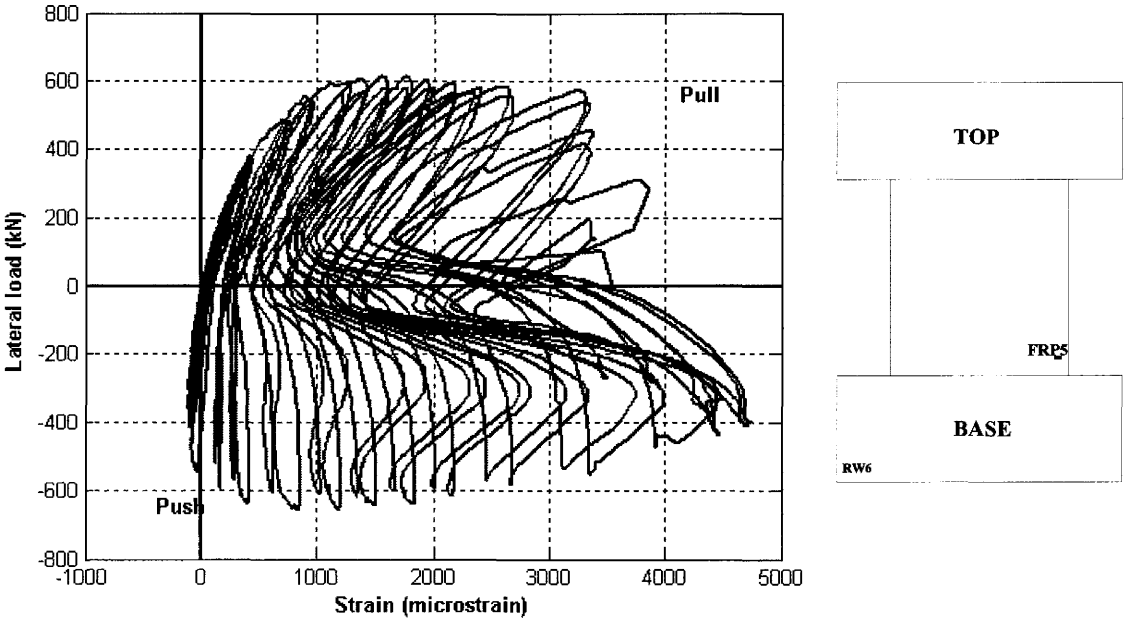

Figure 4- 54 RW6 Strain in CFRP gauge SG 5 -Lateral load relationship.

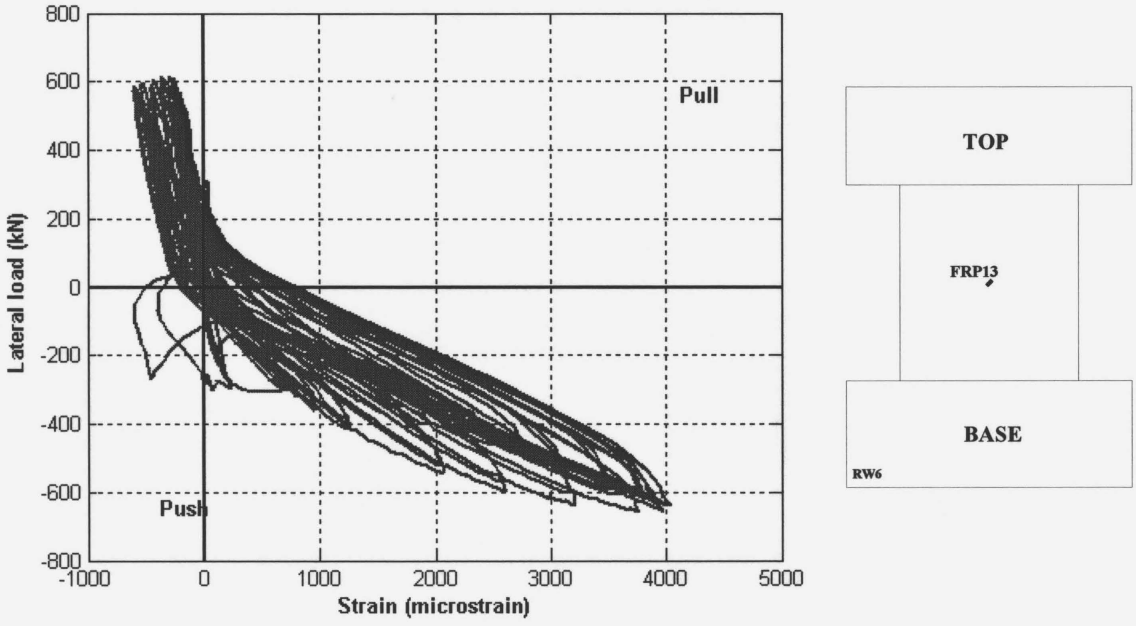

Figure 4- 55 RW6 Strain in CFRP gauge SG 13 -Lateral load relationship.

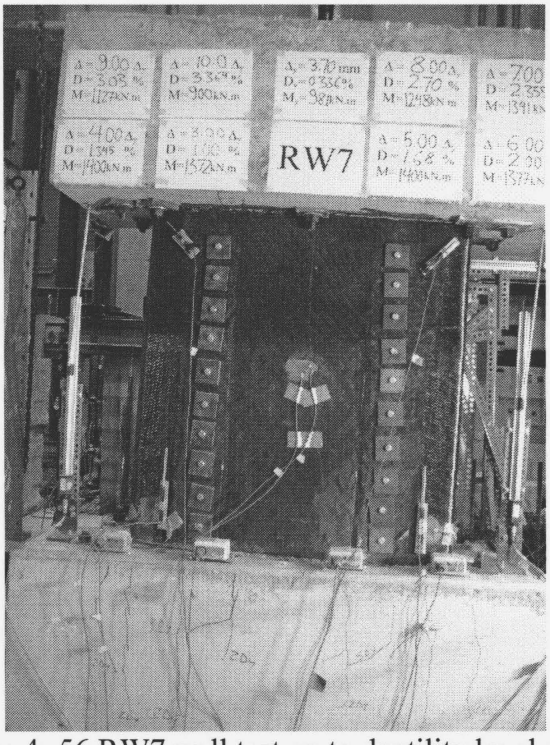

Figure 4- 56 RW7 wall test up to ductility level of 10.

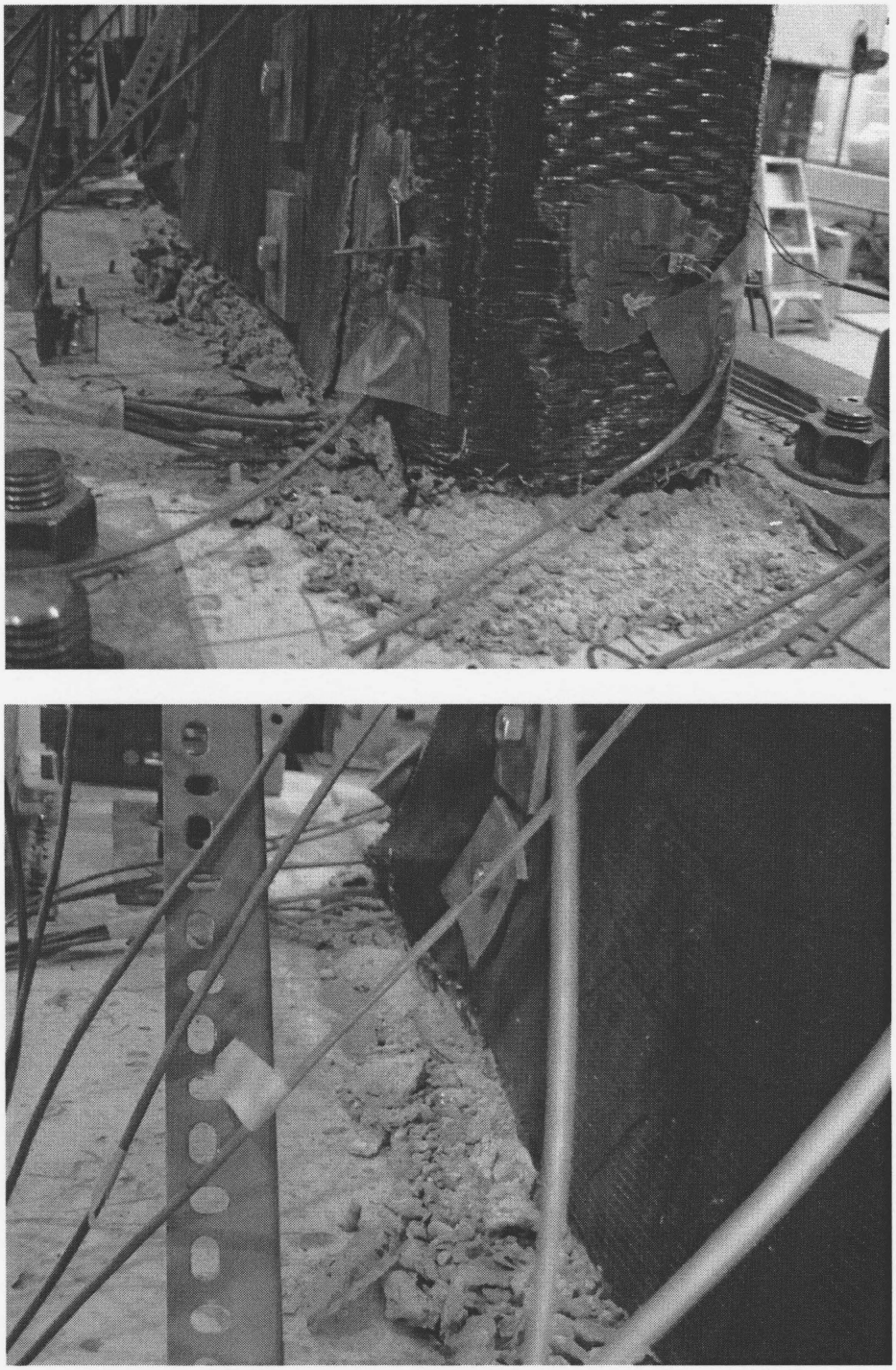

Figure 4- 57 Concrete crushing at the bottom of wall RW7.

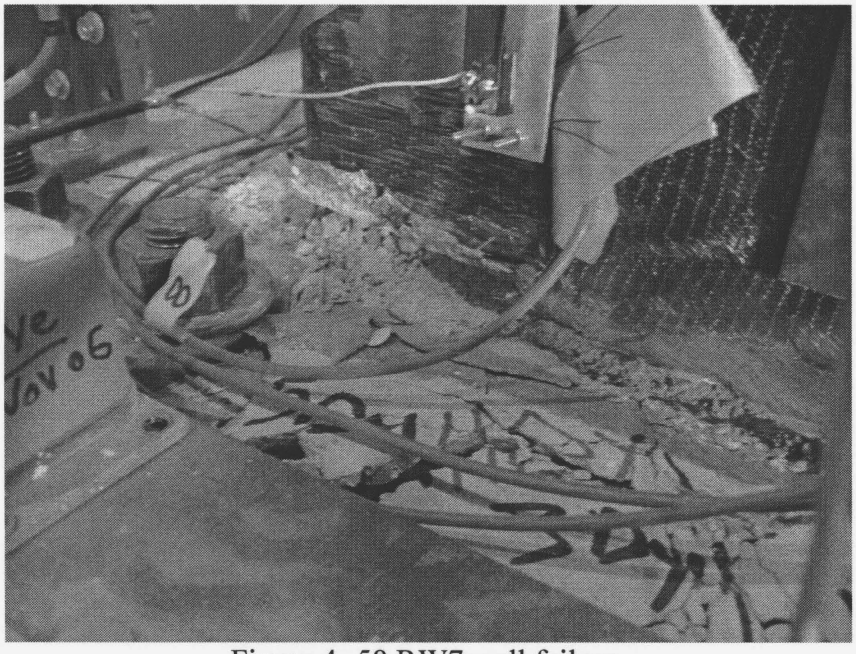

Figure 4- 58 RW7 wall failure.

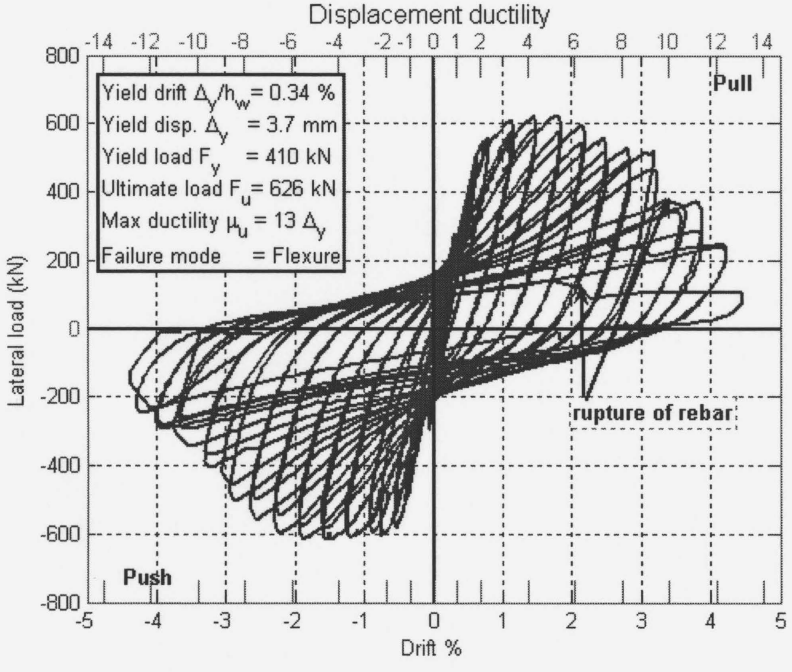

Figure 4- 59 RW7 Drift ratio-Lateral load relationship.

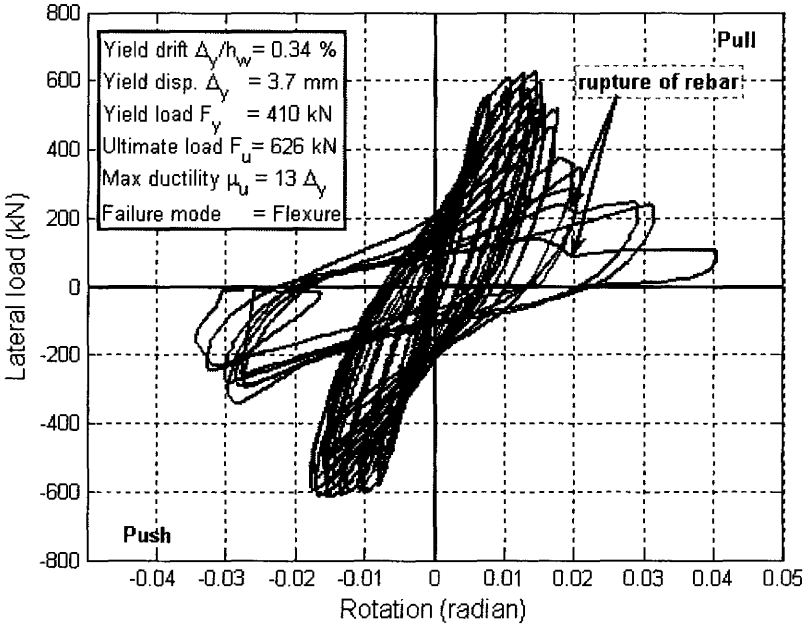

Figure 4- 60 RW7 top rotation-Lateral load relationship.

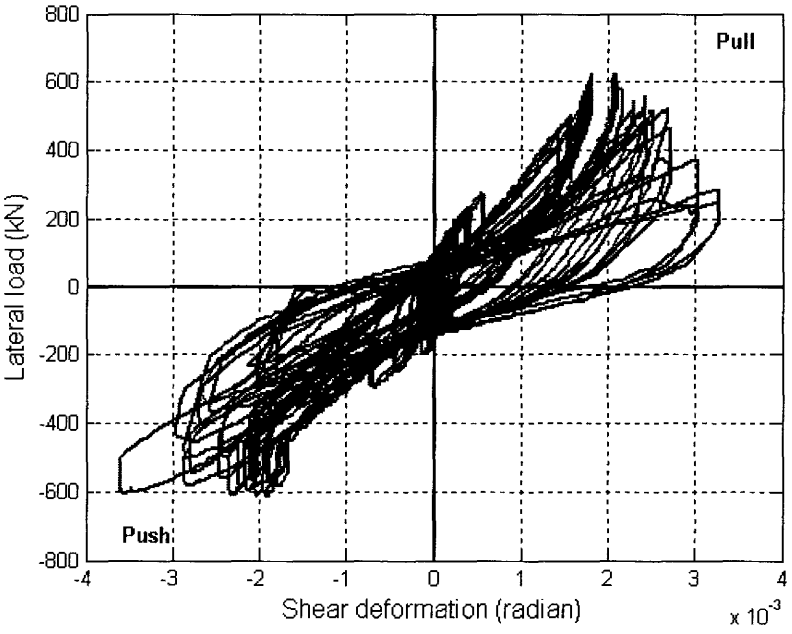

Figure 4- 61 RW7 Shear deformation -Lateral load relationship.

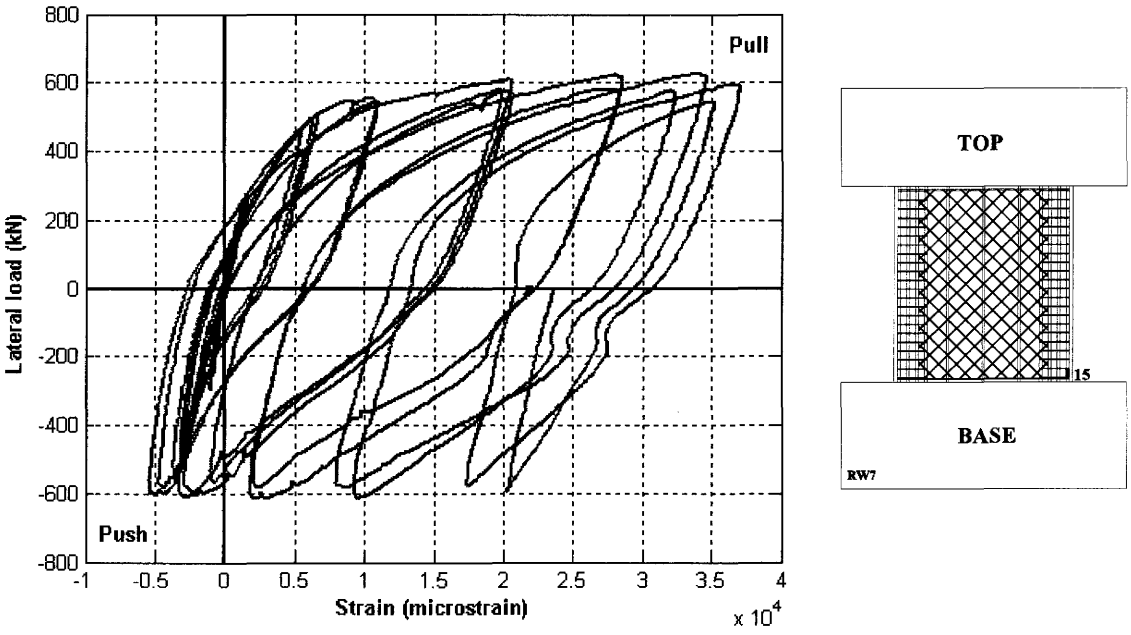

Figure 4- 62 RW7 Strain in gauge SG 15 -Lateral load relationship.

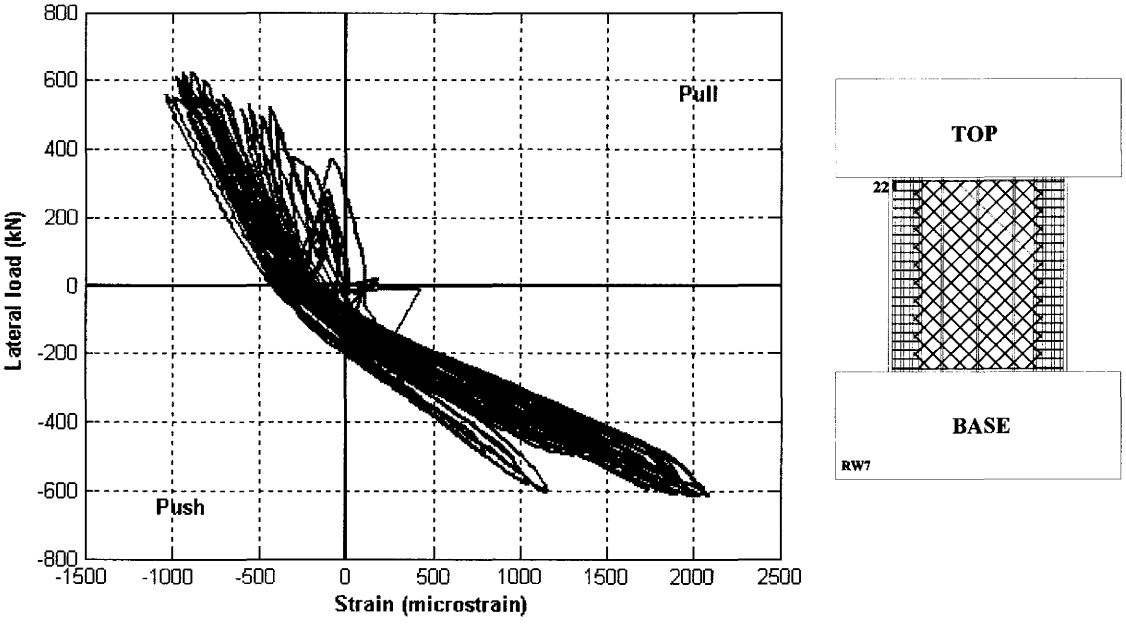

Figure 4- 63 RW7 Strain in gauge SG 22 -Lateral load relationship.

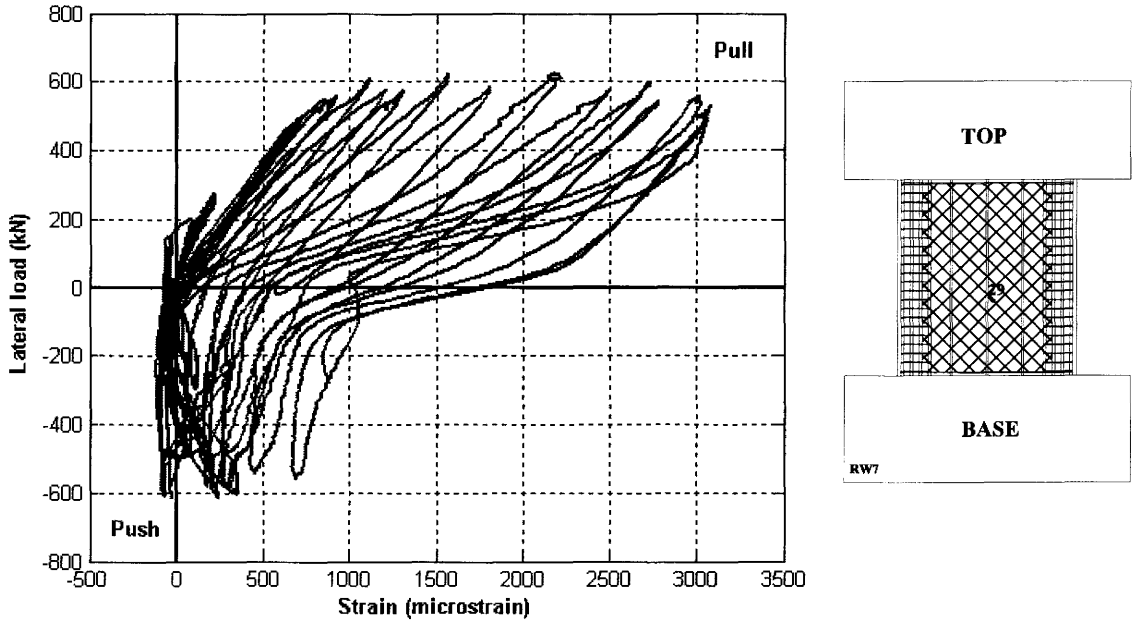

Figure 4- 64 RW7 Strain in gauge SG 29 -Lateral load relationship.

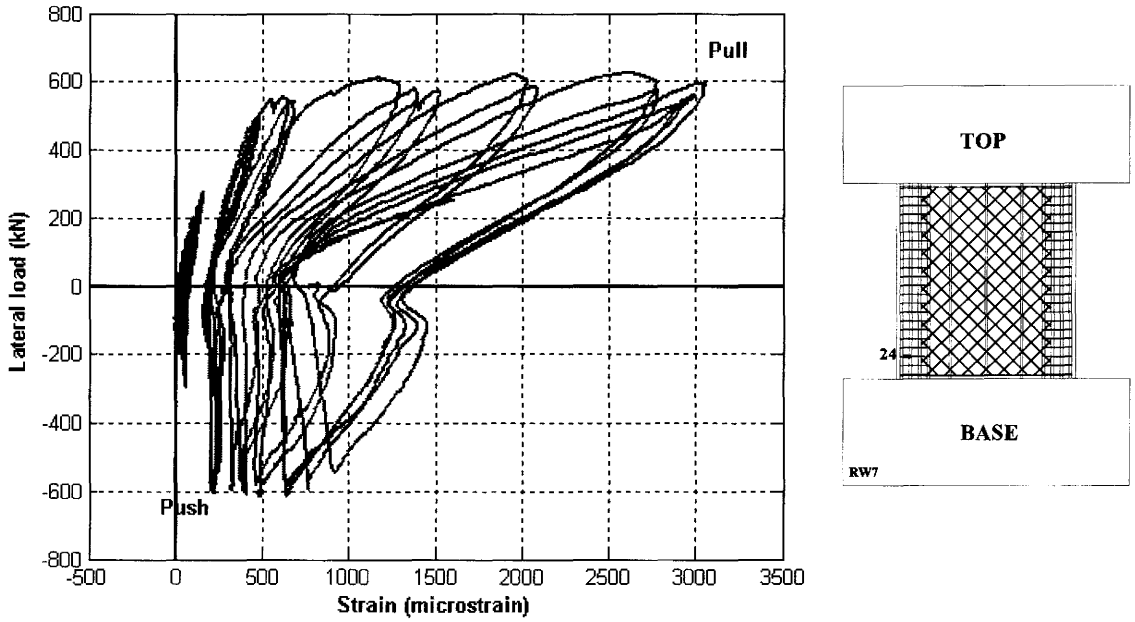

Figure 4- 65 RW7 Strain in confinement ties gauge Strain in gauge SG 24 -Lateral load relationship.

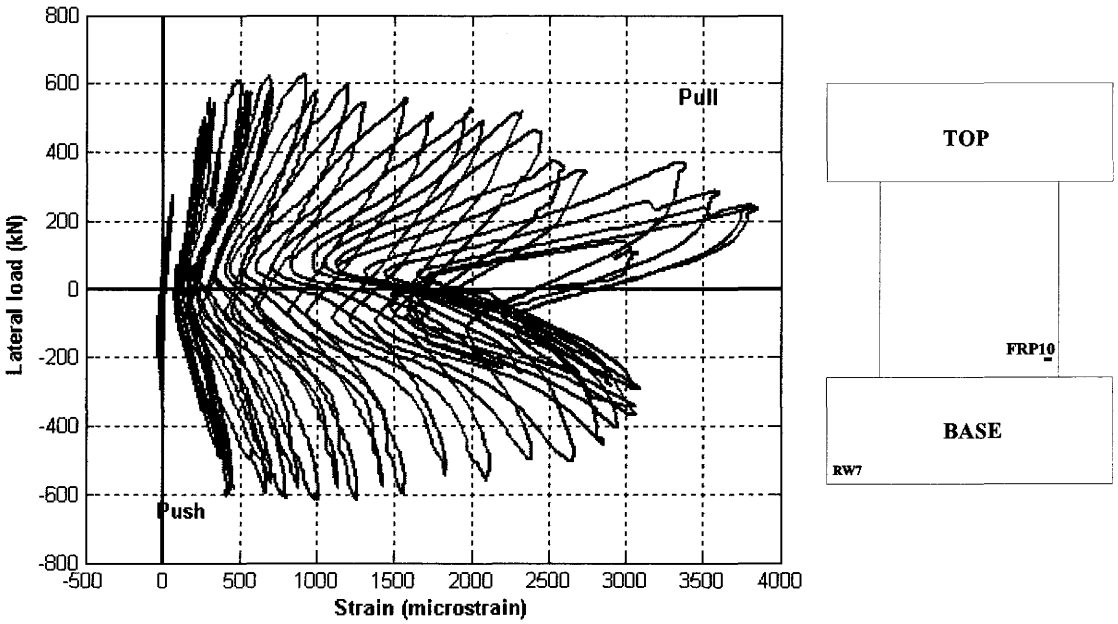

Figure 4- 66 RW7 Strain in CFRP gauge SG 10 -Lateral load relationship.

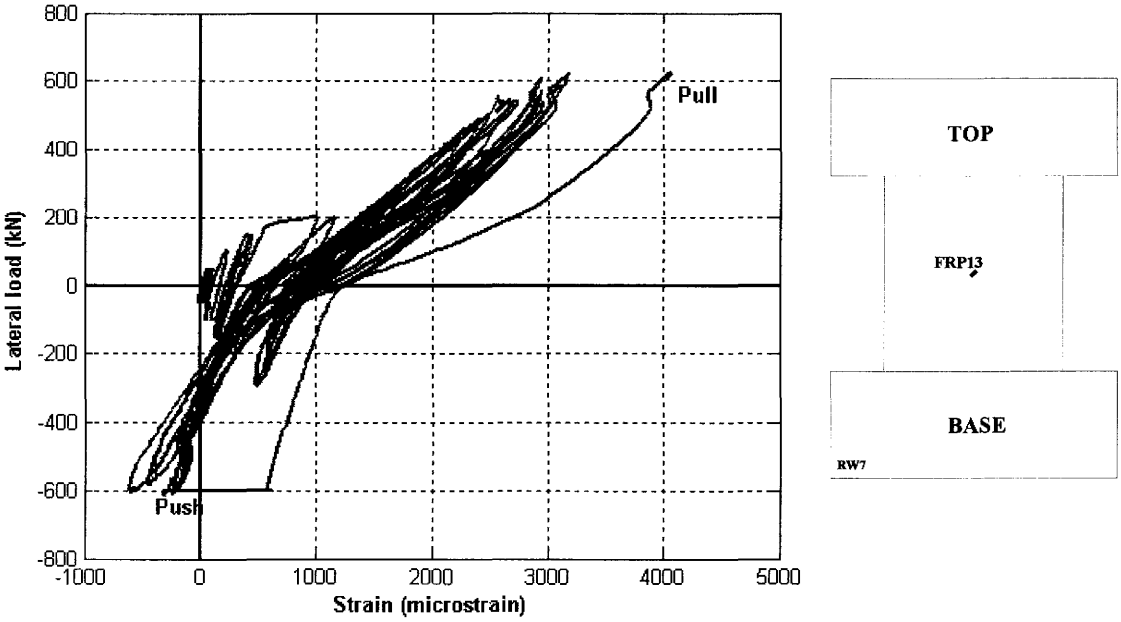

Figure 4- 67 RW7 Shear CFRP: Strain in gauge SG 13 -Lateral load relationship.

Figure 4- 68 RW8 test at ductility level of 7.

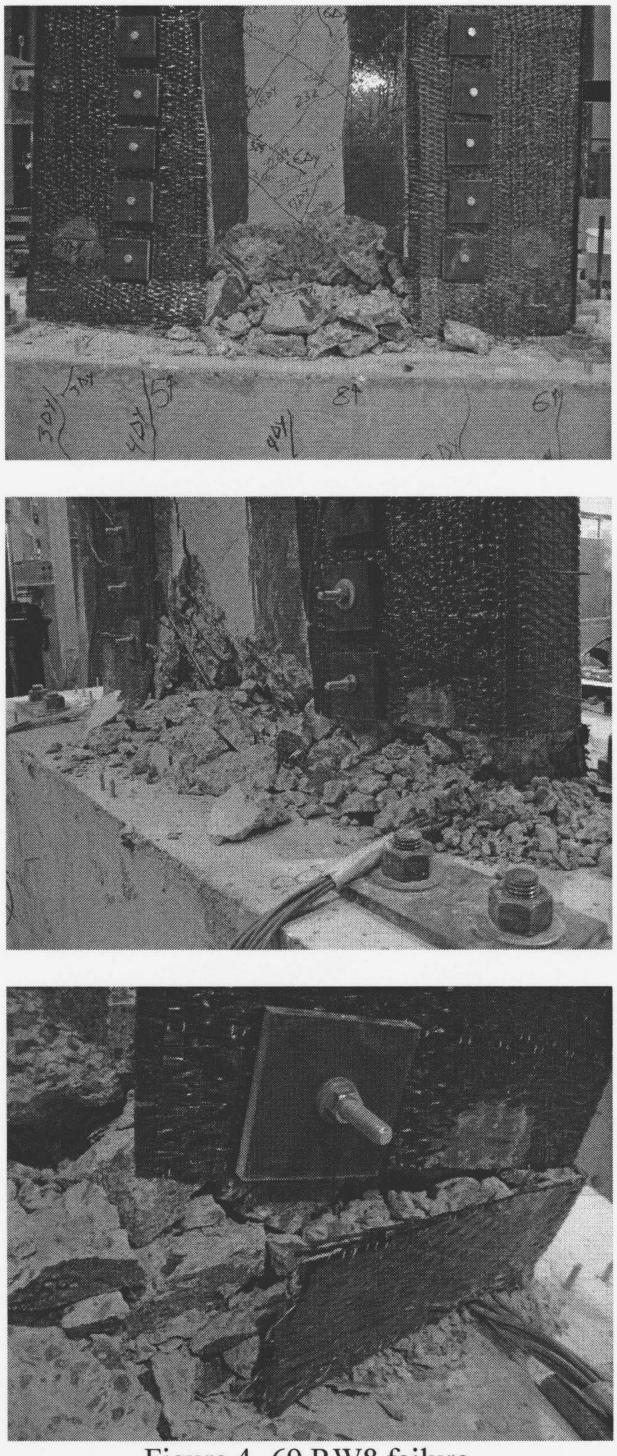

Figure 4- 69 RW8 failure.

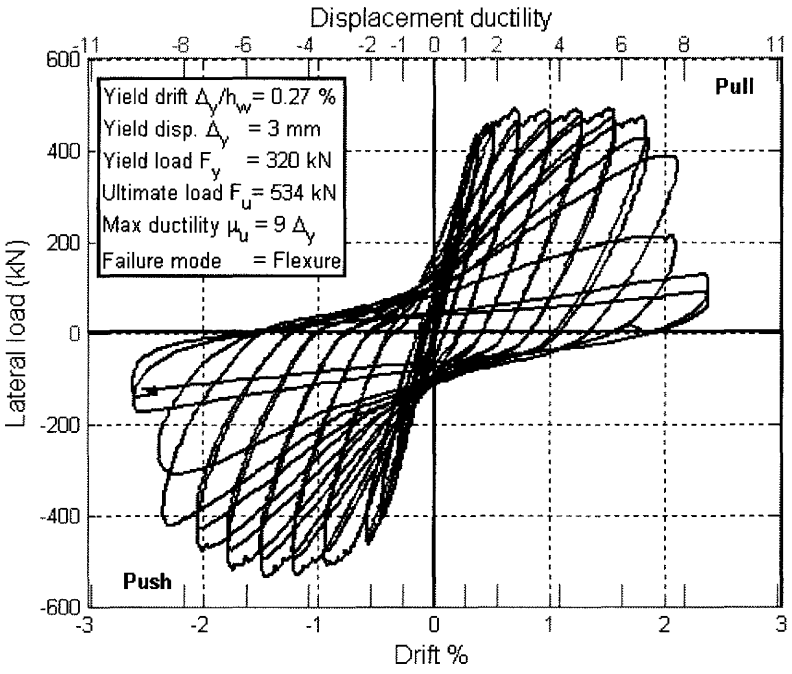

Figure 4- 70 RW8 Drift ratio-Lateral load relationship.

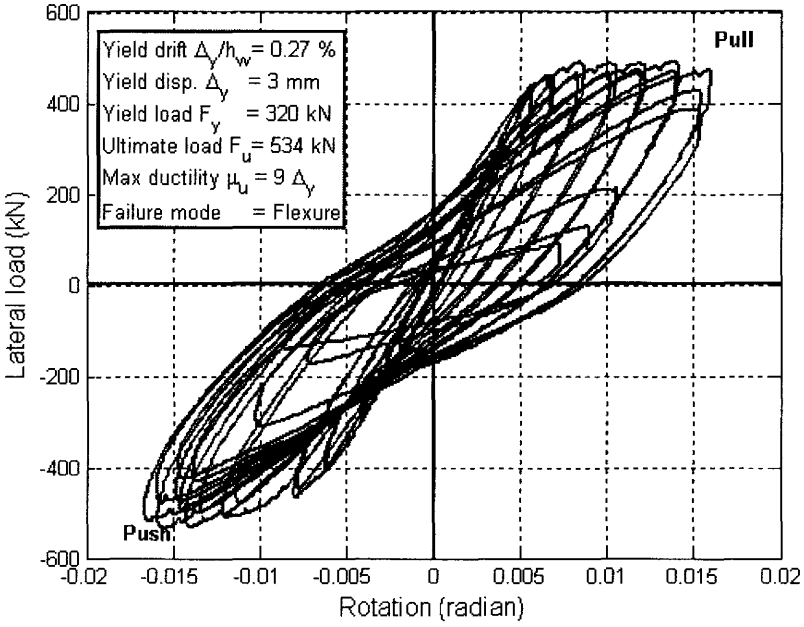

Figure 4- 71 RW8 top rotation-Lateral load relationship.

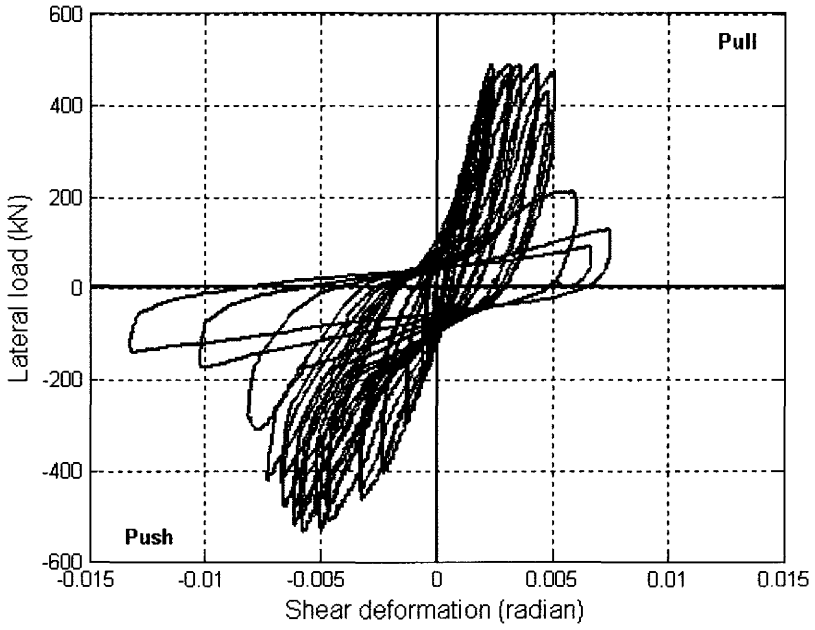

Figure 4- 72 RW8 Shear deformation -Lateral load relationship.

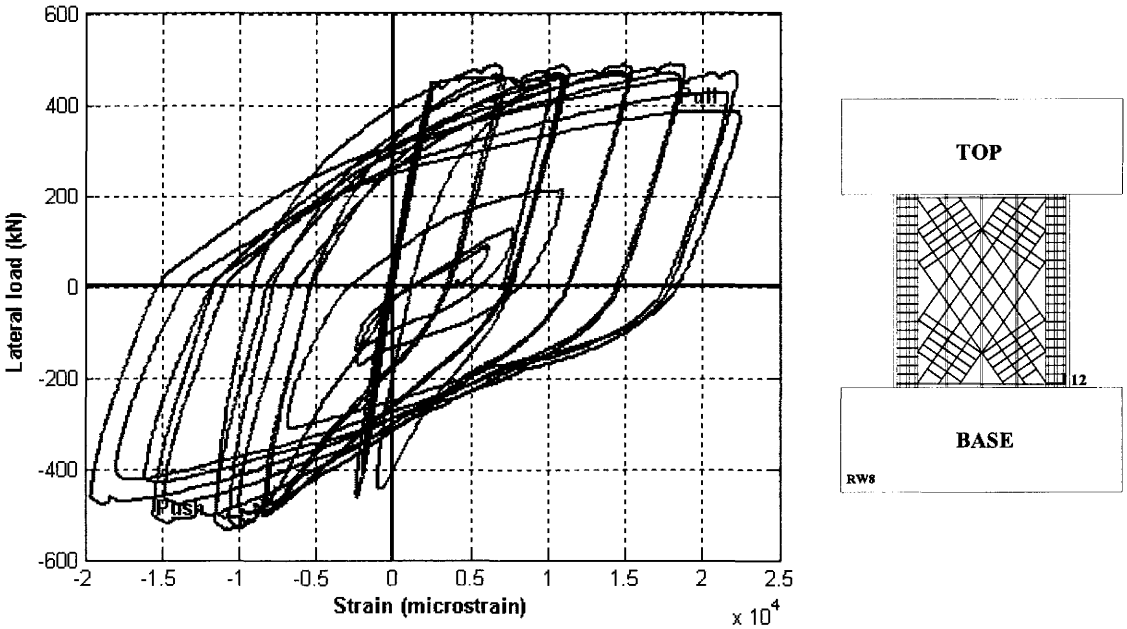

Figure 4- 73 RW8 Strain in gauge SG 12 -Lateral load relationship.

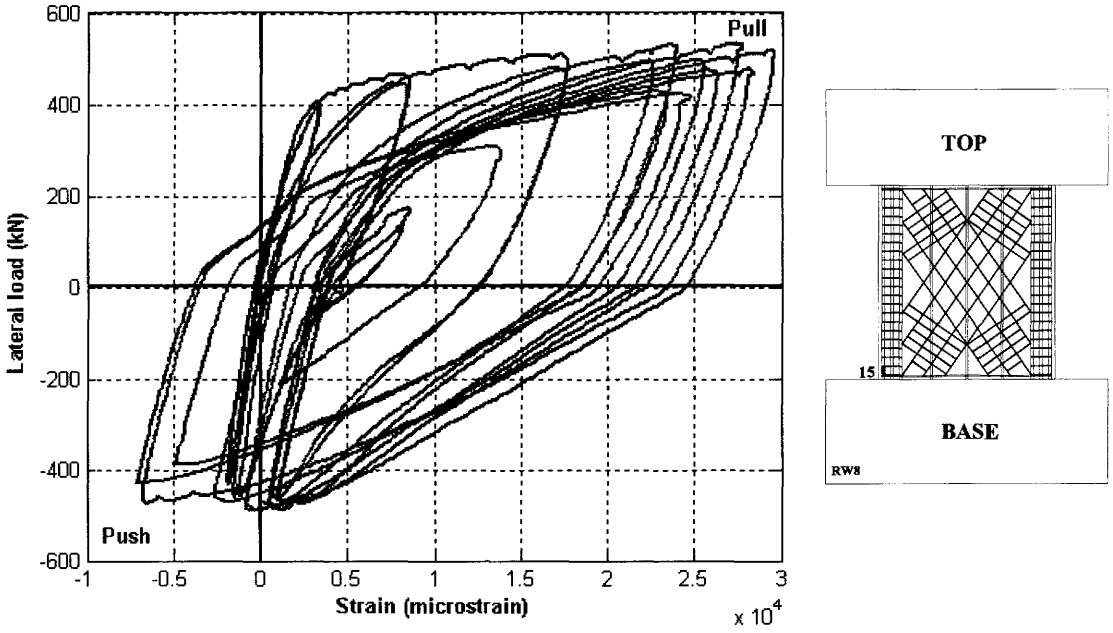

Figure 4- 74 RW8 Strain in gauge SG 15 -Lateral load relationship.

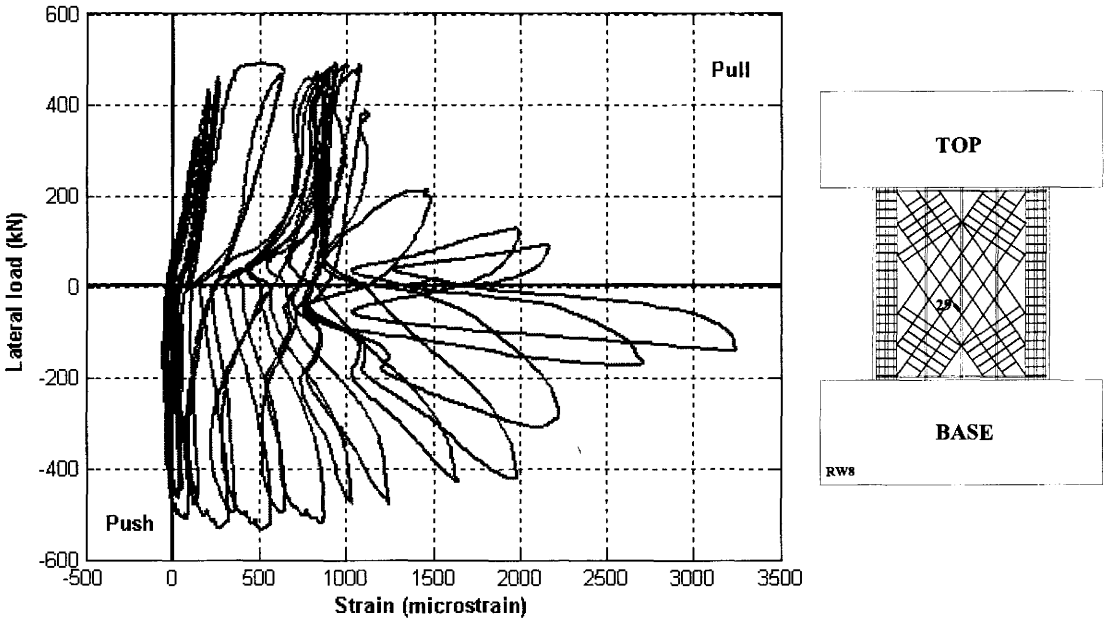

Figure 4- 75 RW8 Strain in gauge SG 29 -Lateral load relationship.

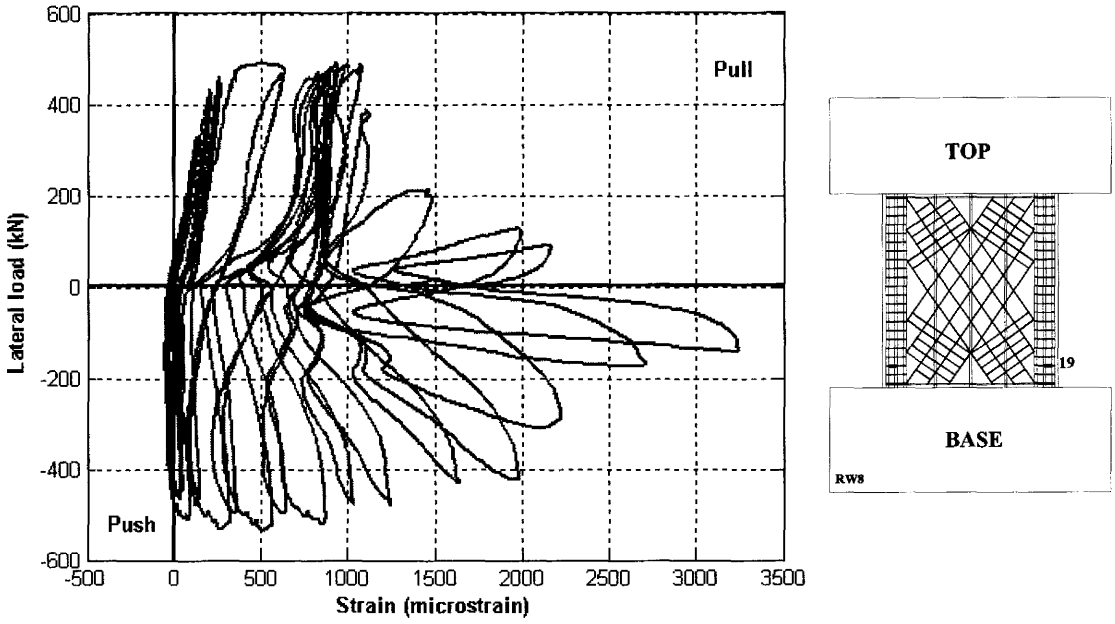

Figure 4- 76 RW8 Strain in confinement ties in gauge SG 19 -Lateral load relationship.

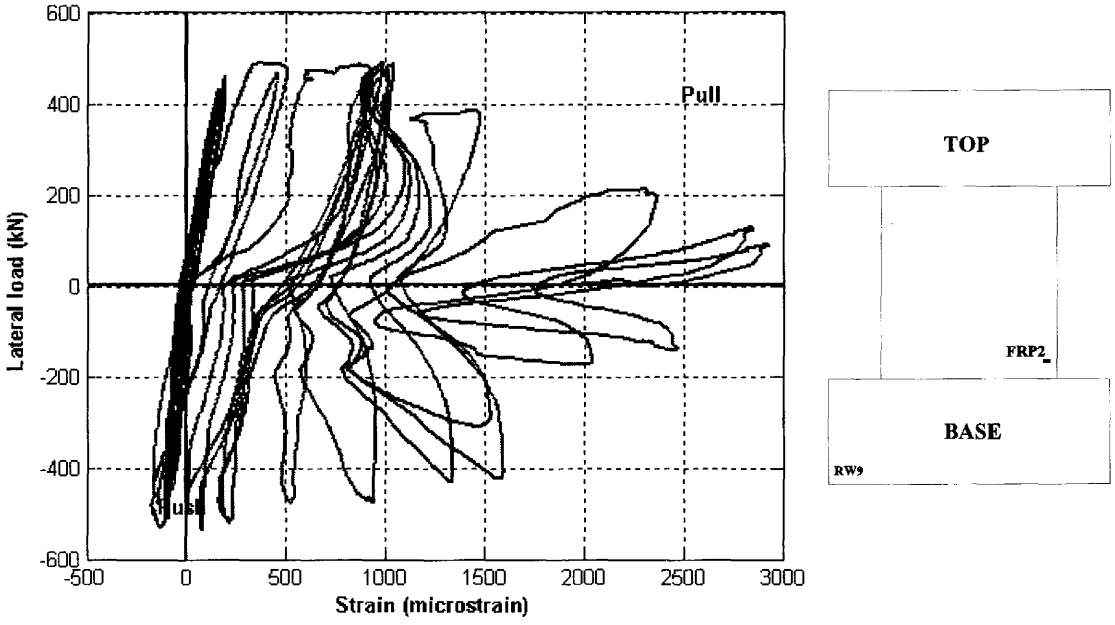

Figure 4- 77 RW8 Confinement CFRP: Strain in gauge SG 2 -Lateral load relationship.

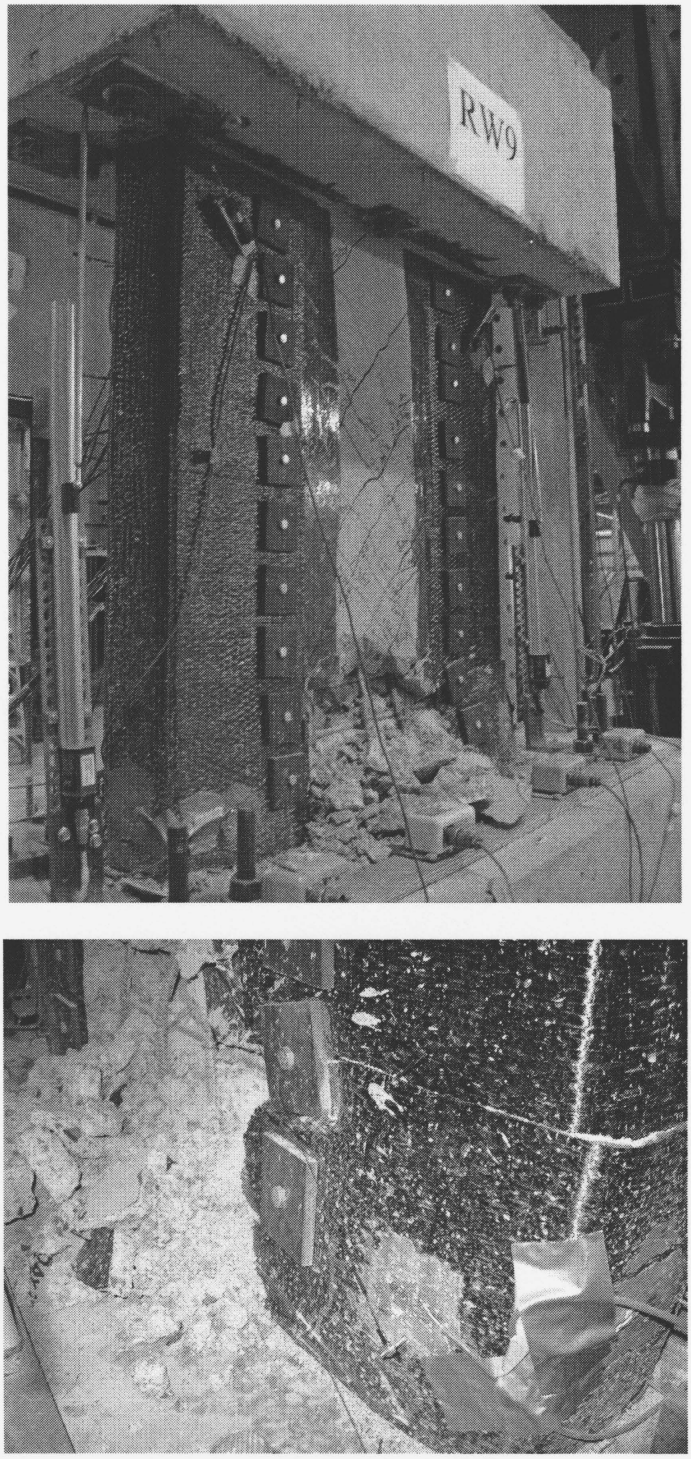

Figure 4- 78 Wall RW9 failure.

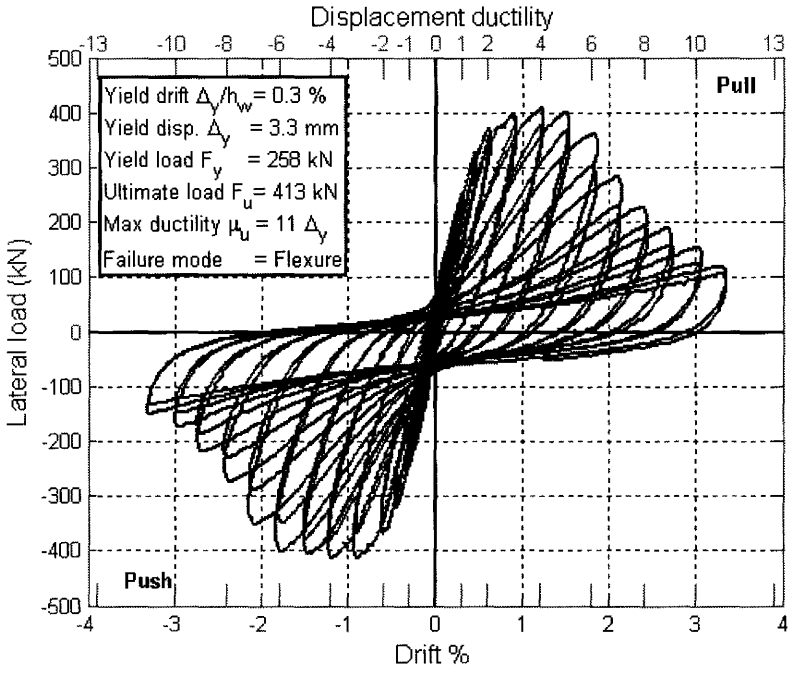

Figure 4- 79 RW9 Drift ratio-Lateral load relationship.

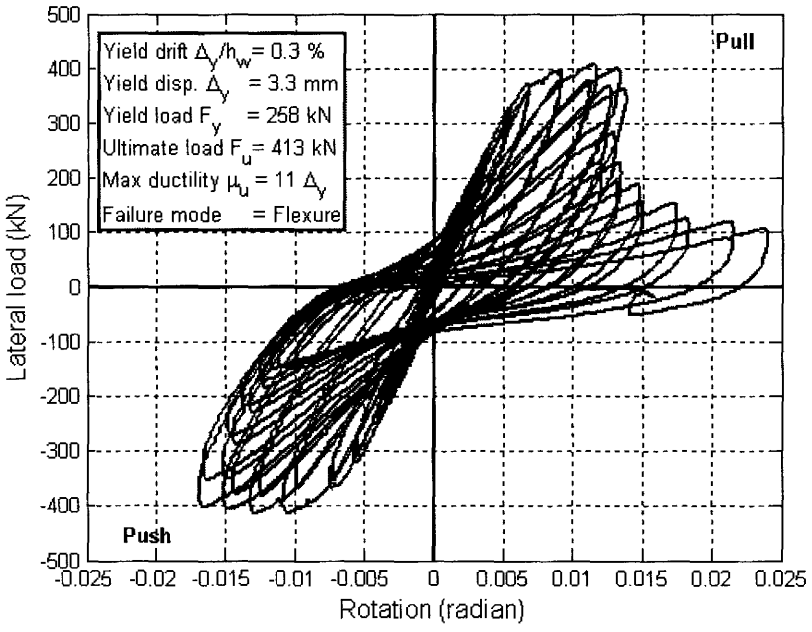

Figure 4- 80 RW9 top rotation-Lateral load relationship.

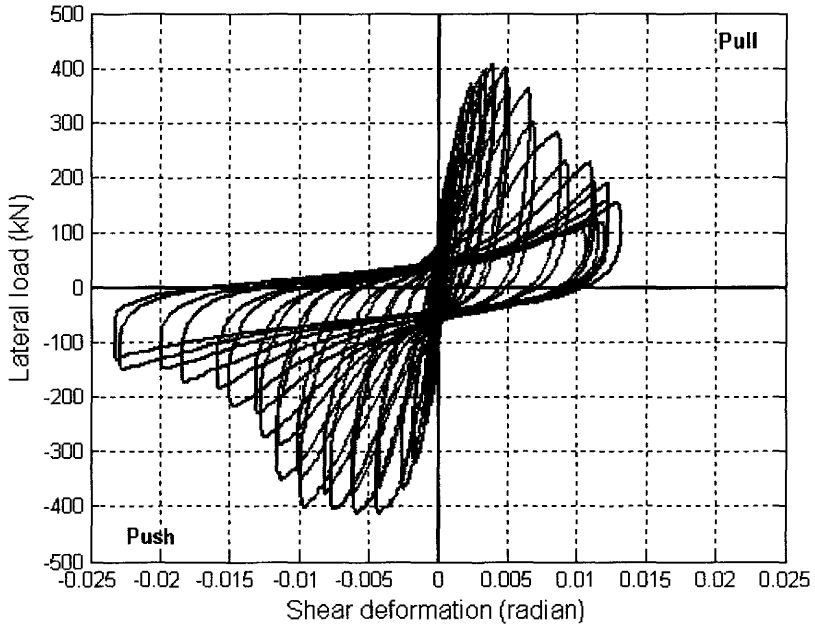

Figure 4- 81 RW9 Shear deformation -Lateral load relationship.

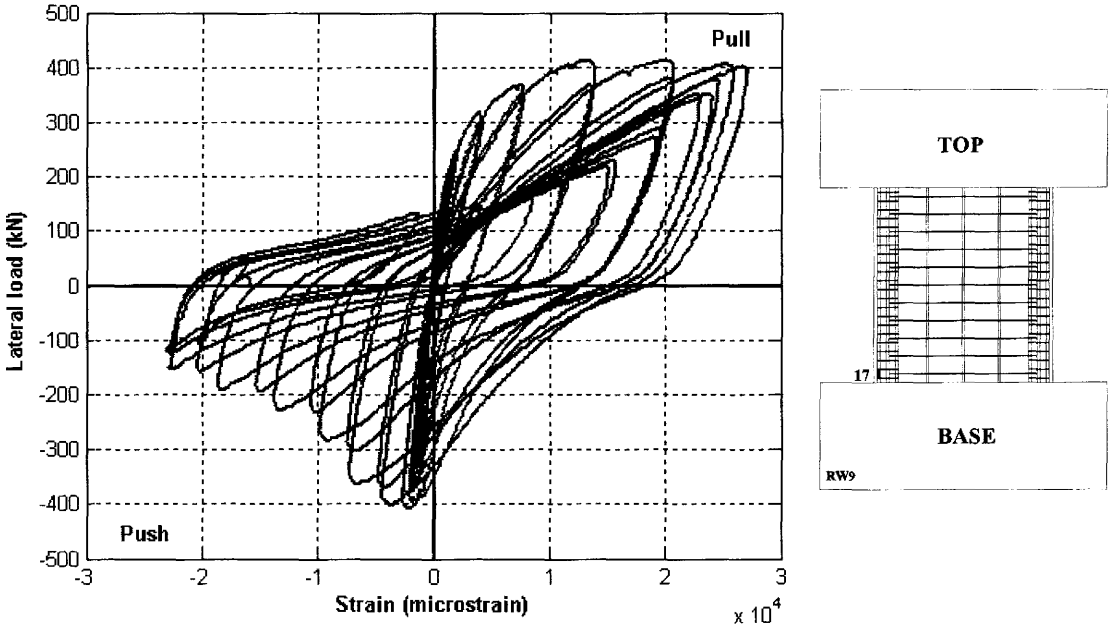

Figure 4- 82 RW9 Strain in gauge SG 17 -Lateral load relationship.

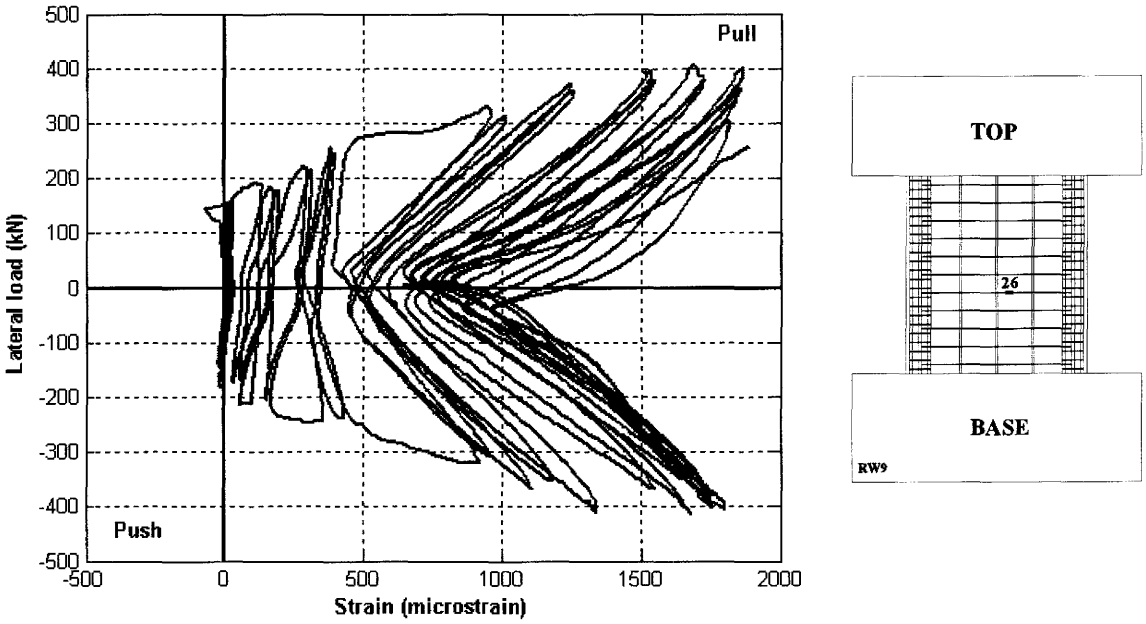

Figure 4- 83 RW9 Strain in gauge SG 26 -Lateral load relationship.

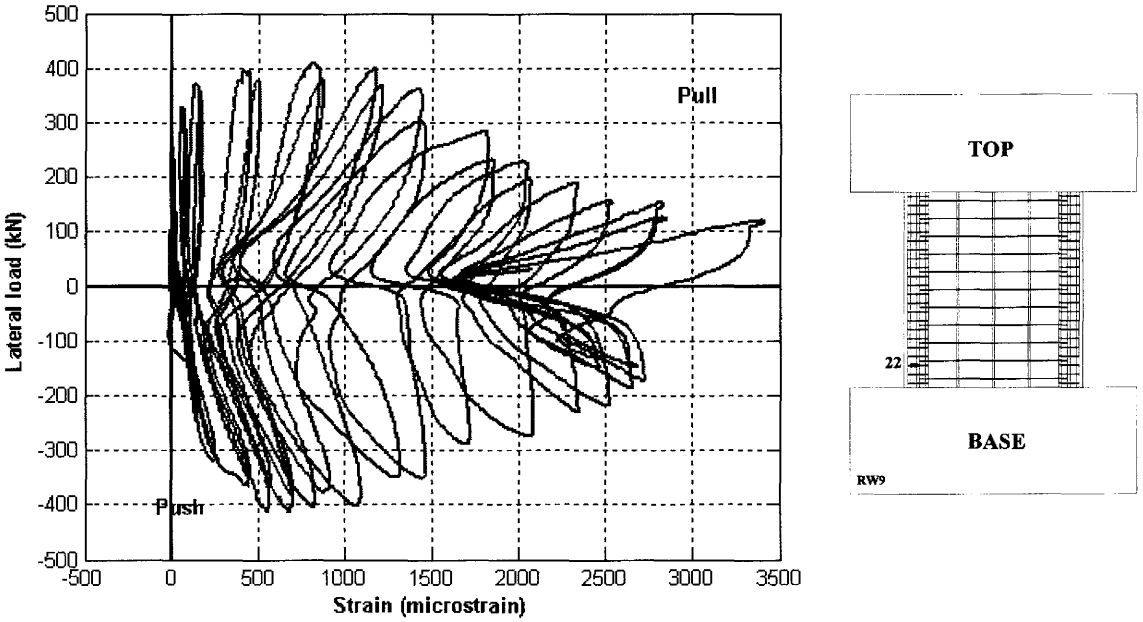

Figure 4- 84 RW9 Strain in confinement ties in gauge SG 22 -Lateral load relationship.

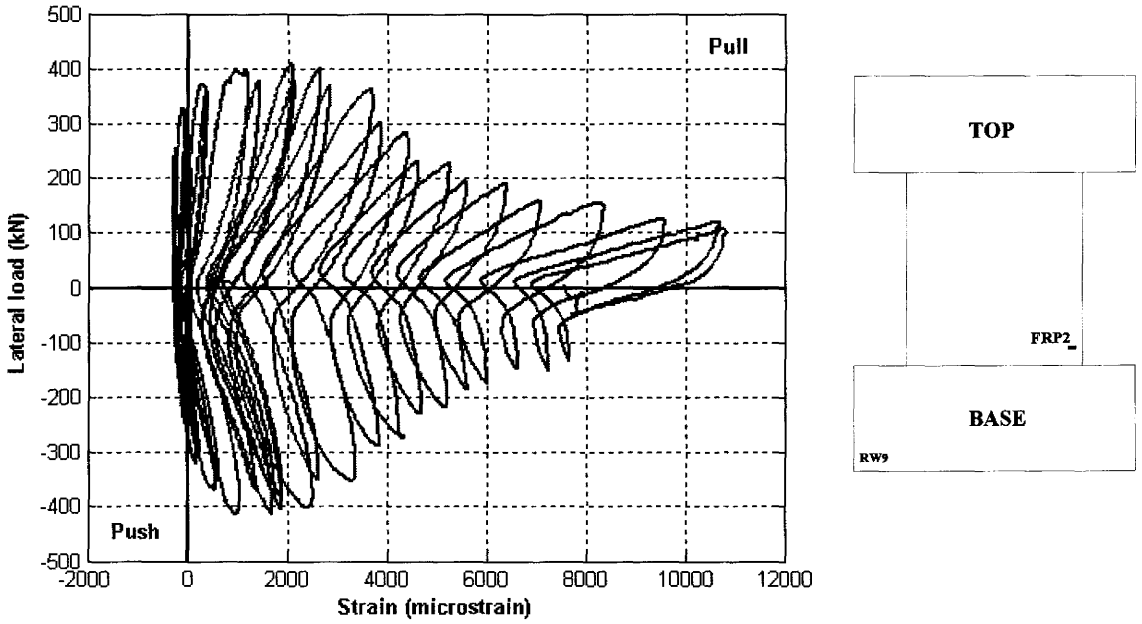

Figure 4- 85 RW9 Confinement CFRP: Strain in gauge SG 2 -Lateral load relationship.

CHAPTER 5

ANALYSIS OF TEST RESULTS

5.1 INTRODUCTION

Analysis of results and comparison of the behaviour of the tested walls are presented in this chapter. Ten walls were tested; three control walls CW1 to CW3 and seven rehabilitated walls RW3 to RW9. Walls CW1 to CW3 represented existing RC structural walls of pre 1970's design practice. To check the control system performance and the range of loading, wall CW1 was tested until it failed unexpectedly in shear. Wall CW2 was tested using high moment to shear ratio to examine flexural behaviour, while CW3 was tested under low moment to shear ratio. Wall RW3 was identical to test wall CW3 but was rehabilitated using CFRP wrapping for shear strengthening and confinement after welding the lap spliced flexural reinforcement. Wall RW4 represented CSA A23.3 (2004) designed wall. Wall RW5 was identical to test wall RW4 but it was rehabilitated using CFRP for shear strengthening and confinement to enhance ductile behaviour. Walls RW6 and RW7 represented rehabilitated walls to strengthen shear resistance and to confine the end columns. The only difference between RW6 and RW7 was the clamping plates attached at the bottom edges of the web CFRP sheets of the RW6. This technique was intended to prevent the debonding of web externally bonded shear strengthening CFRP composite material at the bottom edges. Walls RW8 and RW9 represented CSA A23.3 (2004) code designed walls. To increase the ductility levels of both walls, the end columns were confined using anchored CFRP. The lateral load and the lateral displacement along the height of the wall were recorded. Interstorey drift, shear deformation, top rotation, and wall curvature were calculated from test records plotted against the lateral load. Peak to peak lateral stiffness was calculated to determine the walls' in-plane stiffness. The cumulated dissipated energy was calculated and plotted against interstorey drift ratios.

5.2 TEST RESULTS

Envelopes of the recorded lateral loads during the various loading cycles were plotted against the interstorey drift ratio for the tested walls as shown in Figure 5.1. The peak-to-peak lateral stiffness of the tested walls is presented in Table 5.1. the measured stiffness of the first cycle at each ductility level were plotted against the top lateral drift ratio as shown in Figure 5.2. Figure 5.3 shows the cumulative energy dissipated by tested walls against the lateral drift ratio

5.2.1 Walls with deficient lap splices

The results of the two tested control walls CW2 and CW3 indicated that the two control walls prematurely failed due to bond slip of the lap splice. The strain gauge readings indicated that the horizontal steel did not yield nor did the vertical reinforcement.

5.2.2 Walls with rehabilitated lap splice

The lateral load capacity of the rehabilitated wall RW3 was 4.3 times that of control wall CW2 and twice that of test wall CW3. The significant increase in the lateral carrying capacity was due to the elimination of two brittle failure modes. These failure modes were the lap splice failure and the shear failure mode. In addition, the end column elements were sufficiently confined using CFRP wrapping to provide restraint against buckling of flexural reinforcement and to prevent concrete cover from spalling off under compression. Wall RW3 showed an increase in the lateral load capacity up to ductility level of 6 which corresponded to drift ratio of 2.18%. The shear response remained almost elastic. The maximum lateral load reached by wall RW3 was 435 kN which was twice the yield strength. Figure 5.5 shows the drift ratio plotted against the lateral load for walls CW2, CW3, and RW3, respectively. The figures show the effect of rehabilitation on increasing the lateral load carrying capacity of the wall.

5.2.3 CSA A23.3 (2004) designed walls

Wall RW4 was designed according to the concrete Code CSA A23.3 (2004) provisions. The lateral load capacity was double that of the control wall CW2 as shown in Figures 5.5 and 5.6. The increase in capacity was due to repairing the lap splice deficiency by welding the spliced bars and the elimination of the shear failure by the addition of shear reinforcement. Moreover, the end columns were confined using closed steel ties spaced at 50 mm to provide restraint against buckling of flexural reinforcement under compression. Wall RW4 showed an increase in the flexural strength up to ductility level of 3 which corresponded to drift ratio of 0.91 %, with minor shear cracks. The maximum lateral load resisted by the wall was 415 kN (1.38 times the yield strength). Diagonal shear cracks were observed during the push half of the loading cycle at ductility level 4. Shear failure did not occur. The shear reinforcement remained in the elastic range. The wall lateral load capacity dropped because of concrete cover spalling off and the rupture of two longitudinal flexural rebars. Rebar rupture was due to large plastic strains during loading cycles up to ductility level 6.

Wall RW5 was designed to represent a strengthened wall. Both RW4 and RW5 walls were identical except that wall RW5 strengthening included CFRP web wrapping and end column element CFRP confinement. Test wall RW5 was expected to behave in a ductile manner rather than the nominally ductile response of wall RW4. The maximum lateral load resistance was approximately twice that of the control wall CW2, and 1.05 that of RW4. Wall RW5 sustained twice the ductility level of RW4 before the strength started to deteriorate. This increased ductility was attributed to the CFRP confinement of the end columns and CFRP shear strengthening of wall web. The small increase in lateral load capacity is attributed to the increase in the concrete strength due to the effect of partial confinement of CFRP wrap. At ultimate lateral load for wall RW5 the drift ratio was 1.5%. For wall RW4 the drift ratio was 0.91% at ultimate load. This observation indicated that wall RW5 sustained larger deformation than that of wall RW4 with almost the same ultimate capacity. This led to an increase in the dissipated energy by wall RW5 compared

to wall RW4. Figure 5.6 shows the lateral load resistance of RW5 together with RW4 and control wall CW3 data.

Walls RW6 and RW7 represented walls with shear and confinement deficiencies. The deficiencies were rehabilitated by CFRP composite material. The shear and confinement steel reinforcements were identical to wall RW4. The provided shear reinforcement and confinement ties were not enough to resist high strains associated with the flexural ductile response. The flexural reinforcement ratio in each of the end columns was twice that installed in each of the end columns of tested walls CW1 to CW3, and RW3 to RW5. The intent was to evaluate the effect of the flexural reinforcement ratio parameter on both flexural capacity and ductility levels of the tested walls with the same cross sections. The only difference between RW6 and RW7 was the clamping plates attached at the bottom CFRP sheets in wall RW6. The plates were used to prevent debonding of the wall web externally bonded CFRP. The strengthening technique involved CFRP shear strengthening and confinement of end columns.

The maximum lateral load sustained by wall RW6 was 660 kN (1.53 yield strength). For RW7 the lateral load capacity was 630 kN (1.53 yield strength). In comparison wall RW6 lateral load capacity was 1.06 times that of wall RW7. This was because the added web clamping plate at the bottom edge of the CFRP sheets prevented the concrete from crushing through the web part of RW6. Concrete crushing was limited to near bottom of the two end columns. This increased the number of stable ductile loading cycles that were observed from test wall RW6 and delayed the strength deterioration until 3% top lateral drift ratio as shown in Figure 5.7.

Walls RW8 and RW9 represented walls with confinement deficiency that was rehabilitated using three layers of CFRP. The provided shear reinforcement was sufficient to prevent brittle shear failure mode. However, the confinement ties were not adequate to resist high strains associated with the flexural response. The flexural reinforcement ratio was 1.5 times that of wall RW4. In addition, the shear reinforcement installed in wall RW8

was configured at ±45° while the bars installed in wall RW9 were horizontal. Both walls end columns were confined using three layers of anchored U shaped CFRP sheets.

The lateral load capacity of wall RW8 was 520 kN (1.63 yield strength). For RW9 the lateral load capacity was 430 kN (1.65 yield strength). In comparison, the maximum lateral load capacity of RW8 was 1.21 times that of RW9 as shown in Figure 5.8. The reason for higher load was that the flexural reinforcement for RW9 was previously tested and yielded and had some residual plastic strains. In this case, there was no distinct yield point due to the Bauschinger effect. The shear reinforcement in RW8 was at ±45°. The reinforcement arrested the shear cracks and kept the shear deformation in the elastic range. The load carrying capacity of RW8 was 0.78 times that of RW6, and 1.21 times that of RW5. The vertical flexural reinforcement installed in RW8 was 0.75 that in RW6. The increased flexural reinforcement ratio of RW6 to double that of RW5 increased the flexural capacity by 1.53 times that of RW5.

5.3 COMPARISON OF TEST RESULTS

Comparisons between the measured responses of the different tested walls are discussed in the following sections.

5.3.1 Envelope of load-drift ratio relationship

The envelope of the lateral load-drift ratio relationships of all the test walls are plotted in Figure 5.1. From comparing the response of different walls, the following can be observed:

1- Existing structural walls with 24 bar diameter lap splices at the base are inadequate for desirable ductile seismic response. Retrofitting lap splices by welding eliminates the brittle bond slip failure mode.

2- The moment to shear ratio is a significant factor that affect the behaviour of the structural walls and influence their failure mode. For the tested wall with moment to shear ratio of 5, flexural response was predominant, while for

moment to shear ratio of 2.25 a coupled flexural/ shear response was observed.

3- Retrofitting the walls using CFRP sheets eliminated the brittle shear failure mode. The result is a ductile response and high energy dissipation, which are necessary for the collapse prevention during severe seismic events.
4- The displacement ductility capacity of wall RW4 was not adequate when closely spaced shear reinforcement and confinement ties were used as per CSA A23.3 (2004) code specifications. Ductility level of 3 was reached before a mixed shear/ flexural failure mechanism occurred. This response would be considered as "nominally" ductile. Strengthening may be considered to assure ductile behaviour of the wall.
5- The upgraded CSA A23.3 (2004) code designed wall RW5, showed a significant ductile response and higher energy dissipation level as compared to RW4.
6- Wall RW4 showed a more pinched hysteretic loops than those of wall RW5. This was attributed to the effect of CFRP wrapping on controlling concrete cracks and decreasing the pinching effect in RW5 response.
7- The use of clamping steel plates as an anchoring system for the bottom edge of the web CFRP wrapping system prevented debonding at the bottom edge of CFRP and localized the damage near the bottom of end column zones. In addition, it increased the number of stable ductile loading cycles to almost a ductility level of almost 10, which corresponded to drift ratio of 3.0 %.
8- The use of the ±45° steel shear reinforcement controlled the diagonal shear cracks and as a result the damage was localized in the bottom third of the wall's height.
9- The use of steel anchor bolts as anchoring system for confinement CFRP wraps was successful in creating well confined end columns for the

rehabilitated walls. They closed the hoop of the U-shaped CFRP end column confinement.

10- The design practice based on CSA A23.3 (2004) code specifications does not recognize the effect of the flexural reinforcement ratio on the need for confinement of the end column element of RC structural walls which may lead to nominal ductile response.

11- To calculate the total design shear, all contributions from different constituent materials need to be considered. The following inequality was used to calculate the total shear capacity of RC structural walls (CSA, S806, 2002, Eq. 12.2):

$$V_n \le V_c + V_s + V_f \le V_c + 0.6\varphi_c \sqrt{f'_c} b_w d \qquad (5.1)$$

Where,

V_n = nominal shear strength of the wall

V_c = concrete shear strength contribution from CSA A23.3, Eq. 11.6:

$$V_c = \phi_c \lambda \beta \sqrt{f'_c} b_w d_v \qquad (5.2)$$

$$\beta = 0.18\ , \qquad \phi_c = 1.0, \qquad \lambda = 1.0 \qquad (5.3)$$

$$\sqrt{f'_c} \le 8\ MPa \qquad (5.4)$$

V_s = shear strength from shear reinforcement contribution per Eq. 11.7, CSA A23.3:

$$V_s = \frac{\phi_s A_v f_y d_v \cot\theta}{s} \qquad (5.5)$$

$$\theta = 35^\circ\ , \qquad \phi_s = 1.0 \qquad (5.6)$$

f_y = transverse reinforcement yield strength (5.7)

s = shear reinforcement spacing

V_f = shear strength from CFRP contribution,

$V_f = n_{layer} \times m_{face}\, \varphi_f\, f_{fd}\, t_j\, l_w$ (CSA, S806, 2002, Eq. 11.22)

$f_{fd} = 0.4\, f_{fu} = 0.4 \times \varepsilon_{fu} \times E_f$ (CSA, S806, 2002, Eq. 12.5)

ε =0.004 (maximum allowable strain for shear per ICBO-AC125, 2001)

$E_f = 78\,GPa$ for Tyfo SCH-35, and $E_f = 65\,GPa$ for Tyfo BBC-51

t_f = CFRP wrap thickness in mm,

l_w = the wall length in mm

ϕ_f = resistance factor for CFRP composites

n_{layer} = number of CFRP layers

m_{face} = 1 for single sided CFRP wrap and 2 for two-sided CFRP wrap.

Peak-to-peak lateral stiffnesses of the tested walls are presented in Table 5.1 and Figure 5.2. The wall stiffness given in Table 5.1 was compared with stiffness of the wall as suggested by CSA A23.3 (2004). Based on concrete cylinders compression strength test results, the concrete compression strength f'_c was 38 MPa. The design standard CSA A23.3 clause 8.6.2.3 suggests that the modulus of elasticity of concrete E_c is 2.774 $\times 10^7$ kN/m^2. Therefore, the initial uncracked rigidity of the wall E_cI_g is 2.774 $\times 10^5$ kN/m^2, and CSA A23.3-04 clause 10.14.1.2 suggests that 0.7 of the gross rigidity to be used as the uncracked rigidity and 0.35 of the gross rigidity to be used as the cracked rigidity. Observations from test results as shown in Figure 5.2 and Table 5.1 indicate that the measured stiffness is continuously decreasing with lateral drift ratio increase. Comparison between the measured stiffness and that suggested by the design Code indicated that the wall stiffness suggested by the Code is higher than the measured value. For example, Figure 5.2 shows that the cracked stiffness was 200 kN/mm at drift ratio of 0.2% and approximately 100 kN/mm at first yield of flexural reinforcement. This indicated that the wall rigidity decreased from 0.32 to 0.16 of the gross rigidity, respectively. In addition, past the first yield, the measured wall stiffnesses were continuously deteriorating. Moreover, it was observed that CW2 and CW3 suffered from high stiffness degradation rate, and exhibited brittle response. This was due to the brittle nature of the bond slip

failure of the lap splices. Walls with CFRP wrapping showed slow stiffness degradation and showed almost the same pattern of stiffness degradation rate as shown in Figures 5.9 to 5.12.

5.3.2 Energy dissipation

The energy dissipated by each of the tested walls was calculated as the area enclosed by the load-displacement hysteretic loops. Figure 5.3 shows the cumulative energy dissipated by the tested walls plotted against the lateral drift ratio. Walls RW6 and RW7 reached the highest capacity and ductility. The walls also showed the highest cumulative energy dissipation among all tested walls. On the other hand, walls CW2 and CW3 showed no ductile response and hence provided no significant cumulative energy dissipation. Tested walls with CFRP rehabilitation technique showed improvement in the energy dissipation as compared to those without CFRP wrapping. This was clear from the comparion between the cumulative energy dissipated by RW4 with that dissipated by wall RW5. Figures 5.13 to 5.16 show the cumulative energy dissipated by the tested walls.

5.3.3 Load-longitudinal strains relationship

No yielding of the longitudinal reinforcement was detected for walls CW2 and CW3. The reason for this was the premature wall failure due to bond slip. Rehabilitated walls RW3 to RW9 exhibited high plastic strains before rupture of some longitudinal reinforcement bars. The entire length of the longitudinal flexural rebars in the end column yielded during the tests.

5.3.4 Load-transverse strains relationship

Test walls CW2 and CW3 failed by bond slip before the adequacy of the provided shear reinforcement was tested. The transverse shear reinforcement was on the verge of yielding. Rehabilitated walls RW3 to RW9 exhibited higher shear forces compared to CW2 and CW3, and no yielding of the transverse reinforcement was observed. This confirms that the rehabilitation techniques were successful in providing the desired high ductility and suppressing the undesirable brittle failure modes.

5.3.5 Load-shear deformation relationship

The shear and flexural strengths of RW6 and RW7 are the highest of the rehabilitated walls, while those observed from RW3 to RW5 were the lowest, and RW8 and RW9 showed intermediate capacity compared to the seven rehabilitated walls. In addition, all of the rehabilitated walls showed significant strength and lateral drift ratio increase over the control walls CW2 and CW3.

Table 5. 1 Experimentally measured peak to peak lateral stiffness in kN/mm

Wall	cycle	$0.5\Delta_y$	Δ_y	$1.5\Delta_y$	$2\Delta_y$	$3\Delta_y$	$4\Delta_y$	$5\Delta_y$	$6\Delta_y$	$7\Delta_y$	$8\Delta_y$	$9\Delta_y$	$10\Delta_y$	$11\Delta_y$	$12\Delta_y$	$13\Delta_y$
CW2	1st	49	NA													
CW3	1st	96	NA													
RW3	1st	58	55	52	46	35	27	21	16	13.5	7.3	NA				
	2nd	58	54	51	45	33	25	18	15	12	7	NA				
RW4	1st	98	86	70	58	40	30	21	11.5	NA						
	2nd	98	86	69	53	37	28	18	8	NA						
RW5	1st	109	98	80	67	49	38	31	24	16	11	9	6	NA		
	2nd	109	97	78	65	47	36	29	23	15	10	7.5	4.5	NA		
RW6	1st	111	105	93	78	56	43	34	29	24	21	18	15.5	12.5	10	4.5
	2nd	111	105	90.6	75	52.7	40.3	32.5	27	23	19	17	14	11.7	9	3.9
RW7	1st	137	114	98	77	55	42	34	27	22	18	16	11	9	6	3.7
	2nd	137	112	90	73	53	40	31.5	25	20.4	16.9	14	9.8	7.2	5.9	3.1
RW8	1st	150	114	93	77	56	46	34	28	20.4	10.8	4.3	NA			
	2nd	150	114	91	74.5	52.7	40.2	32.4	26.4	19.6	6.3	3.7	NA			
RW9	1st	100	86	66	56	41	31	24	20	14	9.5	7	5	3.7	NA	
	2nd	100	82	62.6	53.9	38.6	28.8	22.7	16.6	11.3	8	5.8	4.2	3.3	NA	

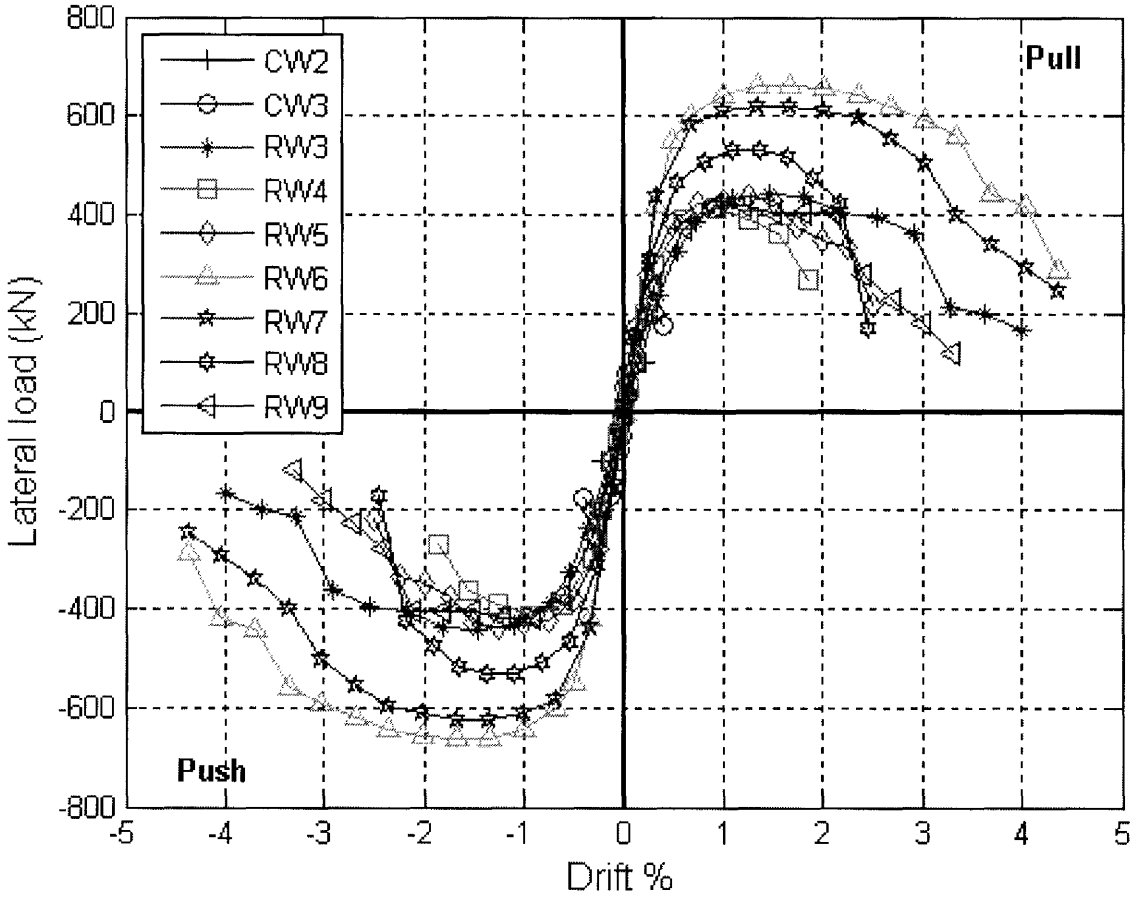

Figure 5. 1 Envelope for lateral load- lateral drift relationship

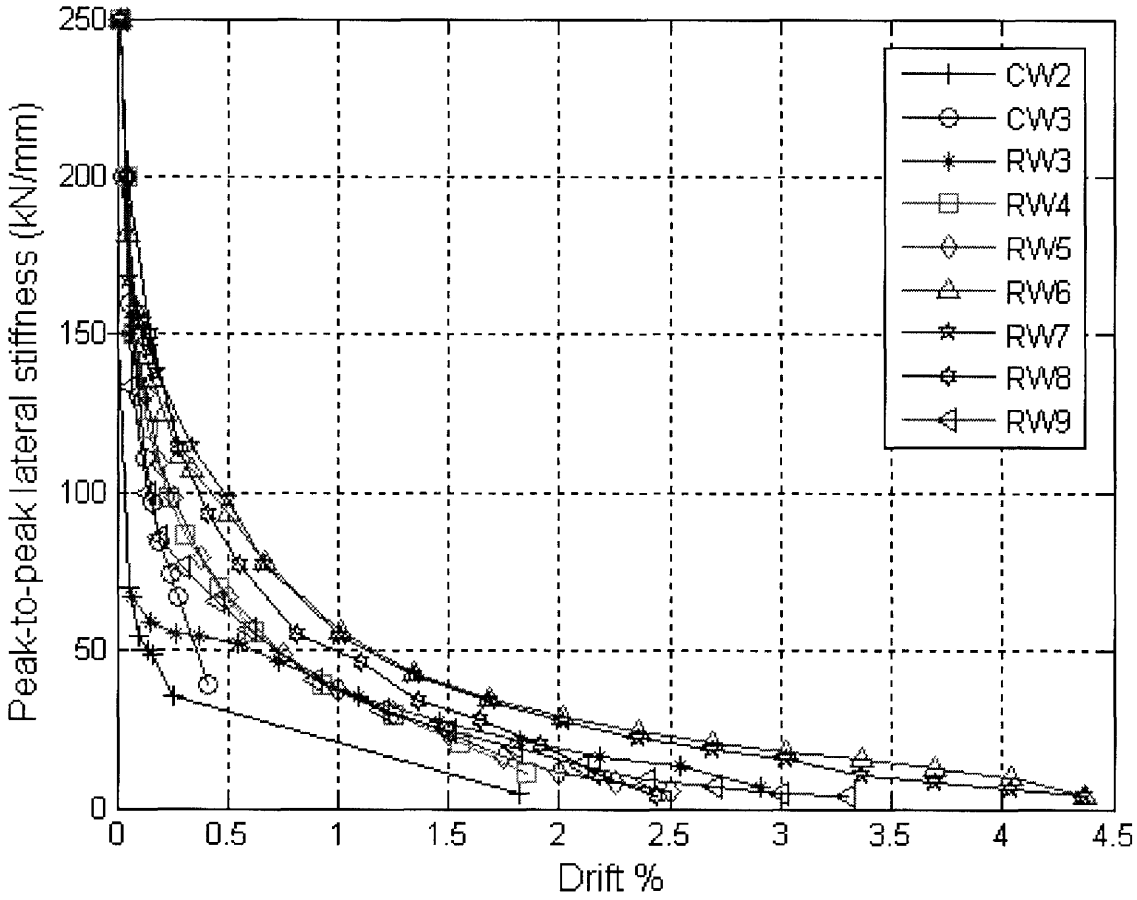

Figure 5. 2 Peak-to-peak lateral stiffness-lateral drift ratio relationship for all tested walls

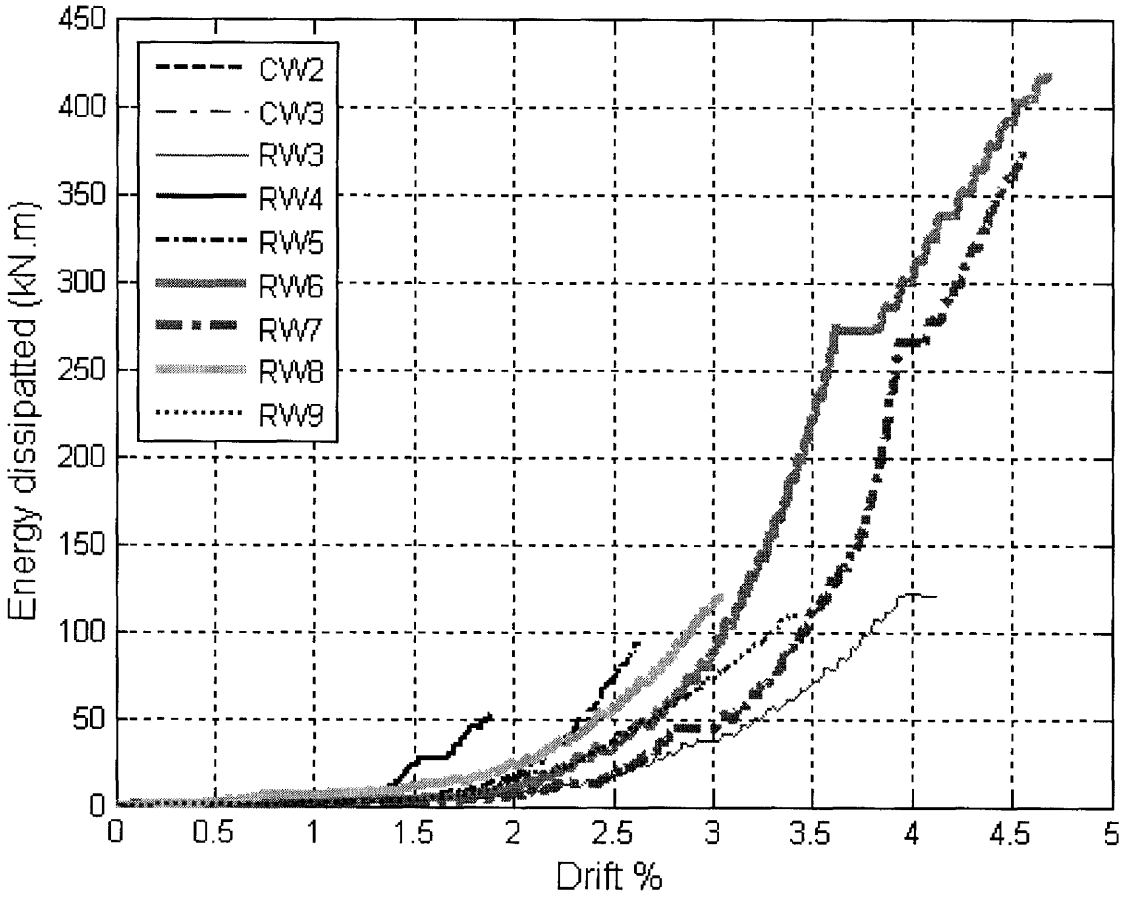

Figure 5. 3 Cumulative energy dissipation of tested walls

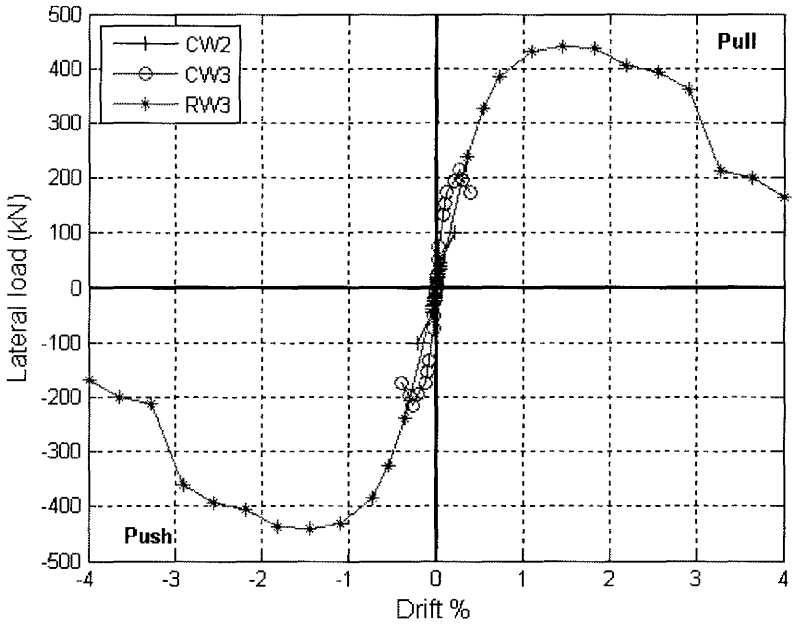

Figure 5. 4 Walls CW2, CW3, and RW3 envelopes for the base shear-drift relationship

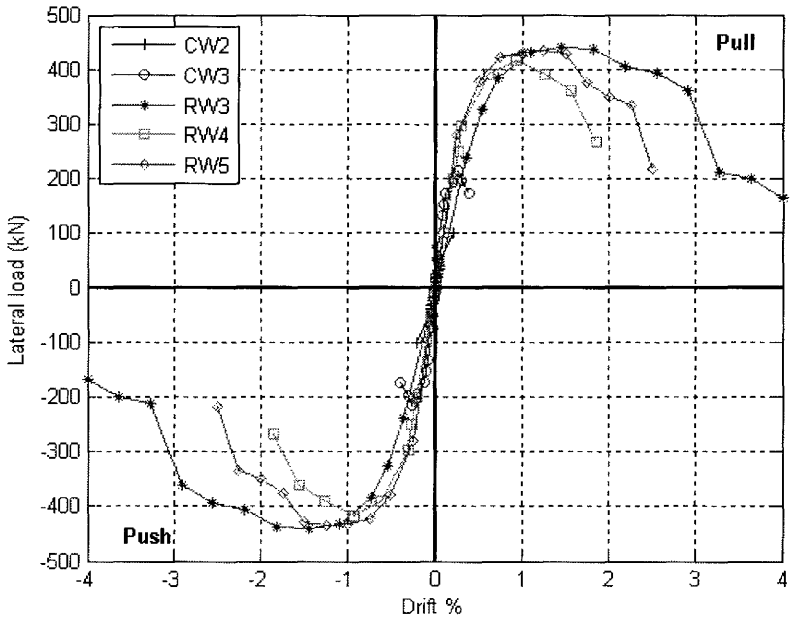

Figure 5. 5 Walls CW2 to RW5 envelopes for the lateral load- drift relationship

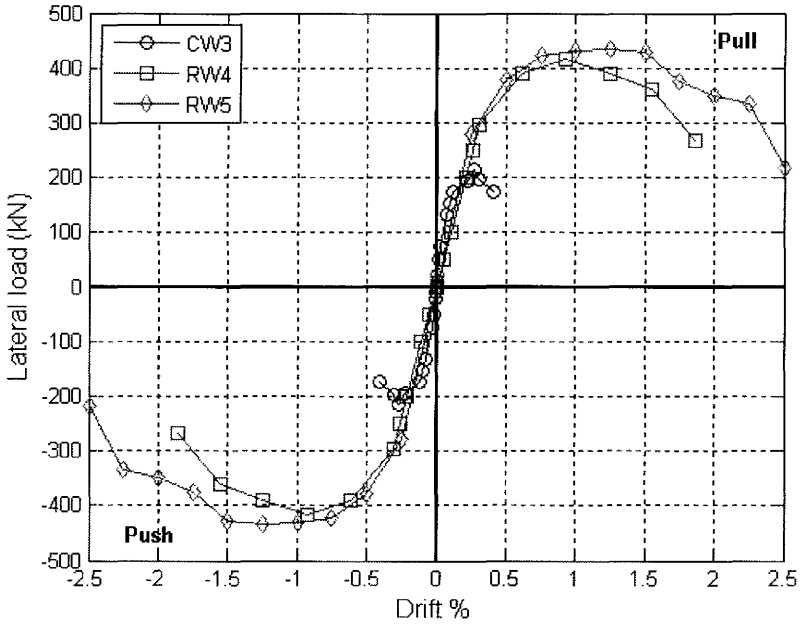

Figure 5. 6 Walls CW3, RW4 and RW5 envelopes for the lateral load- drift relationship

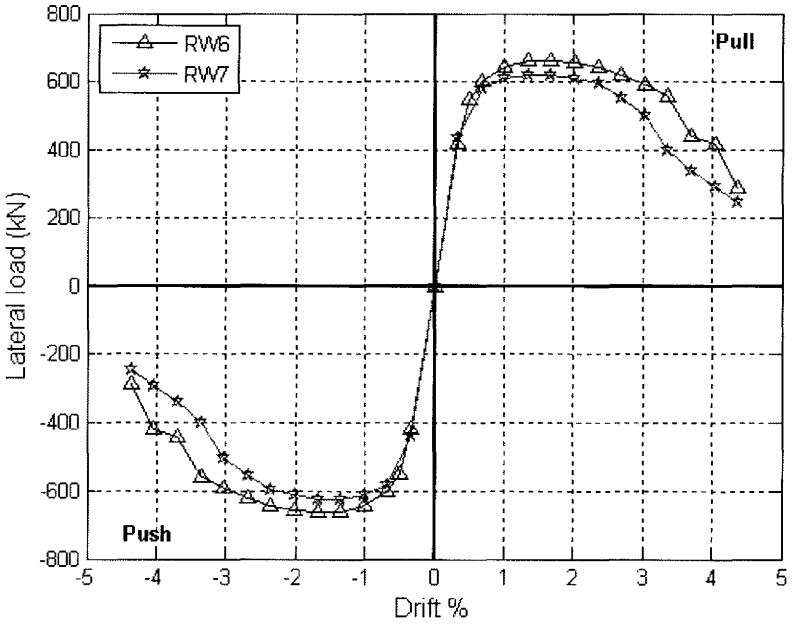

Figure 5. 7 Walls RW6 and RW7 envelopes for the lateral load- drift relationship

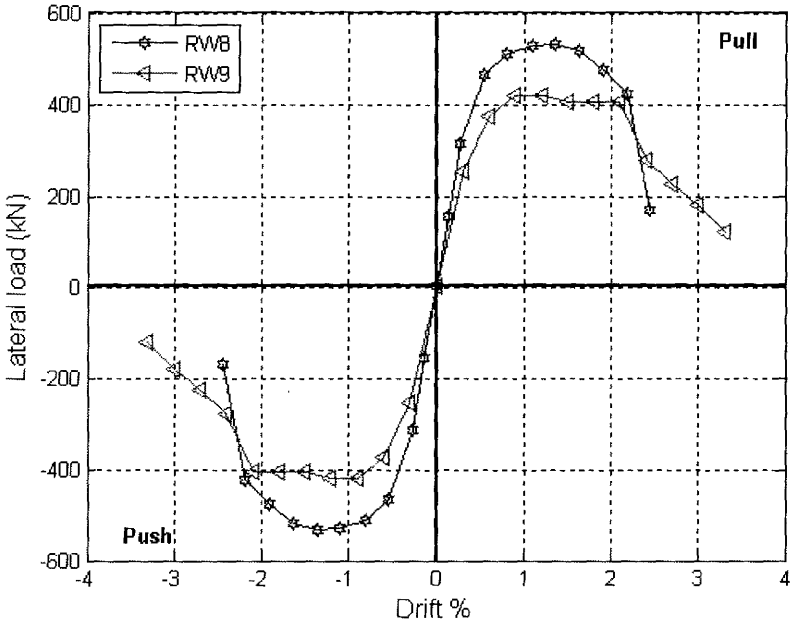

Figure 5. 8 Walls RW8 and RW9 envelopes for the lateral load- drift relationship

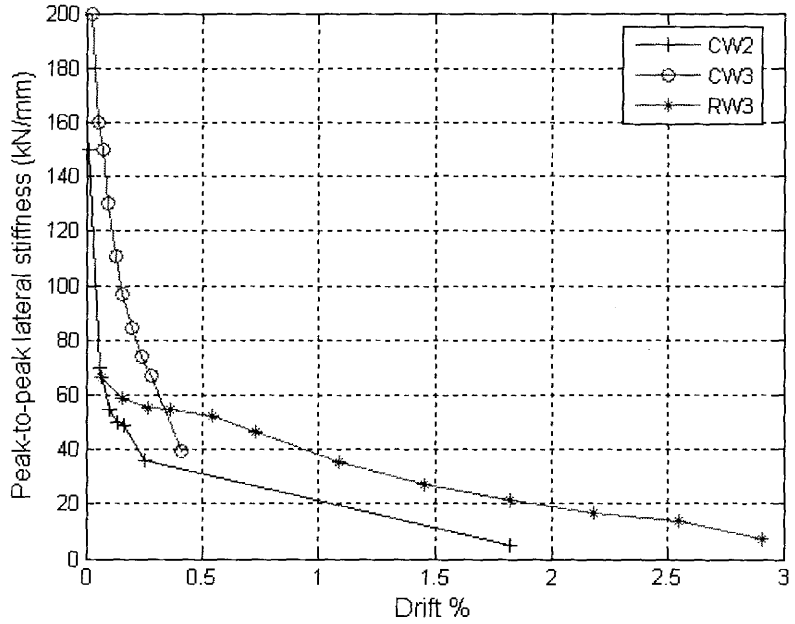

Figure 5. 9 Peak-to-peak lateral stiffness variation with drift for CW2, CW3, and RW3

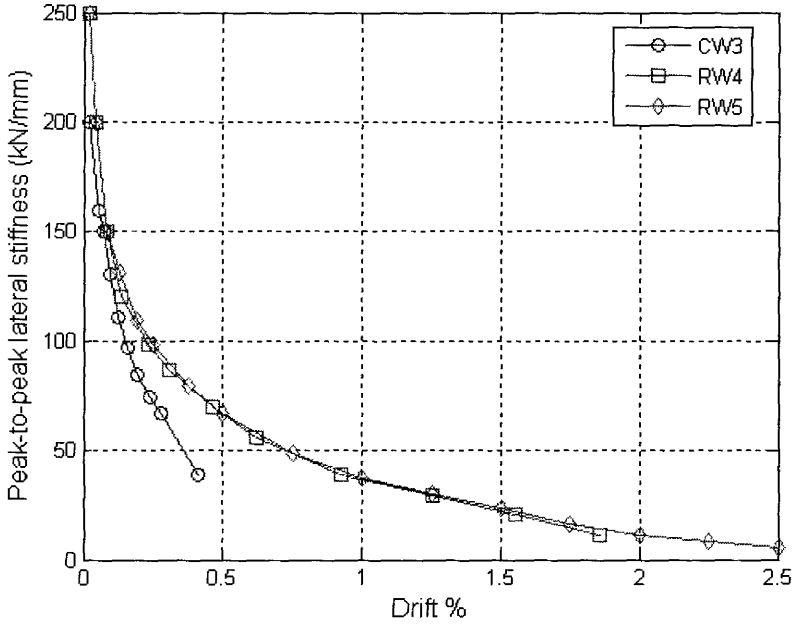

Figure 5. 10 Peak-to-peak lateral stiffness variation with drift for CW2, RW4, and RW5

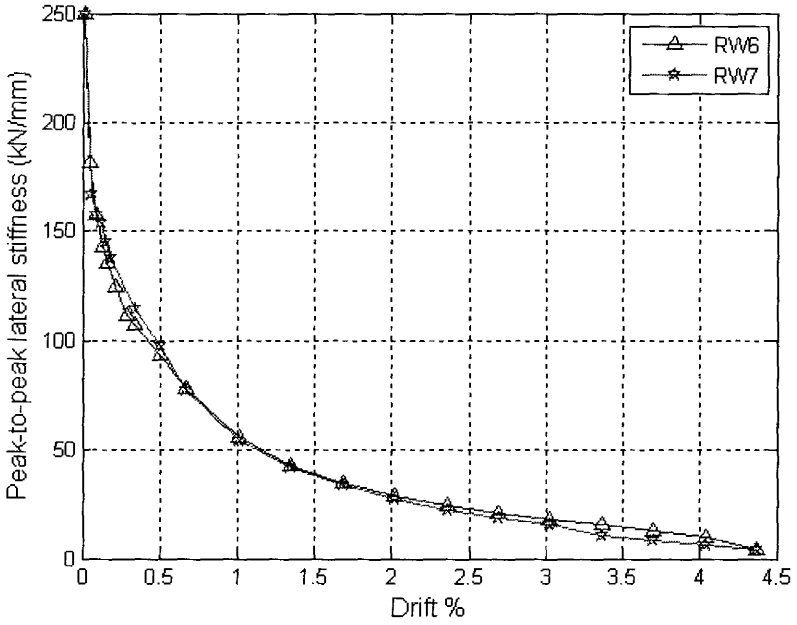

Figure 5. 11 Peak-to-peak lateral stiffness variation with drift for walls RW6, RW7

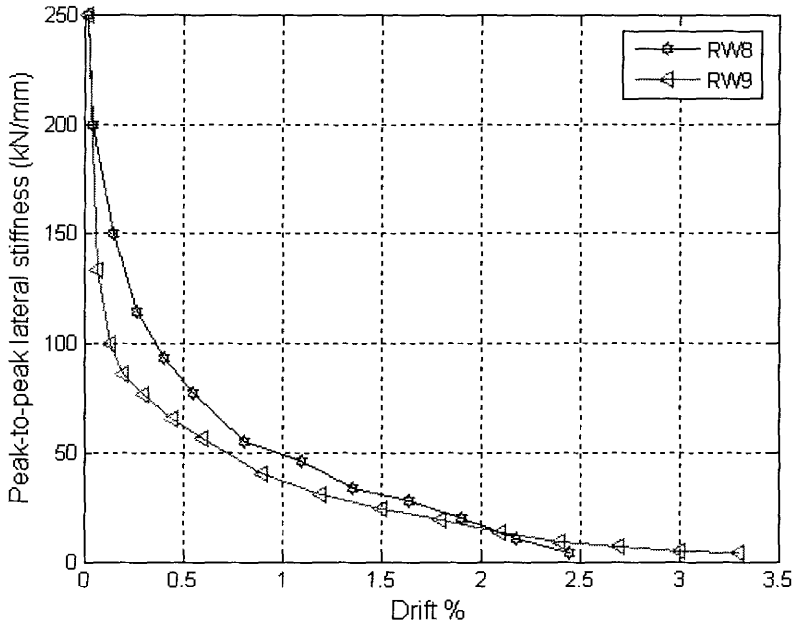

Figure 5. 12 Peak-to-peak lateral stiffness variation with drift for walls RW8, RW9

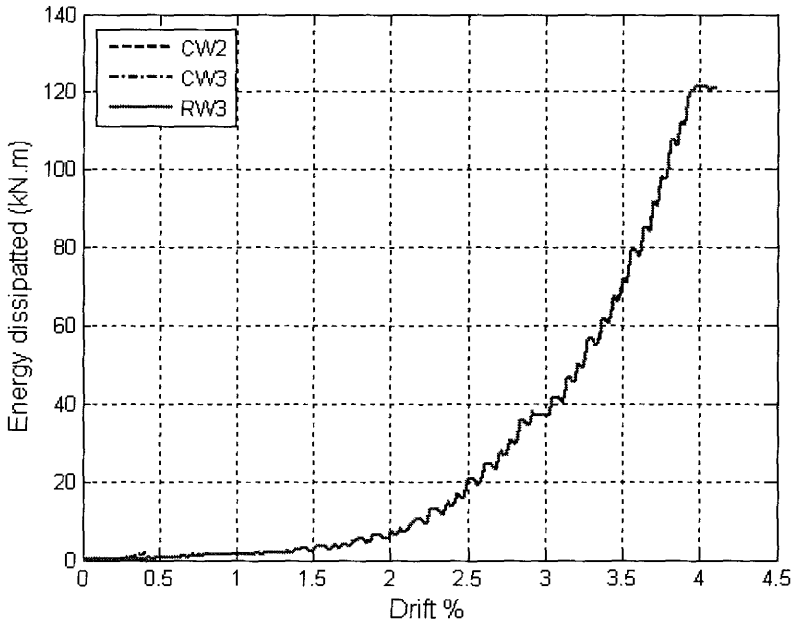

Figure 5. 13 Cumulative energy dissipation of walls CW2, CW3, and RW3

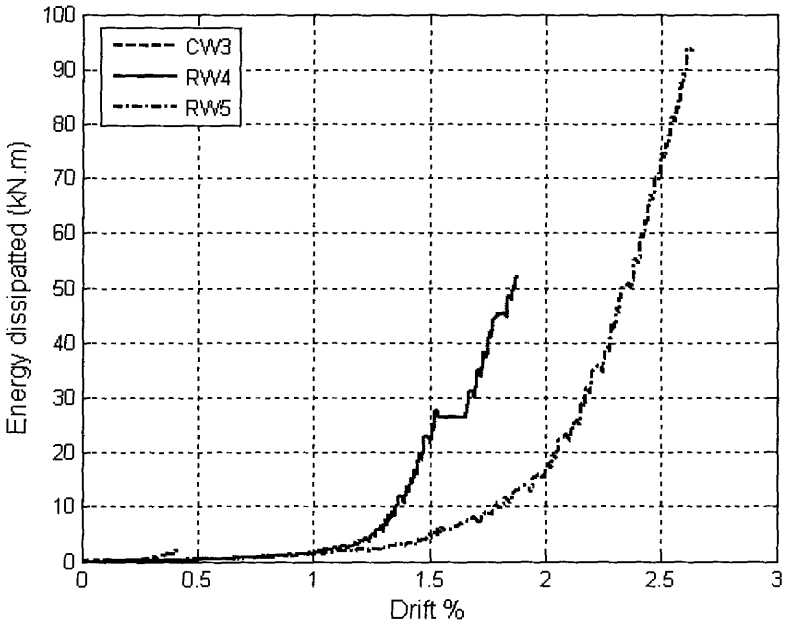

Figure 5. 14 Cumulative energy dissipation of walls CW3, RW4, and RW5

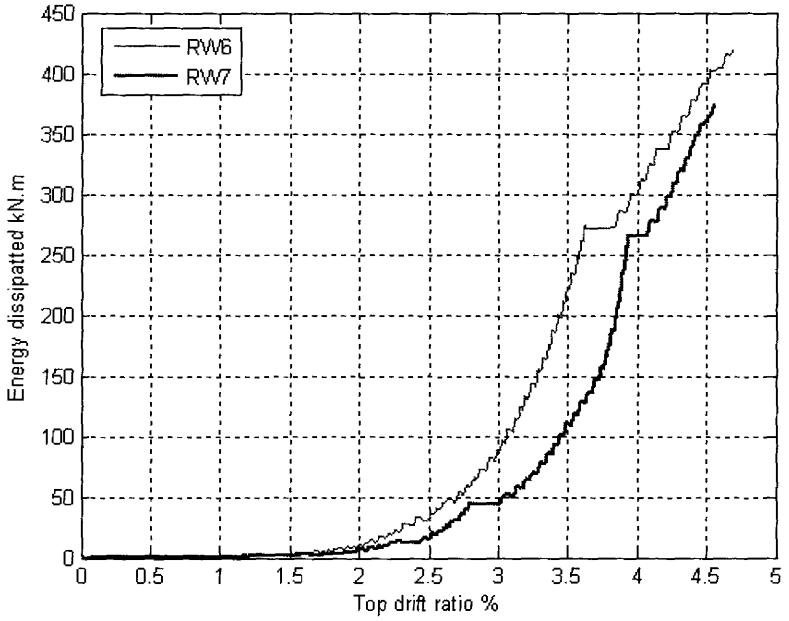

Figure 5. 15 Cumulative energy dissipation of walls RW6, RW7

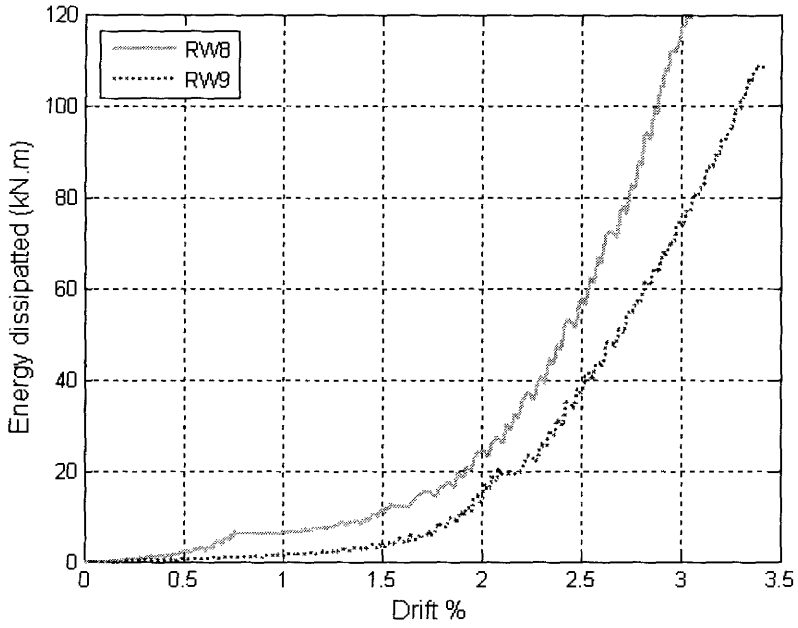

Figure 5. 16 Cumulative energy dissipation of walls RW8, RW9

CHAPTER 6

ANALYTICAL MODEL

6.1 INTRODUCTION

The development of a macroscopic model to represent the behaviour of reinforced concrete structural walls when subjected to static or dynamic loads is described in this chapter. The proposed model is intended to adequately describe the hysteretic behaviour of reinforced concrete wall elements and to be capable of accurately predicting both flexural and shear components of inelastic deformation.

The approach to develop the analytical model was verified by comparing the model results with the experimental results. Cyclic tests result included the hysteretic moment-rotation, shear force-shear deformation, and shear force-lateral displacement relationships. Using cyclic loading test results as a verification of the input to the model parameters ensures that the earthquake dynamic loads are simulated by the analysis.

The use of micro models and finite element models for seismic analysis of a multistory reinforced concrete structure is a time-consuming and complex task, (Ghobarah and Youssef 1999). On the other hand, macro modeling that permits efficient seismic analysis of the multistory RC structural wall is simpler and justified modeling scheme. Therefore, programs such as IDARC2D (Valles et al., 1996), DRAIN-2DX (Prakash and Powell 1993), and OpenSees (Mazzoni et al., 2007), have been used widely for the seismic analysis of structures especially for research purposes. The main advantages of these programs are their simplicity, speed of analysis and the capability to model and analyze a large structure.

To analytically reproduce the response of the tested walls', a model of RC structural walls was developed and implemented into two nonlinear analysis programs. The open source for seismic and earthquake engineering software, OpenSees version 1.74

(2007) and IDARC2D version 6.1 (2006) were used to simulate the tested walls response for verification and comparison between analysis and experimental results. The IDARC2D software is used for inelastic damage analyses of reinforced concrete framed-walls buildings. OpenSees version 1.74 (2007) analysis software was selected because it incorporates a large library of nonlinear material models, which is suitable for fast and simple yet accurate analysis of RC structural walls. IDARC2D version 6.1 (2006) software provides inelastic analysis, and nonlinear damage measurement throughout the analysis. The damage model developed by Park and Ang (1985) was incorporated in IDARC2D to measure the accumulated damage for each structural component at each story level and for the entire structure. Both programs incorporate hysteretic models controlled by parameters that model the stiffness degradation, strength deterioration, and pinching of the hysteretic loops.

6.2 MATERIAL MODELS

The hysteretic rules defining the cyclic force-displacement curves of concrete and reinforcement steel are described in the following sections. Strength degradation and concrete model strength softening due to concrete crushing as well as steel model strength softening due to bond slip failure were used.

6.2.1 Concrete models

The relationship between the force and the deformation (displacement) of the spring representing the concrete constitutes the concrete model. The concrete may be subjected to compression or tension stresses. In this study, the concrete compression envelope proposed by Popovics (1973) for unconfined concrete elements and modified by Mander et al. (1988) for steel-confined concrete elements were adopted. Model of CFRP sheets-confined concrete walls was included in analysis. In the following subsections, the unconfined and confined concrete compression envelopes and the concrete tension envelope are presented.

6.2.1.1 Concrete tension envelope

A linear stress-strain relationship was assumed for concrete in tension until cracking. The element response after cracking depends on the reinforcement ratio in the section. For an unreinforced member, the concrete tensile strength rapidly reduces to zero. The average remaining tensile stress transferred to the concrete after cracking of a member is a function of the bond characteristics between the concrete and steel. This remaining tensile strength is known as tension stiffening.

The concrete tensile stress f_{ct}-strain ε_c relationship, is written as:

$$f_{ct} = E_c \varepsilon_c \tag{6. 1}$$

where E_c is the concrete elastic modulus, and ε_c is the tensile strain

The tension stiffening relationship developed by Stevens et al. (1987) was used in this study. The relationship between the concrete tensile strain and normalized tensile stress is shown in Figure 6.1. The concrete tensile stress f_{ct} is related to tensile strain ε_c by the expression:

$$f_{ct} = f_{cr}\left((1-\alpha_t)e^{-\lambda_t(\varepsilon_c-\varepsilon_{cr})} + \alpha_t\right) \tag{6. 2}$$

where f_{cr} is the concrete cracking strength, α_t is a factor that defines the residual concrete tensile strength and λ_t is a factor that controls the decay rate of the response. These factors were given as:

$$f_{cr} = 0.33\sqrt{f'_c} \tag{6. 3}$$

$$\alpha_t = 75\rho_x / d_b \tag{6. 4}$$

$$\lambda_t = 270/\sqrt{\alpha_t} \leq 1000 \tag{6. 5}$$

where, d_b is the longitudinal bar diameter and ρ_x is the longitudinal steel ratio.

Equation (6.4) gives the value of α_t for the case of axial tensile stresses. In case of bi-directional loading, where the principal tensile stress is inclined to the reinforcement bars in x-direction by an angle θ, then:

$$\alpha_t = \cos^2\theta\,\alpha_{tx} + \sin^2\theta\,\alpha_{ty} \qquad (6.6)$$

Where $\alpha_{tx} = 75\rho_x / d_b$ and $\alpha_{ty} = 75\rho_y / d_b$, ρ_x, ρ_y are the reinforcement ratios in x and y directions, respectively.

6.2.1.2 Envelope of concrete compression confined with steel ties

The response of concrete elements changes significantly under confining lateral pressure. The confining pressure is created because of the lateral dilation of concrete section. For steel-confined concrete, the confining pressure increases until a constant confining pressure, which corresponds to the yield stress of the steel ties, is developed (Mander et al., 1988).

The monotonic concrete compression response follows the model of Popovics, (1973) was the basis for the formulation of the Mander's model (Mander et al., 1988). Popovics model defines the complete behaviour of unconfined concrete under compression including the softening part of the response using one simple formula. The concrete stress f_c that correspond to concrete strain ε_c is given as:

$$f_c = \frac{f'_c \, x \, r}{r - 1 + x^r} \qquad (6.7)$$

where

$$x = \frac{\varepsilon_c}{\varepsilon_o} \qquad (6.8)$$

and

$$r = \frac{E_c}{E_c - E_{sec}} \qquad (6.9)$$

where ε_o is the concrete strain at the peak compressive stress f'_c, E_c is the initial concrete modulus of elasticity and E_{sec} is the secant concrete stiffness at the ultimate concrete strength. Typical values of ε_o and E_c are -0.002 and $5000\sqrt{f'_c}$, respectively.

The ultimate confined concrete strength f'_{cc} was related to the confining stress f'_l due to the confinement ties, as:

$$f'_{cc} = f'_c\left(2.254\sqrt{1+\frac{7.94f'_l}{f'_c}}-2\frac{f'_l}{f'_c}-1.254\right) \quad (6.10)$$

where ε_{cc} is the corresponding concrete strain as given by:

$$\varepsilon_{cc} = \varepsilon_o\left[1+5\left(\frac{f'_{cc}}{f'_c}-1\right)\right] \quad (6.11)$$

the yield stress of the steel ties f_{yh}, the confinement effectiveness coefficient, k_e and the transverse reinforcement ratio ρ_s were related to the confining stress f'_l by the equation:

$$f'_l = k_e f_{yh}\rho_s \quad (6.12)$$

Therefore, the concrete stress-strain relationship for the confined concrete is:

$$f_c = \frac{f'_{cc}\, x\, r}{r-1+x^r} \quad (6.13)$$

where

$$x = \frac{\varepsilon_c}{\varepsilon_{cc}} \quad (6.14)$$

Cross section shape effect on the confinement efficiency of the concrete was taken into account by the confinement effectiveness coefficient k_e, (Mander et al., 1988).

6.2.1.3 Envelope of concrete compression confined with FRP sheets

FRP confinement applies an increasing confining pressure up to failure. This is due to the elastic behaviour of the FRP materials. Therefore, the interaction between the CFRP confinement and the concrete section need to be considered until failure of the CFRP wrapping.

Most of the available analytical models focused on circular concrete sections, rather than square or rectangular sections (Samaan et al., 1998; Spoelstra and Monti, 1999; Fam and Rizkalla, 2001; Assa et al., 2001; and Wang and Restrepo, 2001). El-Amoury

(2004) proposed a model to predict the response of rectangular concrete sections confined with CFRP sheets and subjected to a monotonic axial compressive stress for concrete joints panels. El-Amoury used Mander et al. (1988) model for steel confined concrete to represent the FRP confinement in a manner similar to the steel ties. The confinement analysis for the walls needs to be developed due to the lack of available models. Since they are the most stressed parts of the wall, end zone columns need adequate confinement. For end zone confined concrete with steel ties, the same model of Mander et al. (1988) for confined concrete by assuming constant confinement pressure, can be used. For FRP confinement, the confining pressure increases linearly until FRP failure. The lateral strain compatibility between the CFRP jacket and the concrete section is considered and a constant concrete Poisson's ratio was assumed.

Under axial stress ε_c, the unconfined concrete section deforms laterally in the form:

$$\varepsilon_x = \nu_c \varepsilon_c \tag{6. 15}$$

where ε_x is the lateral concrete strain in x-direction, ε_c is the axial concrete strain and ν_c is Poisson's ratio of the concrete.

Thus, the unrestrained lateral deformations in x and y directions, u_{xf} and u_{yf}, respectively, as shown in Figure 6.2a, are:

$$u_{xf} = \nu_c b_x \varepsilon_c \text{ and } u_{yf} = \nu_c b_y \varepsilon_c \tag{6. 16}$$

where b_x and b_y are the section dimensions in x and y directions, respectively.

Composite CFRP jacket applies confinement lateral pressure by arching action at the corner of rectangular section. Chamfering edges to an appropriate diameter is necessary for better distribution of the compression stresses and for minimizing the stress concentration in the FRP jacket. An appropriate choice of the arching angle must to be made to calculate the effective confined section. Mander et al. (1988) assumed an arching angle value of 45° for steel-confined concrete sections. Wang and Restrepo, (2001) reported that a suitable arching angle for CFRP-confined sections varies between 42° and

47°; depending on the number of plies and they suggested that an average value of 45° for the arching angle. In this study, the concentrated corner confining pressure was distributed as uniform lateral pressure along the end zone sides. The end zone dimensions were assumed equal to the area enclosed by the U shaped CFRP jacket and the steel anchors. Thus, the confining lateral pressure, as shown in Figure 6.2b, is given by the formula:

$$\sigma_x = 2\sigma_r \frac{r_c}{b_y} \quad \text{and} \quad \sigma_y = 2\sigma_r \frac{r_c}{b_x} \tag{6. 17}$$

where σ_x, σ_y and σ_r are the confining lateral pressure in x, y and radial directions, respectively, and r_c is the chamfer radius.

The sectional lateral displacement u_{xr} and u_{yr}, can be estimated by the expressions:

$$u_{xr} = \frac{2\sigma_r r_c}{E_c}\left(\frac{1}{b_y} - \frac{\nu_c}{b_x}\right)b_x \quad \text{and} \quad u_{yr} = \frac{2\sigma_r r_c}{E_c}\left(\frac{1}{b_x} - \frac{\nu_c}{b_y}\right)b_y \tag{6. 18}$$

where E_c is the concrete modulus of elasticity.

The tensile stress induced in the jacket, σ_j due to the lateral pressure at the corner, as shown in Figure 6.2d, is:

$$\sigma_j = \sigma_r \frac{r_c}{t_j} \tag{6. 19}$$

where t_j is the CFRP jacket thickness, and equals the thickness of one FRP sheet multiplied by the number of layers.

The lateral deformation of the jacket due to this lateral pressure, u_{xj}, as shown in Figure 6.2c, is:

$$u_{xj} = \frac{\sigma_r r_c}{E_j t_j} b_x \tag{6. 20}$$

To estimate the lateral confinement pressure, the lateral displacement compatibility is considered. The compatibility equation is written as:

$$u_{xf} - u_{xr} = u_{xj} \tag{6. 21}$$

Thus, the confinement pressure equals:

$$\sigma_r = \frac{\nu_c}{\frac{r_c}{E_j t_j} + \frac{2r_c}{E_c}\left(\frac{1}{b_x} - \frac{\nu_c}{b_y}\right)} \varepsilon_c \tag{6. 22}$$

The evaluation of Poisson's ratio is a challenge for using this technique because it varies with the levels of imposed axial strain and the corresponding confinement pressure. Several researchers attempted to make realistic prediction of this ratio. For example, Wang and Restrepo (2001), reported a constant average Poisson's ratio for evaluating the confinement pressure. Fam and Rizkalla (2001) employed simple regression analysis to predict Poisson's ratio at different constant confining hydrostatic pressure. An empirical formula was suggested by Spoelstra and Monti (1999) to evaluate the lateral concrete deformation using empirical formulas. A conservative estimate of Poisson's ratio was made for the purpose of this study. Poisson's ratio of 0.50 was used to cover most of axial strain values as suggested by Wang and Restrepo (2001).

The effectiveness of the FRP confinement jacket was considered by a confinement efficiency factor k_e as:

$$k_e = 1 - \frac{\sum_i w_i^2}{6 b_x b_y} \tag{6. 23}$$

where w_i is the length of unconfined region in the concrete section, as shown in Figure 6.2e.

Thus, the confined concrete strength, using Mander et al. (1988) model and taking into account the effect of FRP confinement becomes:

$$f'_{cc} = f'_c\left(2.254\sqrt{1+\frac{7.94\,k_e\left(2\frac{r_c}{b_x}\sigma_r\right)}{f'_c}}-2\frac{k_e\left(2\frac{2r_c}{b_x}\sigma_r\right)}{f'_c}-1.254\right) \quad (6.24)$$

and the corresponding concrete strain ε_{cc} is given as:

$$\varepsilon_{cc} = \varepsilon_o\left[1+5\left(\frac{f'_{cc}}{f'_c}-1\right)\right] \quad (6.25)$$

where f'_c is the unconfined concrete strength and ε_o is the corresponding strain.

Hence, the concrete stress f_c that corresponds to a certain strain ε_c is given by Equation (6.13). The stress-strain relationships for unconfined and confined concrete are shown in Figure 6.3. Figure 6.4 shows the stress-strain relationships for unconfined, steel ties confined, and CFRP confined concrete with the unconfined concrete strength from concrete cylinder compression tests, f'_c of 38 MPa.

6.2.2 Reinforcement steel model

The steel model refers to the relationship between the force and deformation in the steel bars. The bar extension and bar anchorage-slip of an embedded bar in concrete element are the main sources of steel spring inelasticity as well as the bond law between the steel rebar and concrete.

Several researchers investigated the bond-slip behaviour of steel bars embedded in concrete experimentally (Marques and Jirsa, 1975; Viwathanatepa et al., 1979; Soroushian et al., 1988; Soroushian and Choi, 1989; Soroushian et al., 1991a). In addition, several analytical models were developed to predict the bond stress-slip relationship of steel bars embedded in concrete (Ciampi et al., 1982; Filippou et al., 1983; Soroushian and Choi, 1991; Soroushian et al., 1991b; Alsiwat and Saatcioglu, 1992; Monti et al., 1997; Youssef, 2000; Galal 2002, El-Amoury, 2004; and Khalil, 2005). The model developed by Alsiwat and Saatcioglu, (1992) was used to establish the monotonic envelope between force-

deformation of steel bars embedded in concrete. This model results correlates well with the experimental results (Galal 2002, El-Amoury, 2004; and Khalil, 2005). Because of its simplicity and reasonable accuracy, El-Amoury, 2004 model is used in this study to plot the monotonic response of embedded steel bars. El-Amoury model is the same as Saatcioglu, (1992) model but with minor refinements.

6.2.2.1 Material constitutive relationships

The bond law of steel bar embedded in concrete can be described by the relationship between local bond stress, τ, and local relative displacement of the bar with respect to the concrete (slip), s. The steel bar diameter, the distribution of the lugs on the bar circumferential surface, the spacing between the longitudinal bars, the concrete tensile and compression strengths, the aggregate size, the level of axial load, the distribution and the diameter of the confining stirrups and the interaction between these factors contribute in complexity of defining the constitutive bond stress-slip relationship.

The bond stress -slip relationship is idealized, as shown in Figure 6.5, as:

$$\tau = \tau_1 \left(\frac{s}{s_1} \right)^a \qquad s < s_1 \qquad (6.26)$$

$$\tau = \tau_1 \qquad s_1 \le s < s_2 \qquad (6.27)$$

$$\tau = \tau_1 - \frac{(\tau_1 - \tau_3)}{(s_3 - s_2)}(s - s_2) \qquad s_2 \le s < s_3 \qquad (6.28)$$

$$\tau = \tau_3 \qquad s \ge s_3 \qquad (6.29)$$

Suggested values for these paramteres elsewhere, Eligehausen et al. (1983). The values were based on extensive experimental results of 25 mm diameter steel bar with clear bar spacing of $4d_b$. The concrete compression strength was 30 MPa.

To estimate the ultimate bond strength for different bar diameters and concrete strengths, a general equation was proposed by Soroushian et al. (1991b) as:

$$\tau_1 = (20 - d_b/4)\sqrt{\frac{f'_c}{30}} \qquad \text{in MPa} \qquad (6.30)$$

where d_b is the bar diameter in mm.

The frictional resistance of concrete, τ_3 is assumed related to the ultimate bond strength, τ_1 as:

$$\tau_3 = \tau_1 / 3 \qquad (6.31)$$

The slip values s_1 and s_2 are assumed dependent on the concrete compressive strength (Alsiwat and Saatcioglu, 1992), such that:

$$s_1 = \sqrt{\frac{30}{f'_c}} \qquad \text{in mm} \qquad (6.32)$$

$$s_2 = 3 s_1 \qquad (6.33)$$

The slip value s_3 is assumed equal to the clear spacing between the lugs in the bar.

A model that relates the bond stress along the hook length to the slip at the hook tip, that is similar to the bond-slip relationship of straight bars, was proposed (Filippou et al., 1983). A general model that relates the pullout force to the hook slip was also proposed (Soroushian et al., 1988). The model parameters are:

$$P_h = P_1 \left(\frac{s_h}{2.54} \right)^{0.2} \qquad (6.34)$$

$$P_1 = 271(0.05 d_b - 0.25) \qquad \text{in kN} \qquad (6.35)$$

$$P_3 = 0.54 P_1 \qquad (6.36)$$

$$s_{h1} = 2.54 \text{ mm} \qquad (6.37)$$

$$s_{h2} = 3\, s_{h1} \qquad \text{in kN} \qquad (6.38)$$

$$s_{h3} = 15\, s_{h1} \qquad (6.39)$$

Where P_h and s_h are the resistance of the hook and the slip at the tip of the hook, respectively. Figure 6.6 shows the model prediction.

A bilinear steel constitutive relationship with two slopes was assumed for steel bar anchored in concrete element. The first slope is up to the onset of yield strain and the second slope starts from yielding of the steel to the ultimate strength.

6.2.2.2 Proposed model

To predict the deformation of steel bars embedded in concrete elements under pull only, pull and push and hooked bars El-Amoury (2004) model was used. Refinements that El-Amoury made to to Alsiwat and Saatcioglu (1992) model included accounting for post-peak effects on bond stress-slip relationship. Figure 6.7 shows the main assumptions that were made by Alsiwat and Saatcioglu (1992), Galal (2002) and El-Amoury (2004) to model the bond stress-slip relationship.

Bar deformation consists of the bar extension δ_{ext}, and the anchorage-slip s. The extension of the steel bar is expressed as:

$$\delta_{ext} = \frac{\varepsilon_y l_e}{2} + \frac{(\varepsilon_s + \varepsilon_{sh}) l_{pl}}{2} \qquad (6.40)$$

where ε_y is the bar yield strain, l_e is the length of elastic part of the tensile bar, ε_s is the bar strain at the pull side of the bar, ε_{sh} is the bar strain hardening, l_{pl} is the length of the inelastic region of the tensile bar.

The bond stress is assumed constant along the length of each of the elastic and plastic subregions. For the elastic region, the average bond stress τ_e as proposed by ACI (1985) is:

$$\tau_e = \frac{f_y d_b}{4 l_d} \qquad (6.41)$$

$$l_d = \frac{440\, A_b}{3 d_b \sqrt{f_c'}} \frac{f_y}{400} \geq 300\, mm \qquad (6.42)$$

where f_y is the bar yield strength in MPa, d_b and l_d are the bar diameter and the bar development length in mm.

The length of the elastic region can be determined as:

$$l_e = \frac{f_y d_b}{4\tau_e} \quad (6.43)$$

The length of the plastic region can be determined as:

$$l_{pl} = \frac{(f_s - f_y)d_b}{4\tau_f} \quad (6.44)$$

$$\tau_f = (5.5 - 0.07\frac{S_L}{H_L})\sqrt{\frac{f_c'}{27.6}} \quad (6.45)$$

For most practical cases, $\tau_f = 5\sqrt{\frac{f_c'}{27.6}}$ (6.46)

Where, τ_f is the frictional bond stress in MPa (Galal, 2002), S_L and H_L are clear spacing of bar lugs and the clear height of the lugs, respectively.

The frictional bond stress can be assumed as a ratio of the ultimate bond strength τ_1 as indicated in Equation 6.30. By increasing the tension force at the bar pull side until the bar slip s equals to s_1, the following equations are used:

$$l_e' = l_{bar} - l_{pl} \quad (6.47)$$

$$\tau = \frac{f_y d_b}{4l_e'} \quad (6.48)$$

Then substite in local bond stress-slip relationship to obtain the bar slip s:

$$\tau = \tau_1\left(\frac{s}{s_1}\right)^a \qquad s < s_1 \quad (6.49)$$

Once slip occurred, the control is switched from force control to displacement control by applying incrementally increasing bar slip s at the cut off end. The slip was increased from S_1 to S_2 and the average bond stress was constant and equals to τ_1. Therefore,

$$l'_e = \frac{f_y d_b}{4\tau_1} \tag{6. 50}$$

By increasing the slip from S_2 to S_3, the average bond stress decreases from τ_1 to τ_3. Therefore,

$$l'_e = \frac{f_y d_b}{4\tau} \tag{6. 51}$$

$$\tau = \tau_1 - \frac{(\tau_1 - \tau_3)}{(s_3 - s_2)}(s - s_2) \qquad s_2 \le s < s_3 \tag{6. 52}$$

$$l_{pl} = l_{bar} - l'_e \tag{6.53}$$

Finally, the total bar displacement is equal to:

$$\delta_{bar} = \delta_{ext} + s \tag{6. 54}$$

The model predictions agree reasonably well with the experimental data (Galal, 2002; El-Amoury, 2004).

6.3 Structural Wall Shear Model

Several components contribute to the reinforced concrete structural walls shear load resistance. In the elastic range, the concrete can provide a considerable contribution to the lateral load resistance. The concrete contribution deteriorates with crack development and cyclic lateral load reversals. Therefore, the transverse reinforcement is essential to prevent brittle shear failure. Walls with external CFRP shear reinforcement have the additional shear resistance contribution of the FRP. These three shear resistance components behave in different manners under the same loading for the same structural element. For example, FRP behaves linearly up to failure. One other hand, the concrete shows a nonlinear response up to ultimate strain and its strength deteriorates after peak stress in several different ways according to the confinement level. The shear reinforcement behaves linearly up to yield and can be assumed to have isotropic strain hardening after that. These three materials contribute simultaneously to the lateral load

resistance mechanism. The behaviour of the epoxy material that was used in the FRP strengthening and the bond between the steel reinforcement and concrete material are important factors in defining the shear hysteretic envelopes. For cases where an access to a large number of experimental hysteretic envelope curves is limited, the modified compression field theory (MCFT) can be used to define the envelope curve for the hysteretic material model of the shear behviour, Vecchio and Collins (1986). Several researchers, Yousef 2000; Galal 2002; El-Almoury 2004; and Khalil 2005, reported that the MCFT prediction of the shear behaviour of the structural concrete elements can provide a good accuracy when compared experimental data that was available.

6.3.1 Constitutive equations

Concrete model of the MCFT is replaced by Mander et al. (1988) model. The principle compressive stress in concrete is:

$$f_2 = \frac{f_{2max} x r}{r - 1 + x^r}, \quad x \le 1.0 \tag{6.55}$$

$$x = \frac{\varepsilon_2}{\varepsilon_{cc}} \tag{6.56}$$

$$r = \frac{E_c}{E_c - E_{sec}} \tag{6.57}$$

$$E_c = 5000\sqrt{f'_c} \tag{6.58}$$

$$E_{sec} = \frac{f'_{cc}}{\varepsilon_{cc}} \tag{6.59}$$

where ε_2 is the principal compression strain, E_c is the initial concrete modulus of elasticity and E_{sec} is the secant concrete stiffness at the ultimate concrete strength. The confined concrete strength f'_{cc} is expressed as:

$$f'_{cc} = f'_c\left(2.254\sqrt{1+\frac{7.94f'_l}{f'_c}}-2\frac{f'_l}{f'_c}-1.254\right) \quad (6.60)$$

where ε_{cc} is the corresponding concrete strain as given by:

$$\varepsilon_{cc} = \varepsilon_\circ\left[1+5\left(\frac{f'_{cc}}{f'_c}-1\right)\right] \quad (6.61)$$

the maximum concrete strength that corresponds to the principal tensile strain, ε_1 is given as $f_{2\max}$,

$$f_{2\max} = \frac{f'_{cc}}{\left(0.8-0.34\frac{\varepsilon_1}{\varepsilon'_{cc}}\right)} \le f'_{cc} \quad (6.62)$$

The relation between the average tensile stress f_1 and the average tensile strain ε_1 is:

$$f_1 = E_c\varepsilon_1 \qquad \text{if } \varepsilon_1 \le \varepsilon_{cr} \quad (6.63)$$

where ε_{cr} is the cracking strain and E_c is the modulus of elasticity of concrete.

for $\varepsilon_1 > \varepsilon_{cr}$, the average tensile stress f_1 is given by, (Stevens et al., 1987):

$$f_1 = f_{cr}\left((1-\alpha_t)e^{-\lambda_t(\varepsilon_c-\varepsilon_{cr})}+\alpha_t\right) \quad (6.64)$$

where f_{cr} is the concrete cracking strength, α_t is a factor that defines the residual concrete tensile strength and λ_t is a factor that controls the decay rate of the response. These factors were given as:

$$f_{cr} = 0.33\sqrt{f'_c} \quad (6.65)$$

$$\alpha_t = 75\rho_x / d_b \quad (6.66)$$

$$\lambda_t = 270/\sqrt{\alpha_t} \le 1000 \quad (6.67)$$

where, d_b is the longitudinal bar diameter and ρ_x is the longitudinal steel ratio.

Equation (6.66) gives the value of α_t for the case of axial tensile stresses, where, reinforcement bars are parallel to the tensile stresses. In case of bi-directional loading,

where the principal tensile stress is inclined to the reinforcement bars in x-direction by an angle θ, then:

$$\alpha_t = \cos^2\theta\,\alpha_{tx} + \sin^2\theta\,\alpha_{ty} \qquad (6.68)$$

Where α_{tx} and α_{ty} can be estimated using Equation (6.66) after replacing ρ_x with reinforcement ratio in x and y directions, respectively.

the crack width w is:

$$w = \frac{\varepsilon_1}{\frac{\sin\theta}{S_{mx}} + \frac{\sin\theta}{S_{mv}}} \qquad (6.69)$$

where S_{mx} and S_{mv} are the crack spacing in the x and y directions, respectively.

$$S_{mx} = 2\left(c + \frac{S_x}{10}\right) + 0.1\frac{d_b}{\rho_x} \qquad (6.70)$$

where c is the clear concrete cover, S_x is the spacing between bars in x direction, d_b is the bar diameter and ρ is the ratio of the reinforcement area to concrete area.

Collins and Mitchell (1987) suggested that to limit the shear stresses v_{ci} that could be transmitted across crack to:

$$v_{ci} = \frac{0.17\sqrt{f'_c}}{0.3 + 0.6w} \qquad (6.71)$$

where the crack width w in mm, v_{ci} and f'_c are in MPa, and Collins et al. , (1996) suggested to limit f_1 to:

$$f_{1max} = v_{ci}\tan\theta \qquad (6.72)$$

6.3.2 Compatibility equations

From Mohr's circle of strains shown in Figure 6.8:

$$\varepsilon_1 = \varepsilon_x + \frac{\gamma}{2}\cot\theta \tag{6.73}$$

$$\varepsilon_2 = \varepsilon_v - (\varepsilon_1 - \varepsilon_v)\cot^2\theta \tag{6.74}$$

$$\varepsilon_v = \varepsilon_1 + \varepsilon_2 - \varepsilon_x \tag{6.75}$$

where ε_x is the longitudinal strain at the mid-depth of the web, ε_t is the transverse strain, ε_1 is the principle tensile strain, ε_2 is the principle compressive strain, γ is the shear strain and θ is the angle of inclination of the diagonal compression.

$$\tan 2\theta = \frac{\gamma}{(\varepsilon_v - \varepsilon_x)} \tag{6.76}$$

6.3.3 Element equilibrium

The shear force V, can be calculated from:

$$V = \frac{\frac{a_v f_v d_v}{S} + f_1 b_v d_v}{\tan\theta} \tag{6.77}$$

The shear stress v, is given by:

$$v = \frac{\frac{a_v f_v}{S\, b_v} + f_1}{\tan\theta} \tag{6.78}$$

where a_v and f_v are the area and yield strength of shear reinforcement, respectively, b_v is the effective thickness of the section, d_v is the effective depth of the section, and S is the spacing between the web reinforcement of walls.

Mohr's circle of stresses is shown in Figure 6.9. In that figure, f_{cx} is the concrete stress in x direction, f_{ct} is the concrete stress in transverse direction, v is the shear stress, f_x is the steel stress in the x direction and f_t is the steel stress in the transverse direction. To achieve equilibrium the following equation should be satisfied:

$$\text{error} = f_2 + f_1 - \left(\tan\theta + \frac{1}{\tan\theta}\right)\frac{V}{b_v d_v} = 0 \qquad (6.79)$$

The axial load can be calculated from, Collins and Mitchell (1987):

$$N = A_{sx} f_{sx} + f_1 b_v d_v - V\cot\theta \qquad (6.80)$$

where A_{sx} and f_{sx} are the area and stress of longitudinal bars, respectively.

6.3.4 Solution strategy

Iterations are carried out over an incrementally increasing shear strain strain, γ. For each iteration a value of γ was imposed, ε_x and ε_v were assumed, then principal strains and stresses were estimated. The shear force was calculated and the axial force was estimated and until equilibrium was achieved. The process was repeated by imposed another shear strain incement.

6.4 Modeling of CFRP-Shear Strength Contribution

When modeling RC structural wall strengthened with FRP composites, the effect of the composite jacket with anchored ends can be idealized as distributed ties in the RC wall. The response of concrete wall with externally bonded FRP composites was evaluated using MCFT. The problem is represented by three sets of equations. They are the constitutive laws, compatibility conditions and equiliprium conditions.

6.4.1 Constitutive Laws

The constitutive relationships of the concrete and the composite sheet materials are presented in this section. The principal compressive concrete stress is given as:

$$f_2 = \frac{f_{2max} x r}{r - 1 + x^r}, \quad x \le 1.0 \tag{6.81}$$

$$f_2 = f_{2max} + E_g(\varepsilon_2 - \varepsilon'_{cc}), \quad x > 1.0 \tag{6.82}$$

where E_g is the tangent stiffness of the stress-strain relationship of the concrete, and f_{2max} is the maximum concrete strength as estimated by Equation (6.62) where f'_{cc} in Equation (6.60) is the confined concrete strength as estimated by the FRP-confined concrete model. The elastic constitutive relation of the composite FRP materials is written as:

$$f_{FRP\ sheet} = E_{sheet}\varepsilon_{sheet} \tag{6.83}$$

where $f_{FRP\ sheet}$ is the tensile stress in the FRP sheets that is corresponding to a tensile strain of ε_{sheet} and E_{sheet} is the modulus of elasticity of the FRP sheets.

6.4.2 Compatibility

This set of equations relates the average axial and shear strains through Mohr's circle of strains. The angle of inclination of principal concrete stress was taken equal to the angle of principal strain and the angle of the crack inclination. Compatibility equations (6.73) to (6.76) are implemented in this set.

6.4.3 Equilibrium

The equilibrium of stresses can be derived from Mohr's circle of stresses as described in Section 6.3.2. The shear resistance of the RC structural wall strengthened with FRP composites is evaluated as:

$$V = \frac{\frac{a_v f_v d_v}{S_{ties}} + A_{FRP\ sheet} f_{FRP\ sheet} + f_l b_v d_v}{\tan\theta} \tag{6.84}$$

where $A_{FRP\ sheet}$ is the cross sectional area of the FRP sheets, a_v and f_v are the area and yield strength of shear reinforcement, respectively, b_v is the effective thickness of the

section, d_v is the effective depth of the section, and S_{ties} is the spacing between the web reinforcement of structural walls.

The equilibrium of stresses as given by Mohr's circle, gives:

$$\text{error} = (\cot\theta + \tan\theta)\frac{V_j}{b_v d_v} - f_1 - f_2 \qquad (6.85)$$

The axial load resistance of the section is given as (Collins and Mitchell, 1987):

$$N = A_{sx} f_{sx} + f_1 b_v d_v - V\cot\theta \qquad (6.86)$$

To build the shear force-shear strain envelopes, a value of the shear strain, γ was assumed and then the axial strains, ε_x and ε_y were evaluated.

6.5 ANALYSIS OPTIONS

6.5.1 Element material properties from test data

Two options for defining the material properties for each element were available. Either the analysis program generates the envelopes for the elements based on concrete and reinforcement materials properties, or the program is provided with complete moment-curvature envelope data from tests. If access to experimental envelopes is not available, it is possible to use other programs to generate the envelopes of the moment-curvature and shear force-shear deformation. In this analysis, the first option was used to generate the moment-curvature and shear force-shear deformation envelopes for each wall element. In order to check the accuracy of the program predictions, its results were compared with the available experimental envelopes and a good agreement was observed. This ensures that the effects of reduced stiffness are included in the analysis. By using the first option, (i.e. providing the material properties for program to generate envelopes), and taking into account the stiffness degradation of the reinforced concrete members, it can result reliable and accurate analytical model results in the case of seismic loading.

6.5.2 Hysteretic rules

The hysteretic values should characterize stiffness degradation, strength deterioration, and pinching behaviour for the RC structural walls. For simulation of the experimental results, the values were obtained by a trial and error process. Therefore, after determination of the element properties for RC structural walls, several analyses were carried out with different values of hysteretic parameters and those that yielded the most comparable results to the experiments were selected to be implemented in the simulation of the tested walls. Ductile walls have small values of stiffness degradation, strength deterioration and bond slip. The rehabilitated walls have large volumes of well-anchored longitudinal reinforcement and the CFRP shear strengthening helped to fully mobilize the mechanism of the shear resistance of the walls. For modeling the inelastic behaviour of the tested walls, a model which takes into account stiffness degradation parameter (HC), strength deterioration parameter (HBD, HBC), and slip-lock parameter (HS) was used. Typical ranges of values for hysteretic parameters and their effect on the hysteretic behavior of the structure are shown in Table 6.1. The values of the hysteretic parameters determined for simulation of the tested walls are as presented in Table 6.2. Tables 6.3 and Table 6.4 include the parameters used to represent flexural properties for analysis. The parameters used to represent shear properties for analysis are presented in Tables 6.5 and Table 6.6.

6.5.3 Hysteretic model

The above solution strategy described in Section 6.3.4 establishes the envelope curve for the shear elements. Every point on this curve was evaluated for the corresponding axial force acting on the structural wall represented by the shear element. The modified compression field theory has the ability of determining the point at which degradation in shear strength will start and thus modelling of failure is included in the shear element. To account for the continually varying stiffness and energy absorption characteristics under cyclic loading, suitable hysteretic rules are needed. Hysteretic rules are discussed in Section 6.5.2. The proposed wall model is shown in Figures 6.10 to 6.13.

The model employs the fiber section technique for modeling flexural response along with a hysteretic shear model. Distinction was made between unconfined, steel confined, and CFRP confined concrete areas in the concrete modeling. The hysteretic shear model incorporated important features such as stiffness degradation, strength deterioration, and pinching effects.

The hysteretic model is shown in Figure 6.13. The figure describes a typical reversed shear cycle. As loading is increased, a significant reduction in the tangent stiffness occurs which represents the pinching effect experienced by RC structures under cyclic loading. The proposed model is characterized by its simplicity and its ability to describe the pinching experienced because of shear deformations under cyclic loading by using simple loading and unloading rules. The envelopes of the moment-curvature were generated using sectional analysis. The parameters in Figure 6.13 are defined as follows, Mazzoni et al. (2007):

ePf1, ePf2, ePf3, ePf4 are floating point values defining force points on the *positive* response envelope.

ePd1, ePd2, ePd3, ePd4 are floating point values defining deformation points on the *positive* response envelope.

eNf1, eNf2, eNf3, eNf4 are floating point values defining force points on the *negative* response envelope (default: negative of *positive* envelope values).

eNd1, eNd2, eNd3, eNd4 are floating point values defining deformations points on the *negative* response envelope (default: negative of *positive* envelope values).

rDispP is a floating point value defining the ratio of the deformation at which reloading occurs to the maximum historic deformation demand.

rForceP is a floating point value defining the ratio of the force at which reloading begins to force corresponding to the maximum historic deformation demand.

uForceP is a floating point value defining the ratio of strength developed upon unloading from *negative* load to the maximum strength developed under monotonic loading.

rDispN is a floating point value defining the ratio of the deformation at which reloading occurs to the minimum historic deformation demand (default: **rDispP**).

rForceN is a floating point value defining the ratio of the force at which reloading begins to the force corresponding to the minimum historic deformation demand (default: **rForceP**).

uForceN is a floating point value defining the ratio of the strength developed upon unloading from a *positive* load to the minimum strength developed under monotonic loading (default: **rForceP**).

The following paramters were defined to control stiffness and strength degredations of the hysteretic model. They are:

gK1, gK2, gK3, gK4, gKLim are floating point values controlling cyclic degradation model for *unloading stiffness degradation.*

gD1, gD2, gD3, gD4, gDLim are floating point values controlling cyclic degradation model for *reloading stiffness degradation.*

gF1, gF2, gF3, gF4, gFLim are floating point values controlling cyclic degradation model for *strength degradation.*

6.5.4 Analysis type

The objective of the modeling is to reproduce the behaviour of the tested walls using a simple and accurate analytical modeling. The tests were conducted using cyclic displacement histories under displacement control of the three synchronized actuators. The same displacement histories, imposed on the tested walls during tests, were used as an input to the simulation analysis. The solution was performed incrementally assuming the properties of the structure such as the flexural stiffness, do not change during the time step. The analysis uses the pseudo time to perform the cyclic static analysis under displacement control with user input time step. Analysis step size 0.01 mm was enough to balance between the time needed for the analysis and the accuracy of the results compared to the experimental results.

6.6 ANALYTICAL MODEL RESULTS

The validation and accuracy of the developed model was established by using the model to reproduce the hysteretic behaviour of the tested walls. The validation of the hysteretic rule parameters controlling the behaviour of the tested walls has been achieved by reproducing the experimental results, with 10 % variation from the experimental results, of the tests using two analysis programs. Both OpenSees version 1.74 and IDARC2D version 6.1 were used for simulations of the tested wall results. Good agreements were obtained from the analyses of the tested walls using both programs. Figures 6.14 to 6.30 show the comparisons between the predicted and recorded test results. The comparisons show that the model implemented in both programs predicted the response with a good accuracy. Envelopes of the drift ratio against lateral load from the test results, Idarc analysis, and OpenSees analysis are shown in Figures 6.22 to 6.30. Observations from Figures 6.14 to 6.30 indicated that the stiffness degradation, strength deterioration and pinching behaviours were accurately simulated using the developed model. It was observed that there were some discrepancy between the analytical response of test wall RW9 as shown in Figures 6.21 and 6.30. This was because the test wall RW9 steel reinforcement was previously yielded before the wall was repaired then retested.

Comparison between OpenSees and IDARC2D programgs results indicated that both programs represented the inelastic response of walls until failure. The time needed for IDARC2D program to perform one analysis run was significantly less that that was required for OpenSees. This was attributed to the refined macro-fiber modeling technique in modeling the wall in OpenSees, which included modeling the wall section through larger number of fiber elements than IDARC2D. Only wall end column elements and wall web can be defined in IDARC2D analysis. Figures 6.22 to 6.30 show the comparison between the predicted walls response from both program along with the experimental envelopes. These figures indicate that Opensees was more representive to walls response and more accurate than IDARC2D.

Table 6. 1 Typical range of values for hysteretic parameters, IDARC2D

Parameter	Effect	Value
Stiffness degrading parameter (HC)	No degrading	200.0
	Mild degrading	15.0
	Moderate degrading	10.0
	Sever degrading	4.0
Ductility-based strength degrading parameter (HBD)	No degrading	0.01
	Mild degrading	0.15
	Moderate degrading	0.30
	Sever degrading	0.6
Energy-based strength degrading parameter (HBE)	No deteriorating	0.01
	Mild deteriorating	0.08
	Moderate deteriorating	0.15
	Sever deteriorating	0.6
Crack-closing or slip parameter (HS)	No pinching	1.00
	Mild pinching	0.40
	Moderate deteriorating	0.25
	Sever deteriorating	0.05

Table 6. 2 Hysteretic values for each type of walls, IDARC2D

Type	Rule	HC	HBD	HBE	HS
Gravity load design GLD (Walls CW1 to CW3)	Flexure	2	0.25	0.20	0.25
	Shear	2	0.50	0.50	0.05
Nominally ductile (Wall RW4)	Flexure	5	0.25	0.20	0.40
	Shear	5	0.02	0.01	0.40
Ductile (Walls RW3, RW5 to RW9)	Flexure	10	0.25	0.10	0.50
	Shear	10	0.02	0.01	0.50

Table 6. 3 Input properties for cyclic flexural test simulation, IDARC2D

Parameter*	Control walls			Rehabilitated walls						
	CW1	CW2	CW3	RW3	RW4	RW5	RW6	RW7	RW8	RW9
KHYSW	1	1	1	1	1	1	1	1	1	1
EA/h	1667	1667	1667	1667	1667	1667	1667	1667	1667	1667
EI	31.25e10	31.25e10	31.25e10	31.25e10	31.25e10	31.25e10	31.25e10	31.25e10	31.25e10	31.25e10
PCP	9.00e5	4.00e5	3.50e5	5.00e5	6.50e5	7.00e5	9.70e5	10.00e5	10.50e5	7.00e5
PYP	9.30e5	5.00e5	5.00e5	9.50e5	9.90e5	9.10e5	14.10e5	14.50e5	11.50e5	9.60e5
UYP	6.00e-6	3.50e-6	2.00e-6	4.00e-6	4.00e-6	3.88e-6	6.00e-6	7.70e-6	6.00e-6	10.00e-6
UUP	30.00e-6	30.00e-6	30.00e-6	50.00e-6	100.0e-6	100.0e-6	200.0e-6	200.0e-6	150.0e-6	150.0e-6
EI3P	1	5	5	1	1	1	1	1	1	1
PCN	9.00e5	4.00e5	4.00e5	5.00e5	6.50e5	7.00e5	9.70e5	10.00e5	10.50e5	7.00e5
PYN	9.30e5	5.00e5	5.00e5	9.50e5	9.30e5	9.80e5	15.00e5	14.20e5	12.00e5	9.60e5
UYN	6.00e-6	3.50e-6	3.50e-6	4.00e-6	4.00e-6	3.88e-6	6.00e-6	7.70e-6	10.00e-6	10.00e-6
UUN	30.00e-6	30.00e-6	30.00e-6	50.00e-6	100.0e-6	100.0e-6	200.0e-6	200.0e-6	150.0e-6	150.0e-6
EI3N	1	5	5	1	1	1	1	1	1	1

*For parameter definition refer to Table 6.4

Table 6. 4 Flexural user input parameters definitions, IDARC2D

Parameter	Definition
KHYSW	Hysteretic rule number
EA/h	Axial stiffness in kN/ mm
EI	Initial flexural stiffness in kN. mm^2
PCP	Positive cracking moment in kN.mm
PYP	Positive yield moment in kN.mm
UYP	Positive yield curvature in radian/mm
UUP	Positive ultimate curvature in radian/mm
EI3P	Positive post yield flexural stiffness as % of elastic
PCN	Negative cracking moment in kN.mm
PYN	Negative yield moment in kN.mm
UYN	Negative yield curvature in radian/mm
UUN	Negative ultimate curvature in radian/mm
EI3N	Negative post yield flexural stiffness as % of elastic.

Table 6. 5 Input properties for cyclic shear test simulation, IDARC2D

Parameter*	Control walls			Rehabilitated walls						
	CW1	CW2	CW3	RW3	RW4	RW5	RW6	RW7	RW8	RW9
KHYSW	2	2	2	2	2	2	2	2	2	2
GA	1.50e6	1.50e6	1.50e6	1.50e6	1.50e6	1.50e6	1.50e6	1.50e6	1.50e6	1.50e6
PCP	350	425	425	851.40	851.40	851.40	851.40	851.40	851.40	851.40
PYP	380	430	430	860	860	860	860	860	860	860
UYP	5.80e-4	2.90e-4	2.90e-4	5.80e-4	5.80e-4	5.80e-4	5.80e-4	5.80e-4	5.80e-4	5.80e-4
UUP	8.00e-3	1.00	1.00	1.00	1.00	1.00	1.00	1.00	1.00	1.00
GA3P	2	2	2	2	2	2	2	2	2	2
PCN	350.0	425.0	425.0	851.40	851.40	851.40	851.40	851.40	851.40	851.40
PYN	380	430	430	860	860	860	860	860	860	860
UYN	5.80e-4	2.90e-4	2.90e-4	5.80e-4	5.80e-4	5.80e-4	5.80e-4	5.80e-4	5.80e-4	5.80e-4
UUN	8.00e-3	1.00	1.00	1.00	1.00	1.00	1.00	1.00	1.00	1.00
GA3N	2	2	2	2	2	2	2	2	2	2

*For parameter definition refer to Table 6.6

Table 6. 6 Shear user input parameters definitions, IDARC2D

Parameter	Definition
KHYSW	Hysteretic rule number
GA	Initial shear stiffness (shear modulus*area)
PCP	Positive cracking shear in kN
PYP	Positive yield shear in kN
UYP	Positive yield shear strain in radian
UUP	Positive ultimate shear strain in radian
GA3P	Positive post yield shear stiffness as % of elastic
PCN	Negative cracking shear in kN
PYN	Negative yield shear in kN
UYN	Negative yield shear strain in radian
UUN	Negative ultimate shear strain in radian
EI3N	Negative post yield shear stiffness as % of elastic

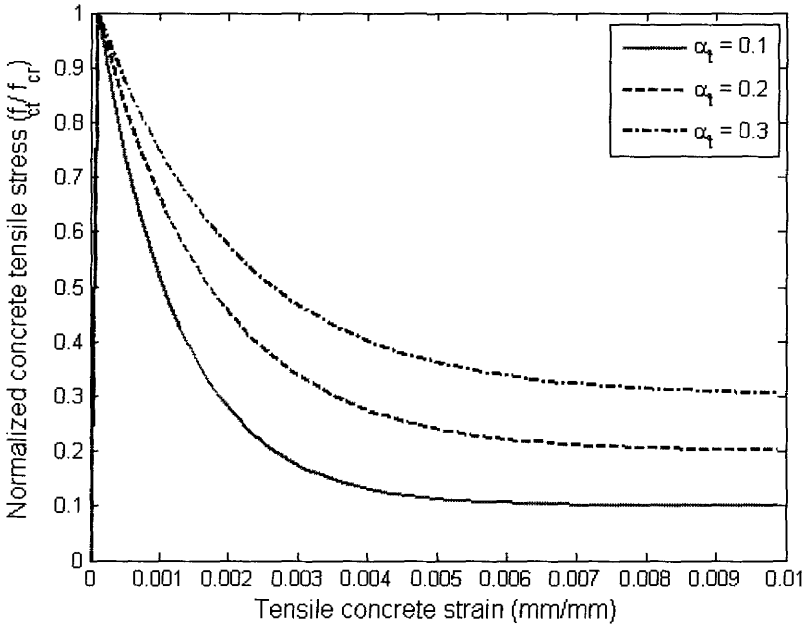

Figure 6. 1 Concrete tension envelope (Stevens et al., 1987)

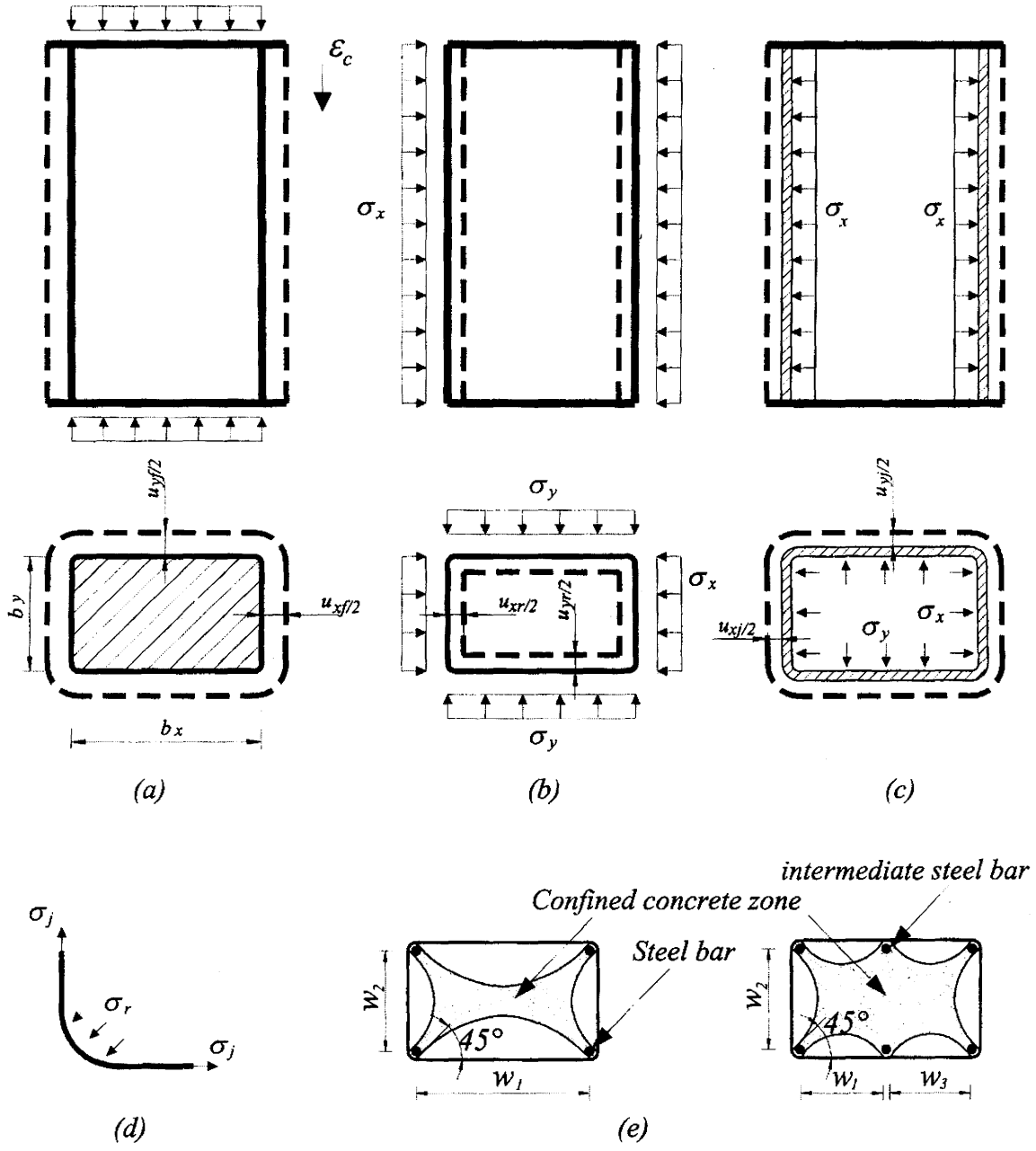

Figure 6. 2 FRP confinement model (El-Amoury, 2004).

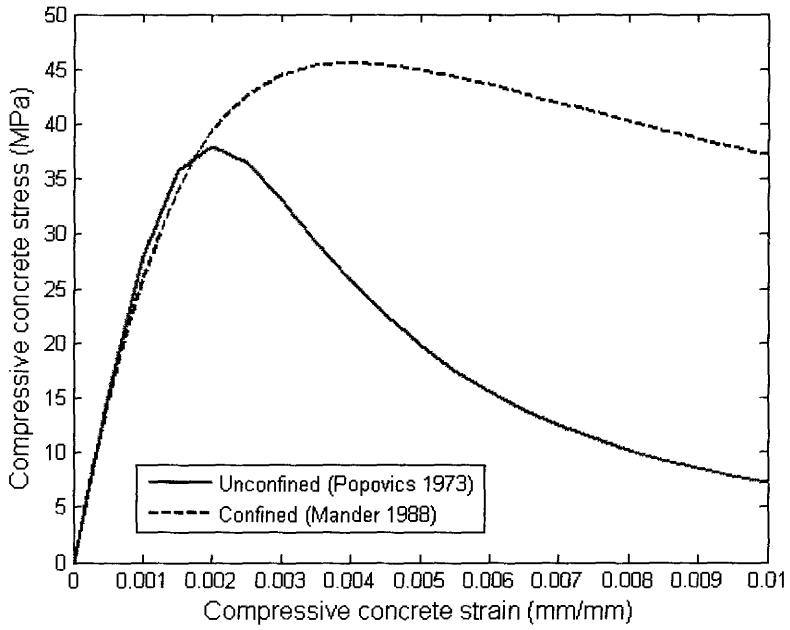

Figure 6. 3 Stress-strain behaviour of unconfined and steel confined concrete members

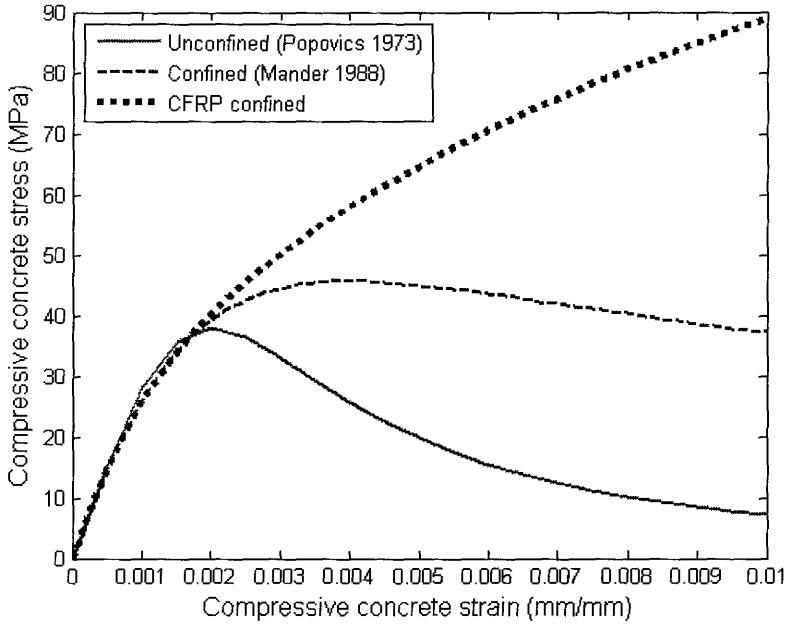

Figure 6. 4 Stress-strain behaviour of unconfined and steel confined concrete members

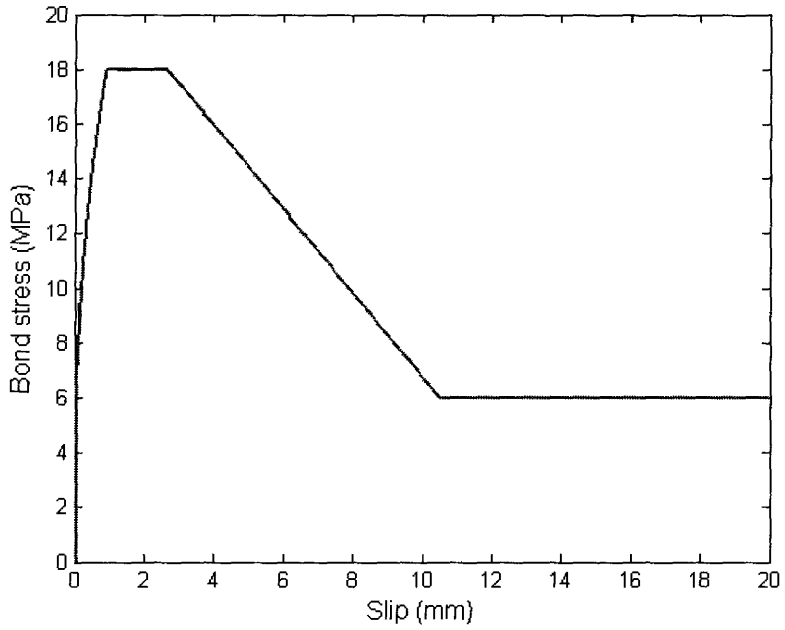

Figure 6. 5 Bond stress-slip relationship for straight bars

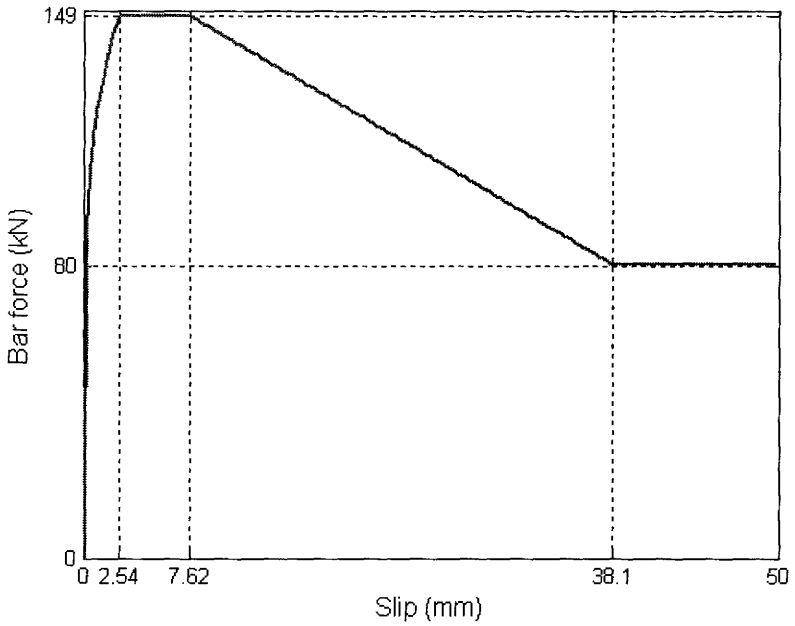

Figure 6. 6 Bond stress-slip relationship for hooked bars

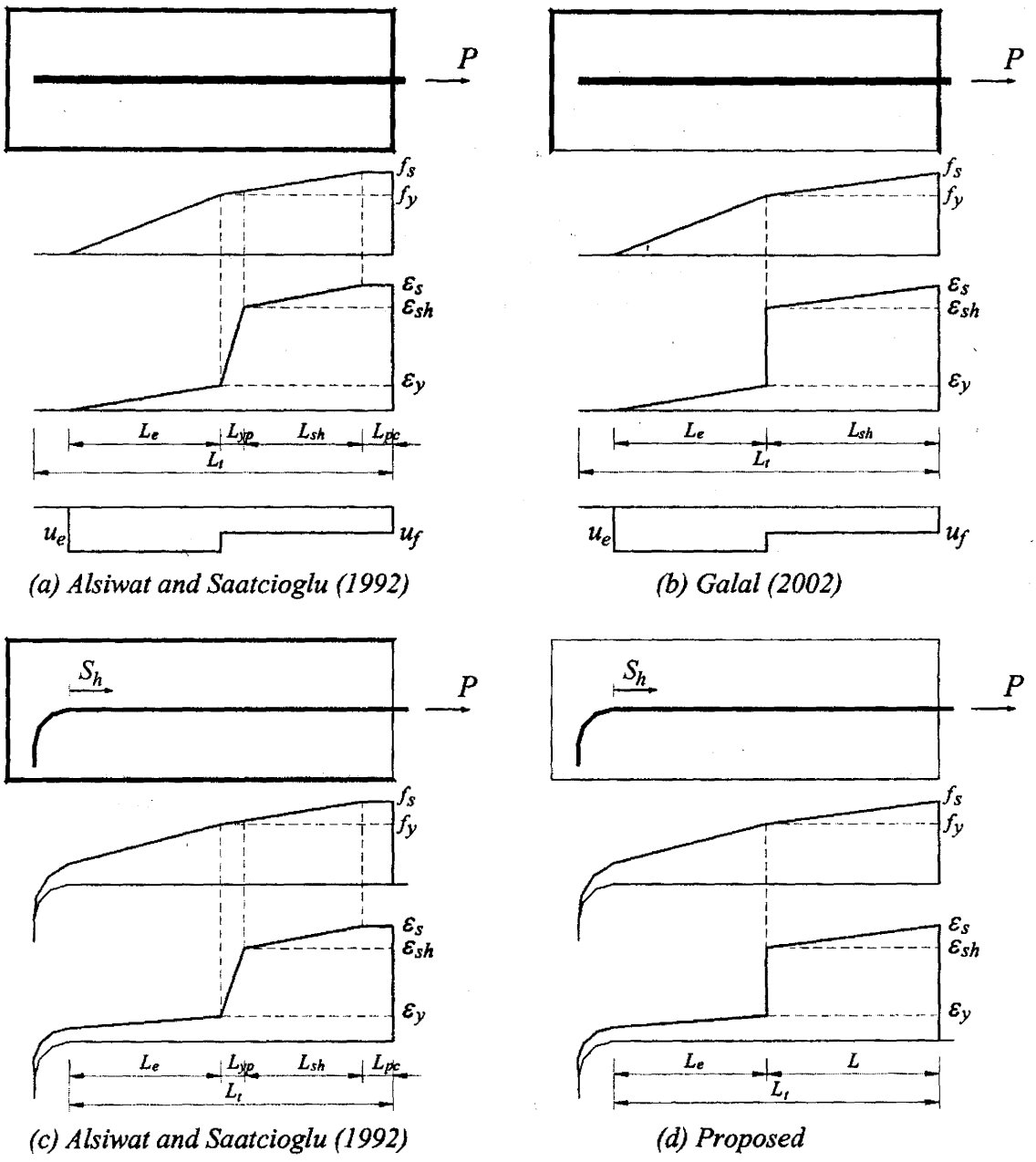

Figure 6. 7 Reinforcing bars with straight or hooked end embedded in concrete, (El-Amoury, 2004).

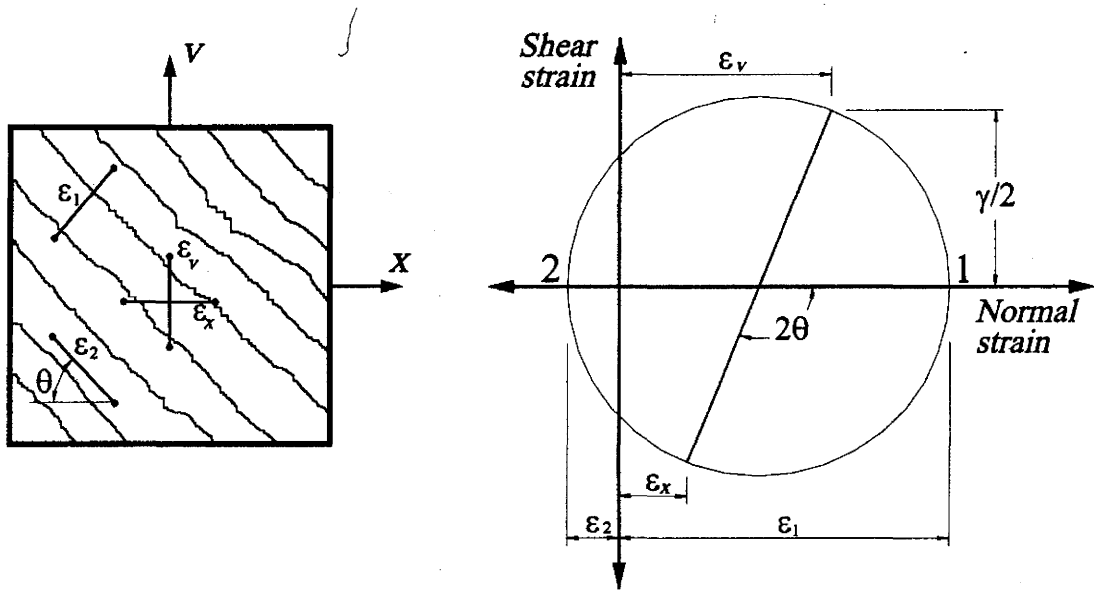

Figure 6. 8 Compatibility conditions for cracked concrete element

(Vecchio and Colins, 1987)

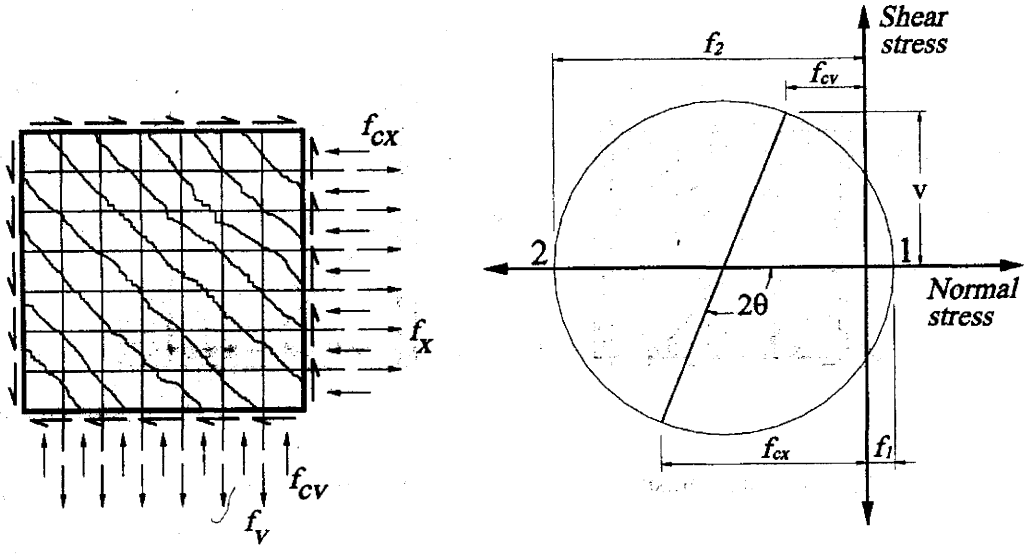

Figure 6. 9 Equilibrium conditions for cracked concrete element

(Vecchio and Colins, 1987).

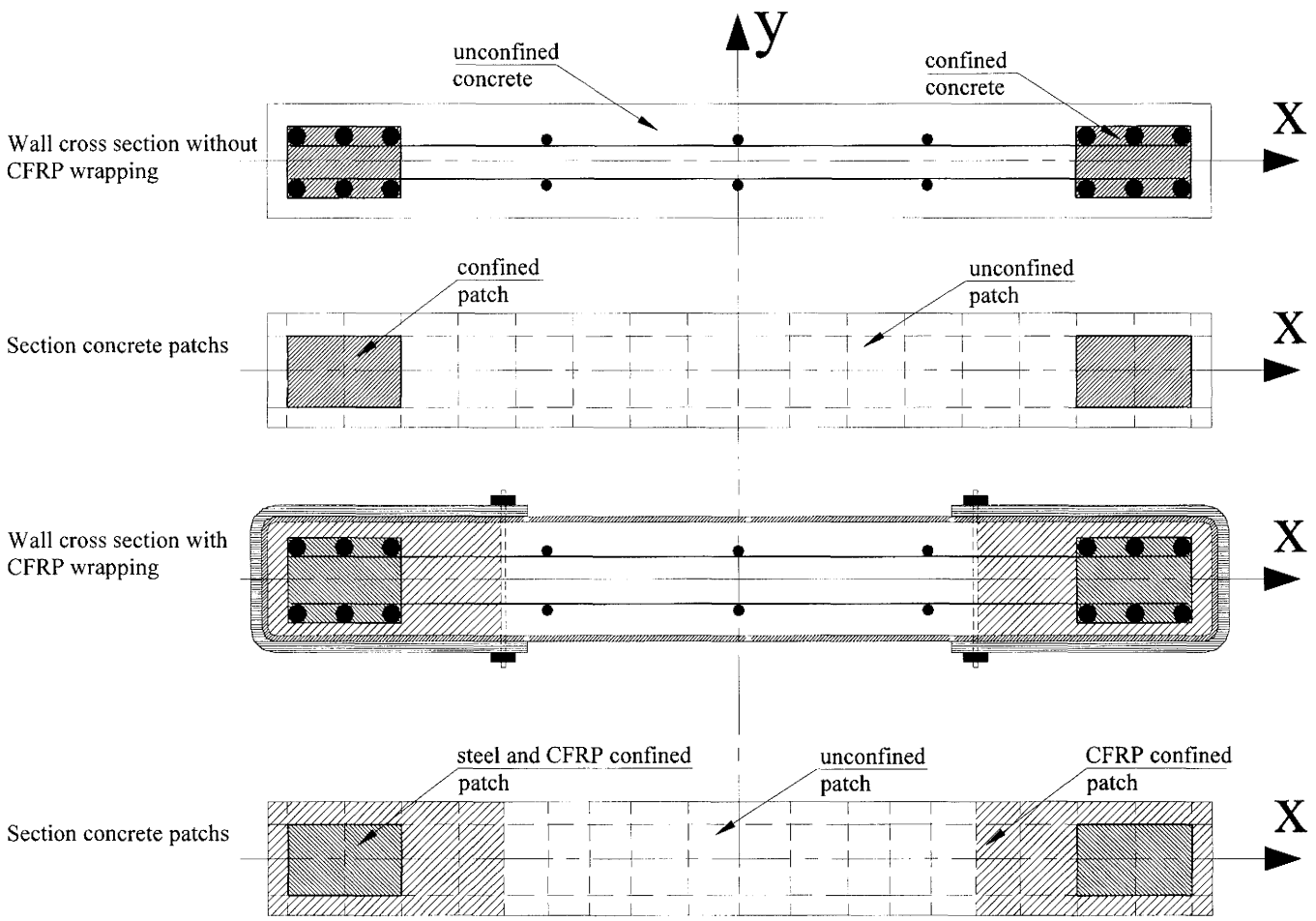

Figure 6. 10 Proposed wall model section meshing

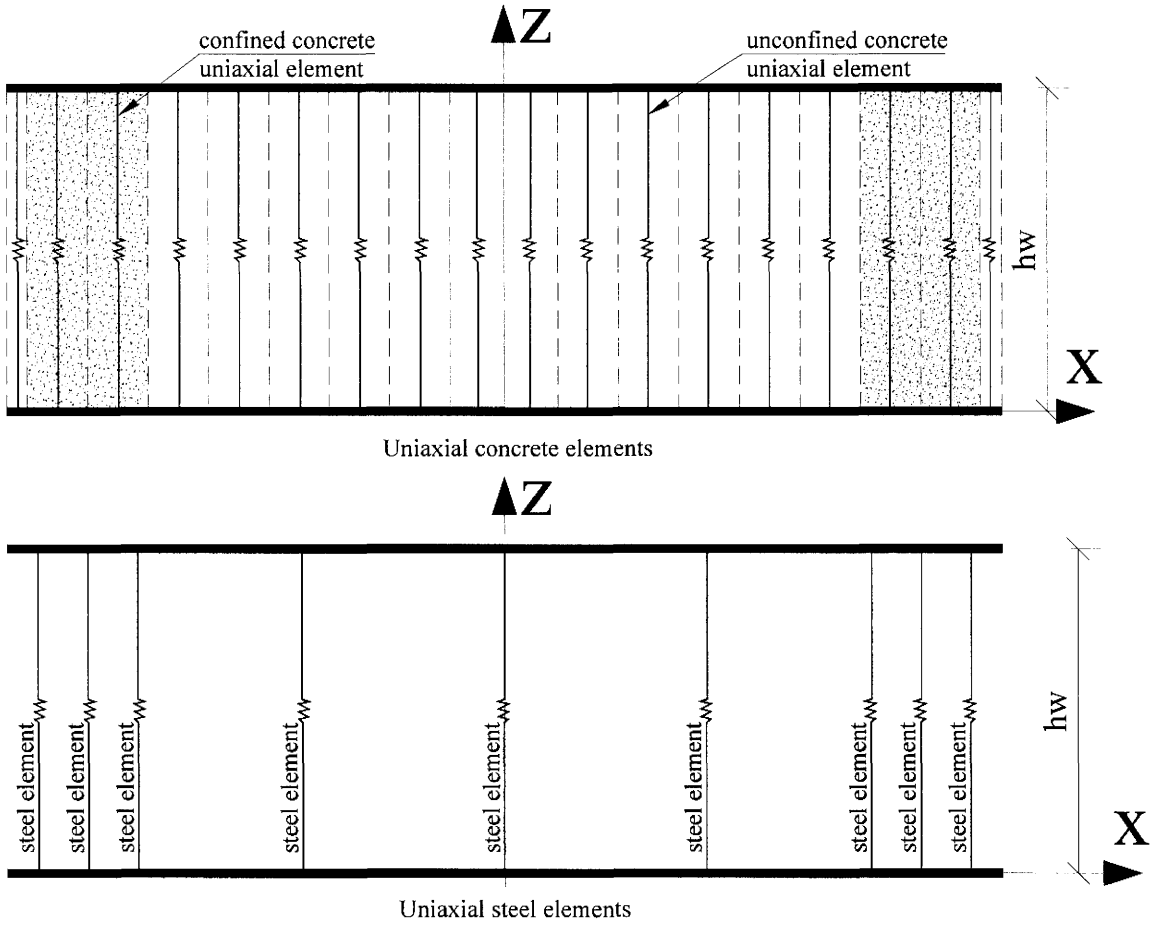

Figure 6. 11 Proposed wall model: steel and concrete elements

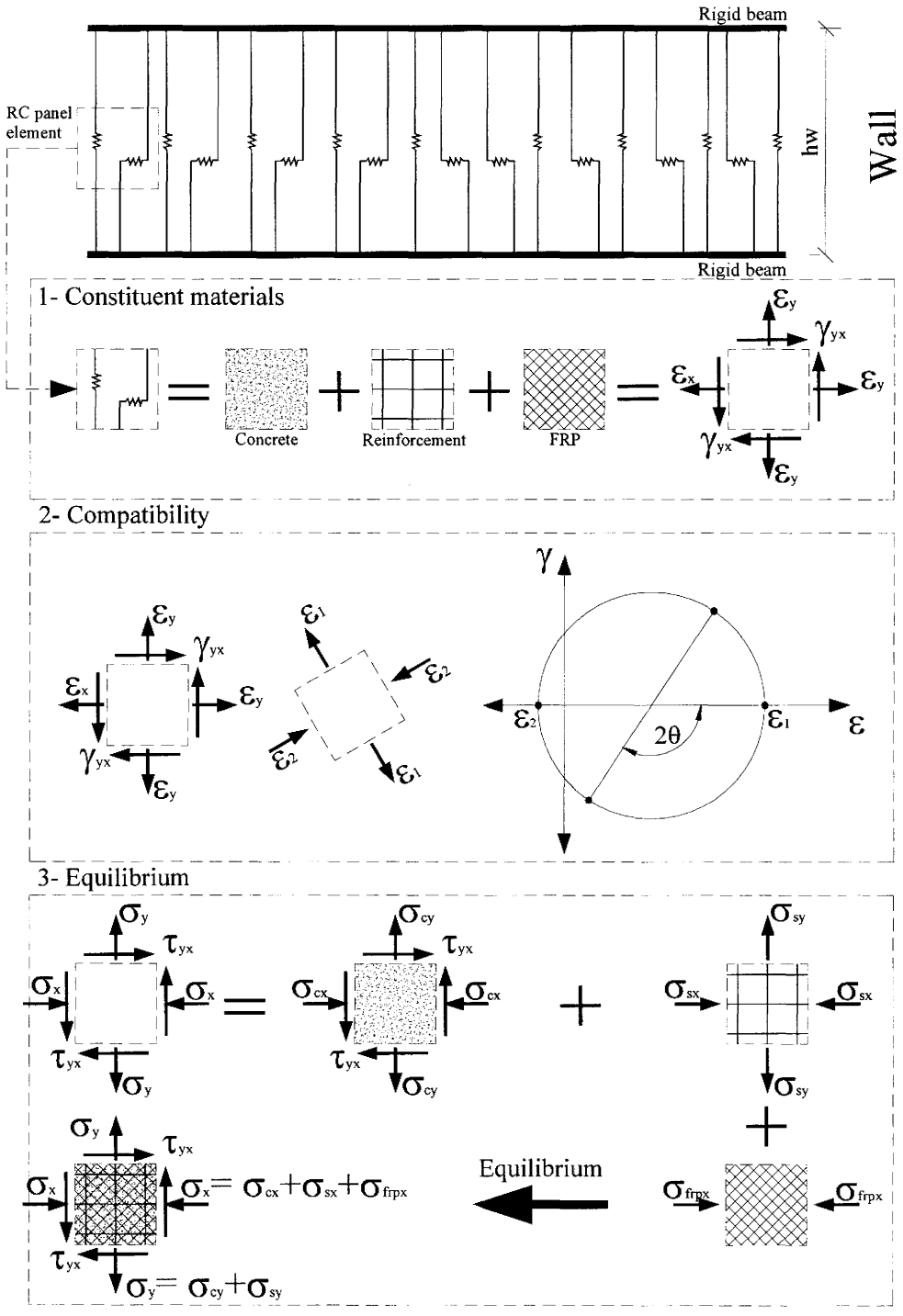

Figure 6. 12 Wall hystertic shear model

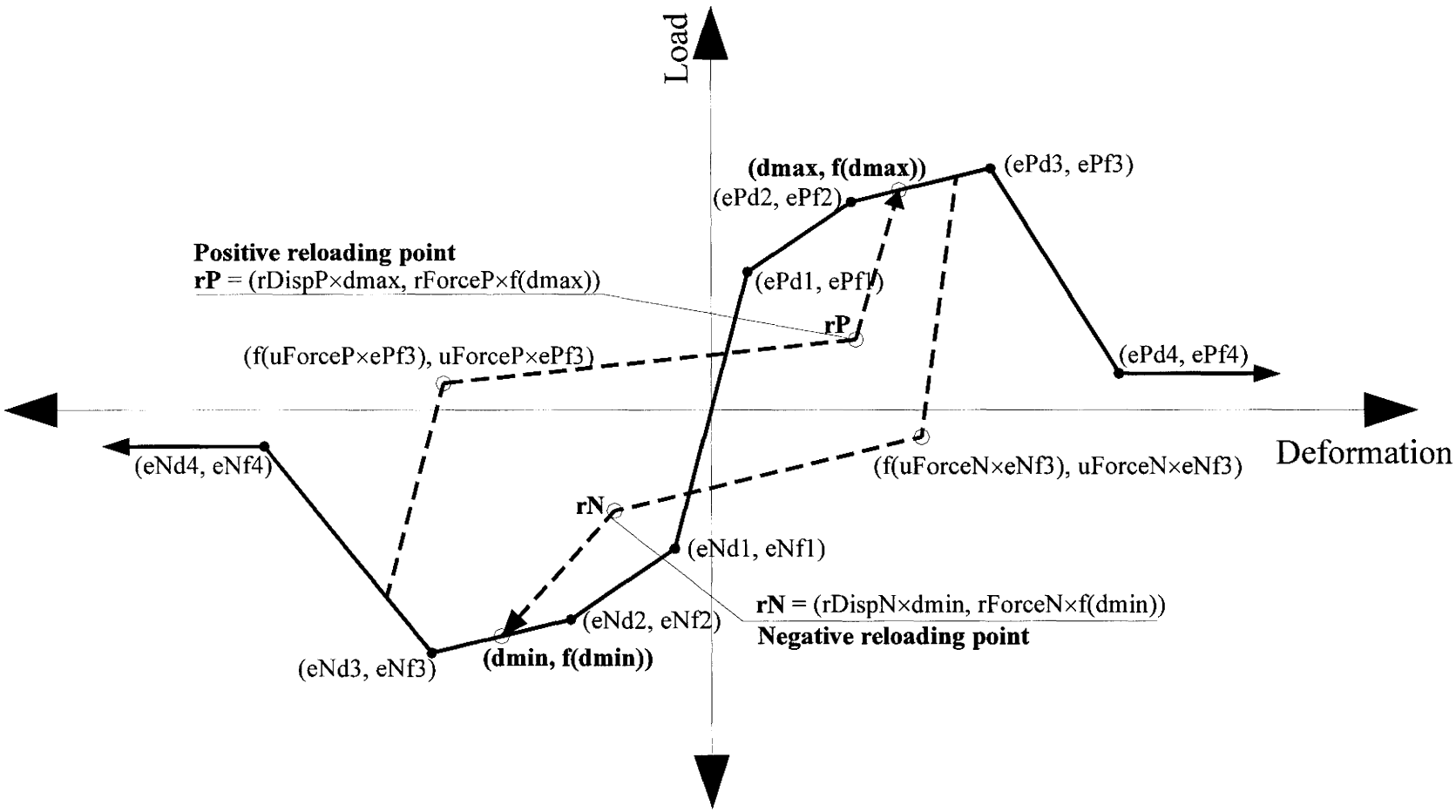

Figure 6. 13 Proposed wall model hysteretic shear modeling (Mazoni et al., 2007)

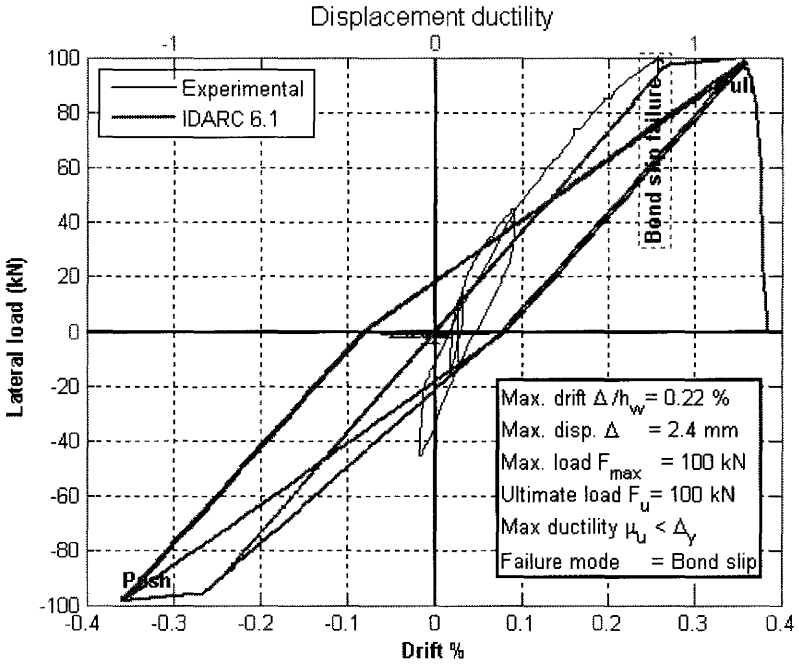

Figure 6. 14 Wall CW2 top drift ratio- lateral load relationship

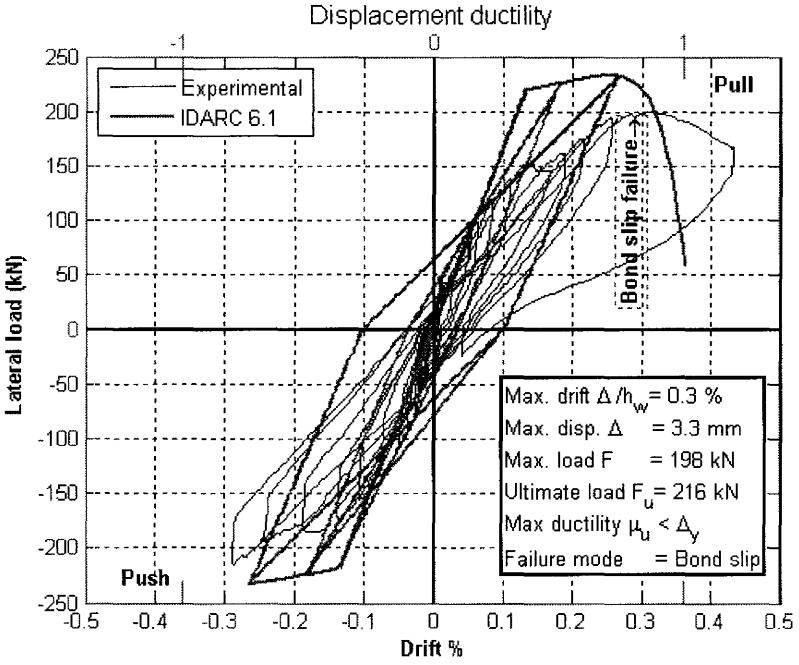

Figure 6. 15 Wall CW3 top drift ratio- lateral load relationship

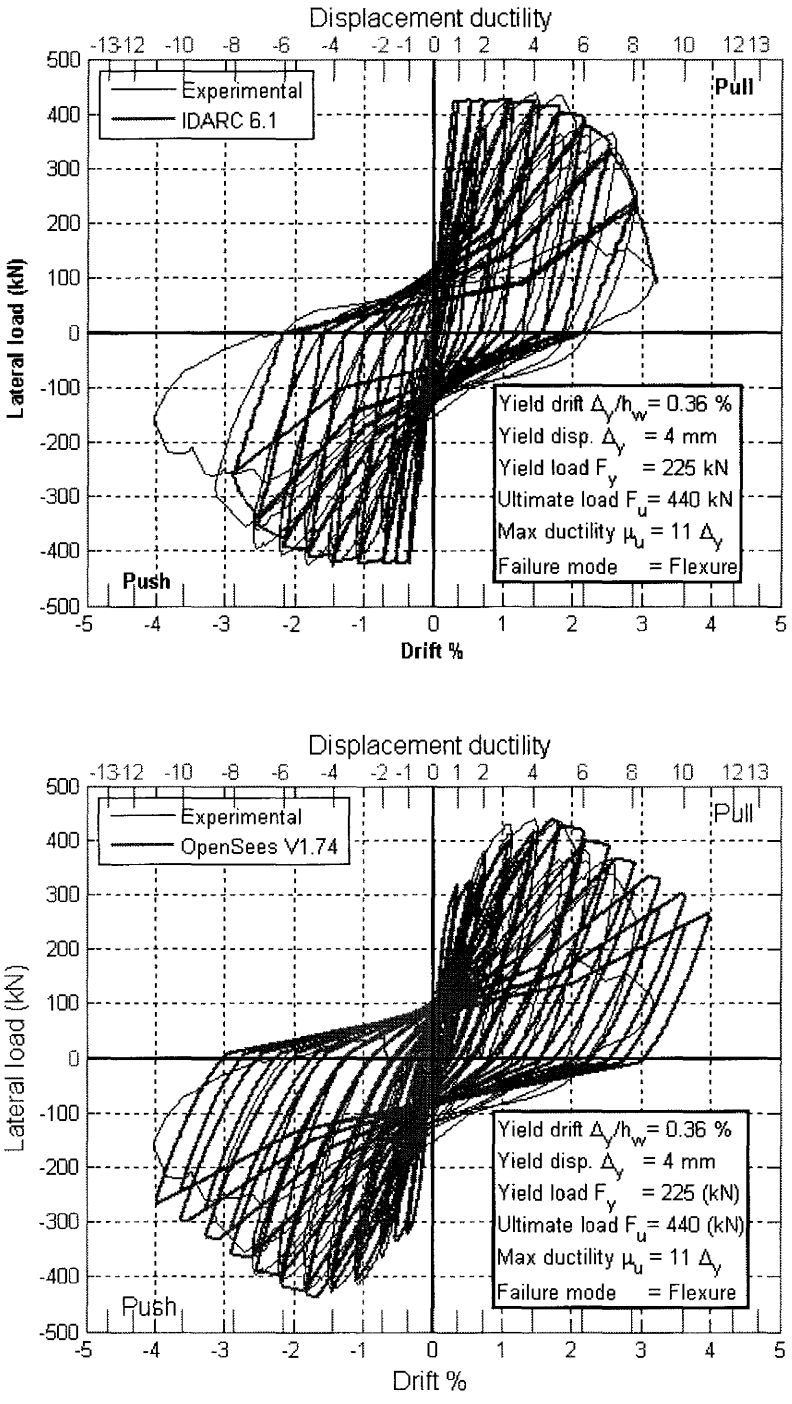

Figure 6. 16 Wall RW3 top drift ratio- lateral load relationship

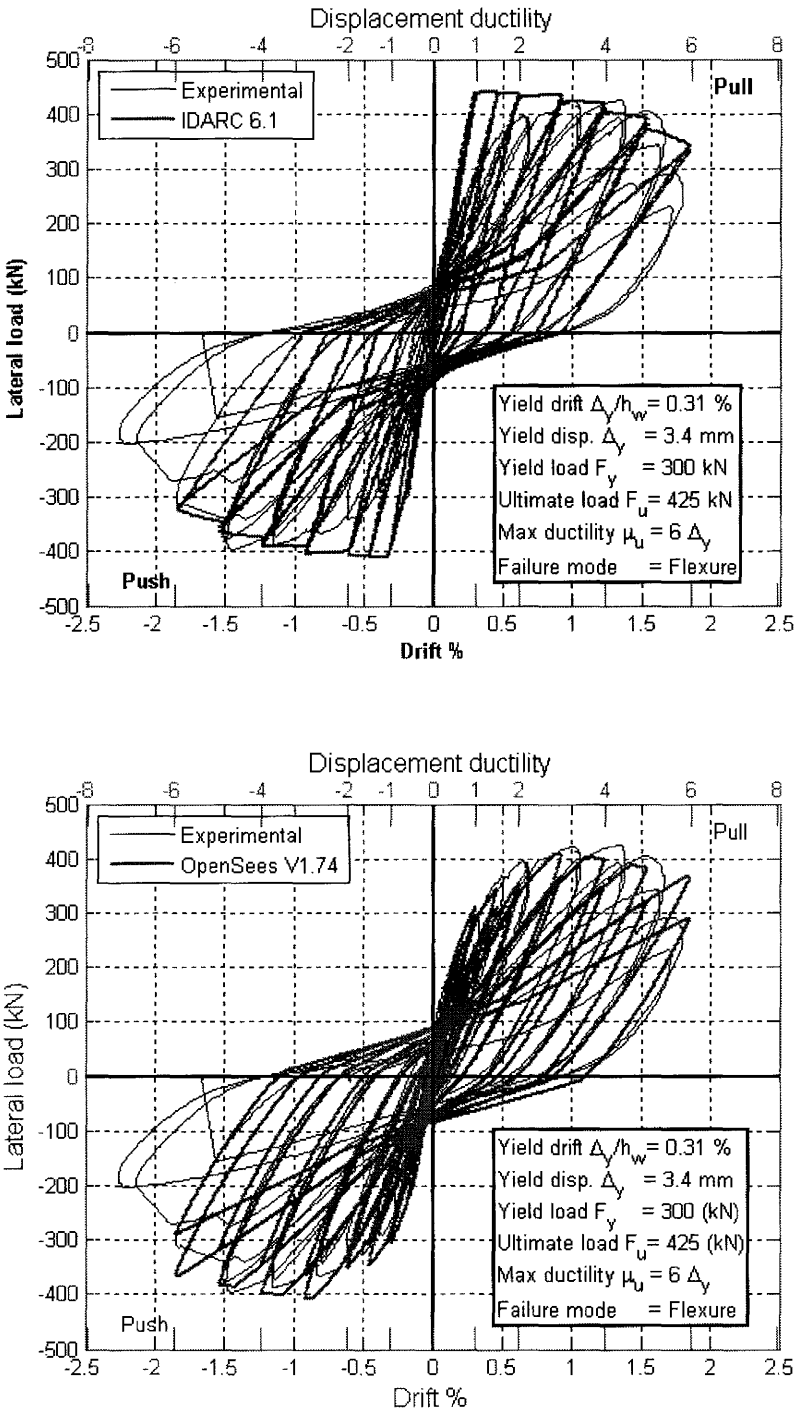

Figure 6. 17 Wall RW4 top drift ratio- lateral load relationship

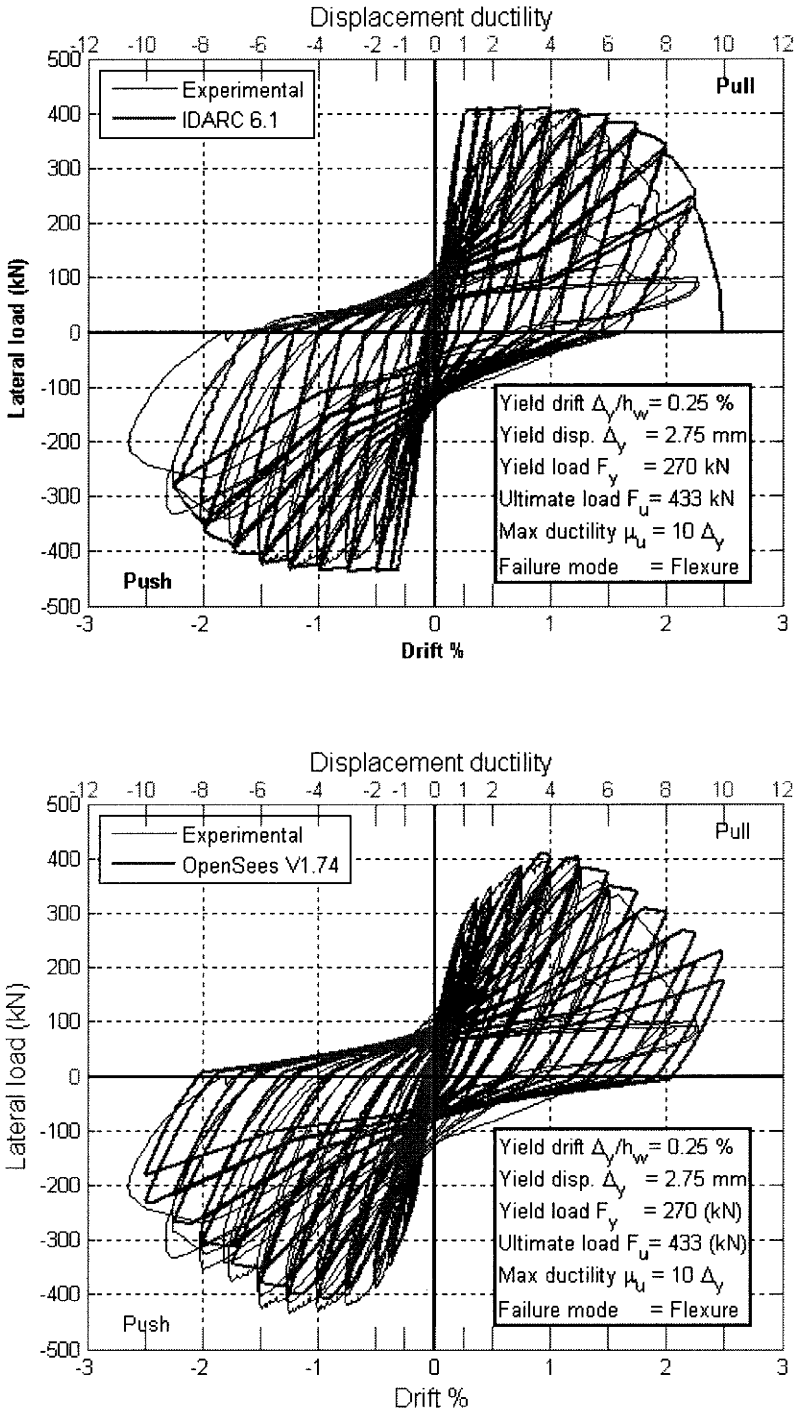

Figure 6. 18 Wall RW5 top drift ratio- lateral load relationship

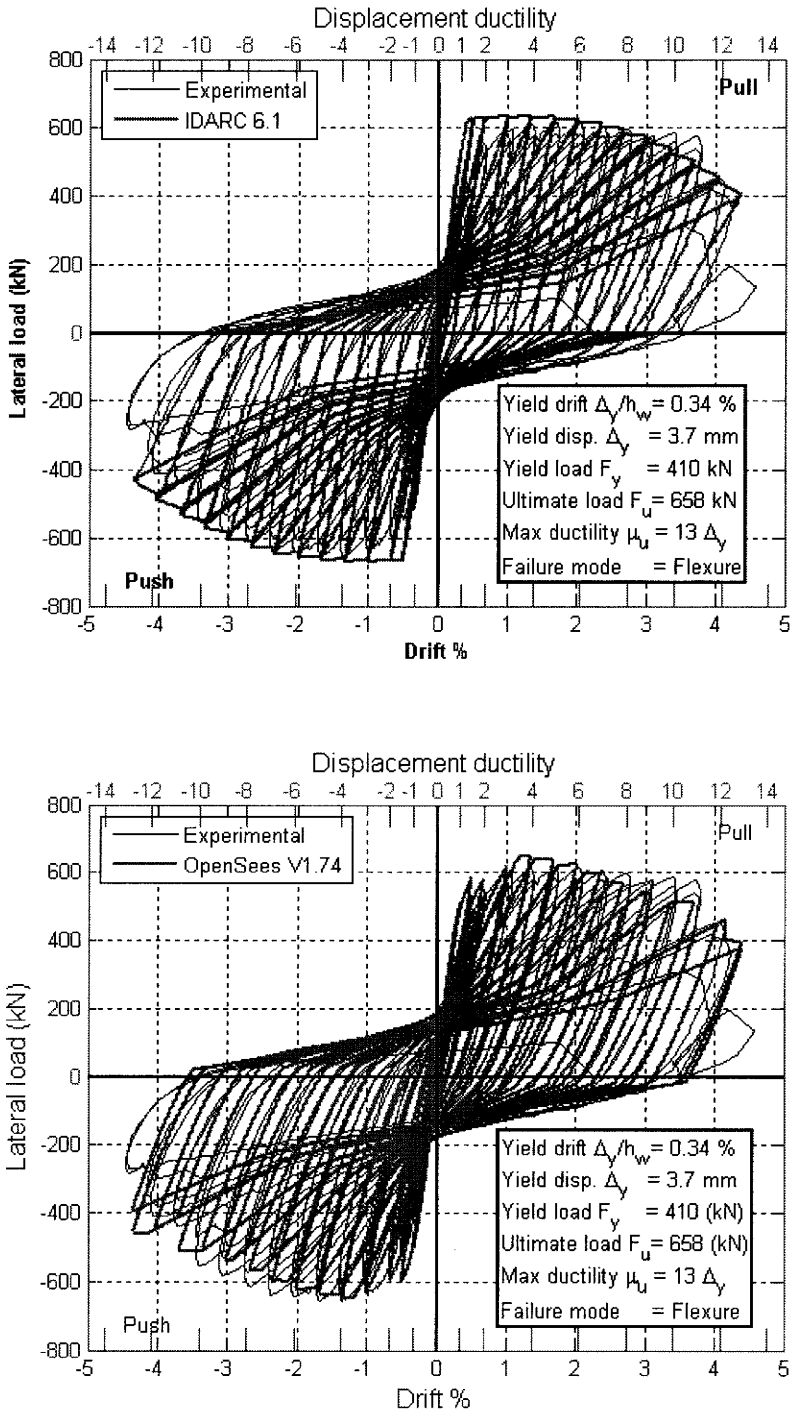

Figure 6. 19 Wall RW6 top drift ratio- lateral load relationship

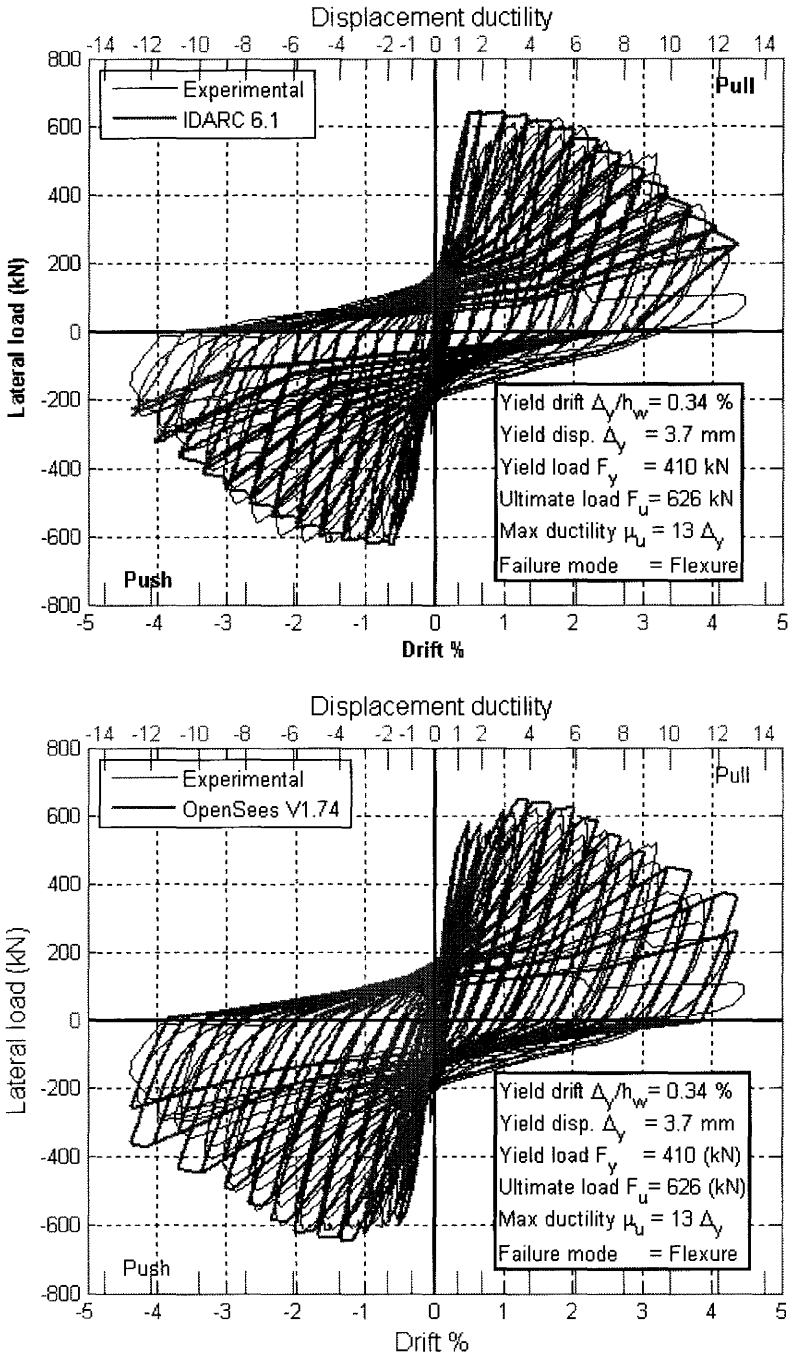

Figure 6. 20 Wall RW7 top drift ratio- lateral load relationship

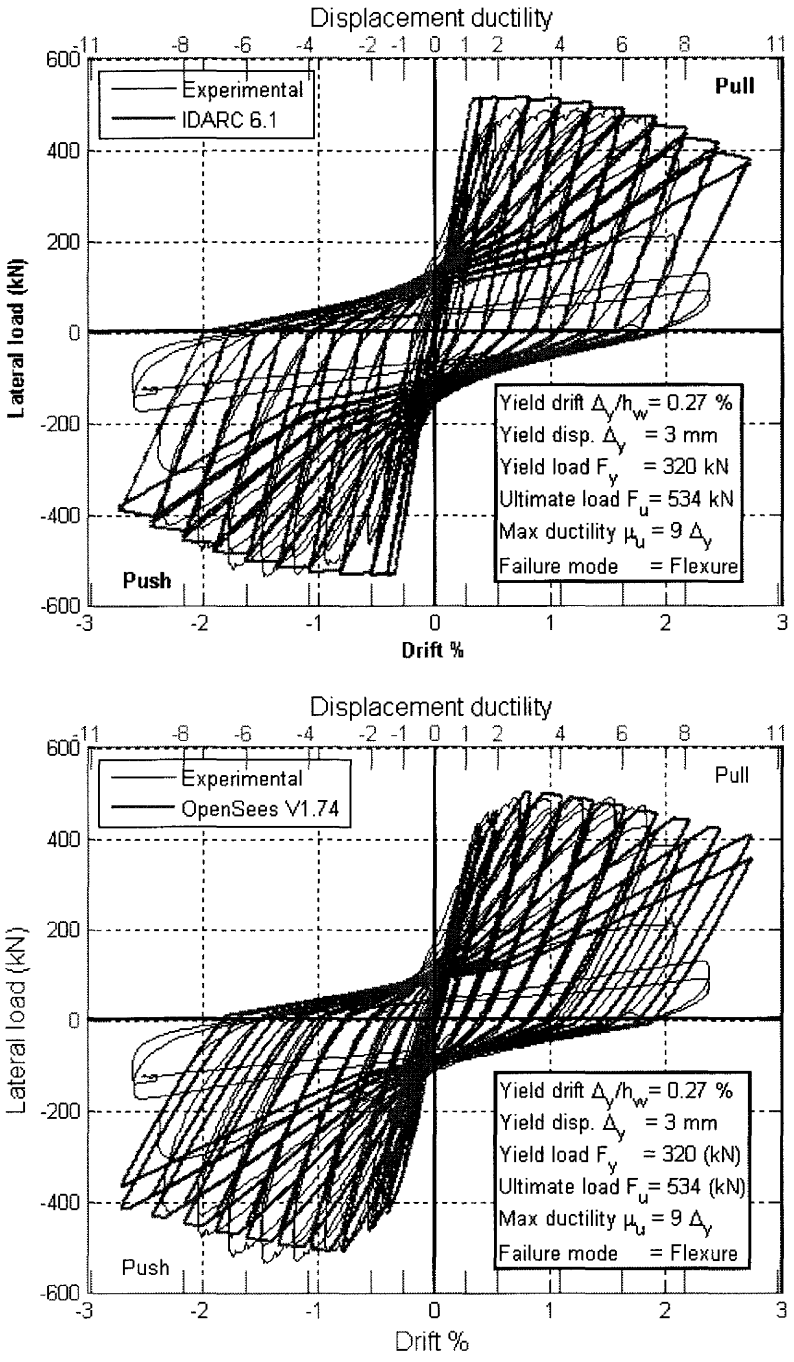

Figure 6. 21 Wall RW8 top drift ratio- lateral load relationship

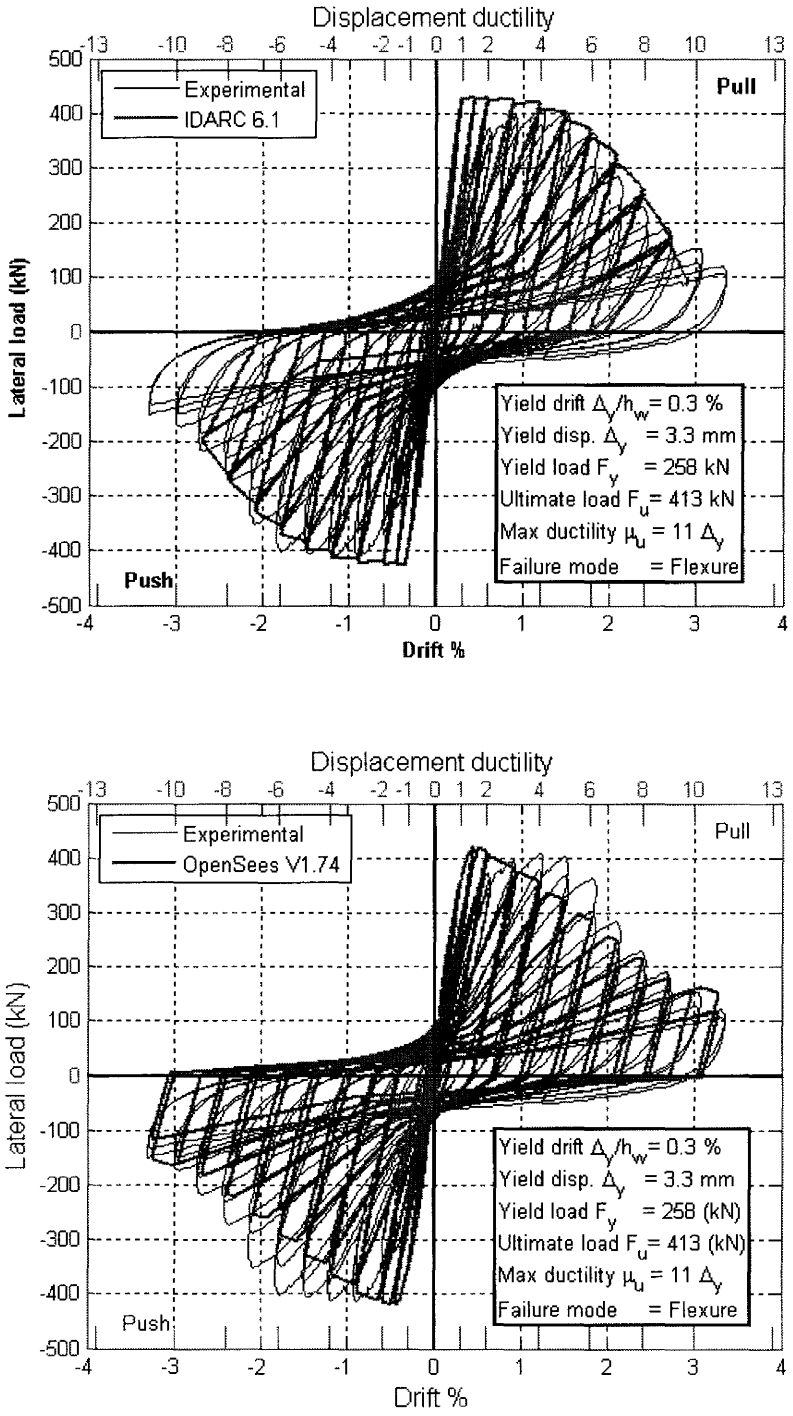

Figure 6. 22 Wall RW9 top drift ratio- lateral load relationship

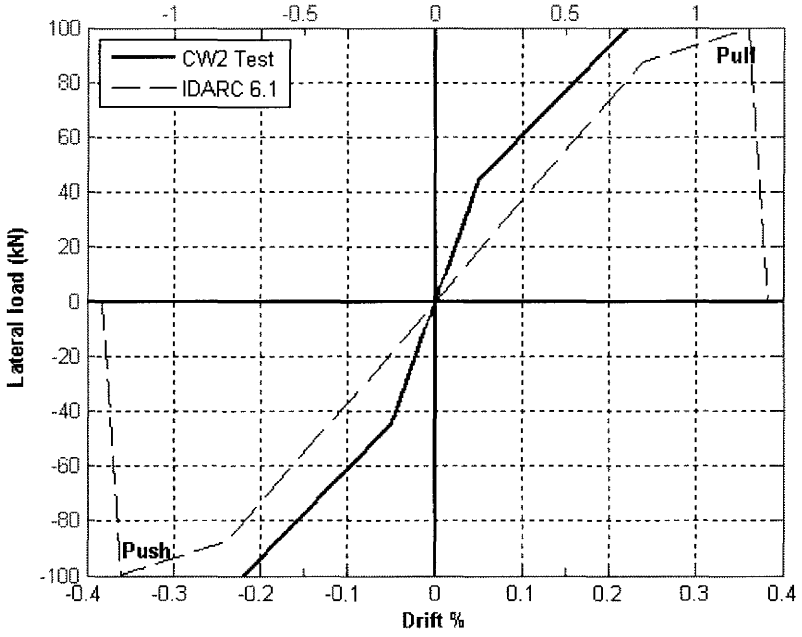

Figure 6. 23 Wall CW2 top drift ratio- lateral load relationship

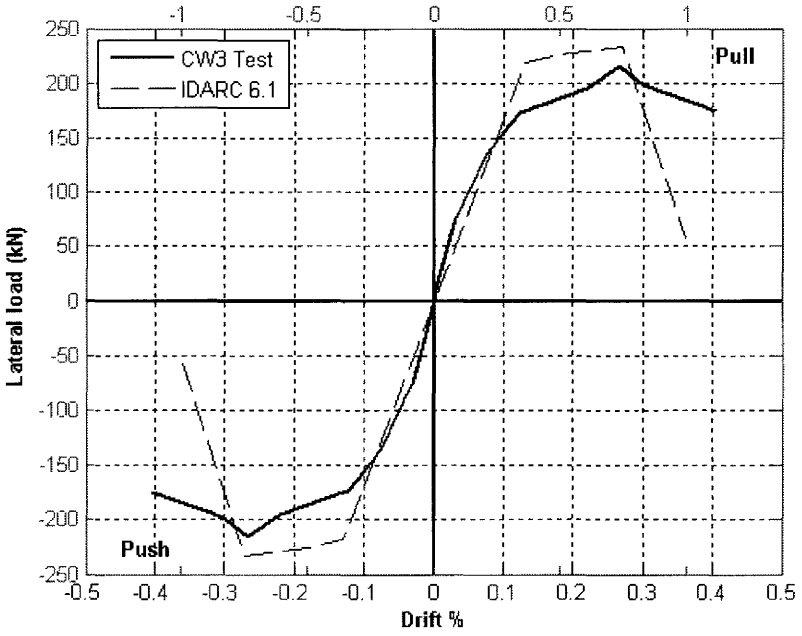

Figure 6. 24 Wall CW3 top drift ratio- lateral load relationship

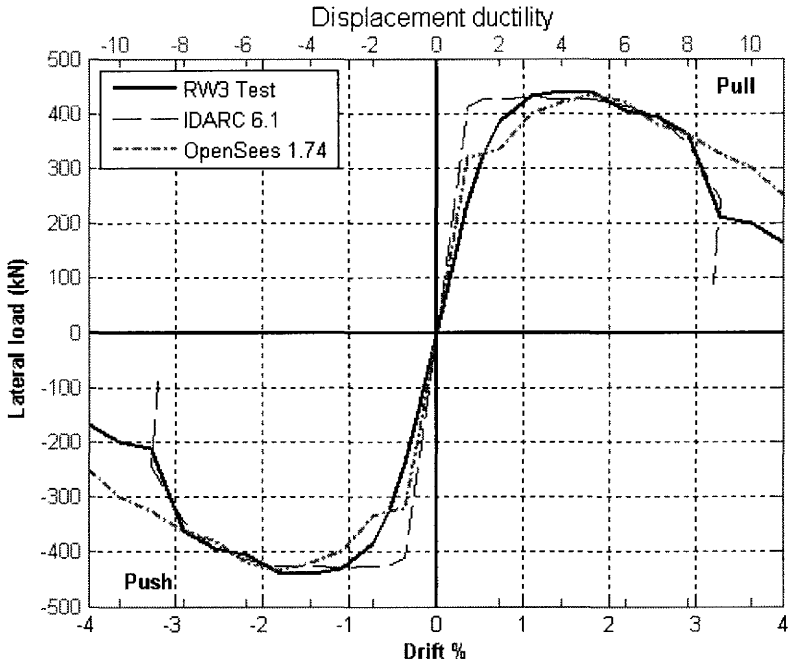

Figure 6. 25 Wall RW3 top drift ratio- lateral load relationship

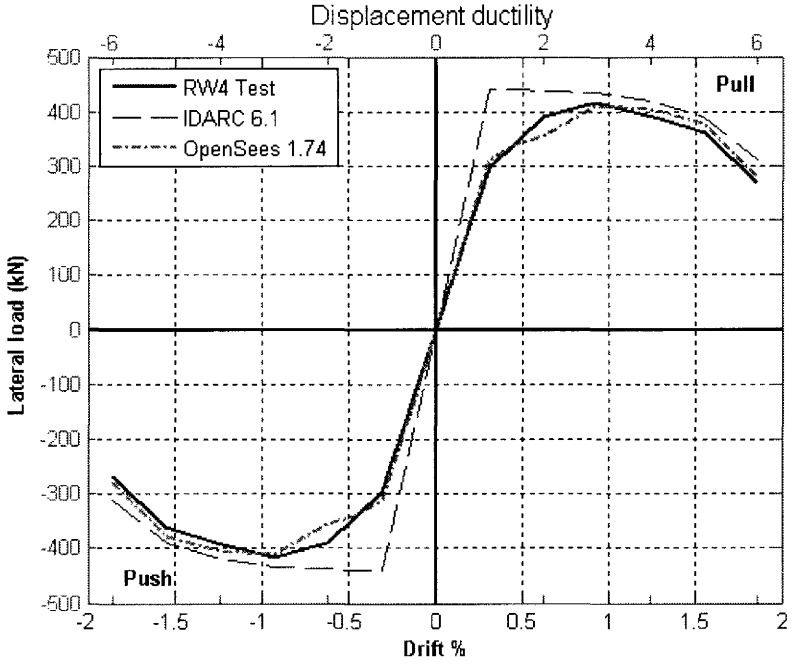

Figure 6. 26 Wall RW4 top drift ratio- lateral load relationship

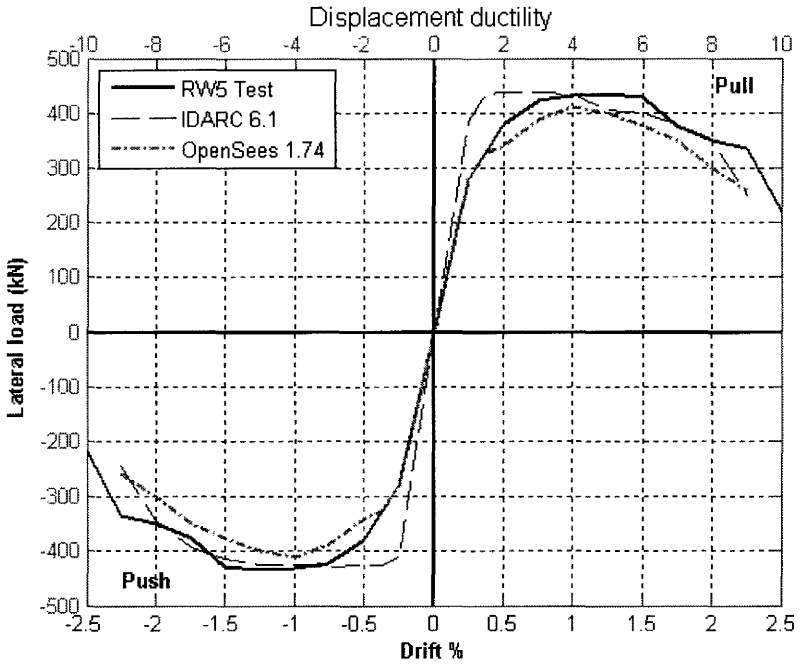

Figure 6. 27 Wall RW5 top drift ratio- lateral load relationship

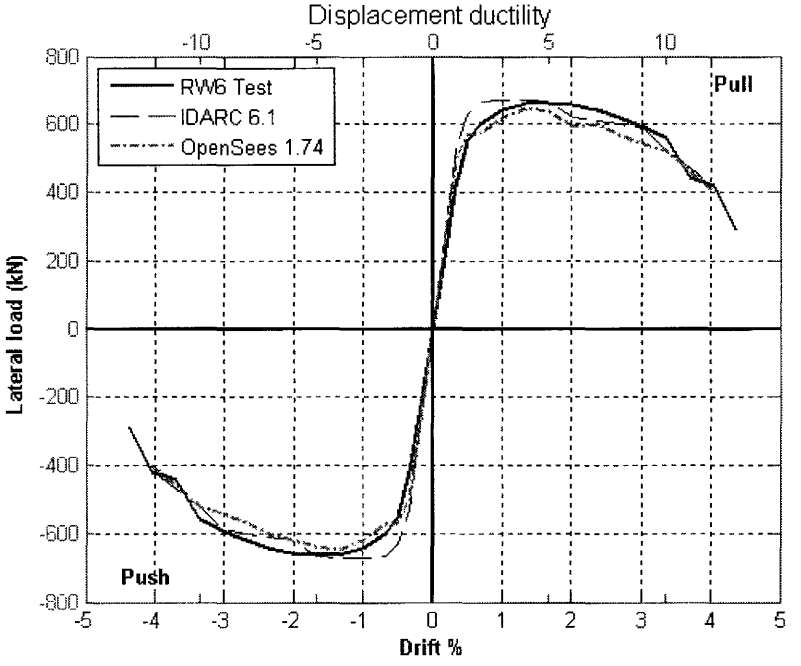

Figure 6. 28 Wall RW6 top drift ratio- lateral load relationship

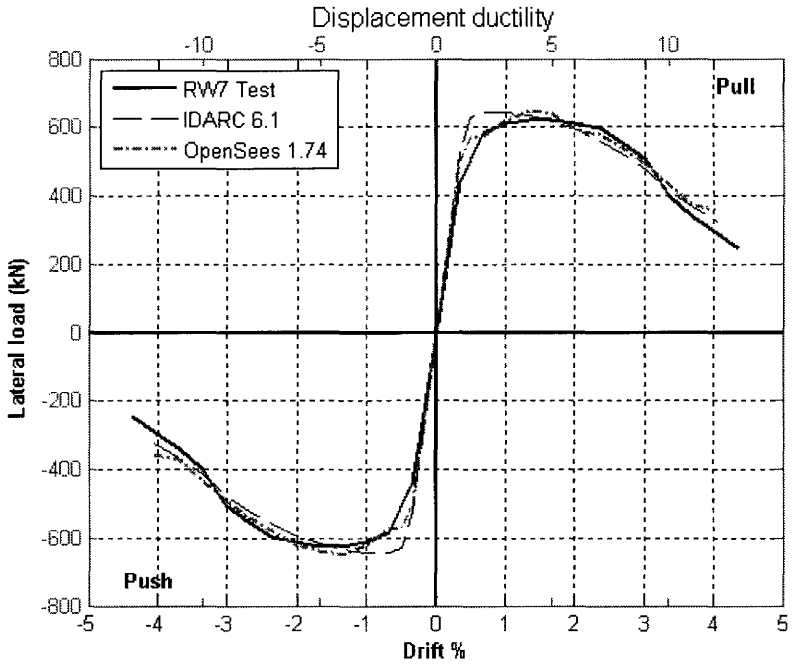

Figure 6. 29 Wall RW7 top drift ratio- lateral load relationship

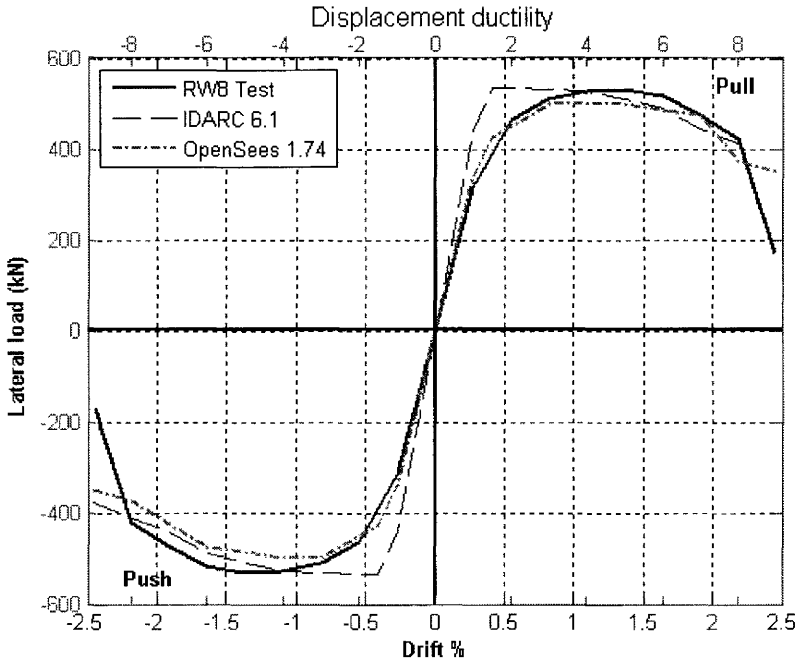

Figure 6. 30 Wall RW8 top drift ratio- lateral load relationship

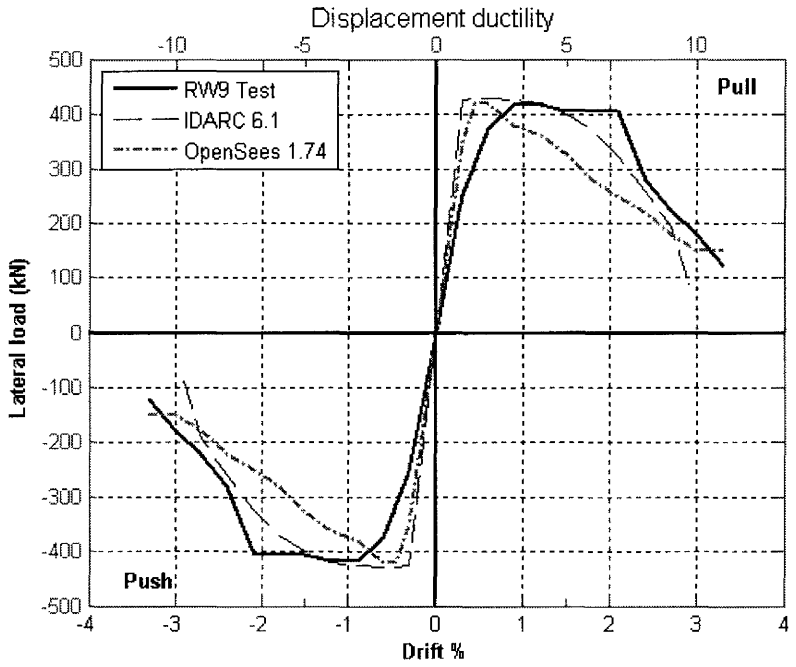

Figure 6. 31 Wall RW9 top drift ratio- lateral load relationship

CHAPTER 7

DYNAMIC ANALYSIS

7.1 INTRODUCTION

Current seismic codes for the design of reinforced concrete structures are based on considerations of inelastic behaviour in the structural members, which requires the formation of desirable plastic hinges at certain well-detailed locations. According to the design practice, well-designed and detailed plastic hinge location of RC structural walls can provide the required ductility and safety to occupants during major earthquakes. Pre-seismic codes designed RC structures may suffer from severe damage or collapse during seismic events. To evaluate an existing RC building, which includes RC structural walls as a lateral resistance system, a nonlinear dynamic analysis is conducted. The building was designed according to the nonseismic codes of the 1960's. The structure was modeled and the bahaviour analyzed when subjected to selected ground motions. The building was rehabilitated, modeled and analyzed again to investigate the effect of the rehabilitation procedures tested earlier on the response of the structure to severe earthquake records.

7.2 DESIGN OF THE EXISTING AND RETROFITTED BUILDINGS

For the purpose of this analytical study, a 10-story RC building was designed. The typical story height was 3.30 m and the building measured 22 m by 30 m in plan. The building dimensions are shown in Figure 7.1. The building was designed according to the American Concrete Institute building code (ACI 318, 1968). The roof and floor slabs were taken as 150 mm thick flat slabs, and the wall cross sections were 360 mm by 3000 mm. The building structural system consisted of flat slabs, columns and RC structural walls. Walls were designed for gravity loads with preseismic shear and lap splice detailing. The lap splice length was 24 times the maximum vertical bar diameter, and it was located at the bottom of walls. The end column elements of the rectangular walls were not adequately

confined to prevent bar buckling and concrete crushing under high reversing compression strains. The loads specified by the Uniform Building Code (UBC, 1964) included only gravity loads. This resulted in minimum shear demands and large spacing between transverse reinforcement. The unfactored design gravity loads for this existing building are taken as 6.00 kN/m^2 dead load and 1.9 kN/m^2 live load.

The deficient RC structural walls of the existing building were retrofitted using the same rehabilitation techniques for RW3 to RW9 as described in Chapter 3 Section 3.7. The results of the experimental program indicated that the rehabilitation techniques were successful in preventing shear and lap splice brittle failure modes and ensuring ductile response of the tested walls.

7.3 NONLINEAR MODELING

The floor slabs are considered as rigid diaphragms in their own horizontal plane. Based on this assumption, one horizontal degree of freedom per floor was considered. The lateral stiffnesses of the columns were neglected compared to that of the RC structural walls. Therefore, the lateral forces were assigned to the RC structural walls, and both columns and RC structural walls carried the vertical loads.

A damping ratio 5 % of critical was assigned to all modes of vibrations. The concept of proportional damping was employed in the nonlinear dynamic analysis. Therefore, the damping was proportional to both the initial stiffness and the mass of RC structural walls. The effects of soil-structure interaction were neglected.

IDARC2D version 6.1, Valles et al., (1996) software was used to perform the inelastic pushover and dynamic time history analyses to evaluate the response of RC structural walls under seismic excitations. The program has the capability of using both lumped plasticity, and spread plasticity concepts. The formulations were based on macro-models in which the nonlinear behaviour was incorporated in the elements formulations. Hysteretic models incorporated in the program simulated the load-deformation of the

structure. The hysteretic models are controlled by parameters accounting for the stiffness degradation, strength deterioration, and pinching of the hysteretic loops.

The damage index developed by Park and Ang (1985) has been incorporated in the program and was used to estimate the accumulated damage sustained by the components of the structure, by each story level, and the global building damage. A global value of the damage index can be used to characterize damage in the entire RC structural walls. This damage index (D) is a simple linear combination of normalized deformation and energy absorption. Calibrations of this damage index model against observed seismic damage, which included at some instances shear and bond failures were the reasons behind using Park and Ang (1985) cumulative damage index model (Williams and Sexsmith 1995). The damage index formula that was suggested by Park and Ang (1985) is:

$$D = \frac{\delta_m}{\delta_u} + \beta_e \frac{\int dE}{F_y \delta_u} \qquad (7.1)$$

Where,

δ_m and δ_u are the maximum and ultimate member displacements, respectively.

β_e = energy based hysteretic strength loss parameter

dE = deformation-related energy

F_y = yield force

A slightly modified version of Park and Ang (1985) index is used in IDARC2D, Park et al. (1987). These modifications included removing the recoverable elastic deformation from the first term in Equation 7.1, and replacing the force and displacement by the moment and curvature as follows:

$$D = \frac{\phi_m - \phi_y}{\phi_u - \phi_y} + \beta_e \frac{\int dE}{M_y \phi_u} \qquad (7.2)$$

Where,

ϕ_m = maximum member curvature

ϕ_u = ultimate member curvature

M_y = yield moment

Park et al. (1985) suggested a value of 0.4 for D to distinguish between repairable and irreparable damage. In addition, they suggested the following classification in 1987:

$D < 0.1$	No damage - localized minor cracking
$0.1 \leq D \leq 0.25$	Minor damage - light cracking throughout
$0.25 \leq D \leq 0.40$	Moderate damage - sever cracking, localized spalling
$0.40 \leq D \leq 1.00$	Sever damage – crushing of concrete, reinforcement exposed
$D \geq 1.00$	Collapsed

Ang et al. (1993) suggested a value of 0.8 for D to define collapse.

The simulation of the hysteretic cyclic behaviour of the tested walls was successfully achieved as presented in Chapter 6. Therefore, in the rest of the current Chapter, the focus is on evaluating the behaviour of existing RC residential buildings that have RC structural walls. The calibration of the hysteretic rule parameters controlling the behaviour of the tested RC walls was achieved by reproducing the test results.

7.3.1 Elements' material properties

Reliable and accurate results can be obtained from inelastic dynamic analysis if the reduced stiffness of the reinforced concrete members was accurately prescribed in the analysis. Access to experimental results that include envelopes of the structure constituent elements is the most realistic approach to the analysis. Since in this study experimental envelopes were available, they were compared with the program generated envelopes. Good correlation between the program generated moment-curvature and the shear force-shear deformation envelopes and the experimental ones.

7.3.2 Hysteretic rules

The hysteretic values that characterize stiffness degradation, strength deterioration, and pinching behaviour for the RC structural walls were incorporated in the model. For simulation of the experimental results, the values were as presented in Table 6.4. The same

hysteretic rules parameters values were implemented in the ten-story building analysis. These parameters were calculated by employing the similitude requirements presented in Table 3.1 and Table 3.2 to the values presented in Table 6.5 and Table 6.6. Table 7.1 and Table 7.2 include the parameters used to represent flexural and shear properties for 10-storey structure. The same tri-linear model as was implemented in the nonlinear cyclic analysis of the tested walls was used in the analysis of ten-story structure analysis.

7.3.3 Analysis type

Dynamic analysis was carried out by specifying a design earthquake record file as an input ground motion data. The program then uses a combination of the Newmark-Beta method, and the pseudo-force method to perform the analysis. The solution was performed incrementally assuming the properties of the structure, such as the flexural stiffness, do not change during the time step. The step size was selected by successive trials until the dynamic response did not change in two consecutive trials, which led to a time step of 0.001 second for performing the analysis.

7.4 PUSHOVER ANALYSIS

The inelastic pushover analysis provides a viable alternative to the inelastic time history dynamic analysis because of its simplicity in estimation of the inelastic performance of structures, Kilar and Fajfar (1999). In addition, the pushover analysis is one of the three analysis options recommended by NEHRP Guidelines for Seismic Rehabilitation of Existing Buildings (FEMA 273, 1997).

Inelastic static pushover analysis of the 10-storey building was performed based on an inverted triangular lateral loading. The pushover analysis procedure involves monotonically pushing the structure under lateral force or displacement control until the roof displacement reaches a certain value in the form of roof lateral drift ratio. The pushover inelastic static procedure eliminates the uncertainty in selecting an appropriate earthquake record; however, one of its drawbacks is its inability to include the inertial

forces in the analysis. Appropriate modeling assumptions and awareness of the pushover analysis limitations are important to obtain reliable results. Successful pushover analysis can be used as a tool to identify the critical weaknesses in the lateral load resisting system of reinforced concrete structures. One of the limitations of the pushover analysis is the assumption that the structure response is dominated by its first fundamental mode of vibration (Krawinkler and Seneviratna 1998). For a stiff building up to 10-storey, this assumption would be a realistic approximation, since higher mode effects are not significant is this case. The local cumulative plastic rotations and overall deformations may be underestimated for high-rise structures that are analyzed using pushover technique, (Fajfar and Gaspersic, 1996). Neglecting the cumulative dissipation energy demand, duration effects, separation between the structural capacity and seismic demand, and incorporation of the strain energy and ignoring the kinetic and viscous damping energy due to the push loading procedure are fundamental drawbacks of the pushover analysis, (Kim and D'Amore 1999). The pushover technique is still used as a useful tool in the seismic design of RC structures. In addition, there are several studies concerning the enhancement of pushover analysis techniques, (Krawinkler and Seneviratna 1998).

Several inelastic analysis programs such as DRAIN 2DX (Prakash and Powell 1993) and IDARC2D (Park et al., 1987; Valles et al., 1996), and OpenSees (Mazzoni et al., 2007) have a built-in pushover analysis capability. In this study, IDARC2D was used to perform the inelastic pushover and time history dynamic analyses to predict the response of RC structural walls under seismic excitations. Results from inelastic pushover analysis are presented in Figures 7.2 to 7.8. The results indicated that the pushover analysis was capable of predicting the yield and the post yield behaviours of both existing and rehabilitated walls. For example, brittle modes of failures in shear for wall CW1 and bond slip for walls CW2 and CW3 were predicted as shown in Figures 7.2 and 7.3. In addition, walls capacities were predicted using inelastic pushover analysis.

7.5 INPUT GROUND MOTION

The magnitude of the earthquake, the epicentral distance, the local geology and the site condition are among the factors, which affect the intensity, duration of strong shaking and frequency content of an earthquake. These factors lead to uncertainty in the earthquake characteristics at a specific site and hence can lead to significant differences in the structural response. Frequency content is one significant indicator that affects the structural response. Short period structures (stiff structures as building with structural walls), i.e. high frequency, are mostly affected by high frequency content earthquakes, while long period structures, i.e. low frequency, would be affected by low frequency content earthquakes. A good indicator of the frequency content of the ground motion is the ratio between the peak ground acceleration PGA, "A" expressed in units of gravitational acceleration "g", to peak ground velocity, "v" expressed in units of m/s. Earthquakes records may be classified according to the frequency content ratio into three categories, high A/v ratio when $A/v > 1.2$, intermediate A/v ratio when $1.2 > A/v > 0.80$ and low A/v ratio when $A/v < 0.80$. From statistical evidence, records with high A/v ratio are associated with stiff soil and rock sites at short epicentral distances, while records on sites with soft conditions at long epicentral distances are characterized by low A/v ratios.

Four actual earthquake records were used to define the input ground motion for performing inelastic dynamic analyses as shown in Figures 7.9 to 7.12. the San Francisco record has high frequency content, the Mexico earthquake has low frequency content and the Imperial Valley and San Fernando records have intermediate frequency contents. For each ground motion, three different maximum PGA scales of 0.20g, 0.50g, and 1.00g, were used as an input for the nonlinear dynamic analysis. Characteristics of the selected earthquake records are presented in Table 7.3.

7.6 DYNAMIC ANALYSIS RESULTS

The behaviour of the ten-storey existing residential building was studied under dynamic loading before and after rehabilitation. The lateral load resisting system was RC structural walls. The existing building has shear and lap splice deficiencies at the critical sections of the lateral load resisting RC structural walls. The structure was analyzed using four selected earthquakees.

7.6.1 Dynamic characteristics of structural walls

To determine the periods of free vibrations of the ten-storey building, IDARC2D version 6.1 was used. The calculated period was compared to the fundamental period estimated using the NBCC (2005) provision. From the program analysis the fundamental period of the structure was 1.035 second, which classifies the structure to have frequency content in the intermediate range. The fundamental period estimated using the NBCC (2005) clause 4.1.8.11.3c provision was 0.69 second. Therefore, the calculated fundamental period was 1.49 times that estimated by the NBCC (2005). The program estimated fundamental period of the structural walls as well as the second and the third mode periods were plotted as shown in Figures 7.13 to 7.16 to identify the locations of the first three modes periods of vibrations on the response spectra of the selected earthquake records. The second and the third mode periods were 0.16 and 0.06 second, respectively. In addition, the relative modal masses were 0.65, 0.20, and 0.07 for the first, second, and third modes of vibrations, respectively. This indicated that the first mode was dominant and the sum of the first three modes was approximately 0.92 of the total modal mass.

7.6.2 Roof displacement time histories

Nonlinear dynamic analysis results for the ten storey building with the ten tested walls are summarized in the form of maximum predicted roof displacement as presented in Tables 7.4 to 7.7. Figures 7.17 to 7.56 show the roof displacement time histories of the walls when subjected to the four selected earthquake records at three different PGA levels of 0.2 g, 0.50 g and 1.0 g. It was observed from the dynamic analysis results that the

displacements histories resulting from the different input ground accelerations are proportional to the levels of the PGAs when the structure responds elastically as in the case of San Francisco earthquake record. This was because the San Francisco earthquake record is rich in high frequency acceleration that does not impart significant energy to the structure to cause inelasticity. For the case of the highest level of ground acceleration considered in this study of 1.0g , there was significant damage and multi-hinge formation in the structural walls. The damage indices and the sequences of the plastic hinge formation are discussed in the next two sections, respectively.

The response of the rehabilitated walls was elastic when the selected earthquakes records were scaled to a PGA of 0.2g. Minor damage was observed in the existing walls CW2 and CW3 with lap splice deficiency when subjected to El Centro earthquake scaled to 0.2g as shown in Figures 7.18 and 7.19 and Table 6.8. In addition, Table 6.8 and Figures 7.38 and 7.39 indicate that major damage occurred when they exposed to Mexico record scaled to PGA of 0.2g. This observation indicated that the rehabilitation techniques were successful in preventing brittle modes of failures.

Except for the case of San Francisco record, the existing walls either failed in shear or in bond slip failure modes when the PGA was scaled to 0.5g. For this PGA level, the response of the rehabilitated walls remained almost elastic with minor cracks except for the case of Mexico earthquake where rehabilitated walls RW3 to RW5 yielded at the first storey with minor damage spreading up to the fourth storey level. This was attributed to the strength of these three rehabilitated walls, which was the lowest amongst the tested rehabilitated walls.

At the extreme case of PGA scaled to 1.0g the rehabilitated walls yielded and flexural plastic hinges formed at the base of the walls. The flexural hinge at the base of the walls was followed by multi-hinges formation under the effect of the selected earthquake records. The exception was the case of the San Francisco earthquake where the response remained elastic and the collapse of the existing walls under the effect of other three earthquake records. Again the most severe damage occurred in the rehabilitated walls was

in walls RW3 to RW5 as well as walls RW8 and RW9. Walls RW6 and RW7 experienced the least damage because of their high strength as compared to the other rehabilitated walls. When the Mexico earthquake scaled to 0.5g was applied to the building the existing walls CW2 and CW3 failed in bond slip as shown in Figures 7.38 and 7.39. However, Figures 7.40 to 7.42 indicate that the rehabilitated walls RW3 to RW5 developed plastic hinge mechanism at the bottom of the walls.

As a general outcome of this analytical study, Mexico earthquake ground motion was the most damaging record compared to the rest of selected group as shown in Figures 7.57 to 7.64. This was because of the effect of the earthquake duration (long duration) that was associated with low A/v ratio. In addition, walls RW6 to RW9 response was elastic throughout the duration of the four selected ground motion as presented in Table 7.6. Table 7.7 presents definitions of the used parameters in Tables 7.4 to 7.6.

7.6.3 Damage index

A benchmark damage model developed by Park and Ang (1985) was slightly modified and included in IDARC2D program to provide a measure of the accumulated damage sustained by the entire structure, by each storey level, and by components of the structure. The ratio of the maximum to ultimate deformations and the ratio of the maximum hysteretic energy dissipated to the maximum monotonic energy are included in this damage index to capture both components of damage. The damage index (D.I.) provided information about both the local component and entire structure damage levels. The damage levels can be classified as light, repairable, irreparable or collapse (Rodriguez-Gomez and Cakmak 1990). For safety reasons, the current seismic design practices accept damage provided that collapse is prevented. The damage index value of 0.0 refers to no damage and D.I. of 1.0 means collapse is imminent. The collapse prevention level is at D.I. of 0.8 as defined by Ang et al., (1993).

The damage index for each wall is presented in Tables 7.8 to 7.10. These tables list only the first four floors, since no damage occurred higher than the fourth floor except in three cases. Moreover, if blank this indicates the damage is zero. Figures 7.57 to 7.64 show

schematic drawings representing cracks and plastic hinges developments in walls when subjected to the four selected earthquake records scaled to three different PGA levels. Light damage was predicted for the case of the selected four earthquakes scaled to PGA of 0.2g, except for the case of CW2 and CW3 when subjected to El Centro and Mexico earthquakes. Table 7.8 shows that for El Centro record scaled to 0.2g walls CW2 and CW3 the D.I. was 0.375 and 0.396, respectively while the D.I. was 0.66 and 0.89, respectively for the same walls CW2 and CW3 when subjected to Mexico record scaled to 0.2g. These observations from the analysis results indicate that walls CW2 and CW3 failed in bond slip for the case of Mexico earthquake and they suffered major damage when subjected to El Centro record while the rehabilitated walls were behaving elastically. In addition, Table 7.9 presents results of the analysis when the walls subjected to the selected earthquake records scaled to PGA of 0.5g. Analysis results indicated that the rehabilitation techniques reduced the damage significantly. The exception is the case of Mexico record scaled to 0.5g where RW4 and RW5 experienced damage indices at the first storey larger than 0.7, which indicated formation of multi-plastic hinges and eventually a collapse mechanism as presented in Table 7.9 and Figure 7.60. At the severe level of PGA scaled to 1.0g, and from Table 7.10 and Figures 6.61 to 6.64 the rehabilitated walls RW6 and RW7 showed the best performance and only sustained repairable damage. This observation indicates that the effective rehabilitation approach addresses both the ductility and the strength of the lateral load resisting system.

7.6.4 Plastic hinge locations

Figures 7.57 to 7.64 show cracks and plastic hinge locations in the walls when subjected to the four selected earthquake records at three different PGA levels. For El Centro record scaled to 0.2g only the existing walls CW2 and CW3 cracked at the first storey and the bottom of the second storey as shown in Figure 7.57. No cracks were detected in the rest of the walls. At the same scale of the PGA but when the walls were subjected to Mexico record, Figure 7.58 shows that a splice failure was detected at base of the existing wall CW3 and wall CW2 with cracks in the first and second storeys. In

addition, rehabilitated walls RW3 to RW5 as well as RW9 cracked at the first storey and the bottom of the second storey but no plastic hinges were developed as shown in Figure 7.58.

All walls cracked when subjected to either El Centro or Mexico records scaled to PGA of 0.5g. The cracks spread up to the fourth storey for existing walls CW2 and CW3, which had a lap splice failure as shown in Figures 7.59 and 7.60. Figure 7.60 shows that walls RW3 and RW5 developed plastic hinges at the bottom of the walls. The existing walls CW2 and CW3 showed a lap-splice failure at the bottom of the first storey when subjected to the San Fernando record scaled to 0.5g as presented from in Figures 7.61. The rest of the walls cracked without developing any plastic hinges as shown in Figures 7.61.

Shear failures were detected in all stories of existing wall CW1 when subjected to El Centro record scaled to 1.0g as shown in Figures 7.62. Walls CW2 and CW3 had a splice failure when subjected to the same record with the same PGA level. The rehabilitated walls showed a ductile response and development of plastic hinges at the first storey, which supports the conclusion that the rehabilitation techniques prevented brittle failure modes and provided safety against structural collapse. The same trend of wall performance was predicted when the walls were subjected to Mexico record and San Fernando records scaled to 1.0g with the most severe damage from Mexico record and the least damage from San Fernando record as shown in Figures 7.63 and 7.64.

7.6.5 Envelopes of lateral displacements

The envelopes of the lateral displacements for the three selected levels of peak ground acceleration of the four selected records are shown in Figures 7.65 to 7.67. The figures show that the maximum displacements were due to the Mexico record at all PGA scales. The San Francisco record caused the least lateral displacements of the walls. Moreover, El Centro record caused larger lateral displacements of the walls than San Fernando record. The reason behind this is the energy of the input ground motion. Mexico and El Centro records caused the largest and the San Francisco caused the least energy dissipation compared to the four selected records as shown in Figure 7.16.

Figure 7.65 shows that the lateral displacements for all walls were almost equal when subjected to the same earthquake record at the same PGA level. At this PGA scale of 0.2g the walls almost remained elastic. When the walls subjected to higher level of PGAs as shown in Figures 7.66 and 7.67, a large difference between the lateral displacements of the walls were observed. Analysis of results indicated that the input ground motion characteristics, the structure ductility and strength, and the inelastic response of the structure were to be examined together to understand the performance of the structural system under seismic loads.

7.6.6 Envelopes of interstory drift

The envelopes of the interstory drift ratio for the three scaled levels of peak ground acceleration of the four selected records are shown in Figures 7.68 to 7.70. To avoid structural instability and to control damage, the National Building Code of Canada, NBCC (2005) Cl. 4.1.8.13.3 limits the interstory drift ratio to 2.5% for residential buildings. Figures 7.68 to 7.69 show the maximum interstory drift envelopes when the walls were subjected to PGAs of 0.2g and 0.5g, respectively. It was observed that Mexico record scaled to PGA of 0.5g caused the maximum interstory drift ratios in the walls, however, they were less than 2.5% except for the case of wall RW5 as shown in Figure 6.69.

The maximum interstory drift for the case of the San Francisco record scaled to a PGA of 1.0g was approximately 0.8 % as shown in Figure 7.70, which reinforced the conclusion of small effect of this earthquake record on the walls. Moreover, El Centro record of PGA of 1.0g caused interstory drift ratios less than 2.5 % NBCC (2005) Cl. 4.1.8.13.3 limits for all walls except walls RW3 and RW5. The San Fernando record of PGA of 1.0 g caused interstory drift ratios less than 2.5% except for walls RW3 to RW5. It was observed that the major damage was localized at the first storey because of the formation of plastic hinges at the bottom of the walls. Mexico record scaled to PGA of 1.0g caused the largest interstory drift ratios which exceeded 2.5% for all walls as shown in Figure 7.70.

7.6.7 Envelopes of curvature

The envelopes of the wall curvature for the three scales of peak ground acceleration of the four selected records are shown in Figures 7.71 to 7.73. The last figure indicates that significant yielding has taken place in the walls and a curvature demand was localized at the first story due to the excessive yielding and plastic hinge formation. Curvature demand was the largest when the walls were subjected to Mexico record as compared to other earthquake records. Existing walls failed due to lack of sufficient curvature while rehabilitated walls sustained high curvature levels.

7.6.8 Envelopes of bending moment

The envelopes of the wall bending moment for the three scaled levels of peak ground acceleration of the four selected records are shown in Figures 7.74 to 7.76. As expected the maximum moment was at the base of the walls. Figure 7.74 indicates that the maximum moment demand was due to Mexico record compared to the rest of the records. Existing walls CW2 and CW3 failed due to lack of sufficient flexural capacity while the rehabilitated walls sustained high moments before yielding.

7.6.9 Envelopes of storey shear

The envelopes of the walls storey shear forces for the three scales of peak ground acceleration of the four selected records are shown in Figures 7.77 to 7.79. As expected the maximum shear force was at the base of the walls. The figures indicate that no shear failure occurred before the first story yielded and the plastic hinge was formed for the rehabilitated walls. Shear force demand was the largest when the walls were subjected to Mexico record as compared to the other earthquake records. Existing wall CW1 failed due to lack of sufficient shear strength while rehabilitated walls sustained high shear forces and the shear deformation was in the elastic range.

7.7 SUMMARY

The inelastic static and dynamic analyses of ten-storey existing residential building before and after rehabilitation were conducted. The analysis provided detailed behaviour of the structure and provided insight into the behaviour of the unstrengthened and the rehabilitated walls. The non-ductile detailing at the critical sections of the lateral load resisting RC structural walls of existing building showed brittle failure modes under seismic events. The rehabilitated walls showed ductile response when subjected to the four selected different earthquake records. Unlike constant moment to shear ratio (M/VL) for the cyclic and pushover techniques, the dynamic schemes result a continuously varying moment to shear ratio. The moment to shear ratios of 1.1, 2.25, and 5 in the experimental and cyclic analytical part of this study represent the worst case scenarios for the pure shear dominated, flexure/ shear coupled, and pure flexural responses, respectively. Therefore, they cover the most practical ranges of variations of moment to shear ratio during seismic events.

Table 7.1 User input of flexure properties for dynamic analysis of ten-story building

Parameter*	Control walls			Rehabilitated walls						
	CW1	CW2	CW3	RW3	RW4	RW5	RW6	RW7	RW8	RW9
KHYSW	1	1	1	1	1	1	1	1	1	1
EA/L	10227.27	10227.27	10227.27	10227.27	10227.27	10227.27	10227.27	10227.27	10227.27	10227.27
EI	2.53e13	2.53e13	2.53e13	2.53e13	2.53e13	2.53e13	2.53e13	2.53e13	2.53e13	2.53e13
PCP	261.90e5	108.00e5	94.50e5	135.50e5	175.50e5	189.00e5	261.90e5	270.00e5	283.50e5	189.00e5
PYP	380.70e5	135.00e5	135.00e5	256.50e5	267.30e5	245.70e5	380.70e5	391.50e5	310.50e5	259.20e5
UYP	2.00e-6	1.167e-6	0.667e-6	1.333e-6	1.333e-6	1.293e-6	2.00e-6	2.56e-6	2.00e-6	3.33e-6
UUP	3.30e-6	2.33e-6	2.00e-6	16.66e-6	10.00e-6	10.00e-6	33.33e-6	33.33e-6	23.33e-6	16.66e-6
EI3P	1	5	5	1	1	1	1	1	1	1
PCN	261.90e5	108.00e5	94.50e5	135.50e5	175.50e5	189.00e5	261.90e5	270.00e5	283.50e5	189.00e5
PYN	405.00e5	135.00e5	135.00e5	256.50e5	251.10e5	264.60e5	405.00e5	383.40e5	324.00e5	259.20e5
UYN	2.00e-6	1.167e-6	0.667e-6	1.333e-6	1.333e-6	1.293e-6	2.566e-6	2.56e-6	2.00e-6	3.33e-6
UUN	3.30e-6	2.33e-6	2.00e-6	16.66e-6	10.00e-6	10.00e-6	33.33e-6	33.33e-6	23.33e-6	16.66e-6
GA3N	1	5	5	1	1	1	1	1	1	1

* The parameters definitions were given in Table 6.5

Table 7.2 User input of shear properties for dynamic analysis of ten-story building

Parameter*	Control walls			Rehabilitated walls						
	CW1	CW2	CW3	RW3	RW4	RW5	RW6	RW7	RW8	RW9
KHYSW	2	2	2	2	2	2	2	2	2	2
EA/L	10227.27	10227.27	10227.27	10227.27	10227.27	10227.27	10227.27	10227.27	10227.27	10227.27
GA	13.50e6	13.50e6	13.50e6	13.50e6	13.50e6	13.50e6	13.50e6	13.50e6	13.50e6	13.50e6
PCP	3150.0	3831.3	3831.3	7662.6	7662.6	7662.6	7662.6	7662.6	7662.6	7662.6
PYP	3420.0	3870.0	3870.0	7740.0	7740.0	7740.0	7740.0	7740.0	7740.0	7740.0
UYP	5.80e-4	2.90e-4	2.90e-4	5.80e-4	5.80e-4	5.80e-4	5.80e-4	5.80e-4	5.80e-4	5.80e-4
UUP	0.01	1.00	0.01	1.00	1.00	1.00	1.00	1.00	1.00	1.00
GA3P	2	2	2	2	2	2	2	2	2	2
PCN	3150.0	3831.3	3831.3	7662.6	7662.6	7662.6	7662.6	7662.6	7662.6	7662.6
PYN	3420.0	3870.0	3870.0	7740.0	7740.0	7740.0	7740.0	7740.0	7740.0	7740.0
UYN	5.80e-4	2.90e-4	2.90e-4	5.80e-4	5.80e-4	5.80e-4	5.80e-4	5.80e-4	5.80e-4	5.80e-4
UUN	0.01	1.00	0.01	1.00	1.00	1.00	1.00	1.00	1.00	1.00
GA3N	2	2	2	2	2	2	2	2	2	2

* The parameters definitions were given in Table 6.7

Table 7.3 Characteristics of selected earthquake records

No.	Earthquake	Date	Magnitude	Station name	Epicentral distance (km)	Comp.	Max. Acc. A(g)	Max. Vel. (m/s)	A/ V Ratio	Soil
1	San Francisco CA	Mar. 22, 1957	5.25	Golden Gate Park	11	S80E	0.105	0.046	2.28	Rock
2	Imperial Valley, CA	May 18, 1940	6.60	El Centro	8	S00E	0.348	0.334	1.04	Stiff Soil
3	Mexico	Sept. 19, 1985	8.1	Zihautenejo, Guerrero Array	135	S00E	0.103	0.159	0.65	Rock
4	San Fernando, CA	Feb. 9, 1971	6.40	Hollywood storage P.E. Lot, L. A.	35	N90E	0.211	0.211	1.00	Stiff Soil

Table 7.4 Dynamic analysis results for PGA of 0.20g

EQ.	Symbol*	CW1	CW2	CW3	RW3	RW4	RW5	RW6	RW7	RW8	RW9
El Centro	crack	---	F4.44	F4.44	---	---	---	---	---	---	---
	Yield	---	---	---	---	---	---	---	---	---	---
	Δ_{top}	143.58	143.58	143.58	143.6	143.6	143.6	143.6	143.6	143.6	143.6
	V_{base}	621	621	621	621.1	621.1	621.1	621.1	621.1	621.1	621.1
San Fernando	Crack	---	---	---	---	---	---	---	---	---	---
	Yield	---	---	---	---	---	---	---	---	---	---
	Δ_{top}	105.5	105.5	105.5	105.5	105.5	105.5	105.5	105.5	105.5	105.5
	V_{base}	443.9	443.9	443.9	443.8	443.8	443.8	443.8	443.8	443.8	443.8
San Francisco	Crack	---	---	---	---	---	---	---	---	---	---
	Yield	---	---	---	---	---	---	---	---	---	---
	Δ_{top}	31.6	31.6	31.6	31.6	31.6	31.6	31.6	31.6	31.6	31.6
	V_{base}	317.25	317.25	317.25	317.4	317.4	317.4	317.4	317.4	317.4	317.4
Mexico	Crack	---	F15.39	F15.37	F15.96	F18.55	---	---	---	---	F36.39
	Yield	---	---	F16.0	---	---	---	---	---	---	---
	Δ_{top}	213.35	223.13	222.06	205.05	213.27	213.35	213.35	213.35	213.35	213.35
	V_{base}	977	888.3	2647.5	906.74	963.2	977	977	977	977	977

* for definitions refer to Table 7.7

Table 7.5 Dynamic analysis results for PGA of 0.50g

EQ.	Symbol*	CW1	CW2	CW3	RW3	RW4	RW5	RW6	RW7	RW8	RW9
El Centro	Crack	F4.43	F2.3	F2.03	F2.79	F2.83	F2.85	F4.43	F4.44	F4.47	F2.85
	Yield	---	F2.88	F2.82	---	---	---	---	---	---	---
	Δ_{top}	358.9			287.2	324	323	358.9	358.9	358.9	300.86
	V_{base}	1570.2			1035.6	1171.6	1206	1545.6	1521.1	1552.6	1225.4
San Fernando	Crack	---	F3.1	F2.71	F3.13	F3.62	F3.63	---	---	---	F3.63
	Yield	---	F3.85	F3.15	---	---	---	---	---	---	---
	Δ_{top}	263.7		242.3	262.1	263.3	263.4	263.75	263.75	263.75	262.8
	V_{base}	1109.8		2666.5	1000.8	1050.2	1093.5	1109.4	1109.4	1109.4	1060.3
San Francisco	Crack	---	---	---	---	---	---	---	---	---	---
	Yield	---	---	---	---	---	---	---	---	---	---
	Δ_{top}	79.11	79.11	79.11	79.11	79.11	79.11	79.11	79.11	79.11	79.11
	V_{base}	793.1	793.1	793.1	793.1	793.1	793.1	793.1	793.1	793.1	793.1
Mexico	Crack	F15.38	F11.65	F11.63	F13.35	F13.96	F14.95	F15.38	F15.39	F15.39	F14.95
	Yield	---	F15.47	F13.5	F16.04	---	F15.04	---	---	---	---
	Δ_{top}	501.47	SF16.77	SF15.57	610.04	---	774.73	493.85	476.8	482.52	411.56
	V_{base}	2228.6	3890.6	---	1612.3	---	1939.1	1718.57	1660.6	1893.3	1472.9

* for definitions refer to Table 7.7

Table 7.6 Dynamic analysis results for PGA of 1.00g

EQ.	Symbol*	CW1	CW2	CW3	RW3	RW4	RW5	RW6	RW7	RW8	RW9
El Centro	Crack	F2.33	F1.86	F1.85	F1.88	F2.01	F2.02	F2.33	F2.79	F2.8	F2.03
	Yield	S3.53	F2.33	F1.99	F2.9	F2.86	F2.87	F3.48	---	F2.9	F3.04
	Δ_{top}				929.7	591.52	1524.7	581.5	560.97	599.26	654.4
	V_{base}				2437.2	1592.95	2373.9	2501.3	1909.1	1674.1	---
San Fernando	Crack	F3.13	F2.51	F2.11	F2.52	F2.69	F2.71	F3.13	F3.13	F3.13	F2.71
	Yield	---	F2.7	F2.68	F3.17	F3.16	F3.16	---	---	F3.67	---
	Δ_{top}	531.3			296	762.7	1202.8	527.7	525.26	521.1	541.42
	V_{base}	1849.9			619.3	512.2	3299.2	1983.3	1982.7	2211	1739.9
San Francisco	Crack	---	F1.5	F1.49	F1.66	---	---	---	---	---	---
	Yield	---	---	F1.67	---	---	---	---	---	---	---
	Δ_{top}	158.23	138.51	157.9	156.35	158.2	158.2	158.2	158.2	158.2	158.2
	V_{base}	1585.9	1505.6	3035.1	1544.1	1586.2	1586.2	1586.2	1586.2	1586.2	1586.2
Mexico	Crack	F13.95	F10.63	F10.61	F11.06	F11.61	F11.62	F13.35	F13.35	F13.36	F23.2
	Yield	S15.47	F11.72	F11.08	F13.51	---	F13.48	F15.41	F15.45	F15.42	F26.74
	Δ_{top}	---	---	---	SF16.99	---	---	1074.21	973.83	1826.24	---
	V_{base}	---	3522	3327.7	---	5192.6	5590.6	2745.1	2577.8	4904.1	5903.1

* for definitions refer to Table 7.7

Table 7.7 Dynamic analysis results parameter definitions

Parameter	Definition
Crack	Type of crack and time at crack in seconds
Yield	Type of yield and time at yield in seconds
Δ_{top}	Roof displacement in mm
V_{base}	Base shear in kN
F	Flexural
S	Shear and time of occurrence
SY	Shear yield and time of occurrence
SF	Shear failure and time of occurrence

Table 7.8 Park and Ang (1985) damage index for ten-storey building subjected to records of PGA of 0.20g

EQ.	storey	CW1	CW2	CW3	RW3	RW4	RW5	RW6	RW7	RW8	RW9
El Centro	1st	0.00	0.375	0.396							
	2nd			0.37							
	3rd										
	4th										
San Fernando	1st										
	2nd										
	3rd										
	4th										
San Francisco	1st										
	2nd										
	3rd										
	4th										
Mexico	1st		0.655	0.897	0.079	0.14					
	2nd		0.369	0.407	0.064						
	3rd			0.378							
	4th										

Table 7.9 Park and Ang (1985) damage index for ten-storey building subjected to records of PGA of 0.50g

EQ.	storey	CW1	CW2	CW3	RW3	RW4	RW5	RW6	RW7	RW8	RW9
El Centro	1st	0.678	Collapse	Collapse	0.102	0.202	0.204	0.066	0.067	0.096	0.139
	2nd			0.423	0.082	0.141	0.146				
	3rd			0.404	0.067	0.122					
	4th										
San Fernando	1st		Collapse	Collapse	0.091	0.145	0.153				0.097
	2nd		0.371	0.405	0.071	0.114					
	3rd			0.388	0.059						
	4th										
San Francisco	1st										
	2nd										
	3rd										
	4th										
Mexico	1st	Collapse	Collapse	---	0.256	Collapse	0.765	0.097	0.123	0.204	0.276
	2nd	0.821	0.362	---	0.109	0.22	0.176	0.072	0.067		0.09
	3rd		0.343		0.072	0.162	0.136	0.058			
	4th				0.06	0.122					

Table 7.10 Park and Ang (1985) damage index for ten-storey building subjected to records of PGA of 1.00g

EQ.	storey	CW1	CW2	CW3	RW3	RW4	RW5	RW6	RW7	RW8	RW9
El Centro	1st	Collapse	Collapse	Collapse	0.577	0.602	Collapse	0.125	0.135	0.291	Collapse
	2nd	Collapse	0.529	---	0.106	0.206	0.211	0.083	0.076		---
	3rd	Collapse	0.382		0.091	0.157	0.163	0.064			
	4th	Collapse	0.37		0.078						
San Fernando	1st	1.177	Collapse	Collapse	Collapse	Collapse	Collapse	0.096	0.115	0.216	0.362
	2nd	0.761	---	0.07	---	---	0.197	0.071	0.063		0.223
	3rd	0.565		0.072			0.158	0.056			
	4th			0.108							
San Francisco	1st		0.667	0.706	0.074						
	2nd			0.395							
	3rd										
	4th										
Mexico	1st	---	Collapse	Collapse	Collapse	Collapse	Collapse	0.347	0.383	Collapse	Collapse
	2nd	Collapse	0.39	0.412	---	0.212	0.193	0.092	0.105		0.085
	3rd	---	0.036	0.40		0.152	0.159	0.073	0.066		0.035
	4th					0.128	0.134				

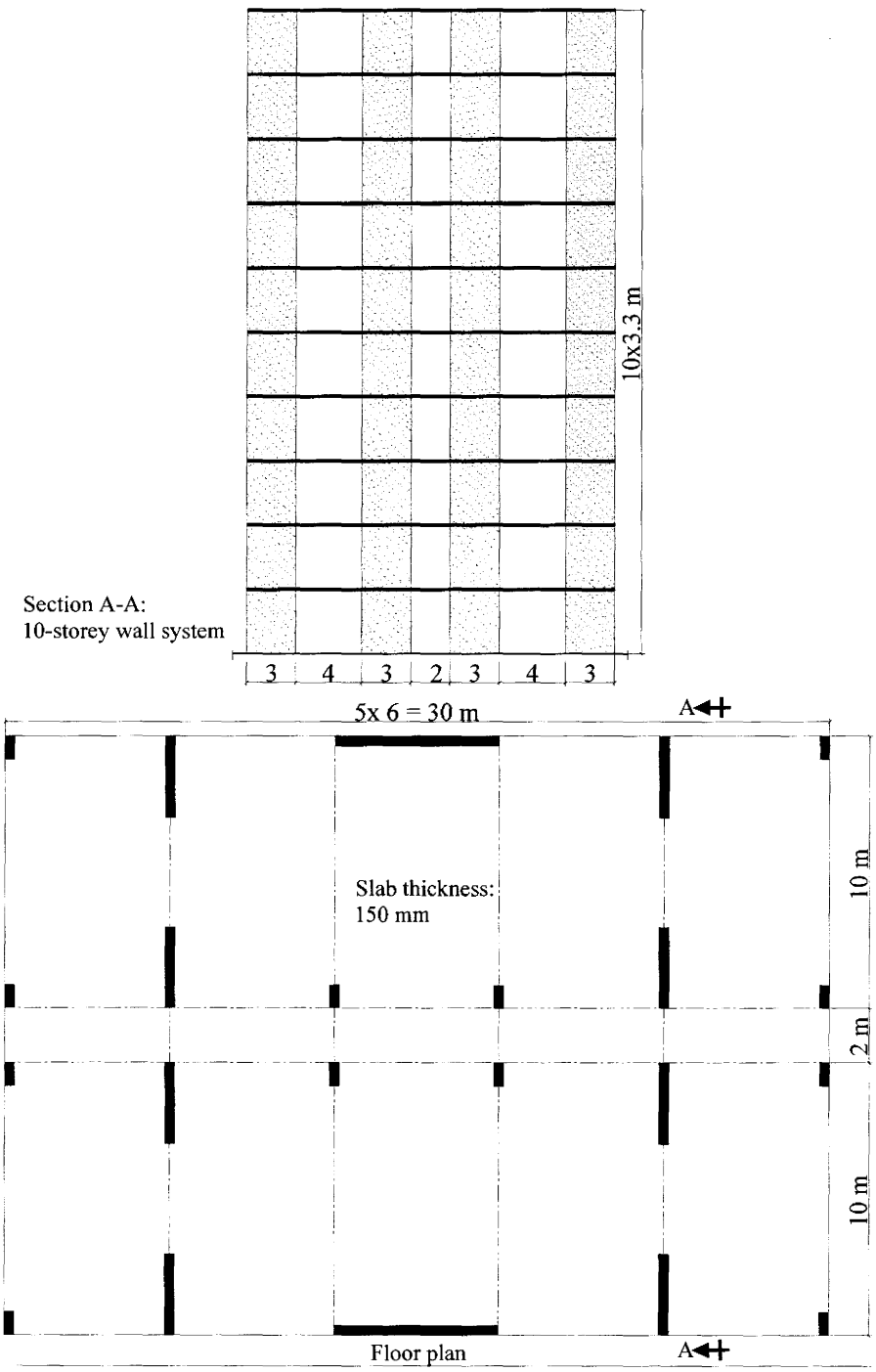

Figure 7. 1 Plan and section elevation for the 10-storey RC building

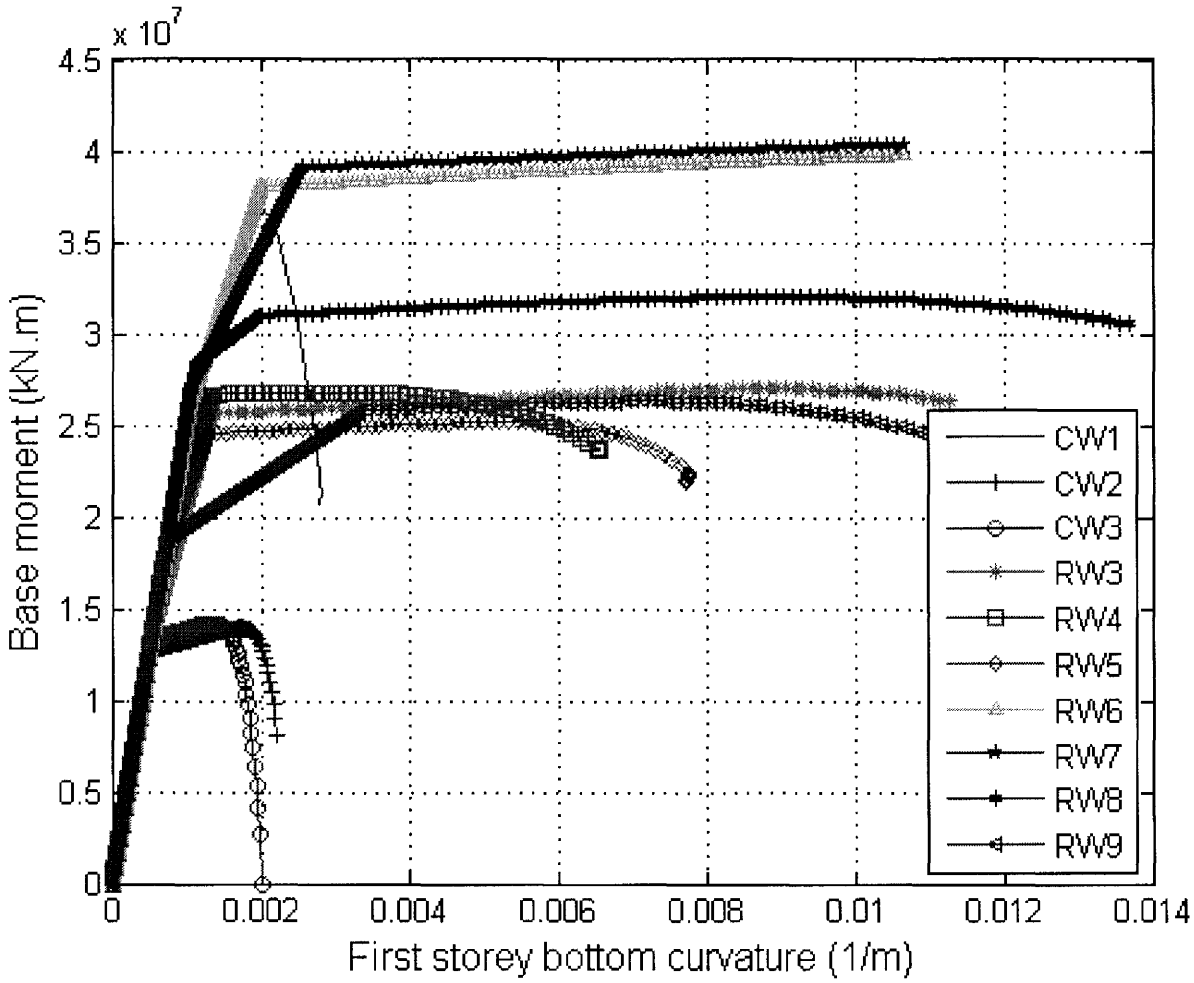

Figure 7. 2 First storey moment-curvature relationship from pushover analysis

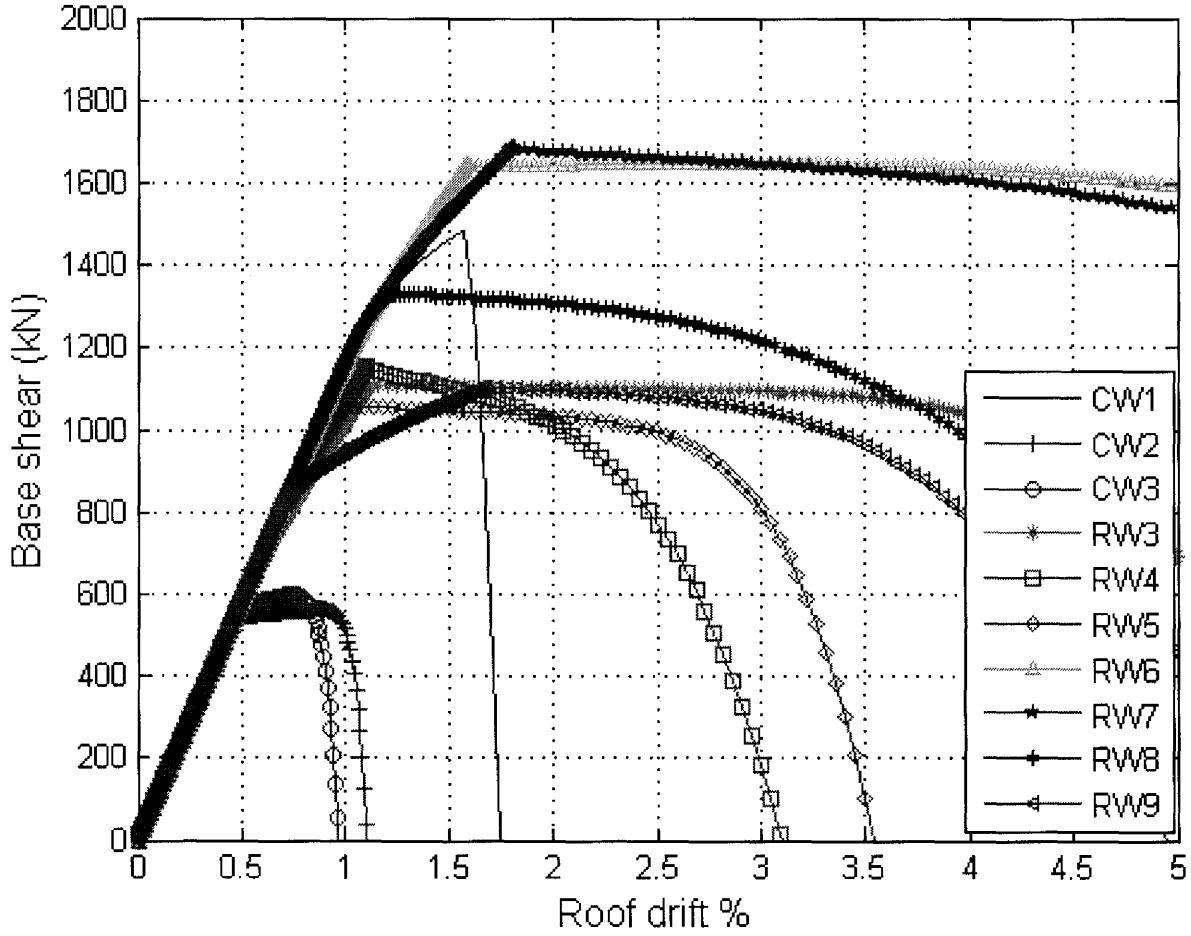

Figure 7. 3 Roof drift ratio-base shear relationship from pushover analysis

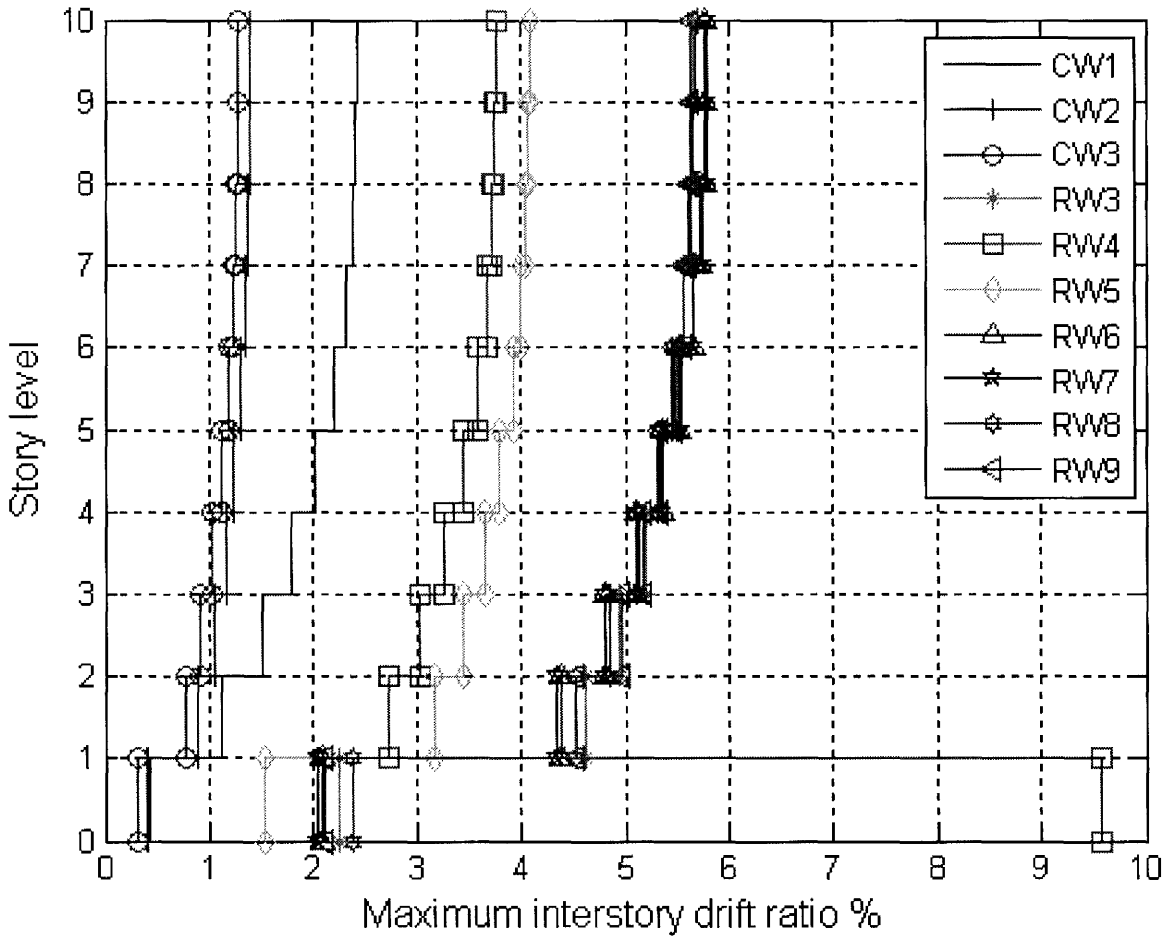

Figure 7. 4 Maximum interstorey drift from pushover analysis

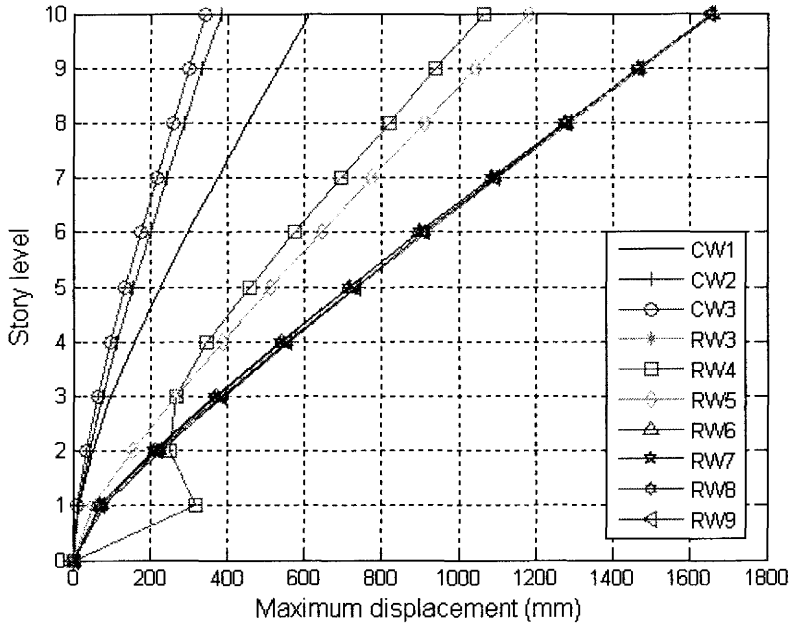

Figure 7. 5 Maximum displacement from pushover analysis

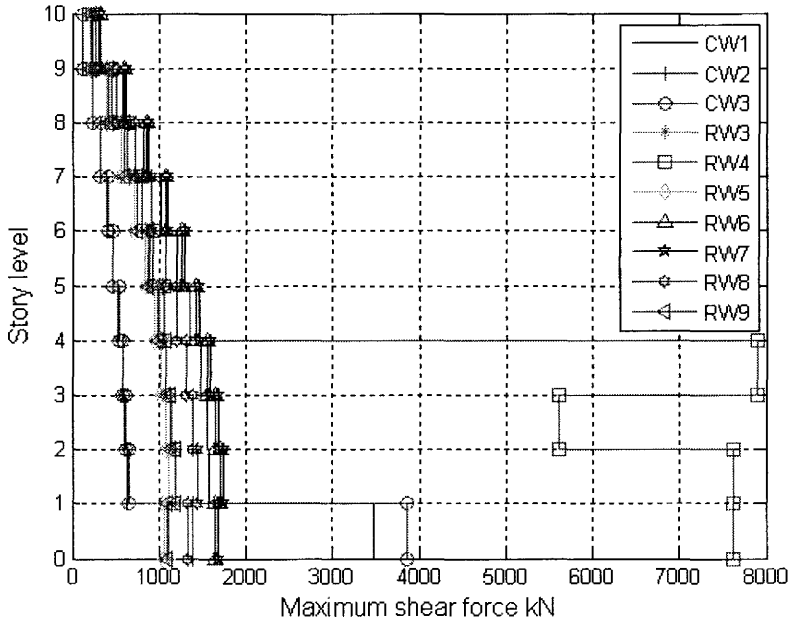

Figure 7. 6 Maximum shear force from pushover analysis

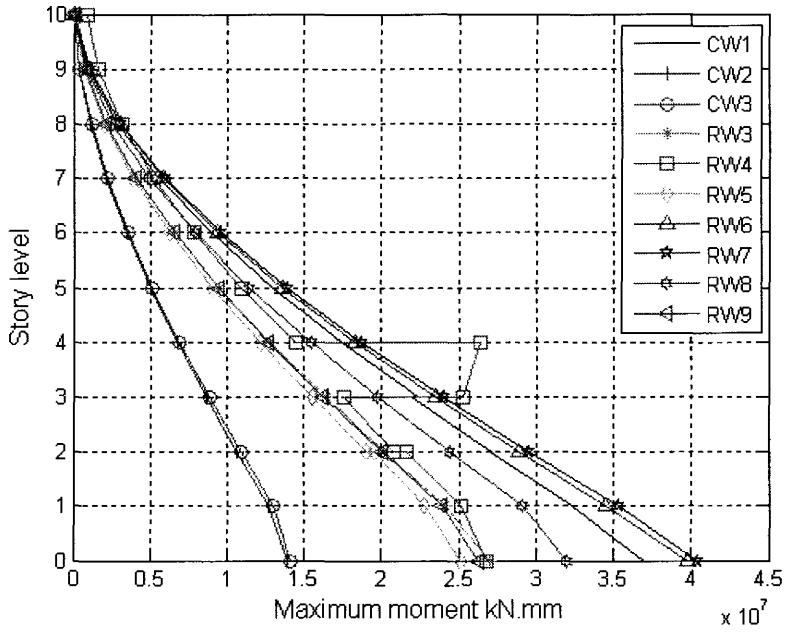

Figure 7. 7 Maximum moment from pushover analysis

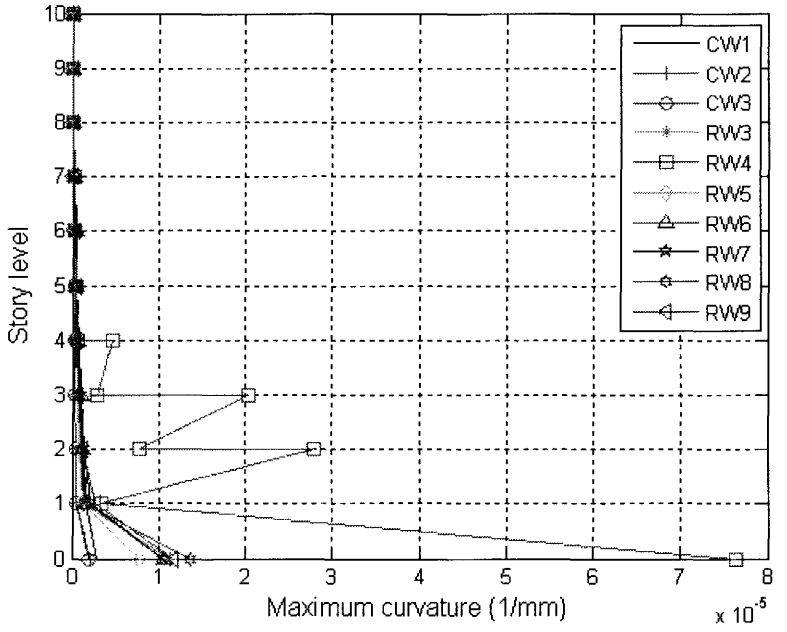

Figure 7. 8 Maximum curvature from pushover analysis

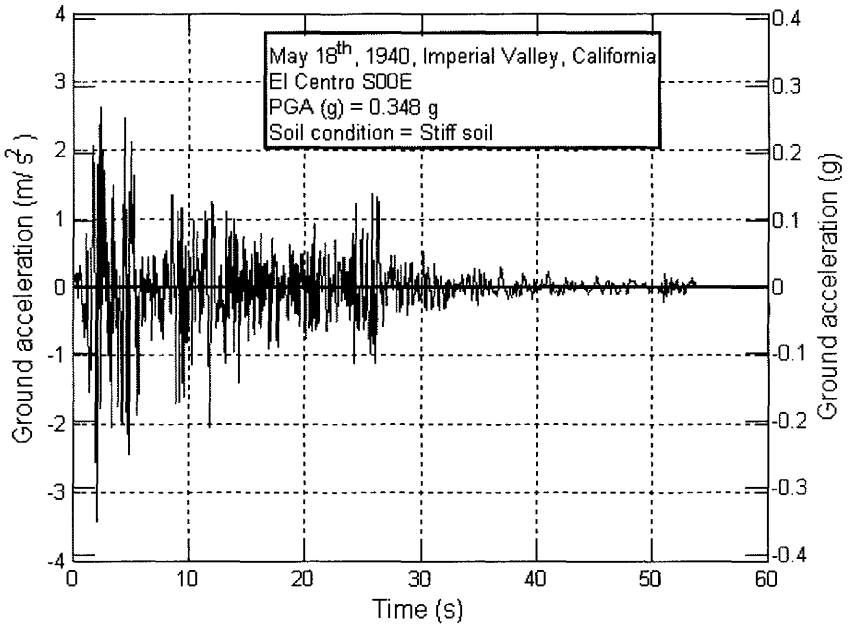

Figure 7. 9 Acceleration time history of the 1940 Imperial Valley EQ. record

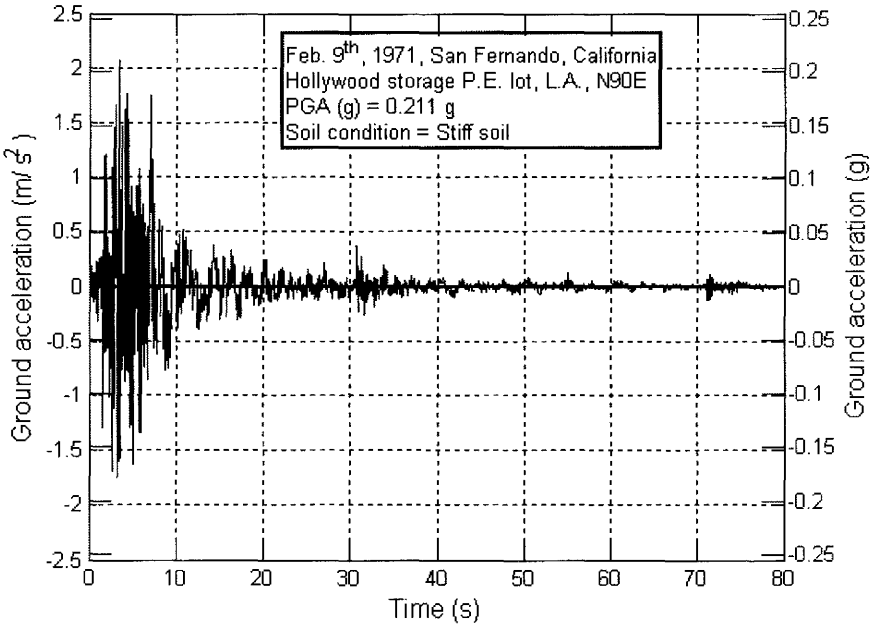

Figure 7. 10 Acceleration time history of the 1971 San Fernando EQ. record

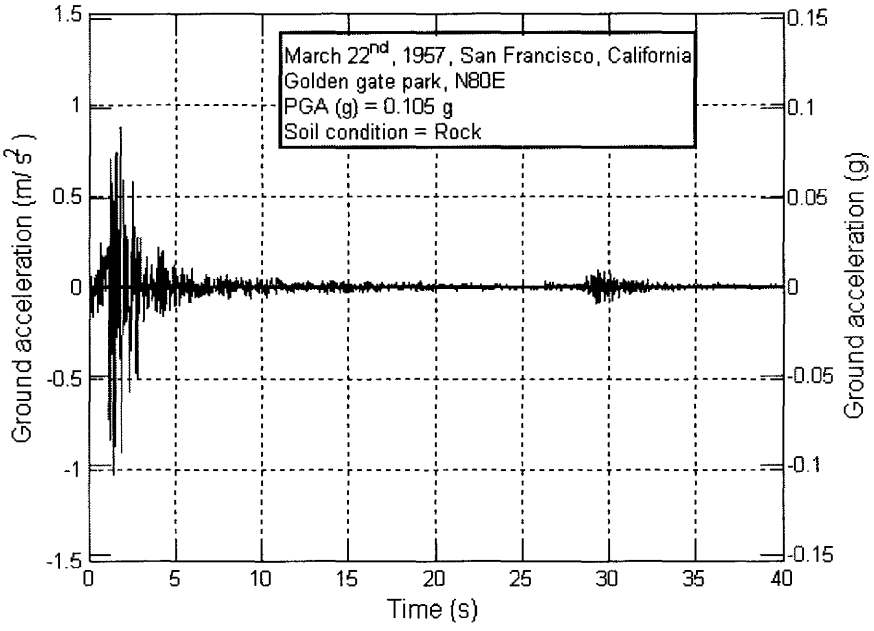

Figure 7. 11 Acceleration time history of the 1957 San Francisco EQ. record

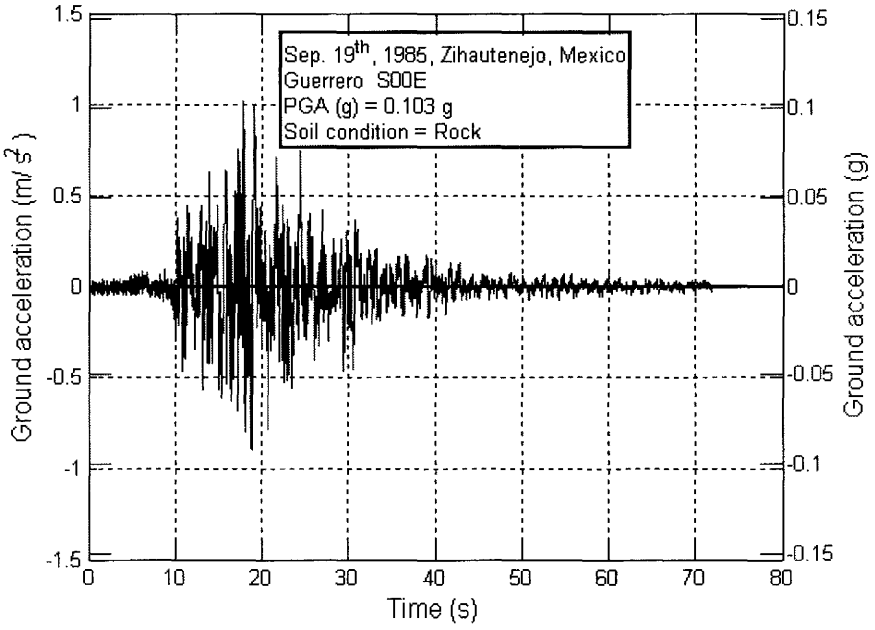

Figure 7. 12 Acceleration time history of the 1985 Mexico EQ. record

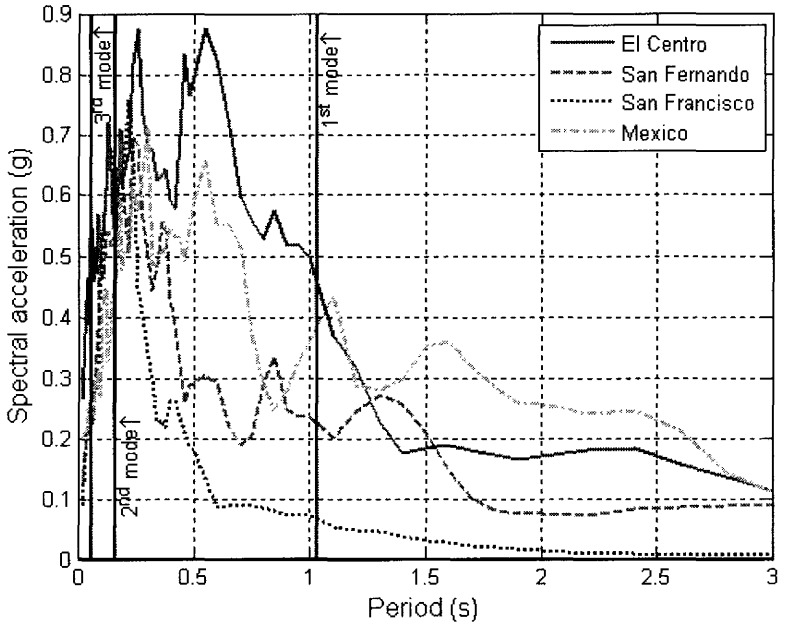

Figure 7. 13 Spectral acceleration for the selected EQ. records

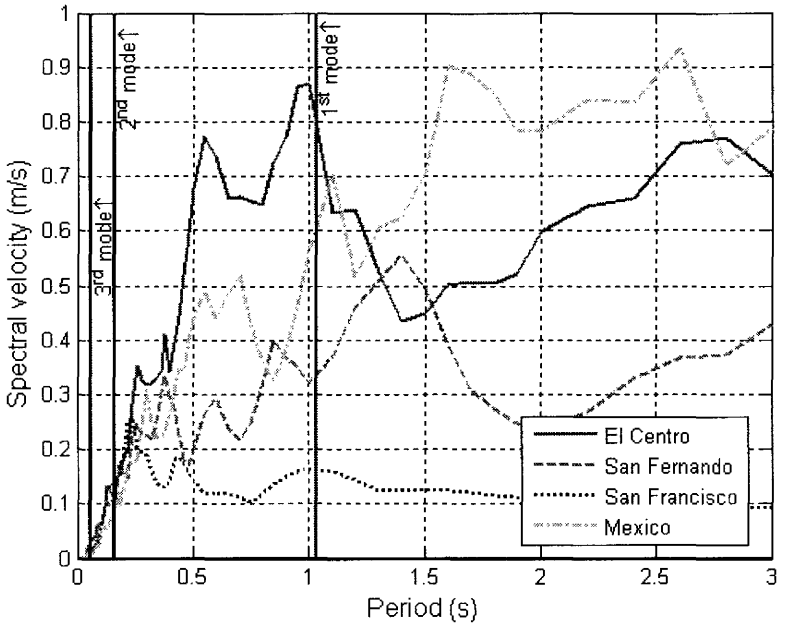

Figure 7. 14 Spectral velocity for the selected EQ. records

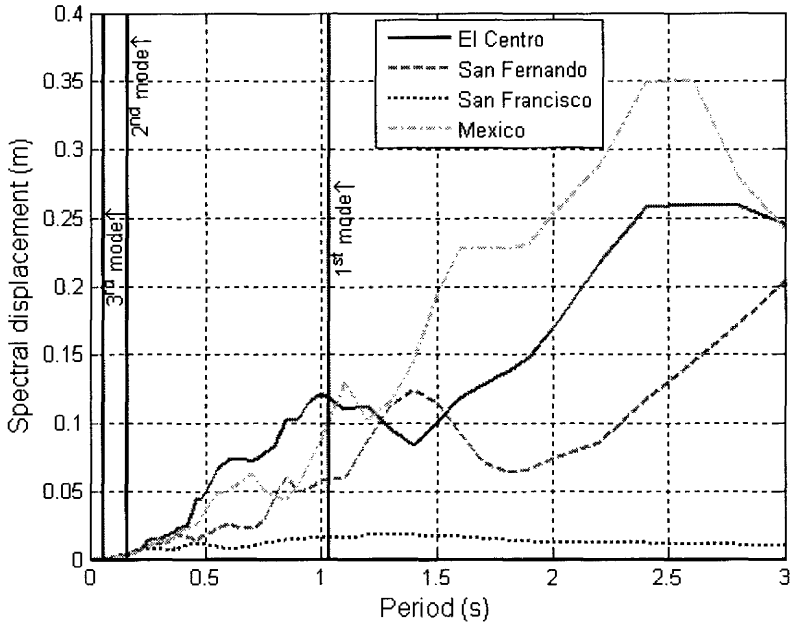

Figure 7. 15 Spectral displacement for the selected EQ. records

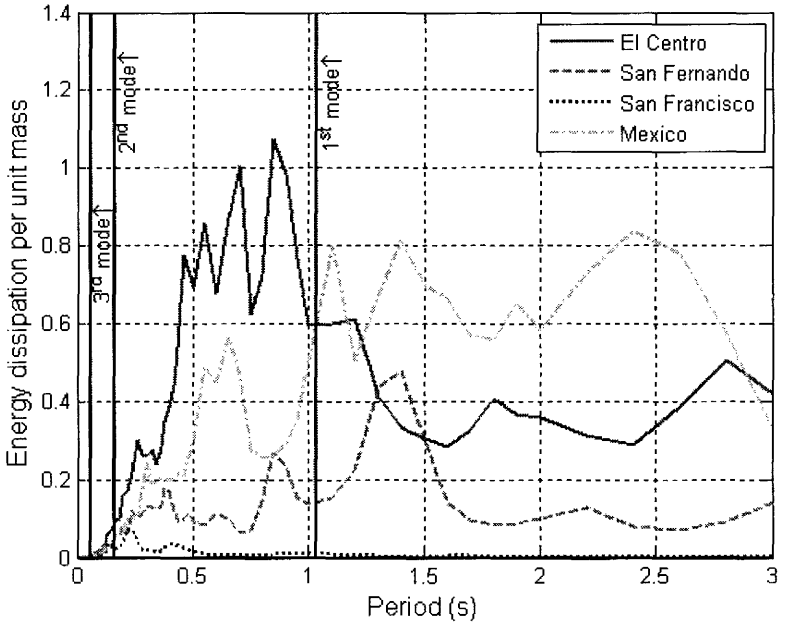

Figure 7. 16 Energy dissipation per unit mass for the selected EQ. records

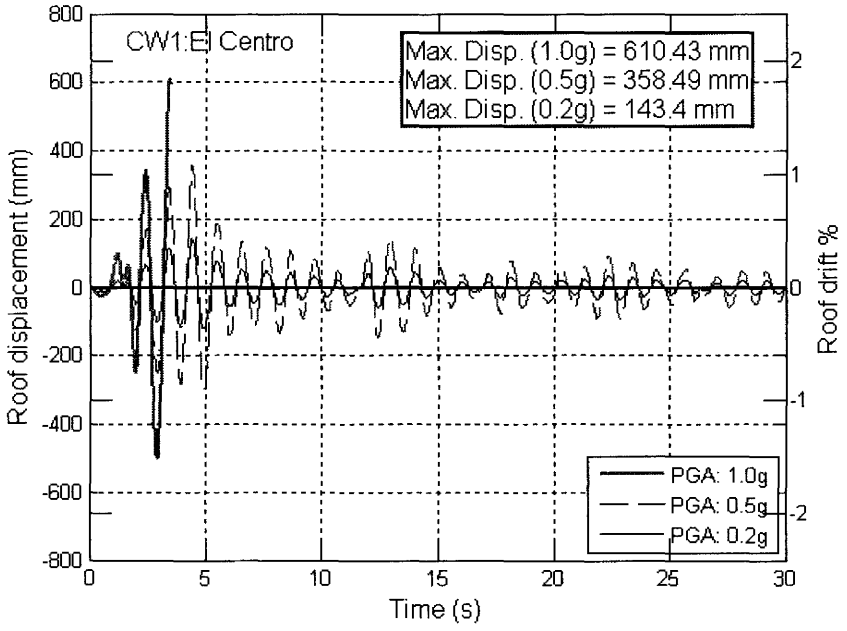

Figure 7. 17 Wall CW1 roof displacement time history due to El Centro EQ. record

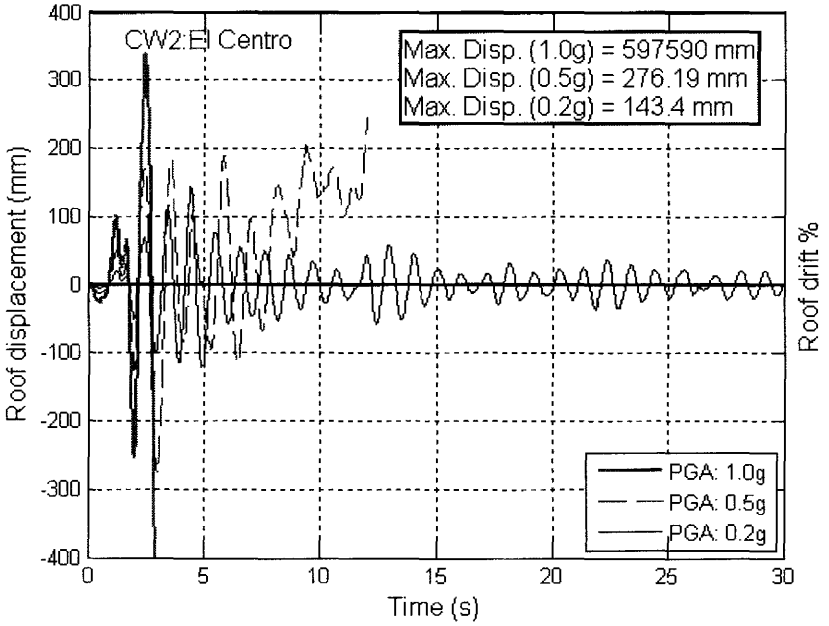

Figure 7. 18 Wall CW2 roof displacement time history due to El Centro EQ. record

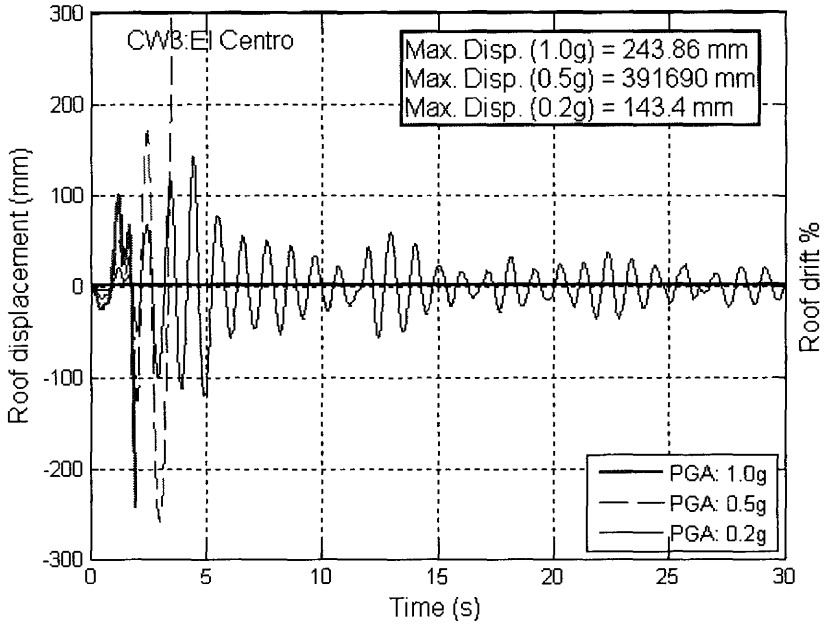

Figure 7. 19 Wall CW3 roof displacement time history due to El Centro EQ. record

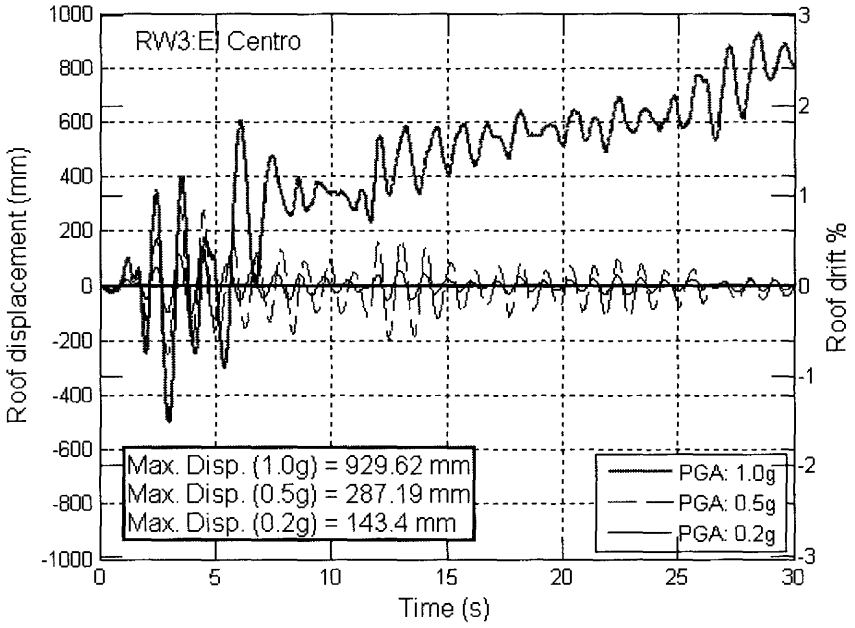

Figure 7. 20 Wall RW3 roof displacement time history due to El Centro EQ. record

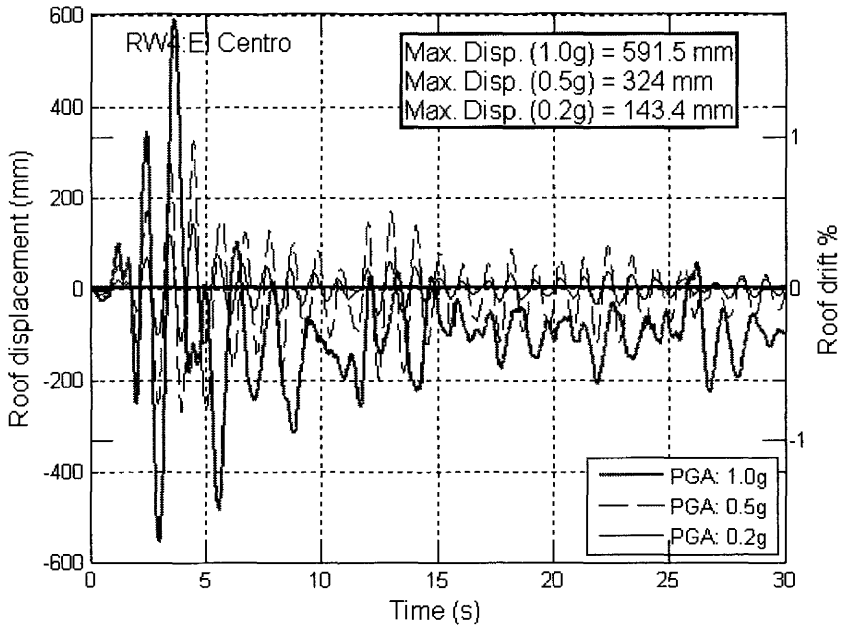

Figure 7. 21 Wall RW4 roof displacement time history due to El Centro EQ. record

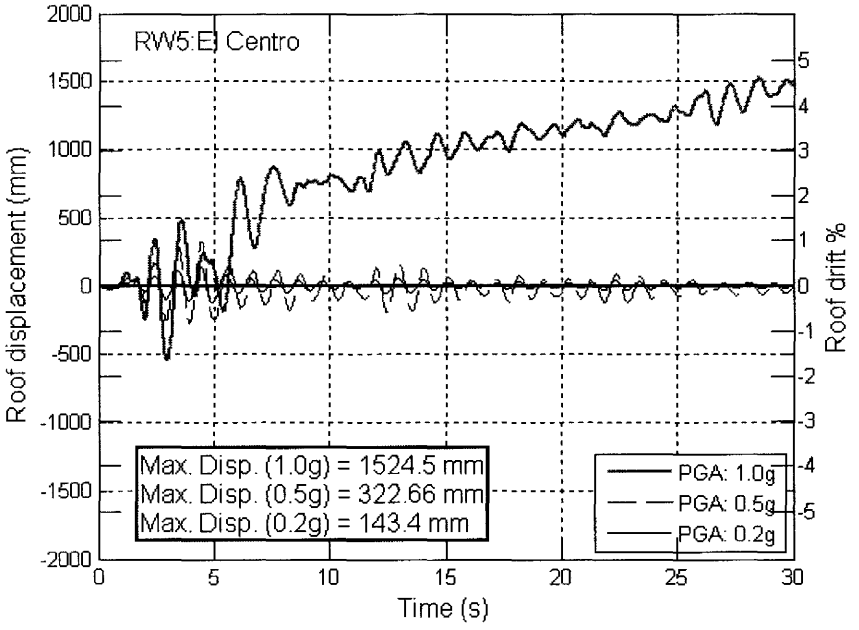

Figure 7. 22 Wall RW5 roof displacement time history due to El Centro EQ. record

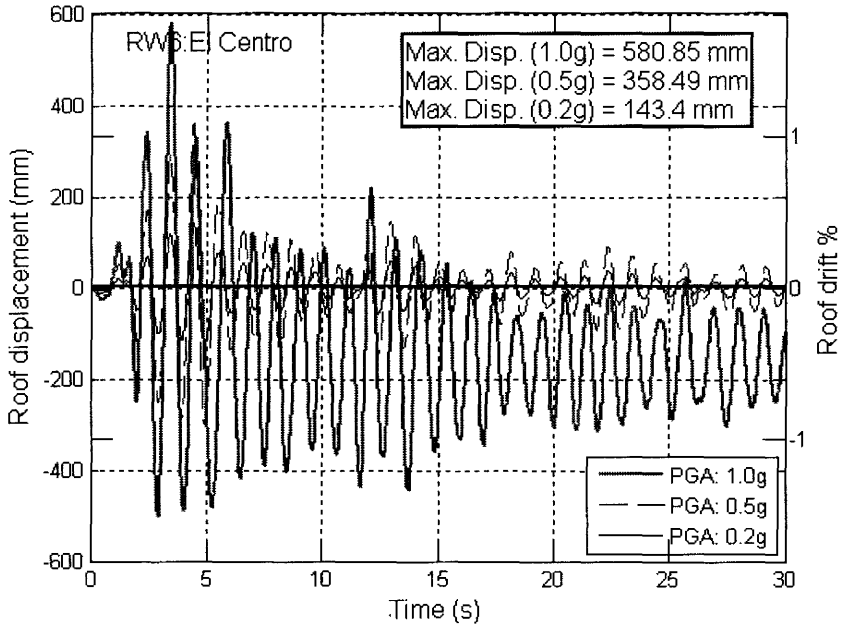

Figure 7. 23 Wall RW6 roof displacement time history due to El Centro EQ. record

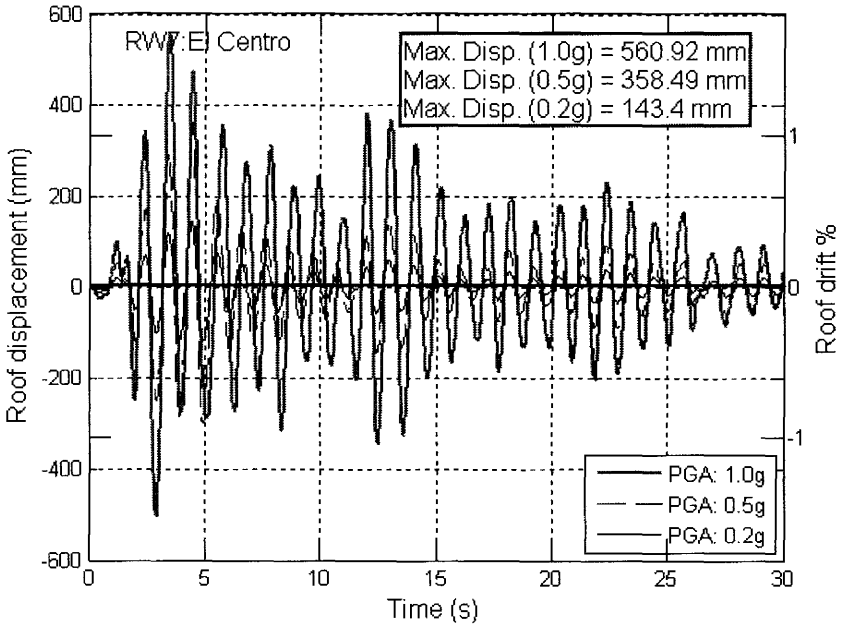

Figure 7. 24 Wall RW7 roof displacement time history due to El Centro EQ. record

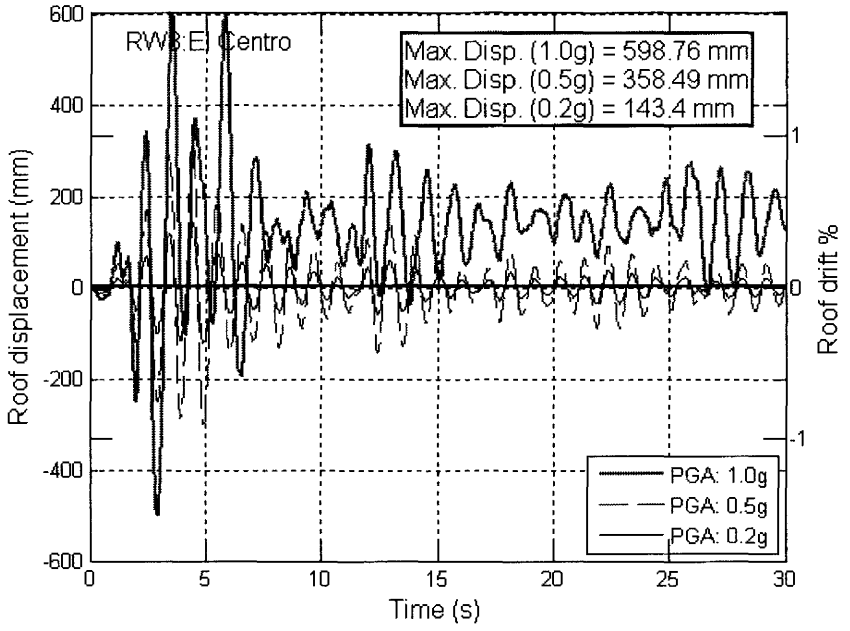

Figure 7. 25 Wall RW8 roof displacement time history due to El Centro EQ. record

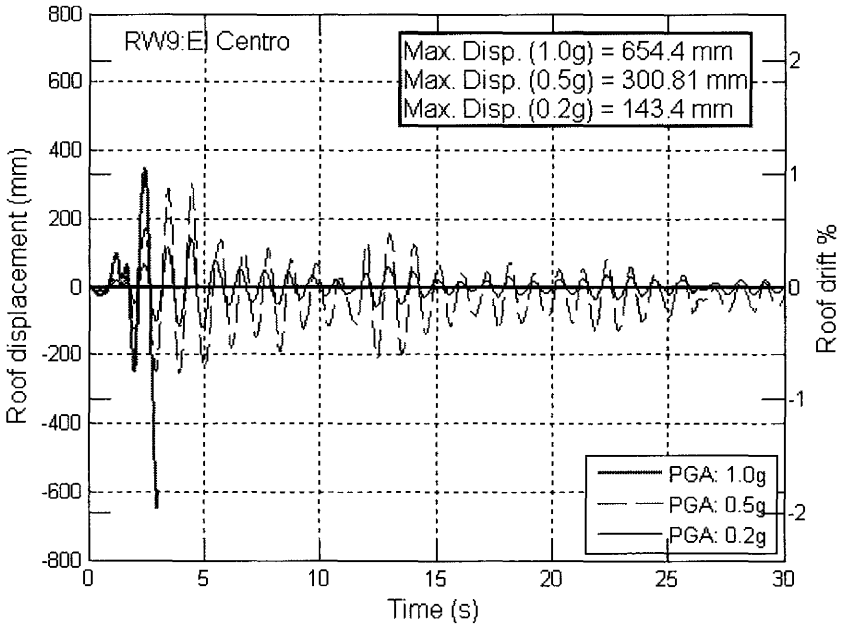

Figure 7. 26 Wall RW9 roof displacement time history due to El Centro EQ. record

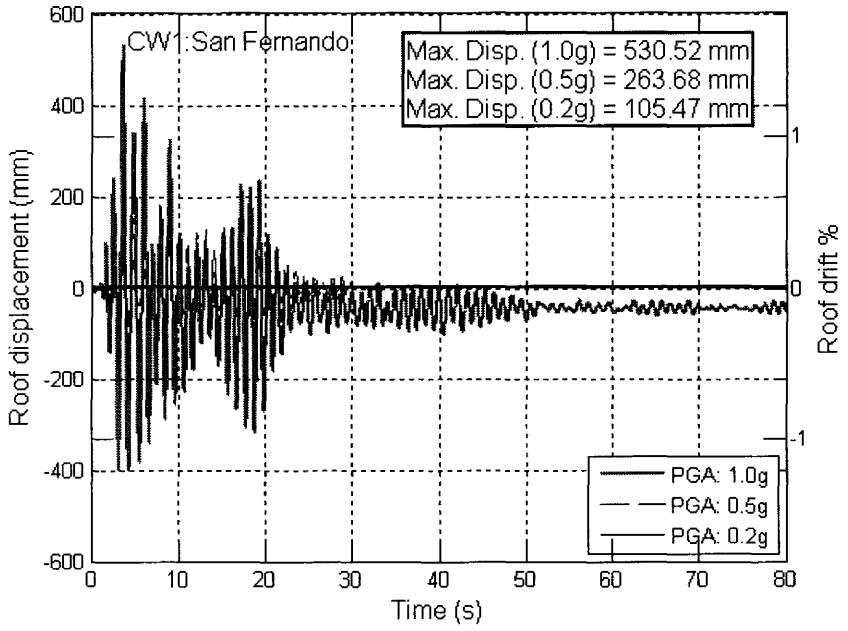

Figure 7. 27 Wall CW1 roof displacement time history due to San Fernando EQ record

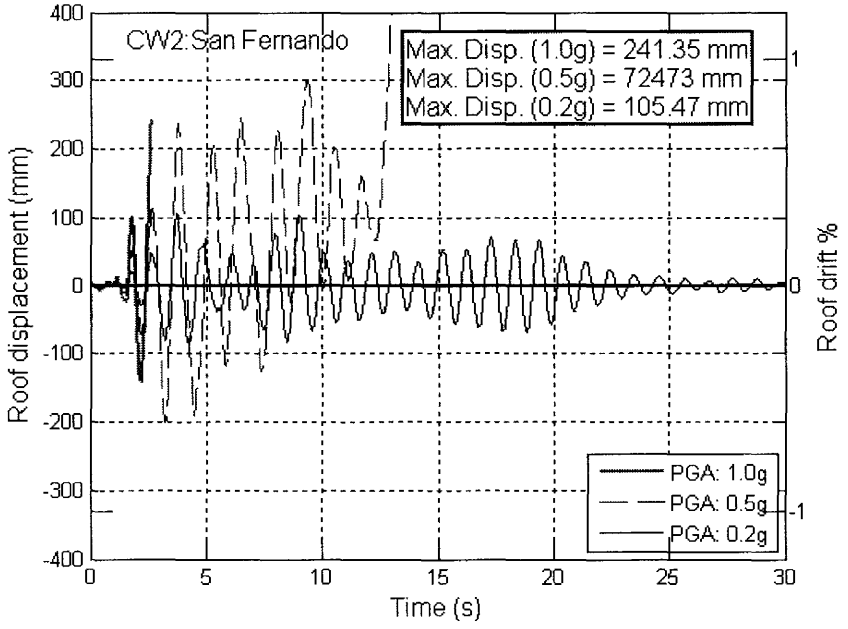

Figure 7. 28 Wall CW2 roof displacement time history due to San Fernando EQ record

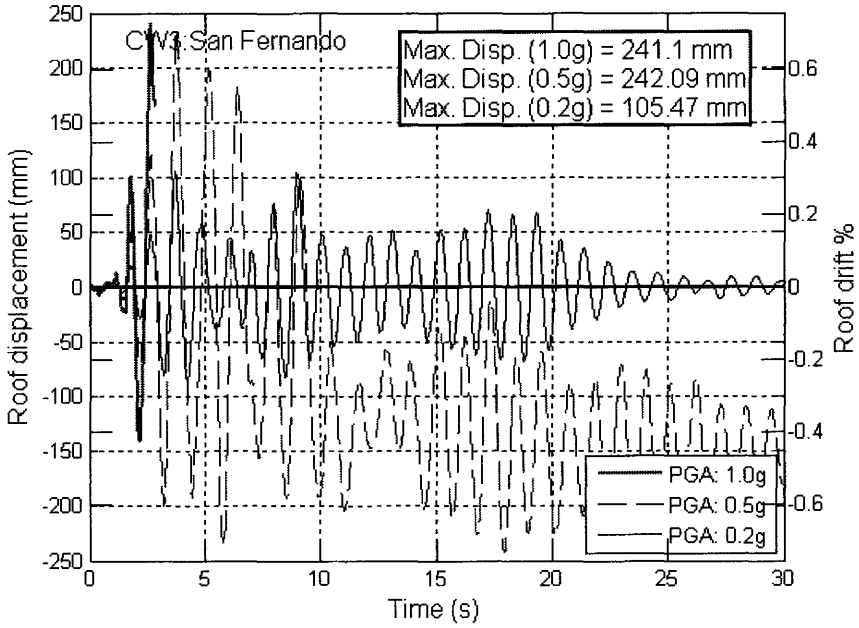

Figure 7. 29 Wall CW3 roof displacement time history due to San Fernando EQ record

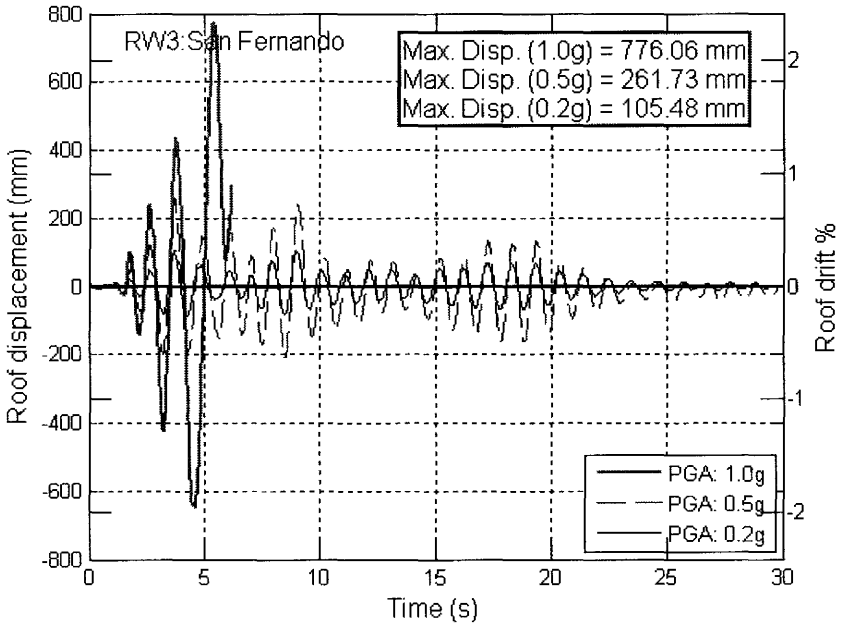

Figure 7. 30 Wall RW3 roof displacement time history due to San Fernando EQ record

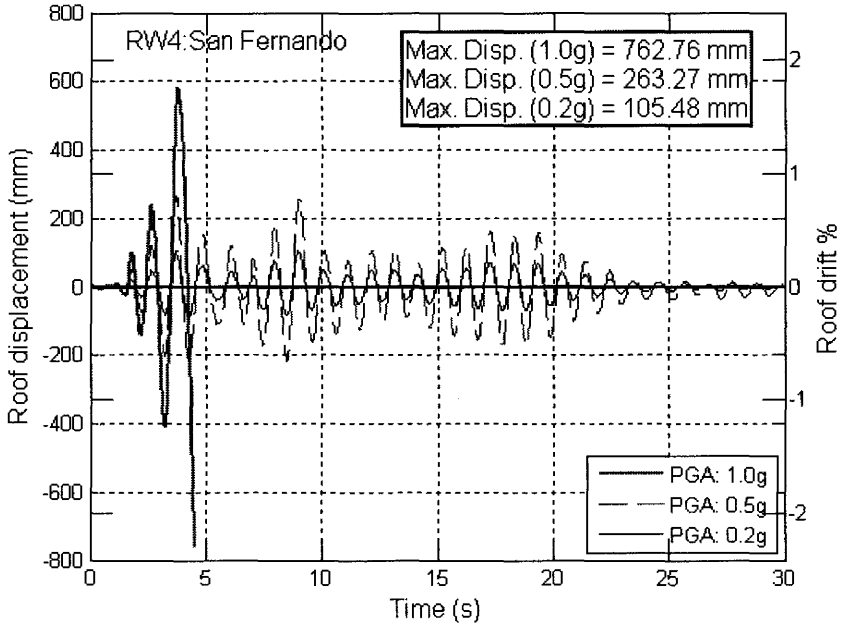

Figure 7. 31 Wall RW4 roof displacement time history due to San Fernando EQ record

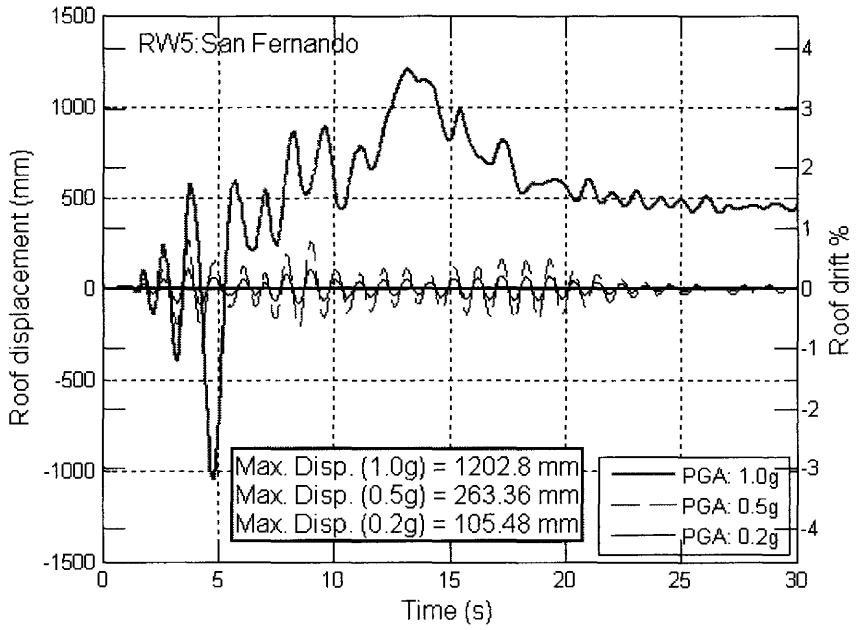

Figure 7. 32 Wall RW5 roof displacement time history due to San Fernando EQ record

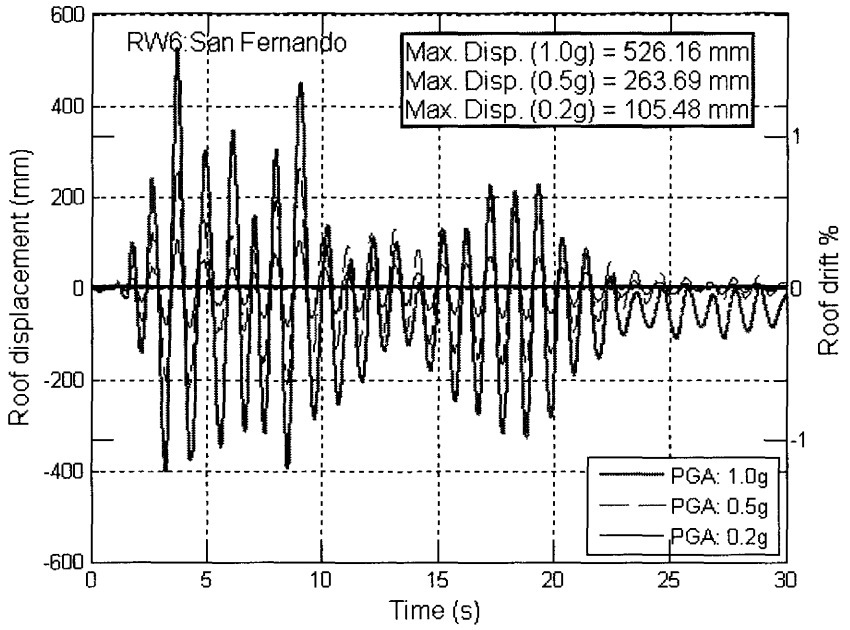

Figure 7. 33 Wall RW6 roof displacement time history due to San Fernando EQ record

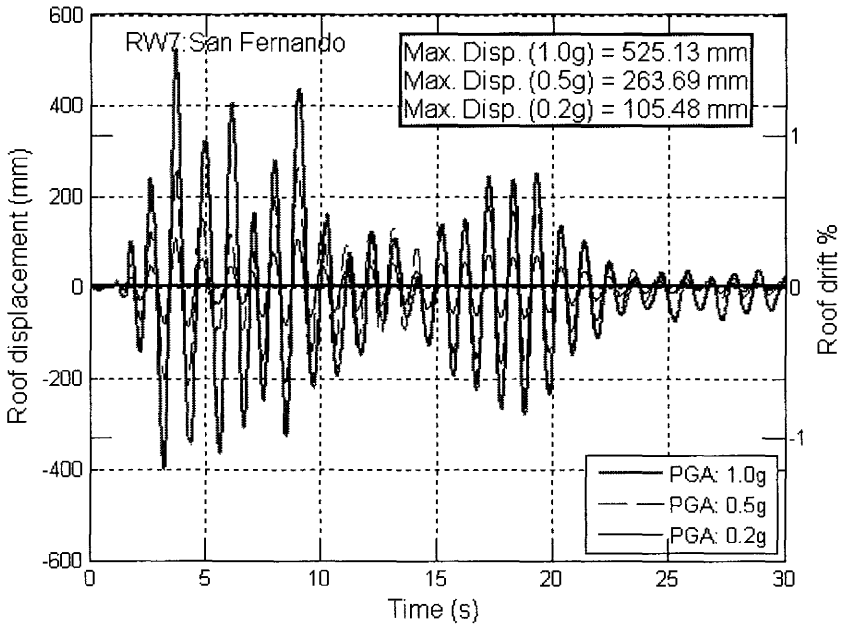

Figure 7. 34 Wall RW7 roof displacement time history due to San Fernando EQ record

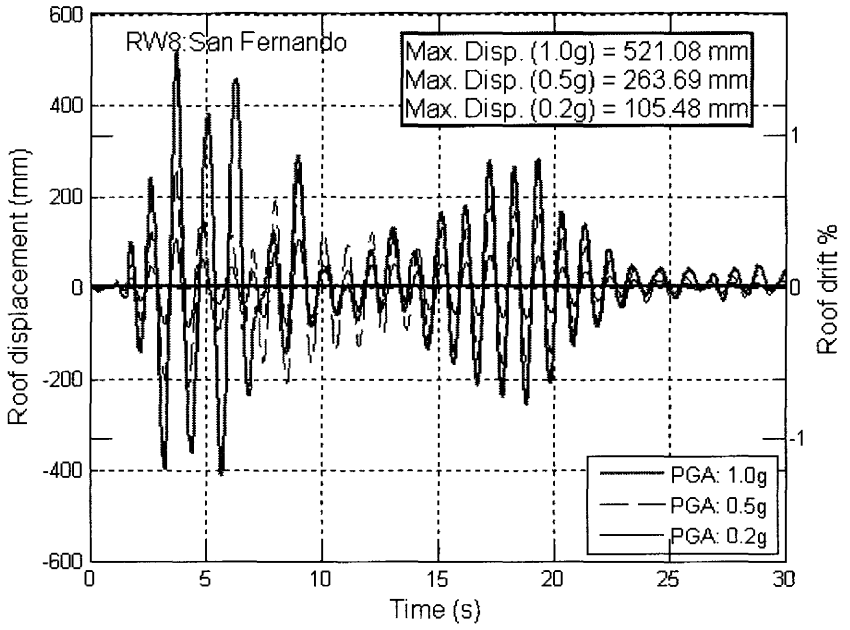

Figure 7. 35 Wall RW8 roof displacement time history due to San Fernando EQ record

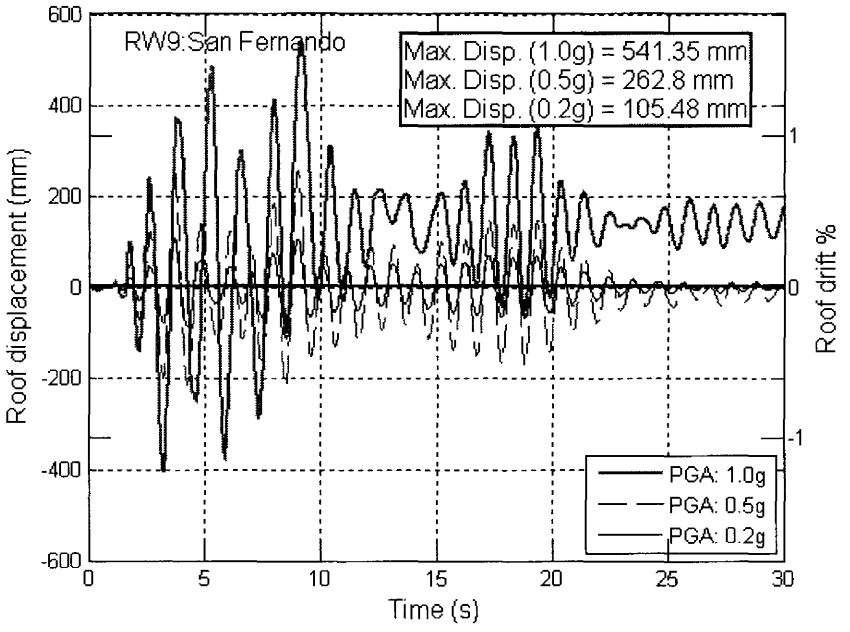

Figure 7. 36 Wall RW9 roof displacement time history due to San Fernando EQ record

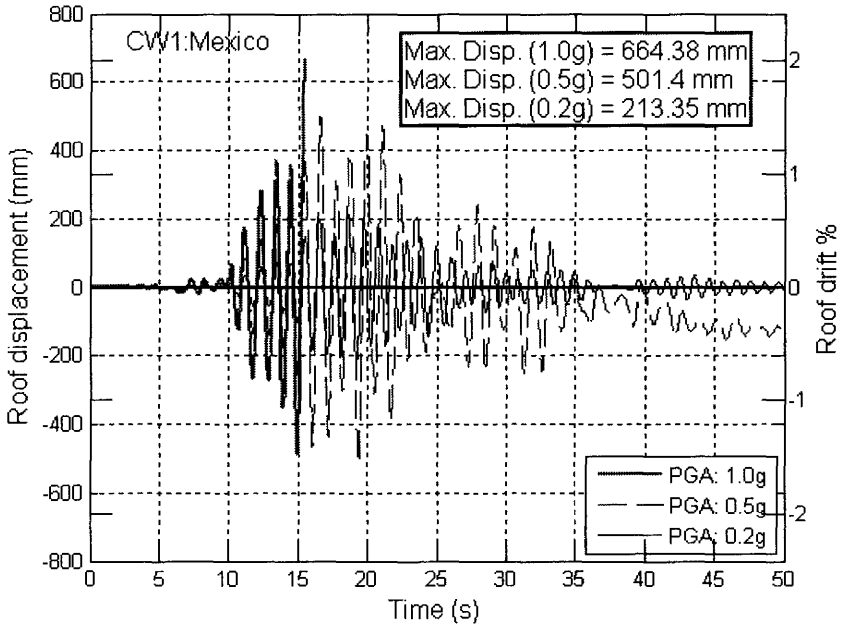

Figure 7. 37 Wall CW1 roof displacement time history due to Mexico EQ record

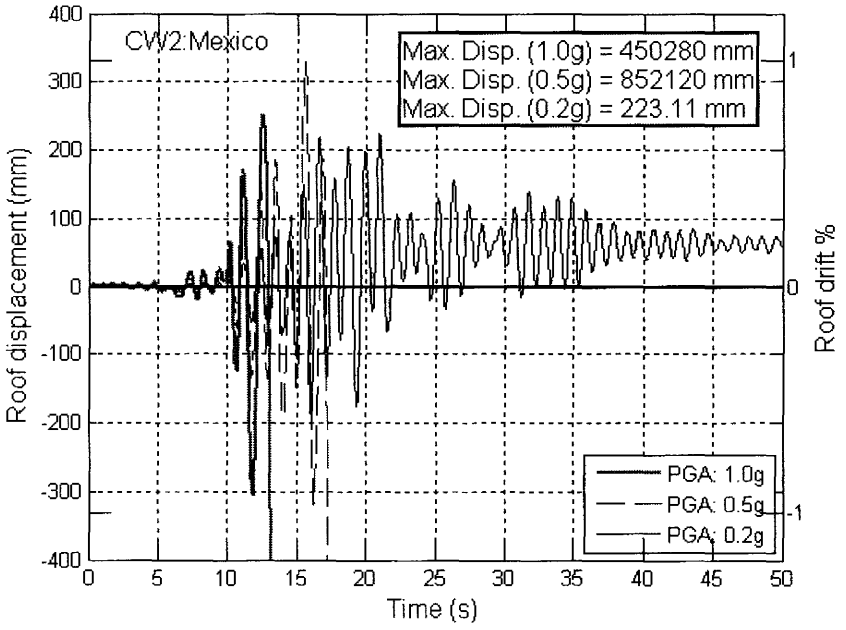

Figure 7. 38 Wall CW2 roof displacement time history due to Mexico EQ record

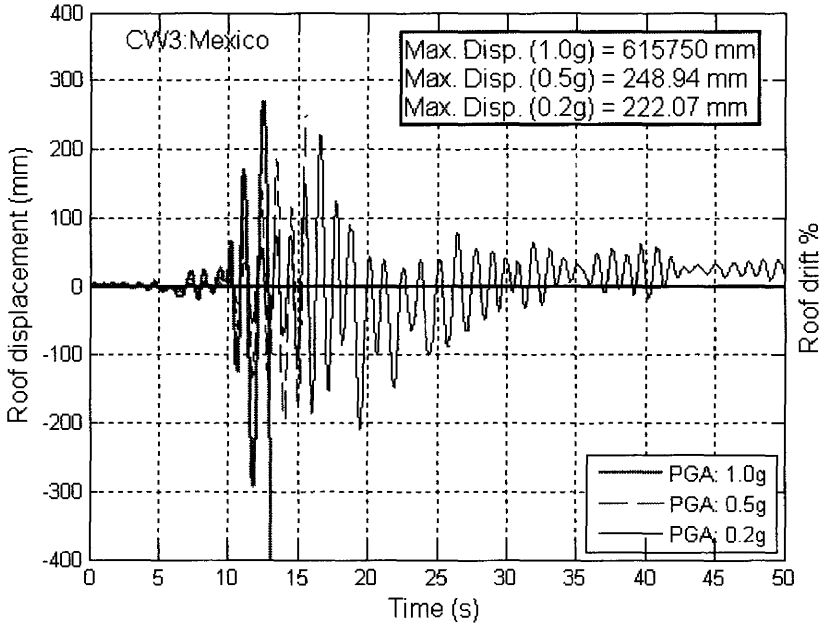

Figure 7. 39 Wall CW3 roof displacement time history due to Mexico EQ record

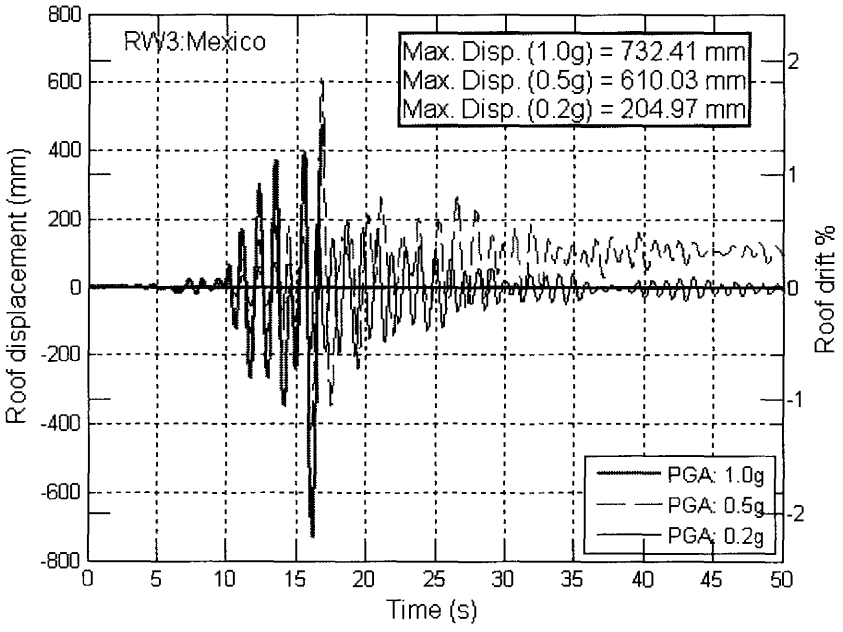

Figure 7. 40 Wall RW3 roof displacement time history due to Mexico EQ record

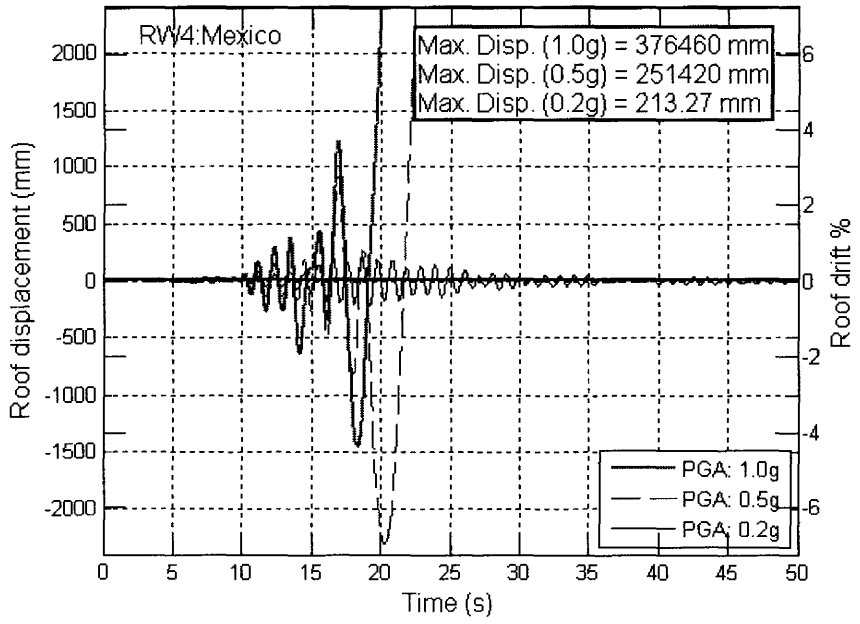

Figure 7. 41 Wall RW4 roof displacement time history due to Mexico EQ record

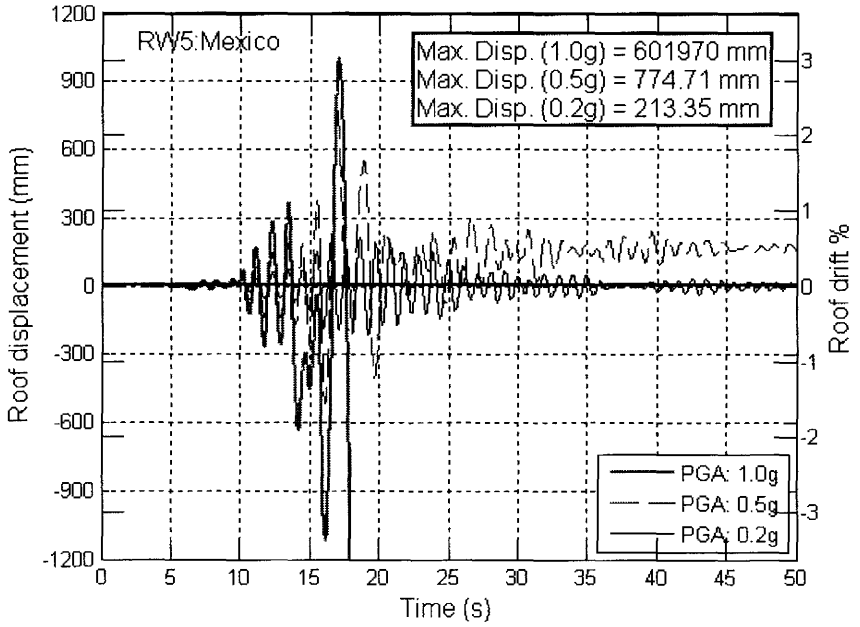

Figure 7. 42 Wall RW5 roof displacement time history due to Mexico EQ record

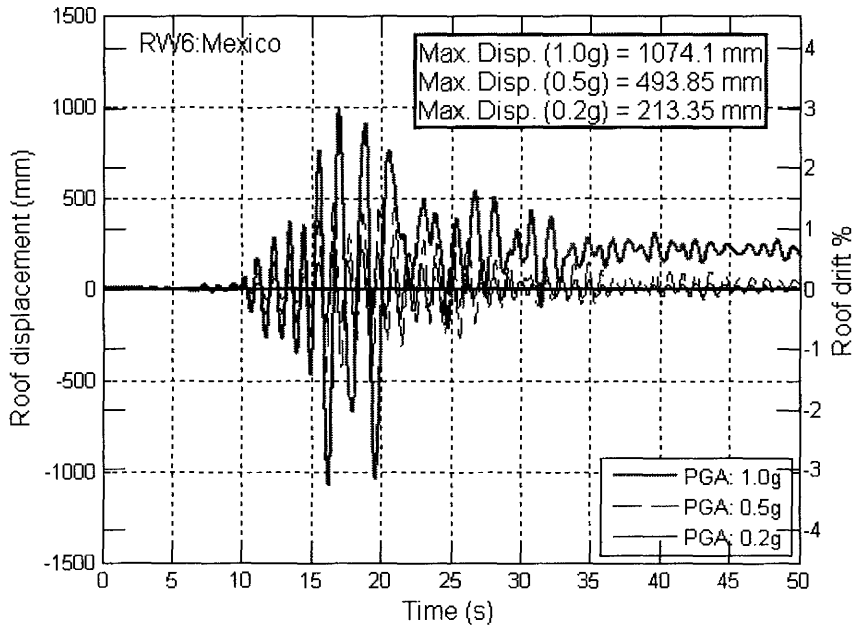

Figure 7. 43 Wall RW6 roof displacement time history due to Mexico EQ record

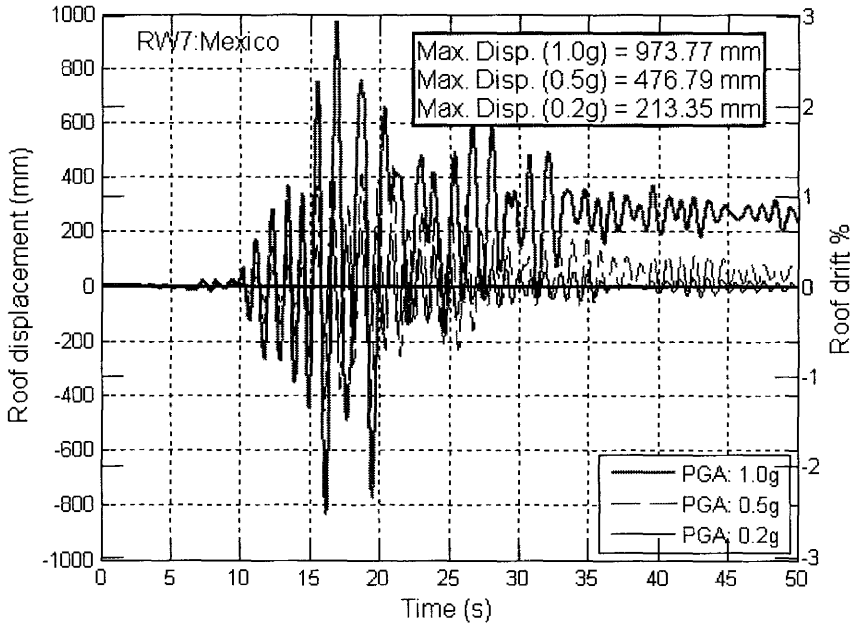

Figure 7. 44 Wall RW7 roof displacement time history due to Mexico EQ record

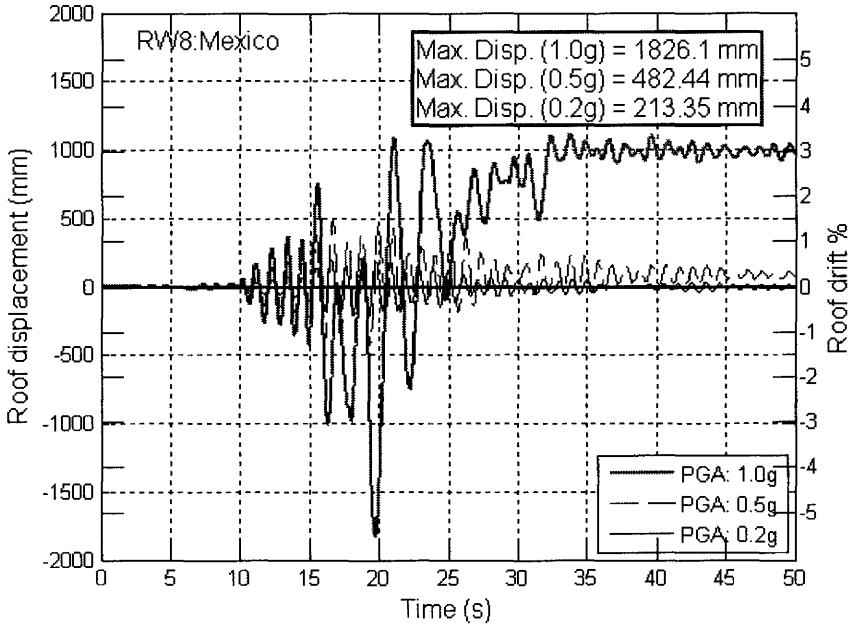

Figure 7. 45 Wall RW8 roof displacement time history due to Mexico EQ record

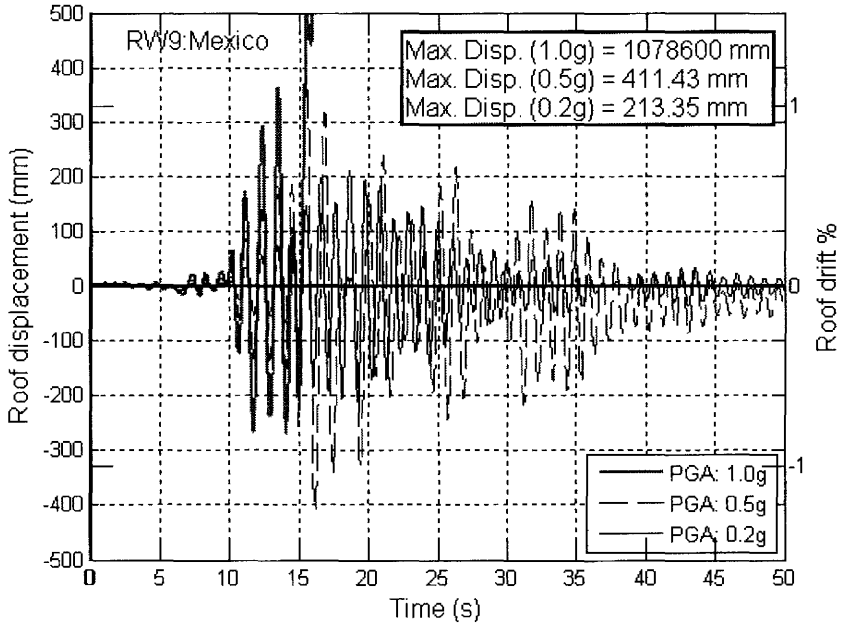

Figure 7. 46 Wall RW9 roof displacement time history due to Mexico EQ record

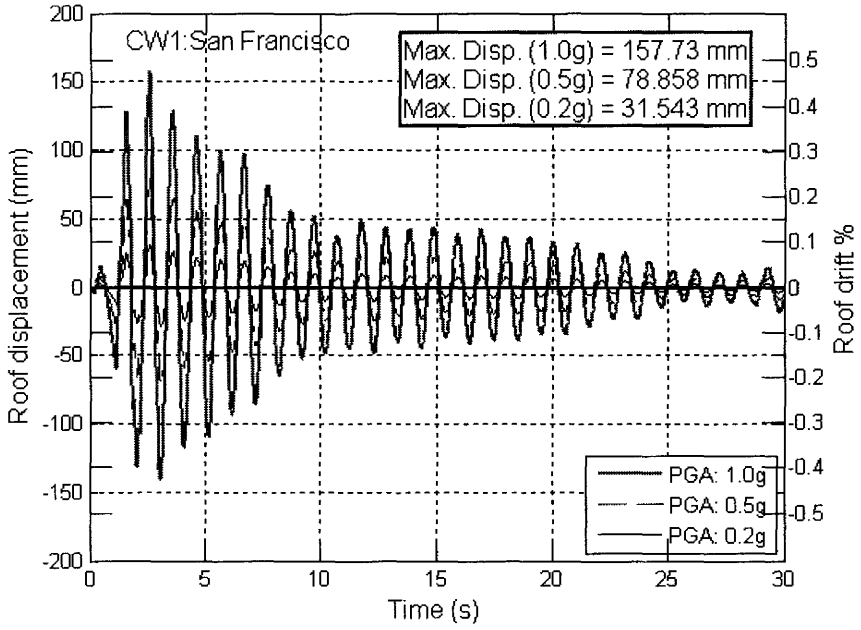

Figure 7. 47 Wall CW1 roof displacement time history due to San Francisco EQ record

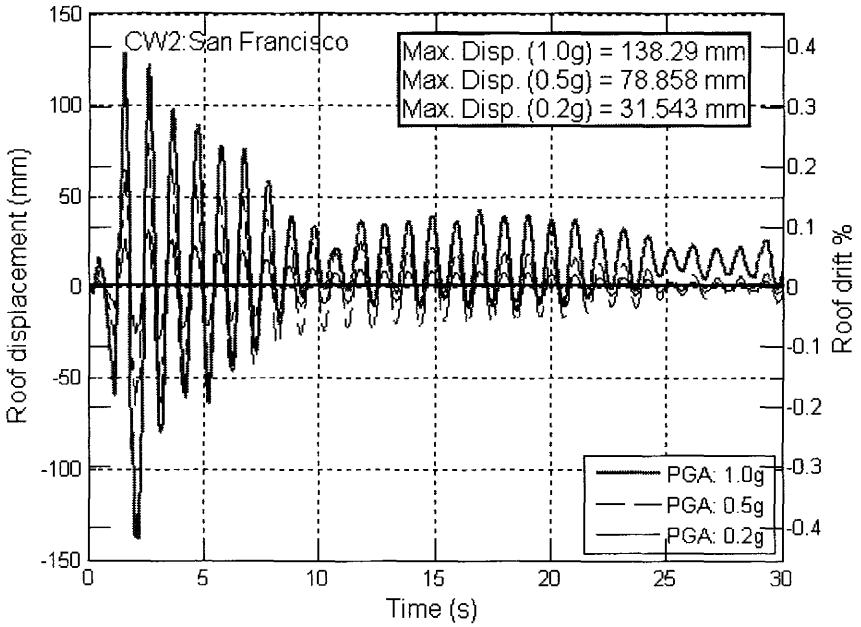

Figure 7. 48 Wall CW2 roof displacement time history due to San Francisco EQ record

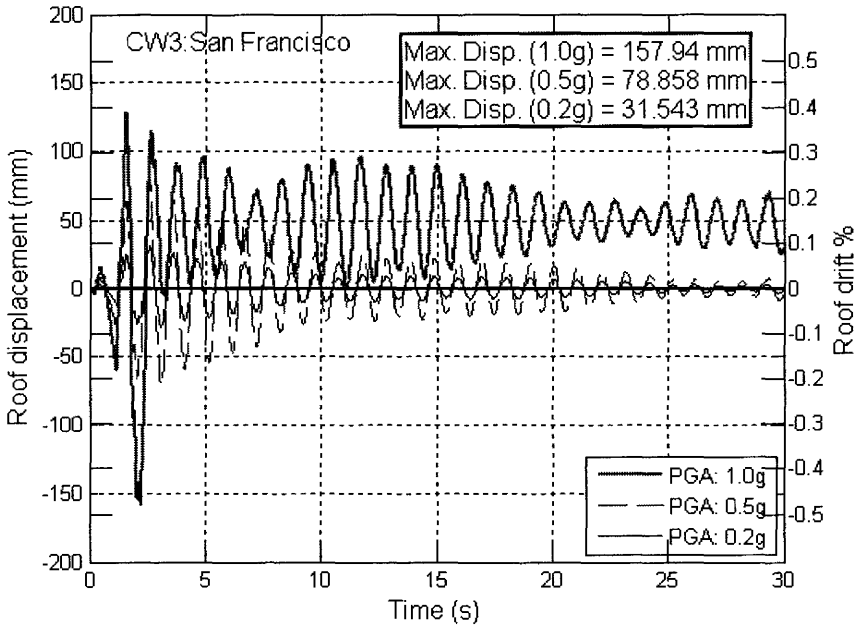

Figure 7. 49 Wall CW3 roof displacement time history due to San Francisco EQ record

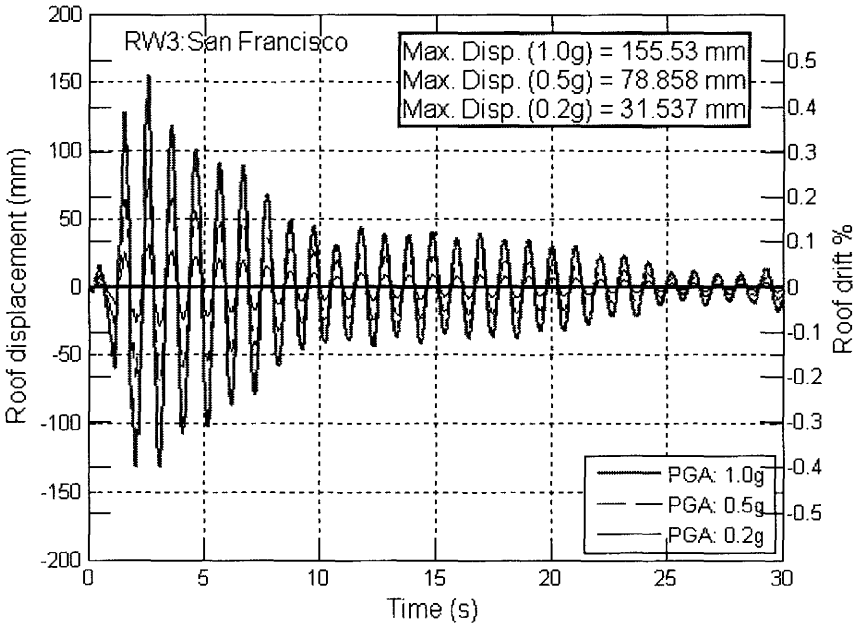

Figure 7. 50 Wall RW3 roof displacement time history due to San Francisco EQ record

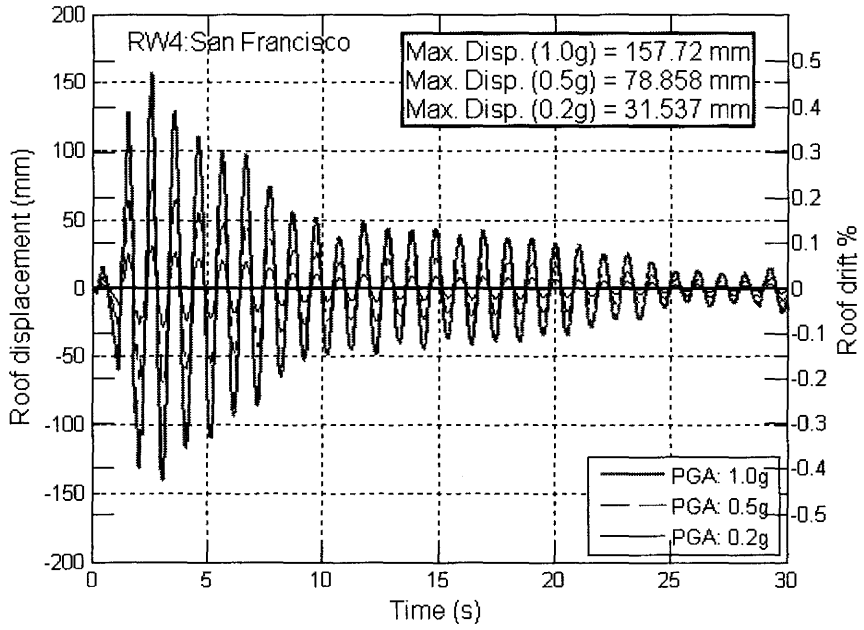

Figure 7. 51 Wall RW4 roof displacement time history due to San Francisco EQ record

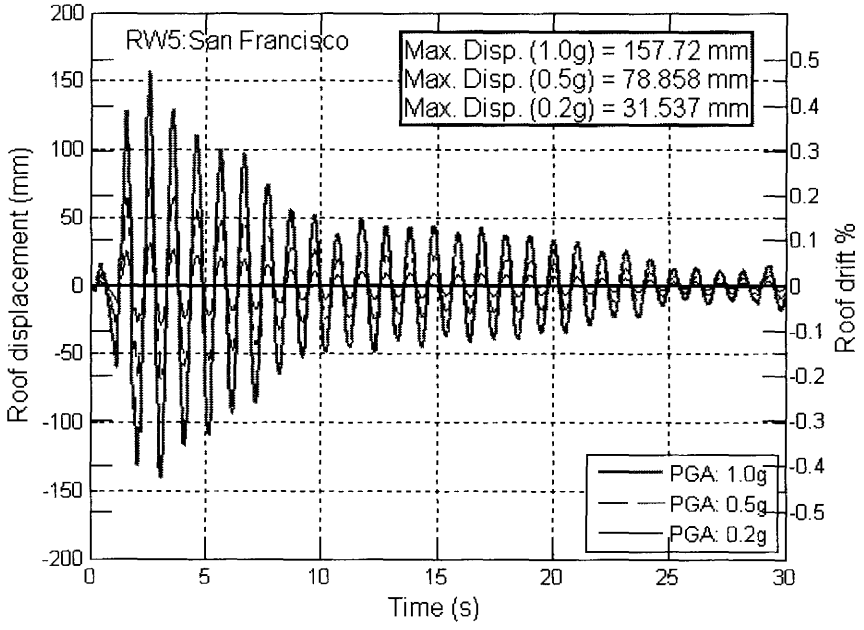

Figure 7. 52 Wall RW5 roof displacement time history due to San Francisco EQ record

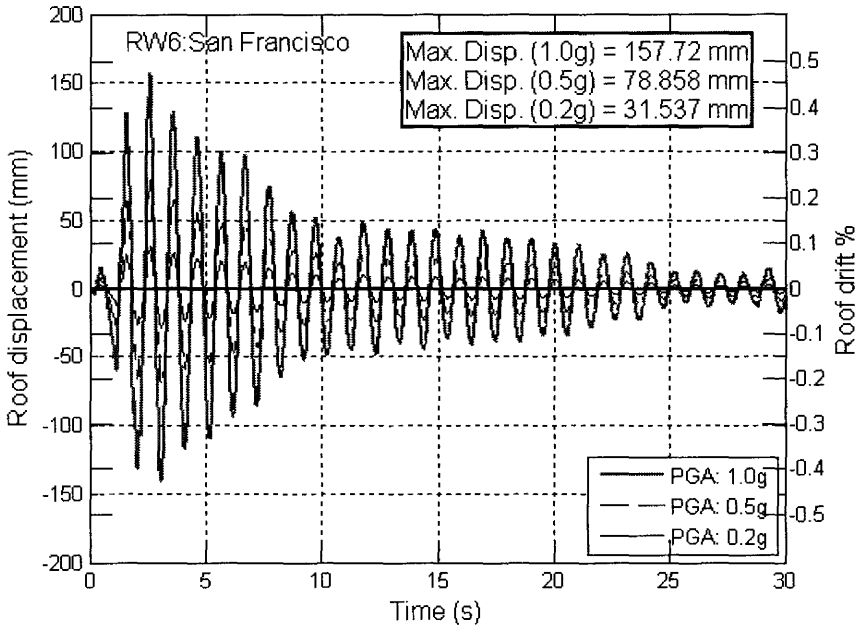

Figure 7. 53 Wall RW6 roof displacement time history due to San Francisco EQ record

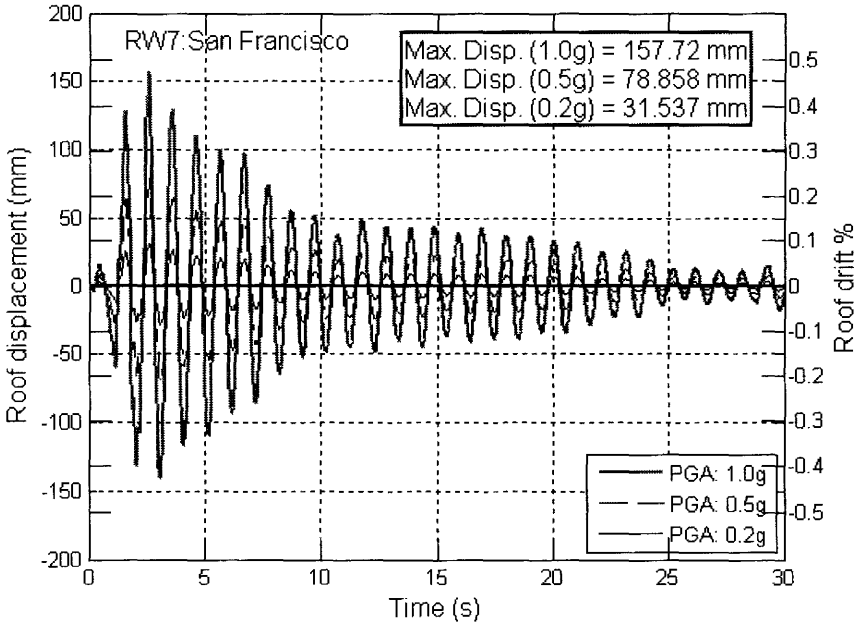

Figure 7. 54 Wall RW7 roof displacement time history due to San Francisco EQ record

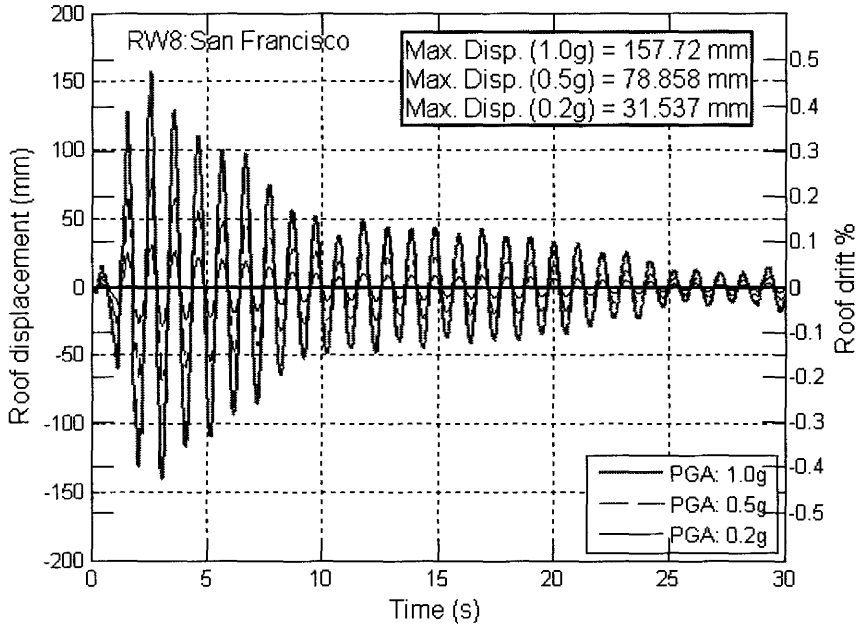

Figure 7. 55 Wall RW8 roof displacement time history due to San Francisco EQ record

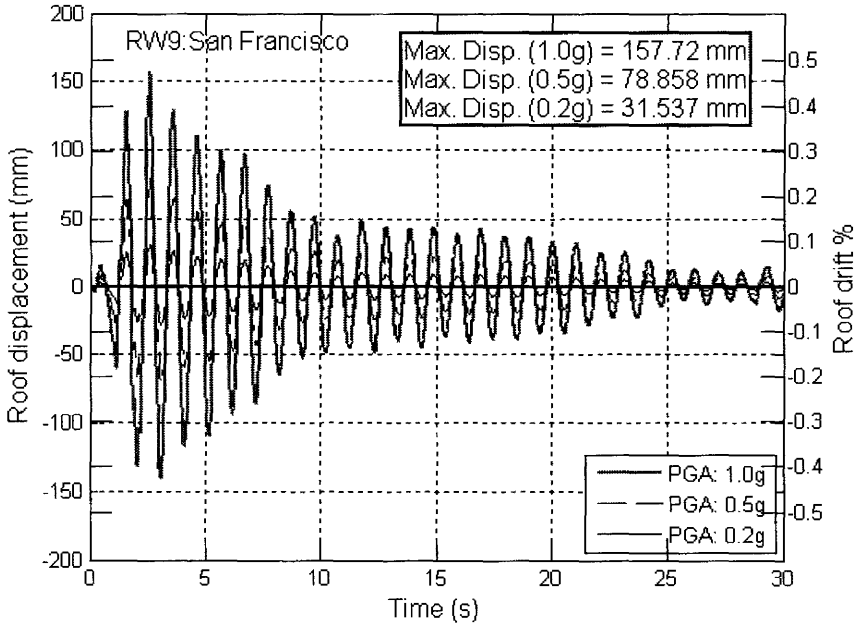

Figure 7. 56 Wall RW9 roof displacement time history due to San Francisco EQ record

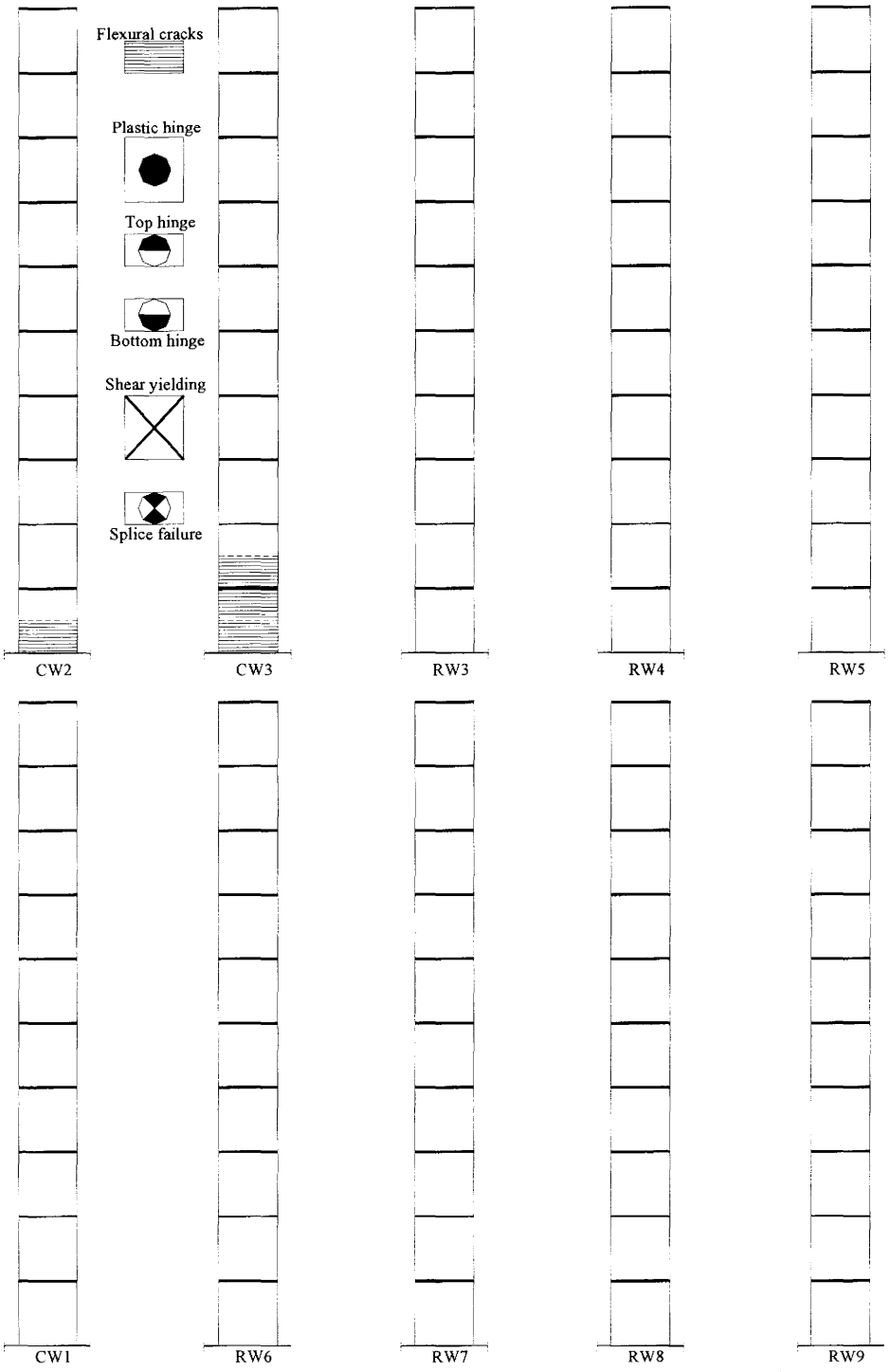

Figure 7. 57 Type of damage and location due to El Centro record with PGA= 0.20g

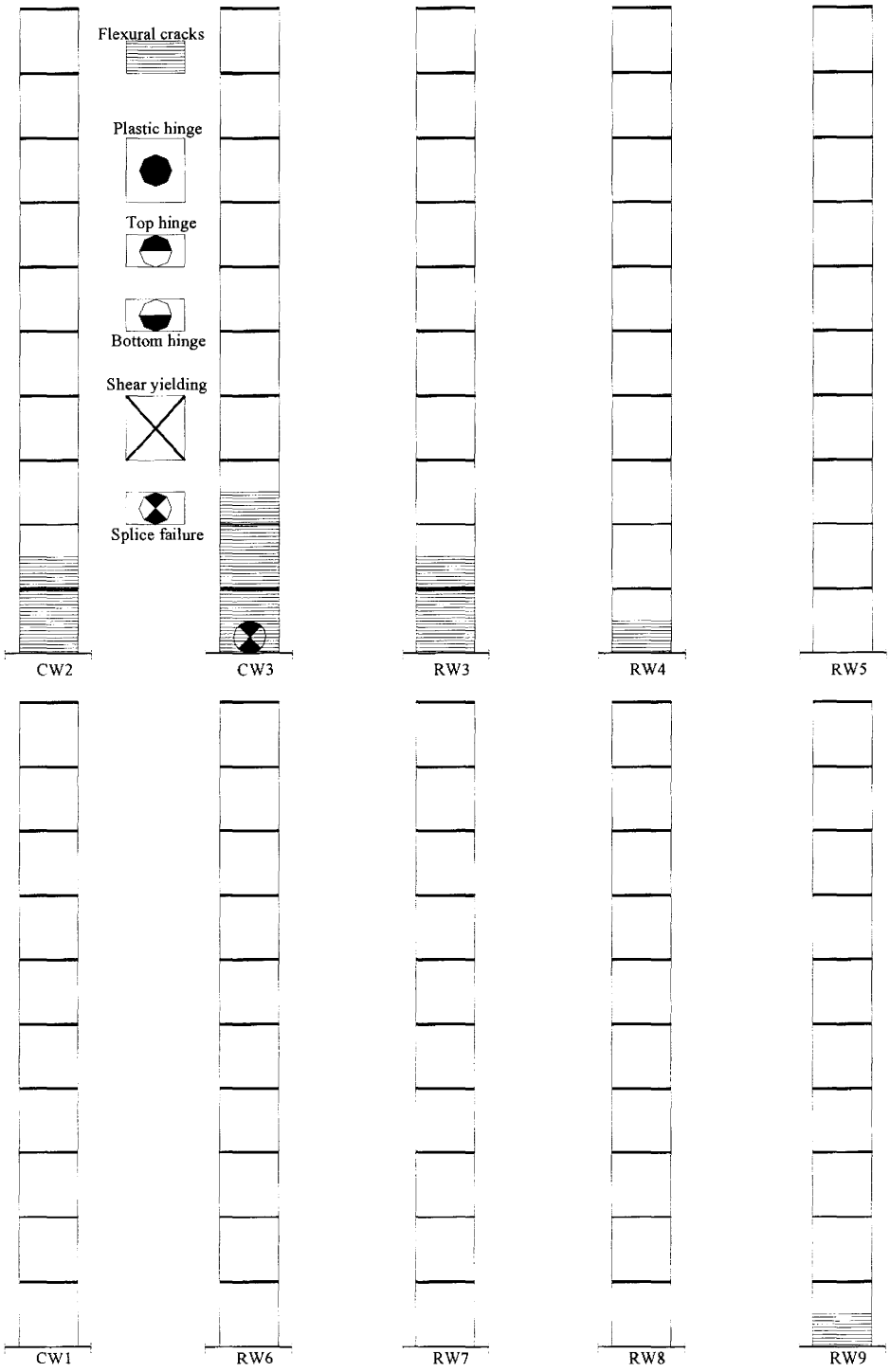

Figure 7. 58 Type of damage and location due to Mexico record with PGA= 0.20g

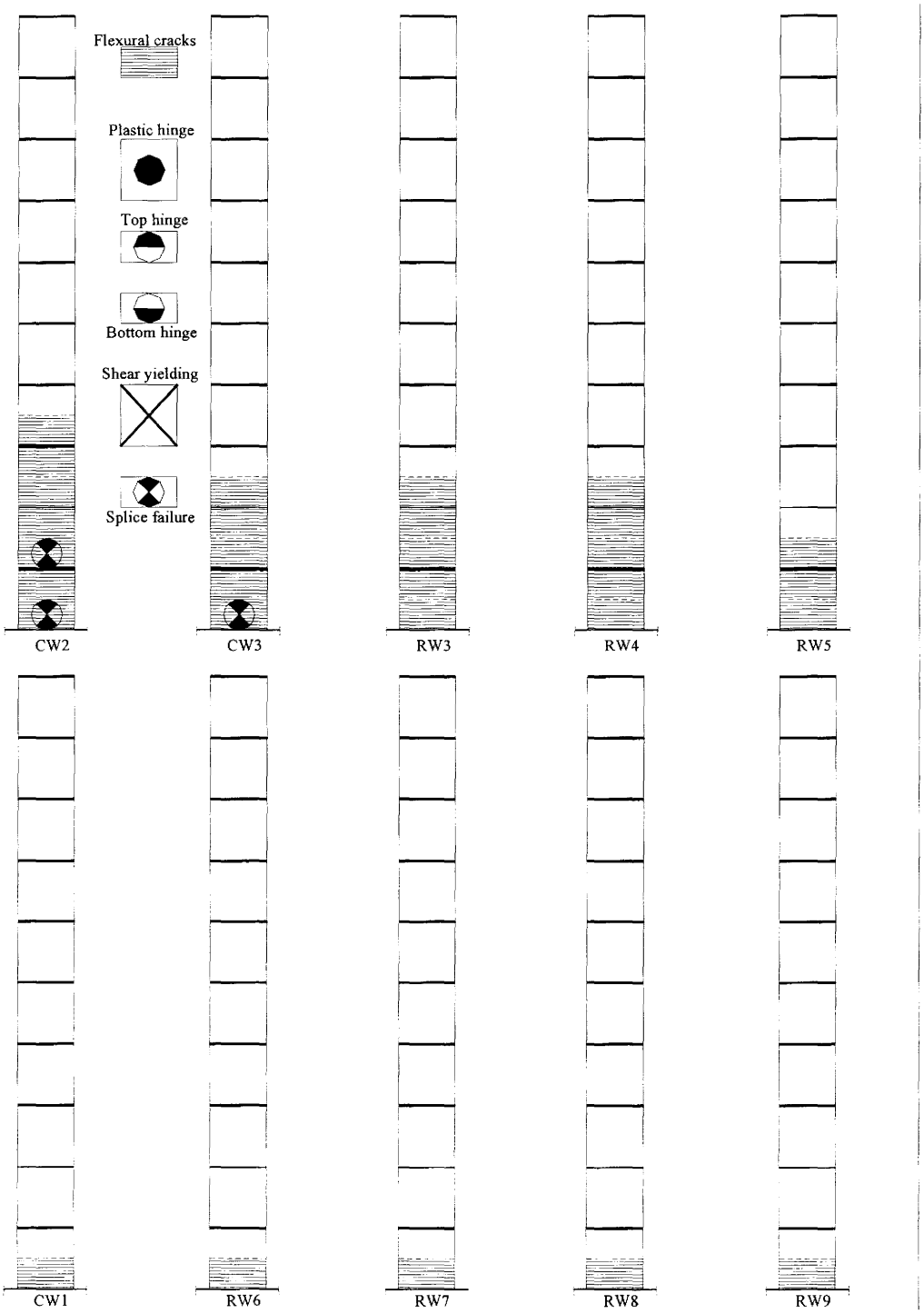

Figure 7. 59 Type of damage and location due to El Centro record with PGA= 0.50g

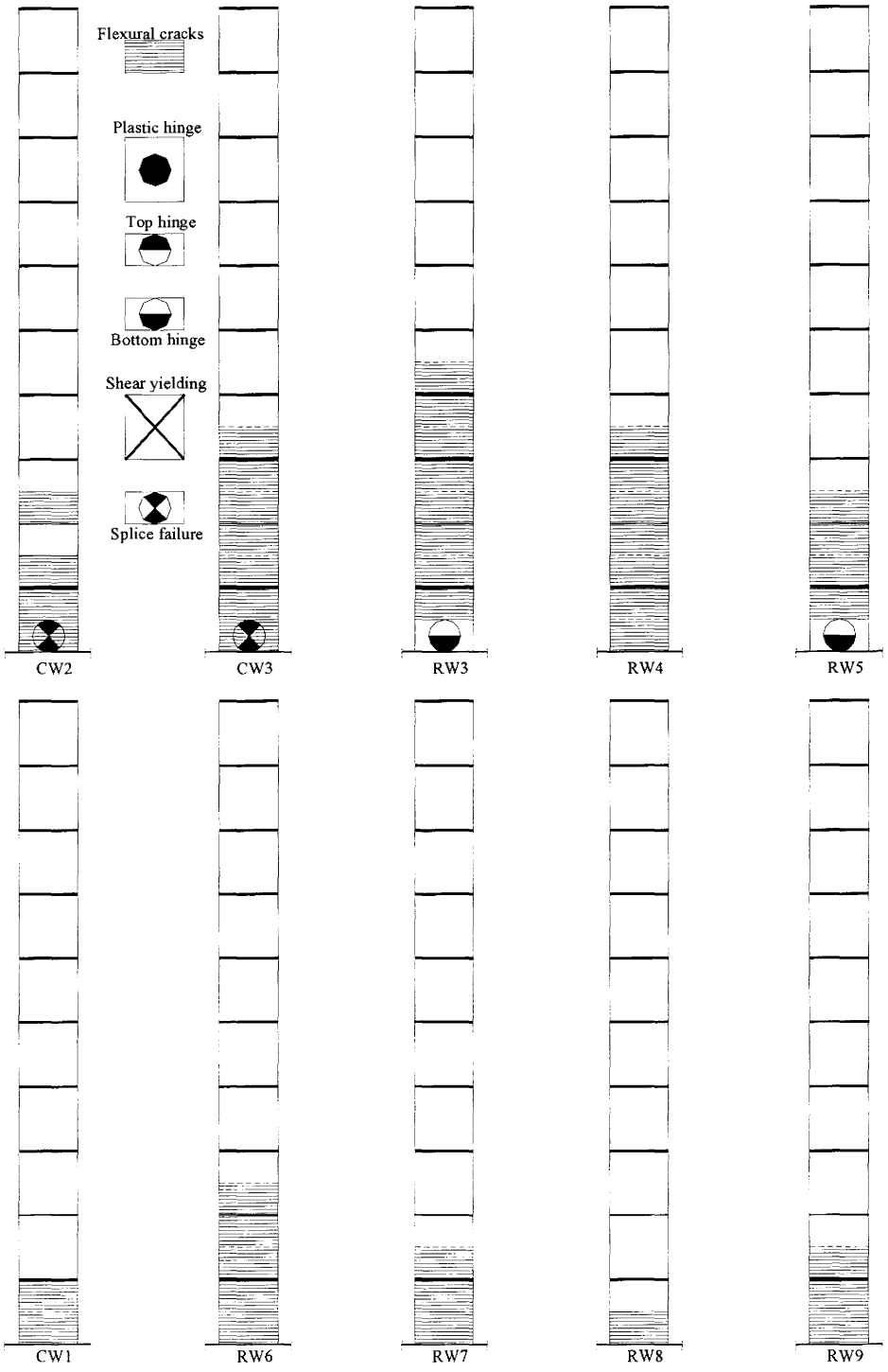

Figure 7. 60 Type of damage and location due to Mexico record with PGA= 0.50g

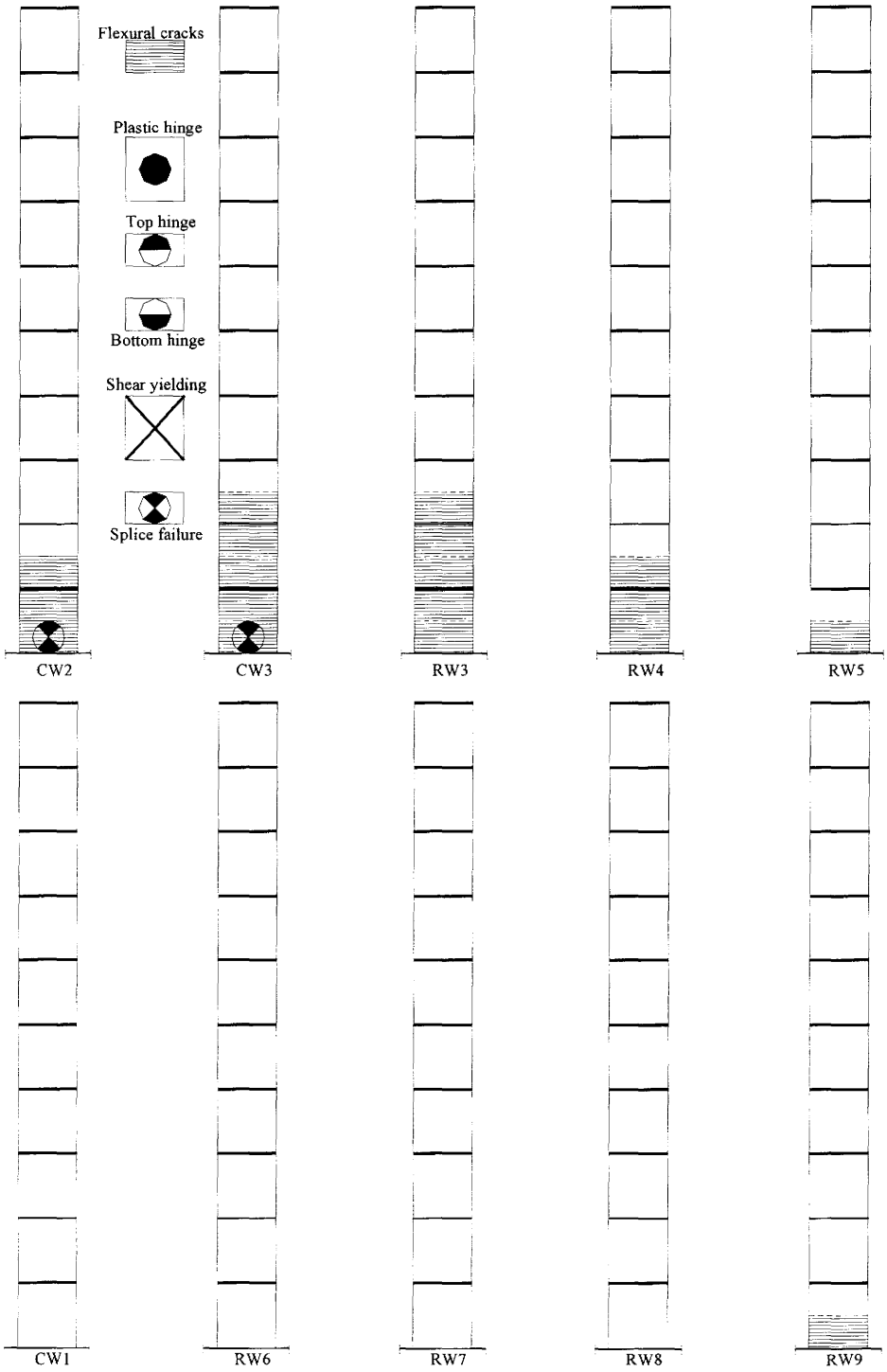

Figure 7. 61 Type of damage and location due to San Fernando record with PGA= 0.50g

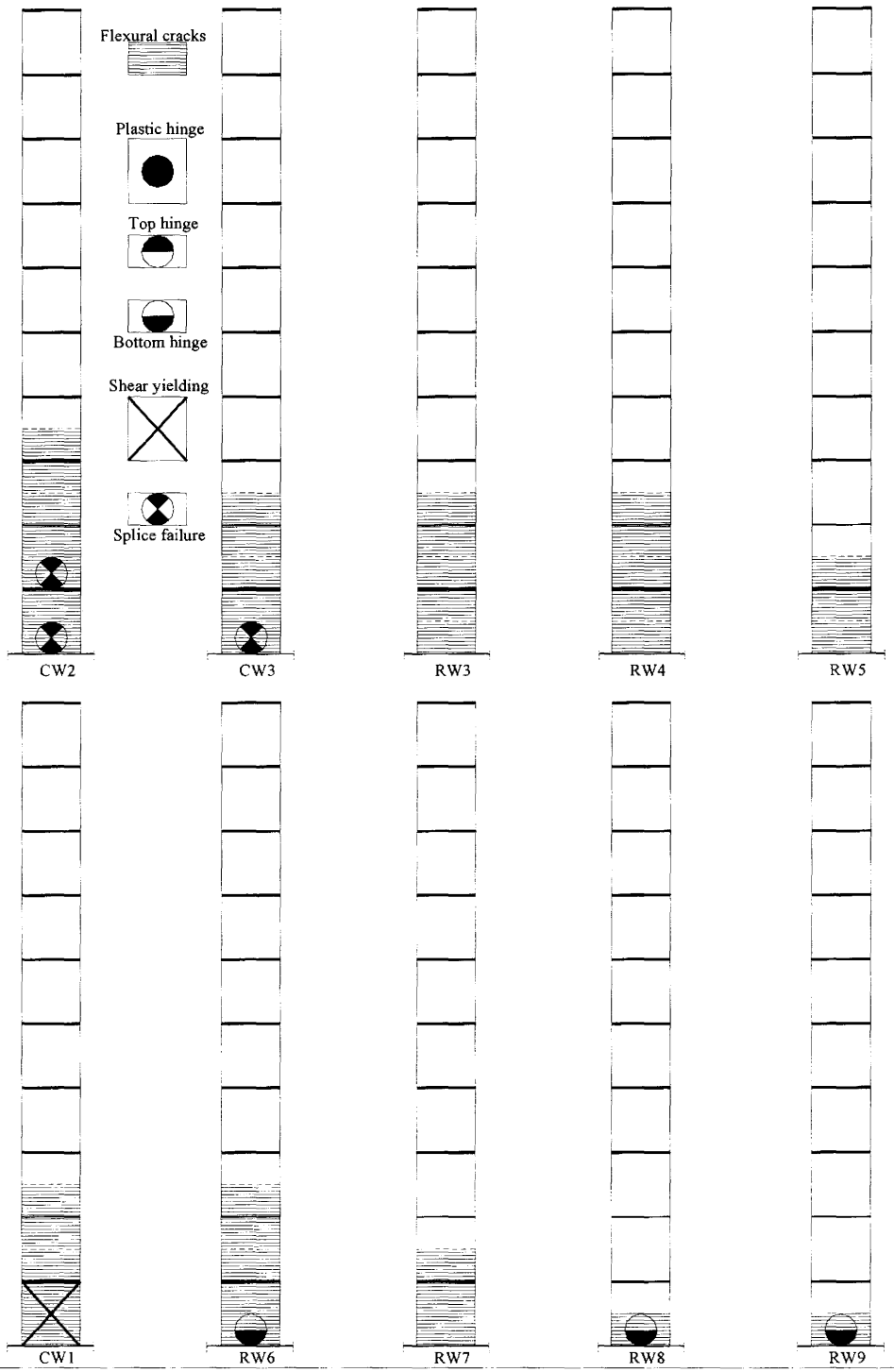

Figure 7. 62 Type of damage and location due to El Centro record with PGA= 1.00g

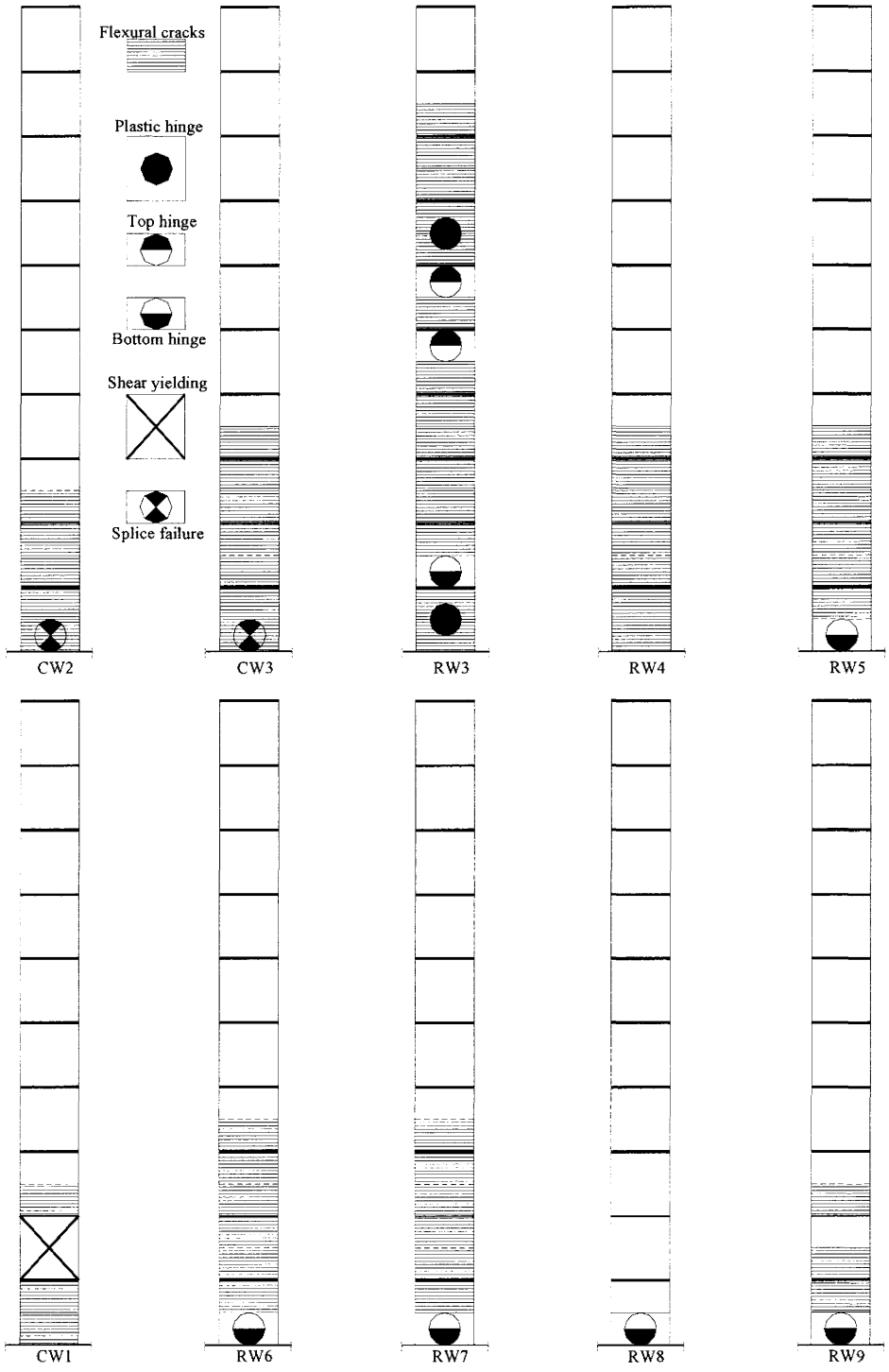

Figure 7. 63 Type of damage and location due to Mexico record with PGA= 1.00g

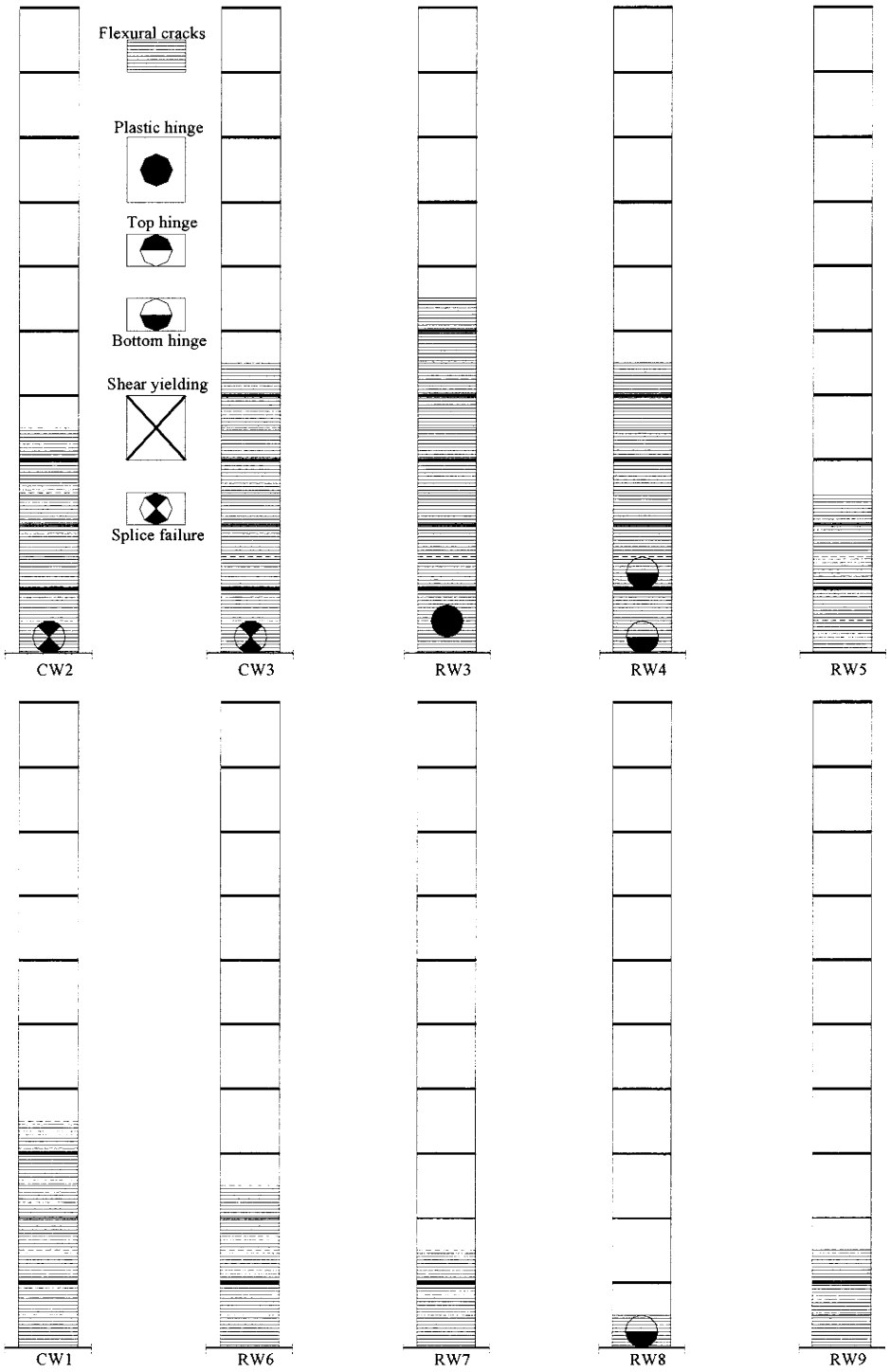

Figure 7. 64 Type of damage and location due to San Fernando record with PGA= 1.00g

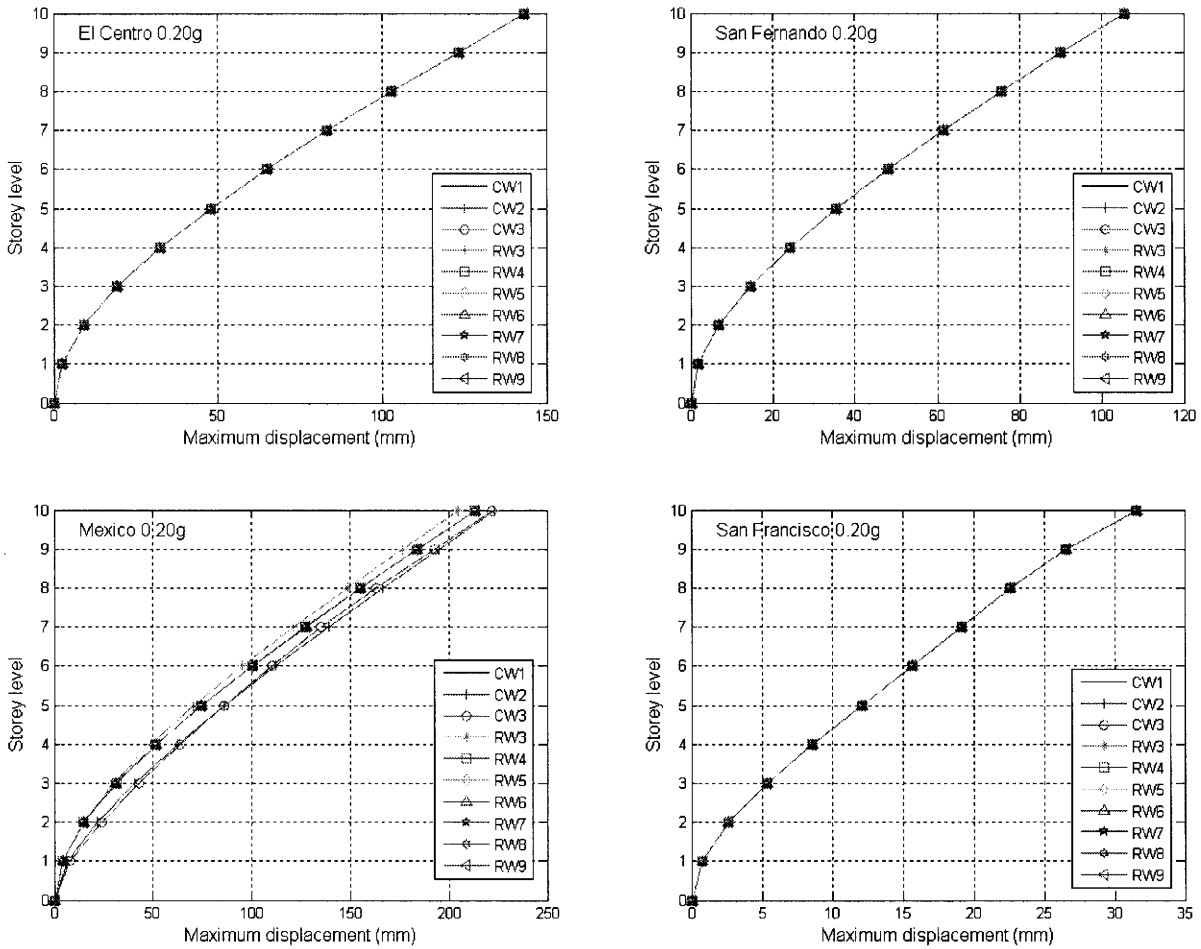

Figure 7. 65 Maximum displacement due to 0.20g PGA

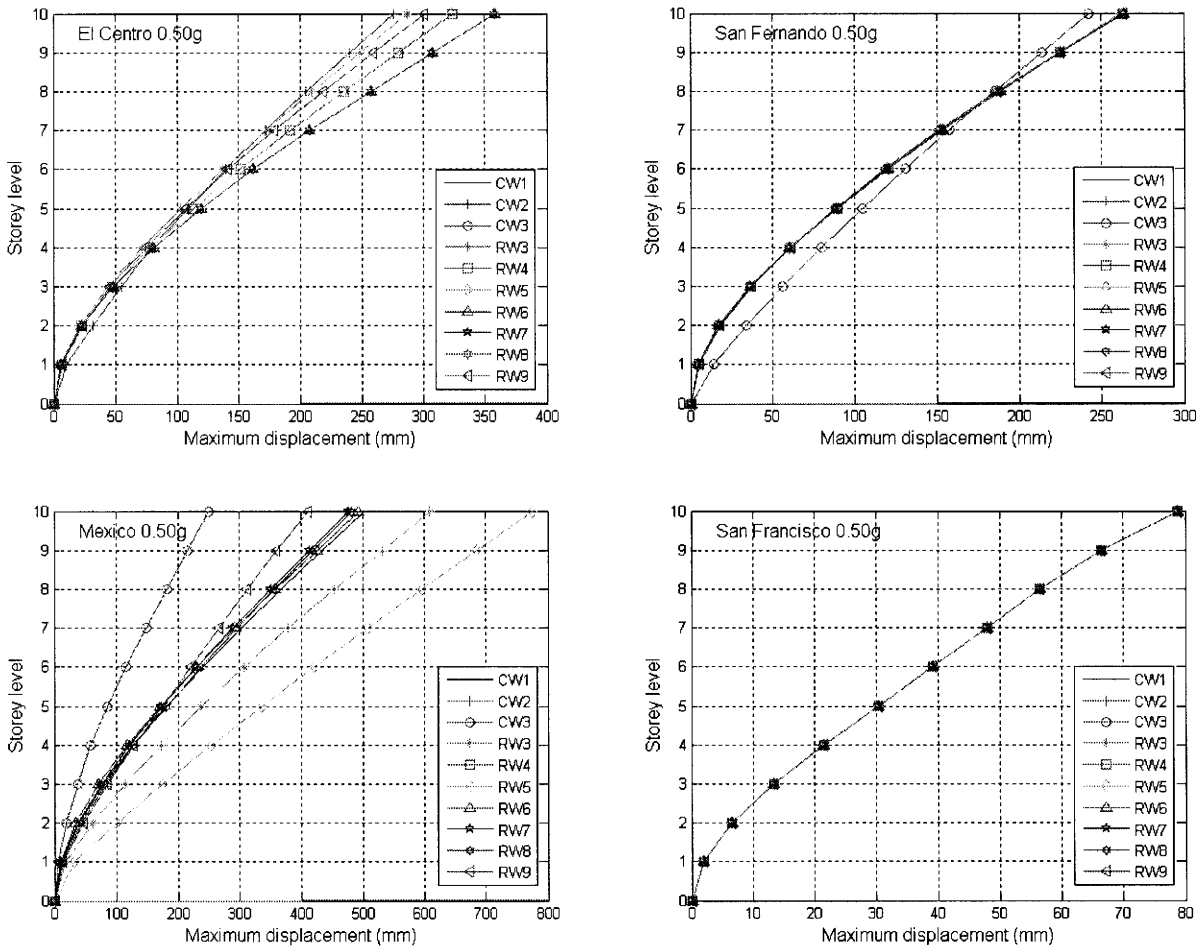

Figure 7. 66 Maximum displacement due to 0.50g PGA

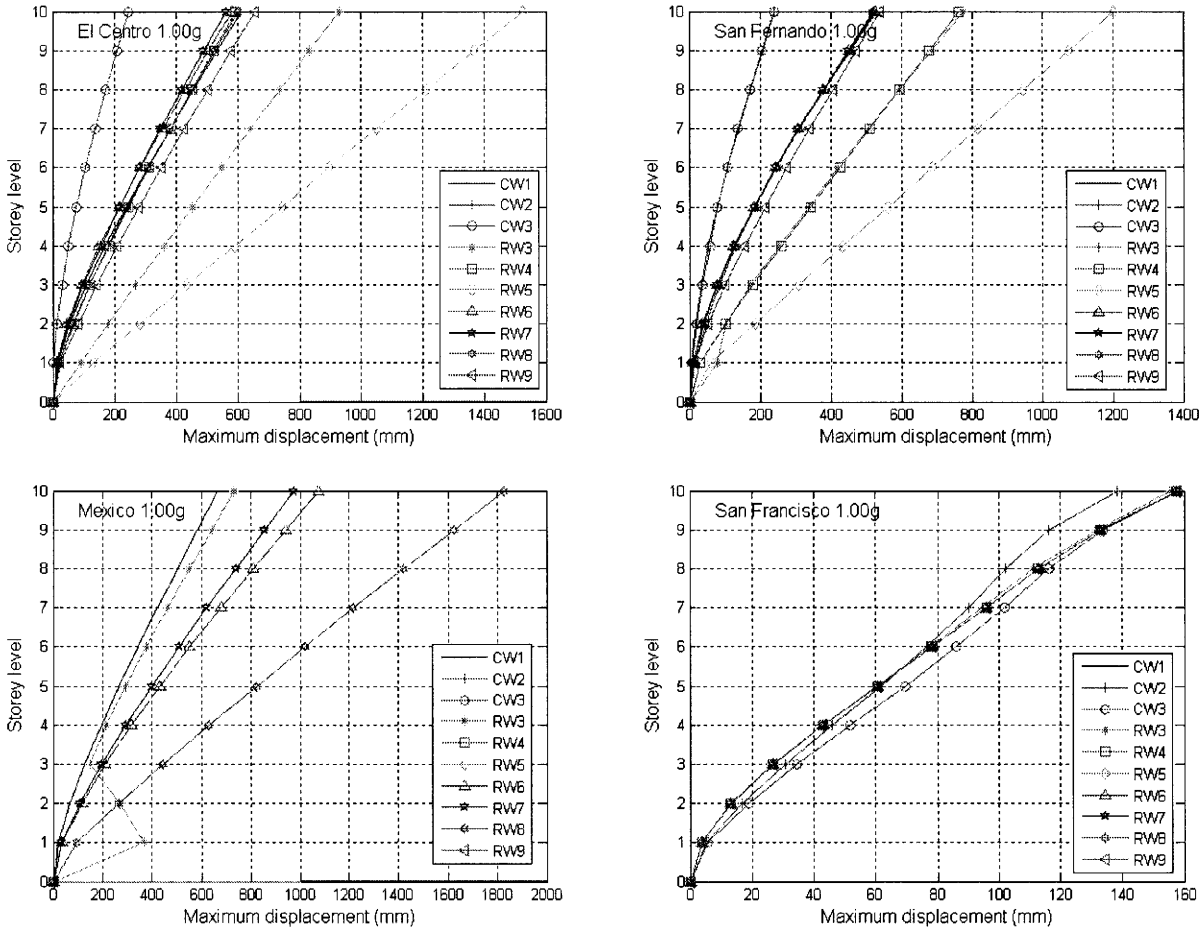

Figure 7. 67 Maximum displacement due to 1.0g PGA

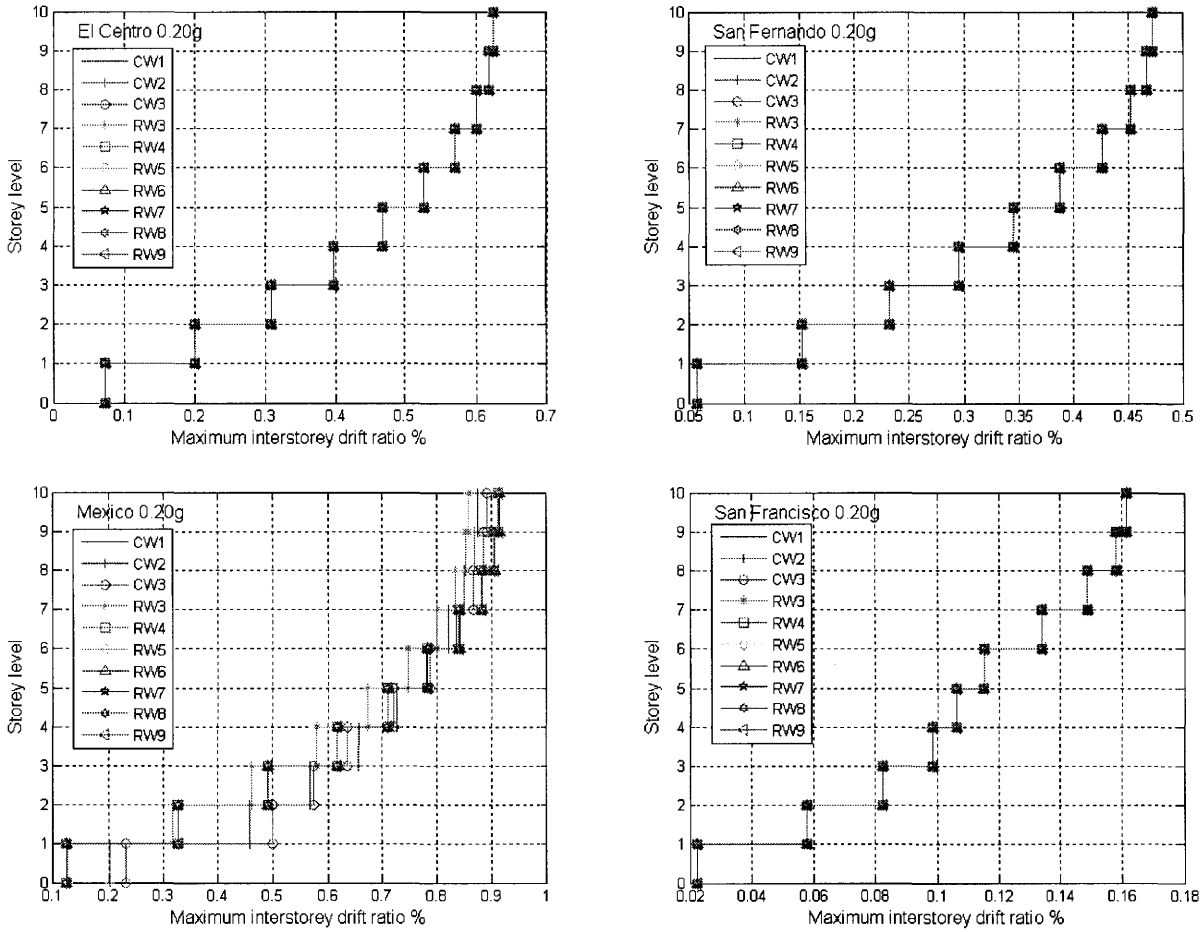

Figure 7. 68 Maximum interstorey drift due to 0.20g PGA

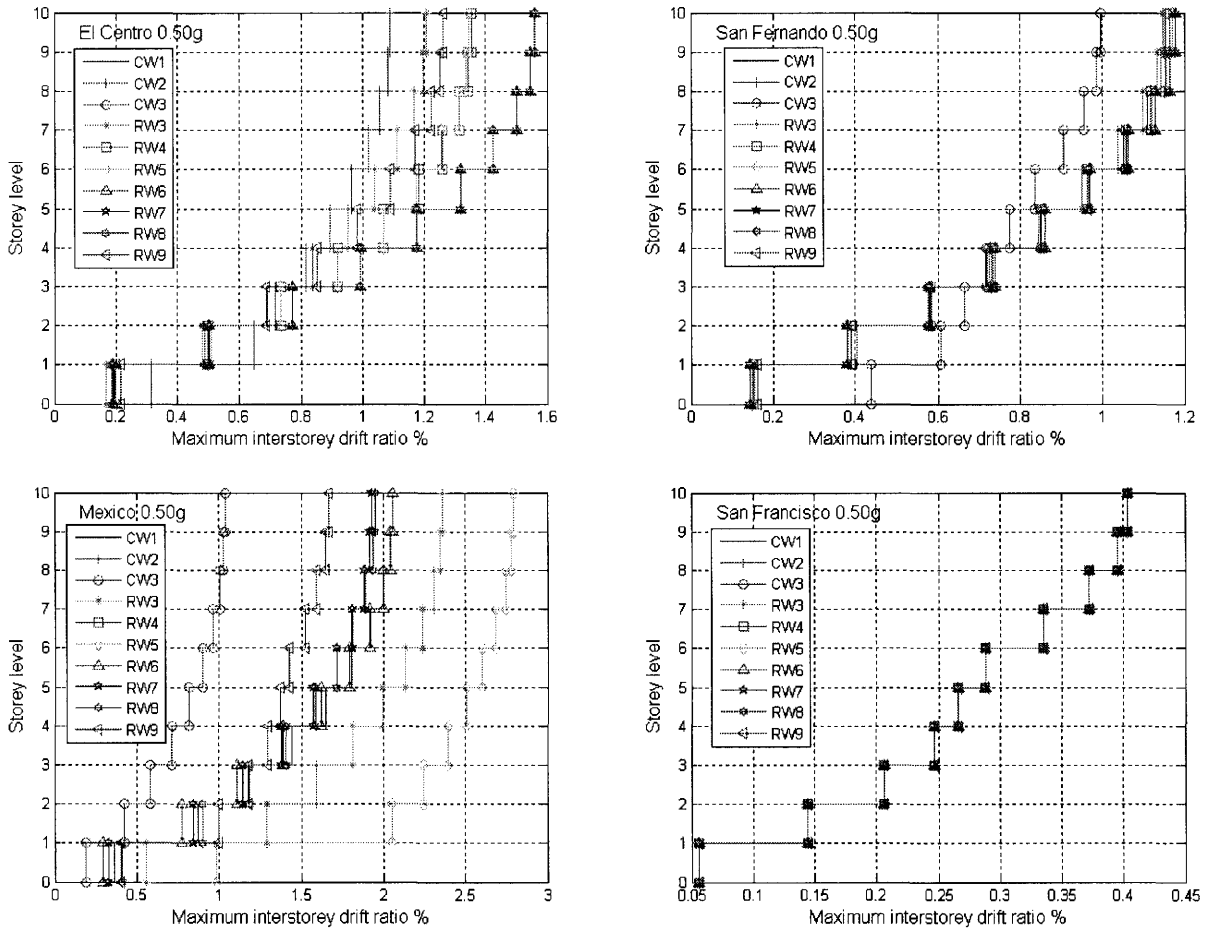

Figure 7. 69 Maximum interstorey drift due to 0.50g PGA

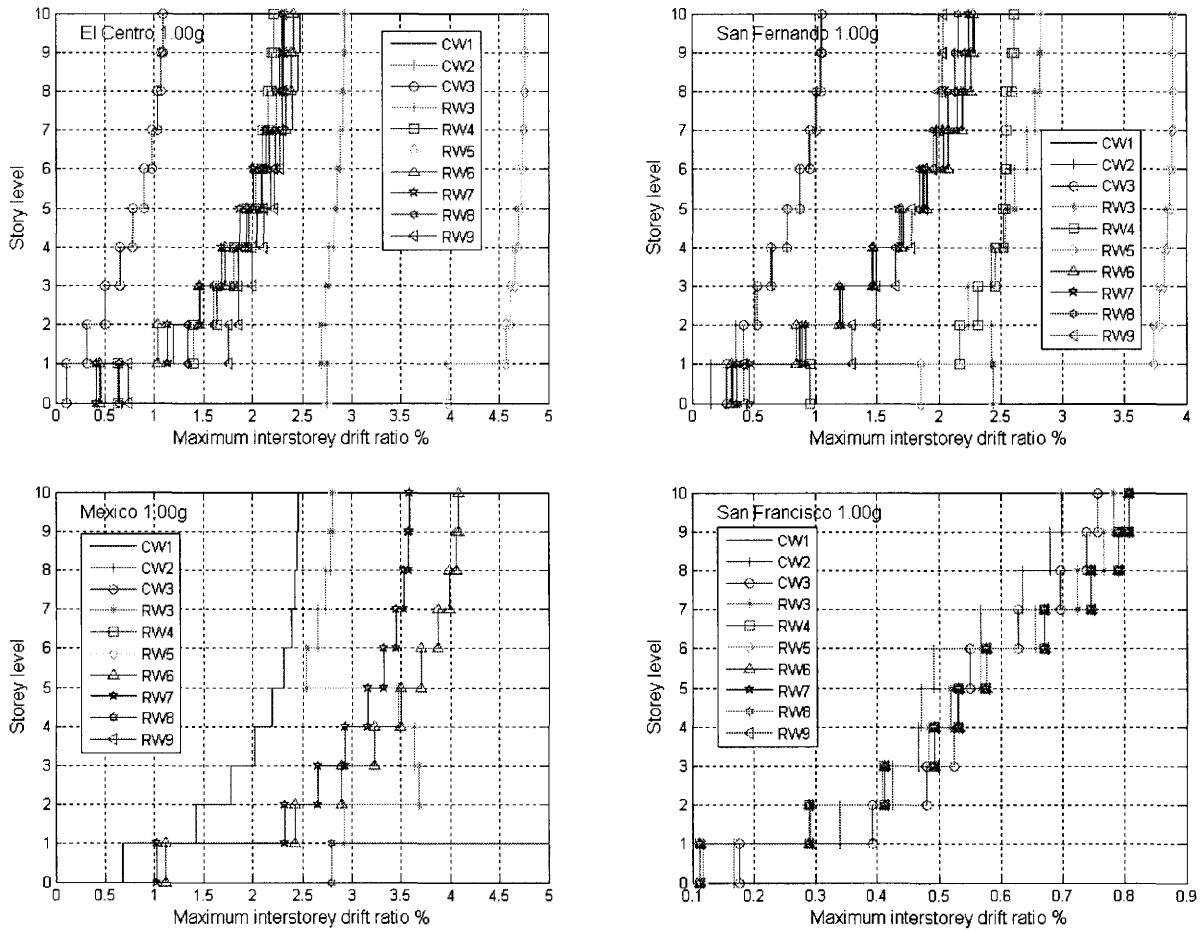

Figure 7. 70 Maximum interstorey drift due to 1.0g PGA

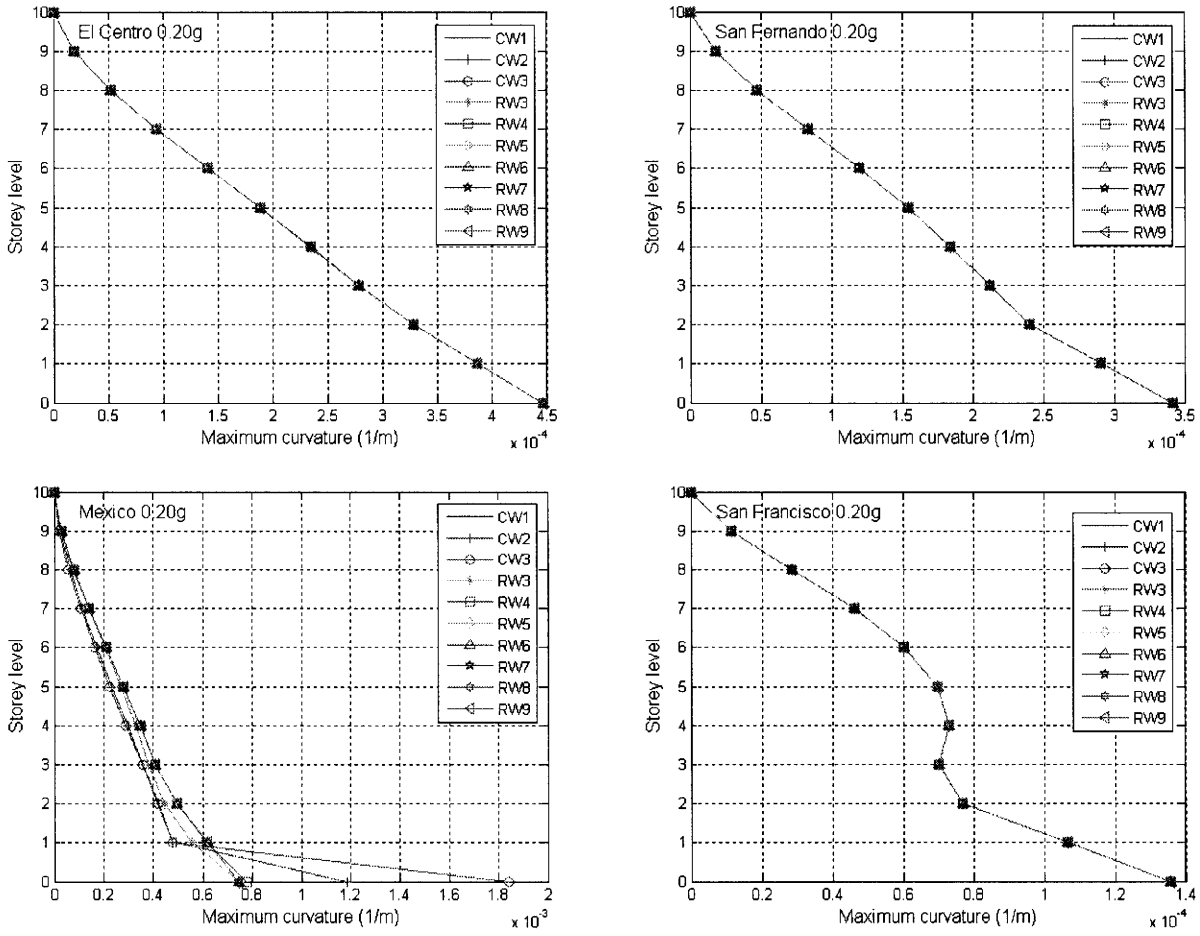

Figure 7. 71 Maximum storey curvature due to 0.20g PGA

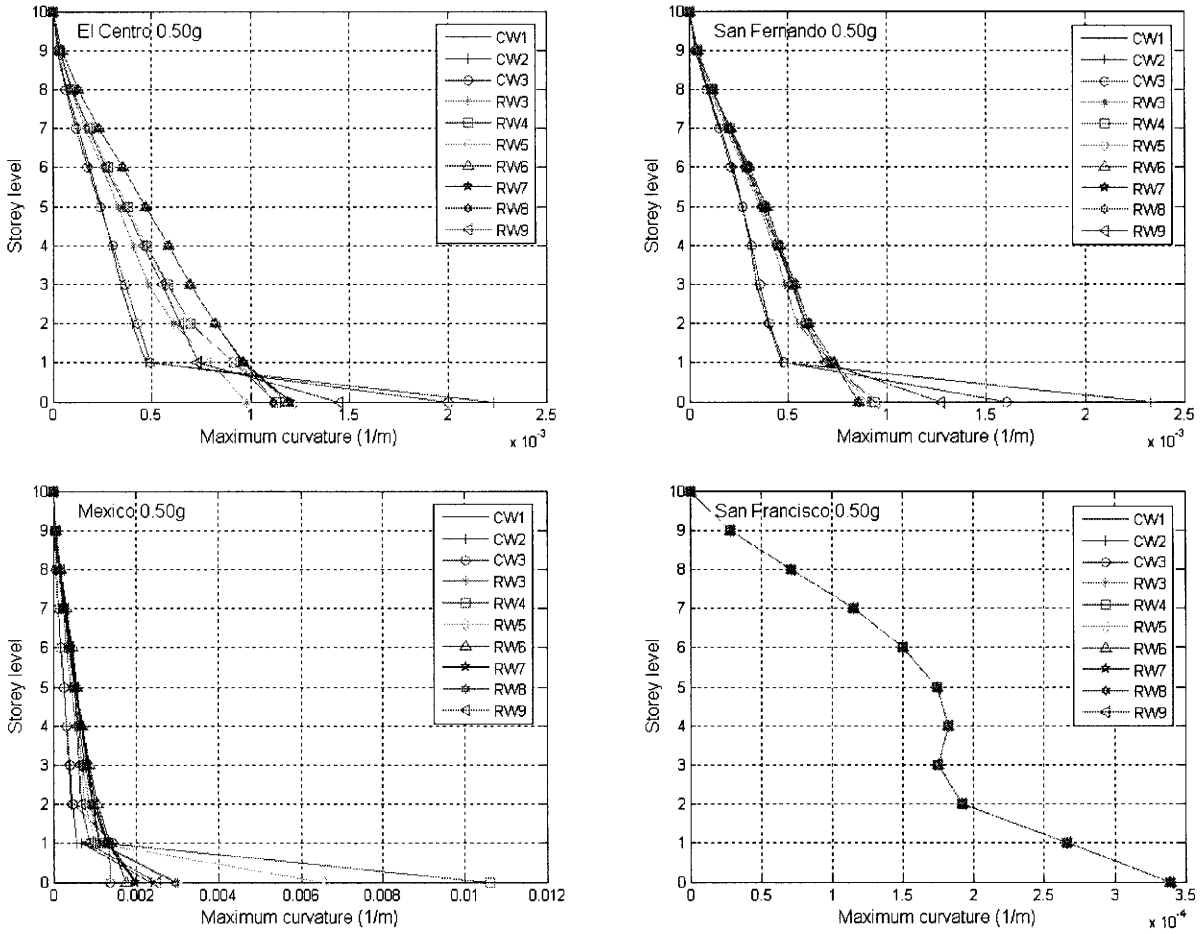

Figure 7. 72 Maximum storey curvature due to 0.50g PGA

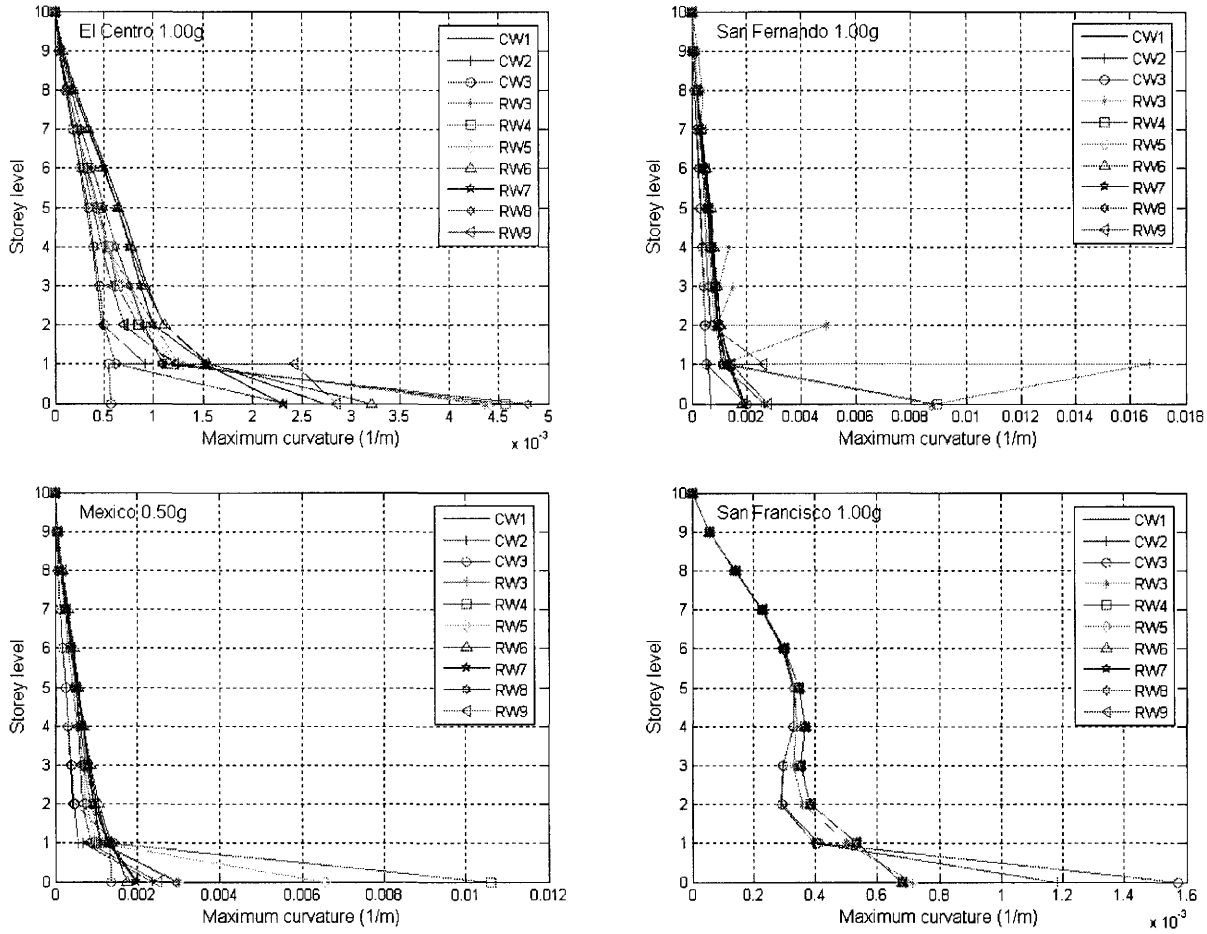

Figure 7. 73 Maximum storey curvature due to 1.0g PGA

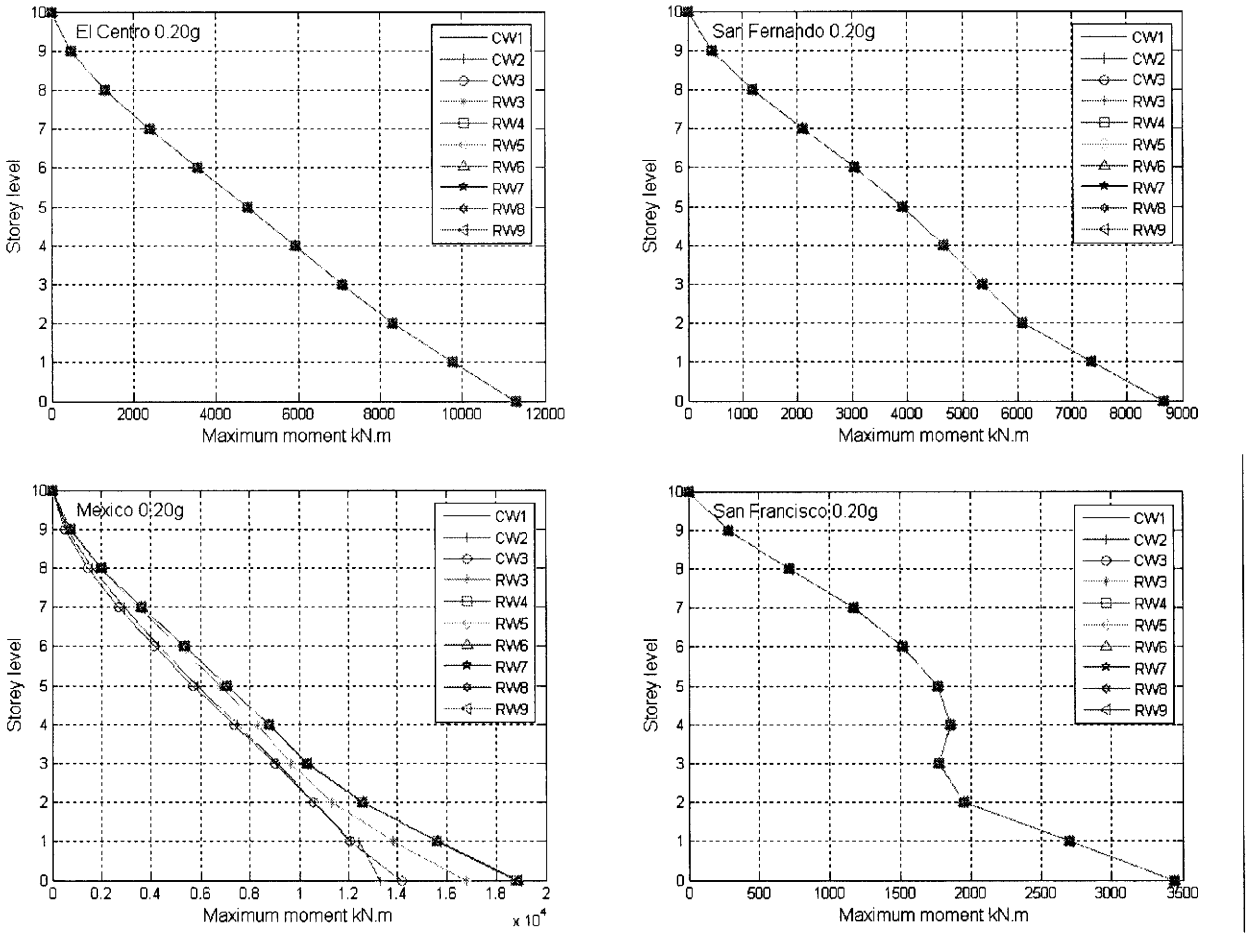

Figure 7. 74 Maximum storey moment due to 0.20g PGA

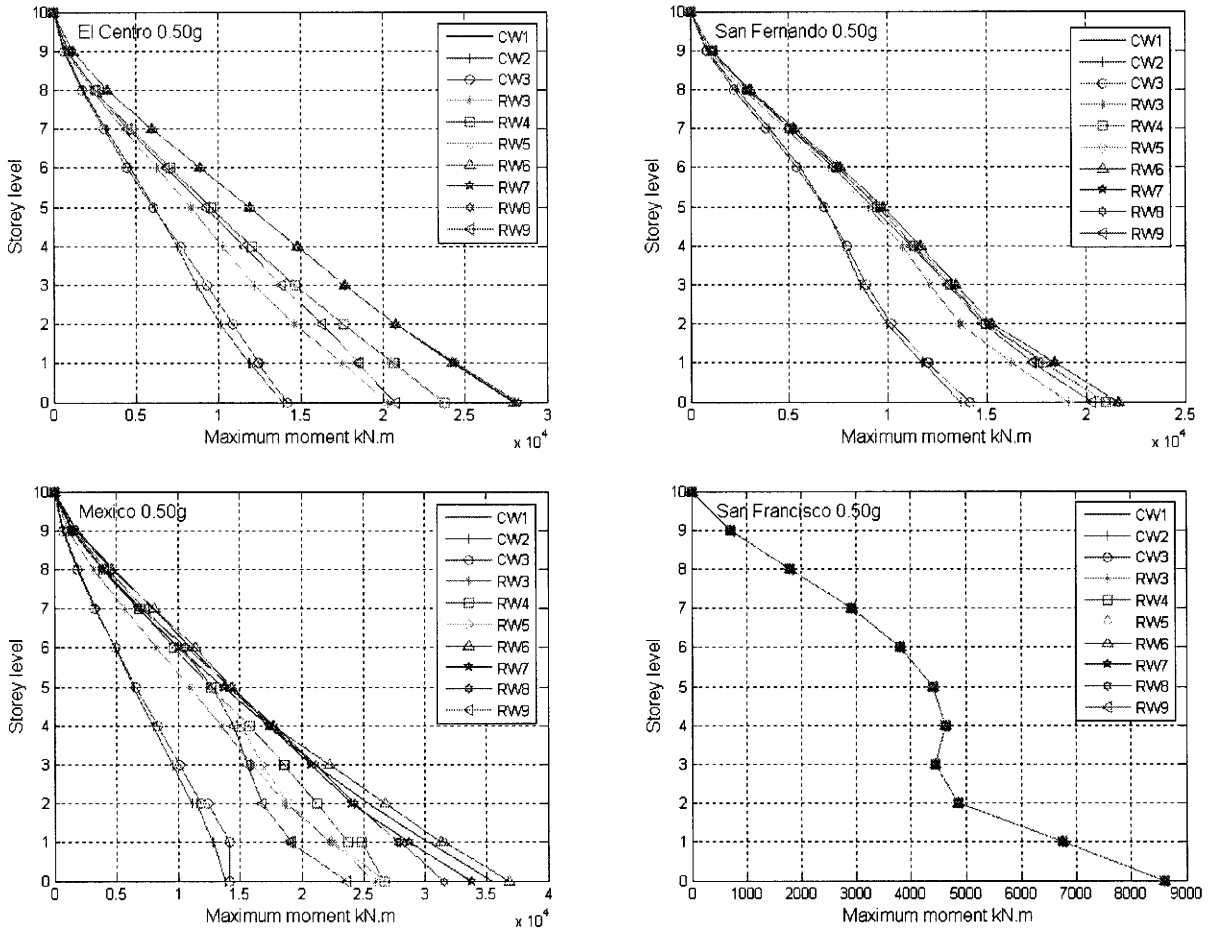

Figure 7. 75 Maximum storey moment due to 0.50g PGA

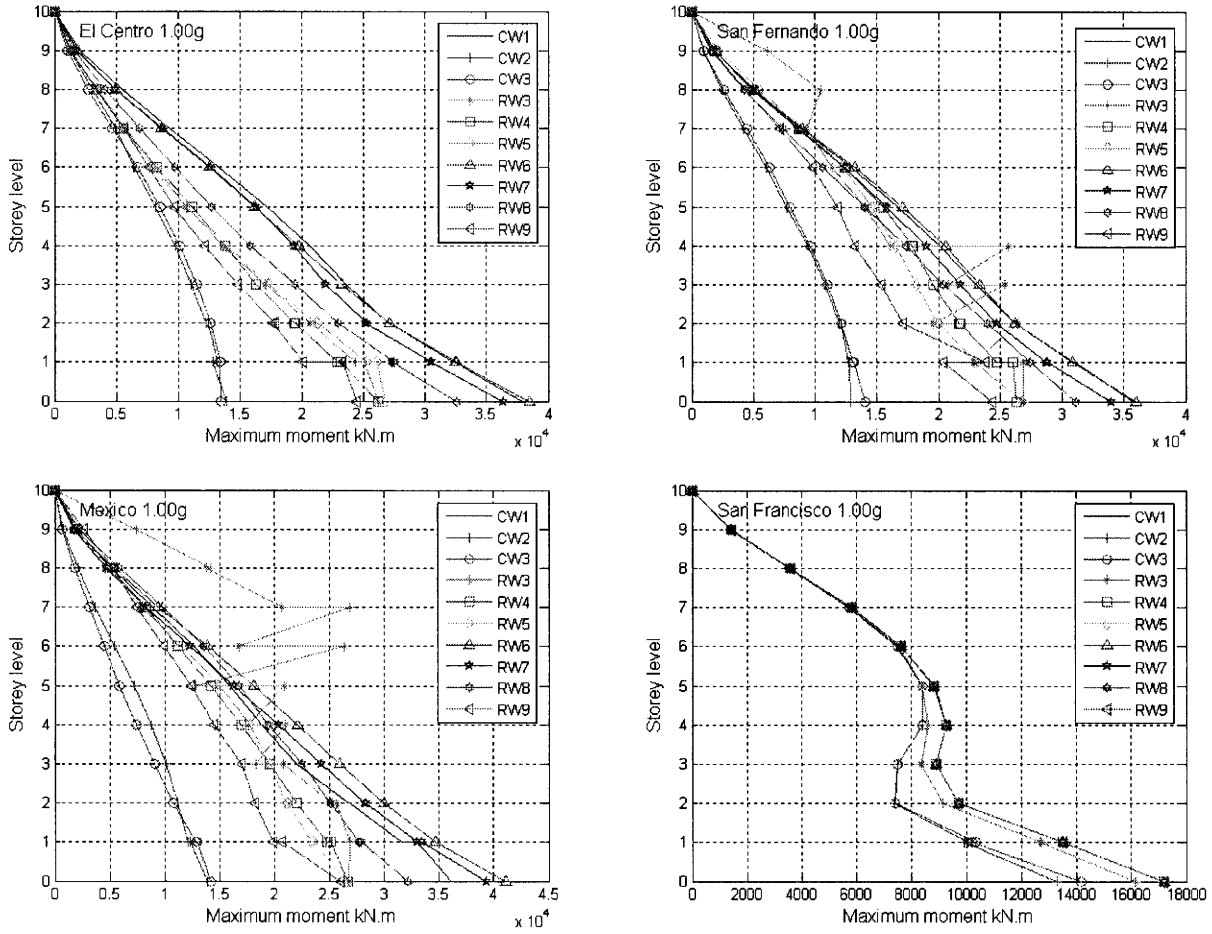

Figure 7. 76 Maximum storey moment due to 1.0g PGA

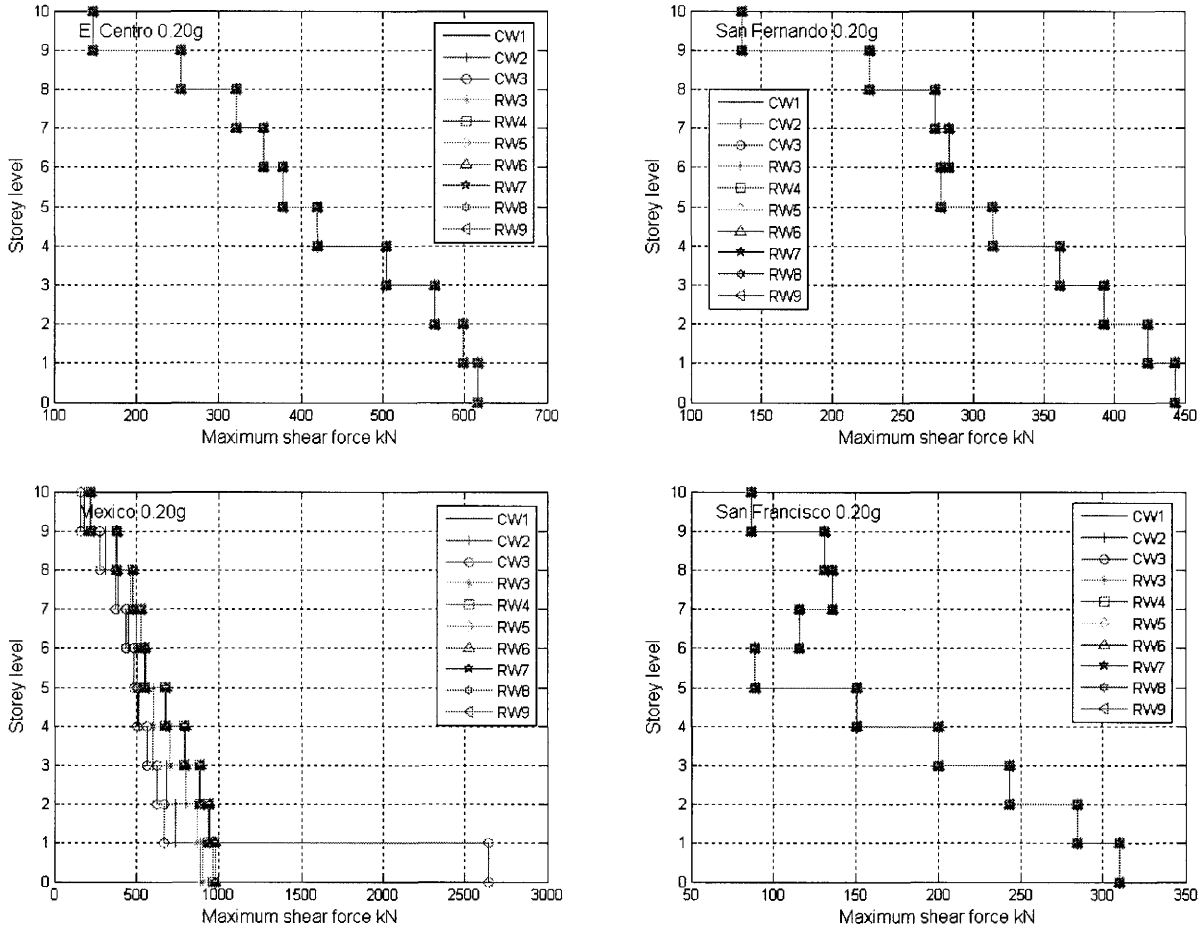

Figure 7. 77 Maximum storey shear due to 0.20g PGA

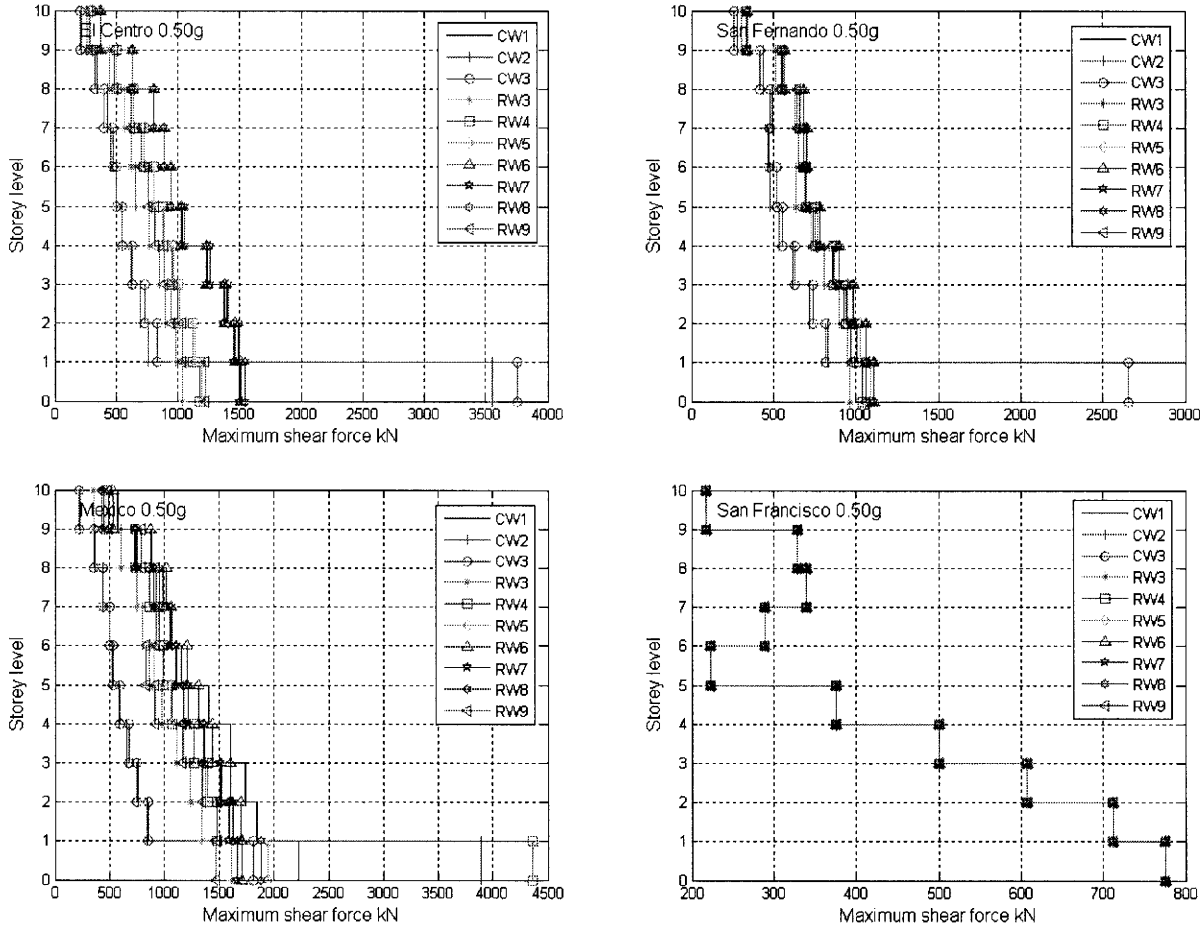

Figure 7. 78 Maximum storey shear due to 0.50g PGA

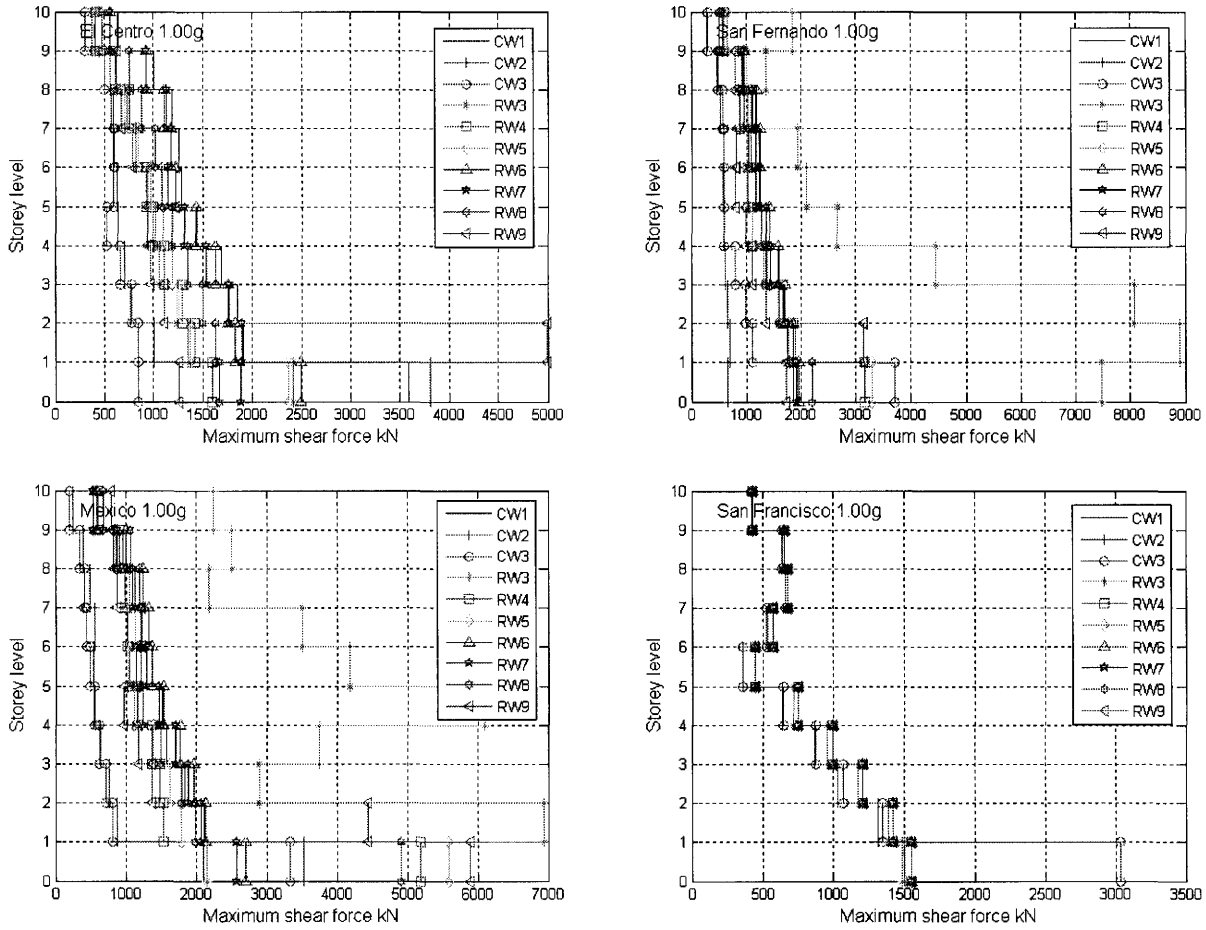

Figure 7. 79 Maximum storey shear due to 1.0g PGA

CHAPTER 8

CONCLUSIONS AND RECOMMENDATIONS

8.1 SUMMARY

The principal objective of this study was to evaluate the seismic behaviour of the non-ductile reinforced concrete structural walls before and after rehabilitation using carbon fibre reinforced polymers. This objective was achieved through experimental and analytical investigations.

The experimental phase of this research involved testing large scale models of the RC structural walls with deficient shear strength and lap splice detailing to reproduce failure modes observed following major seismic events and to evaluate the rehabilitation schemes. Ten reinforced concrete (RC) structural walls were built and tested using cyclic loading procedures. Three control walls were tested as-built with non-ductile detailing and seven walls were rehabilitated before testing. The purpose of the rehabilitation techniques was to prevent brittle failure in shear or bond slip and to improve the ductility and energy dissipation of the RC structural walls.

Ten walls were tested; three control walls CW1 to CW3 and seven rehabilitated walls RW3 to RW9. Walls CW1 to CW3 represented existing RC structural walls of 1970's design practice. Wall CW2 was tested using high moment to shear ratio to examine flexural behaviour, while CW3 was tested under low moment to shear ratio. Wall RW3 was identical to test wall CW3 but was rehabilitated using Carbon Fibre Reinforced Polymers (CFRP) wrapping for shear strengthening and confinement after welding the lap spliced flexural reinforcement. Wall RW4 represented CSA A23.3 (2004) designed wall. Wall RW5 was identical to test wall RW4 but it was rehabilitated using CFRP for shear strengthening and confinement to enhance ductile behaviour. Walls RW6 and RW7 represented rehabilitated walls to strengthen shear resistance and to confine the end columns. The only difference between RW6 and RW7 was the clamping plates attached at

the bottom edges of the web CFRP sheets of the RW6. This technique was intended to prevent the debonding of web externally bonded shear strengthening CFRP composite material at the bottom edges. Walls RW8 and RW9 represented CSA A23.3 (2004) code designed walls. To increase the ductility levels of both walls, the end columns were confined using anchored CFRP sheets.

The analytical phase of this study involved evaluation of the inelastic dynamic response of RC residential building with nonductile structural walls as well as retrofitted walls. An efficient macroscopic model to represent the behaviour of reinforced concrete structural walls when subjected to static cyclic or dynamic seismic loads was developed. The proposed model was intended to adequately describe the hysteretic behaviour of reinforced concrete structural walls and to be capable of accurately predicting both flexural and shear components of inelastic deformation. The model predictions were compared with the experimental results. The analytical model was used to evaluate the nonlinear dynamic behaviour of an existing building under seismic excitation before and after rehabilitation.

8.2 CONCLUSIONS

The following conclusions were reached from the results of this experimental and analytical research:

1- The experimental program was successful in duplicating failure modes observed following earthquakes.
2- Existing structural walls with 24 bar diameter length of lap splices at the base are inadequate for desirable ductile seismic response. Retrofitting lap splices by welding eliminates the brittle bond slip failure mode.
3- The moment to shear ratio is a significant factor that affects the behaviour of the structural walls and influences their failure mode. For the tested wall with moment to shear ratio of 5, the response was predominated by flexural

response. While for moment to shear ratio of 2.25 a coupled flexural/ shear response was observed.

4- Retrofitting the walls using CFRP sheets eliminated the brittle shear failure mode. The result is a ductile response with a high-energy dissipation, which are necessary for the collapse prevention during severe seismic events.

5- The CFRP confined end column elements showed a significant contribution to the tested walls ductile response. In addition, the web CFRP strengthening contributed significantly in controlling the cracks, which reduced the pinching in the hysteretic loops considerably. The increased ductility and the decreased pinching effects significantly improved the energy dissipation of the tested walls.

6- The use of a clamping steel plate as an anchoring system for the bottom edge of the web CFRP wrapping system prevented debonding at the bottom edge of CFRP and localized the damage on the bottom of end columns zones. In addition, it increased the number of stable ductile loading cycles to ductility level of almost 10, which corresponded to drift ratio of 3.0 %.

7- The use of steel anchor bolts as anchoring system for confinement CFRP wraps was successful in creating well-confined end columns for the rehabilitated walls.

8- The rehabilitation systems involved shear strengthening and end columns confinements with steel anchor bolts. Tests results indicated that these systems significantly improved the strength and ductility of the rehabilitated walls.

9- The design practice based on CSA A23.3 (2004) code specifications does not recognize the effect of the flexural reinforcement ratio on the need for confinement of the end column element of RC structural walls, which may lead to nominal ductile response.

10- A model was developed and verified to analytically observe the inelastic cyclic and dynamic responses of reinforced concrete walls.

11- Analytical results showed that damage would occur to existing buildings that were designed to outdated non-seismic Codes.

12- It was observed from inelastic dynamic analysis that the major damage was localized at the first storey because of the formation of plastic hinges at the bottom of the walls. Results from inelastic dynamic analysis of ten-story existing residential building with reinforced concrete structural walls as a lateral load resisting system showed brittle failure modes under seismic events. The analysis results indicated that the rehabilitation techniques were successful in preventing brittle failure modes and ensuring ductile response.

Finally, it should be mentioned that the present analytical results are based on the analysis of a specific residential building. To establish a general conclusion, a comprehensive analytical study is needed.

8.3 RECOMMENDATIONS FOR FUTURE WORK

The following recommendations may be considered in future research involving experimental and analytical study of non-ductile reinforced concrete structural walls:

1- An experimental program that involves pseudodynamic test procedure to investigate the behaviour of reinforced concrete structural walls under the effect of earthquake excitations is needed. The Author did some attempts to conduct this method of testing, but neither the research equipment nor the laboratory space was granted during the fourth year of this study.

2- An experimental program is needed to investigate the bahviour of ductile reinforced concrete structural walls that are designed according to CSA A23.3 (2004) and NBCC (2005).

3- Development and validating, by means of an experimental program, a multipurpose pseudo-dynamic software that consist of two modules (i)

Simulation module, (ii) Test module. The software should simulate the behaviour of the entire building during the test. It should be used for online testing as well as for nonlinear dynamic analysis.

4- An experimental program is needed to investigate the effect of different moment to shear ratios on the walls behaviour.
5- Walls with different geometries such as flanged walls and walls with boundary elements should be tested before and after rehabilitation.
6- An experimental program that involves testing coupled walls and the frame-wall interactions is needed.
7- A rehabilitation system that incorporates the application of externally bonded CFRP strands in the rehabilitation of walls is needed.
8- Moment strengthening of walls needs investigation.
9- Investigation to determine the fragility curves for walls is needed.
10- An analytical study to analyze different types of buildings with different configurations is needed.

REFERENCES

ACI 318 (1968), "Building Code Requirements for Structural Concrete", American Concrete Institute, Detroit, Michigan, USA.

ACI 318 (1985), "Manual of Concrete Practice", Part 3, Committee 408-1R-79, American Concrete Institute, Detroit, Michigan, USA.

Alsiwat, J.M., and Saatcioglu, M. (1992), "Reinforcement Anchorages Slip under Monotonic Loading", Journal of Structural Engineering, ASCE, Vol. 118, No. 9, pp. 2421-2438.

Ang, A.K-S., Kim W.J., and Kim, S.B. (1993), "Damage Estimation of Existing Bridge Structures", Structural Engineering in Natural Hazarads Mitigation, Proceeding of ASCE Structures congress, Irvine, CA, Vol.2, pp.1137-1142.

Antoniades, K., Salonikios, T., and Kappos, A. (2003), "Cyclic Tests on Seismically Damaged Reinforced Concrete Walls Strengthened Using Fiber-Reinforced Polymer Reinforcement", ACI Structural Journal, Vol. 100, No.4, pp.510-518.

Assa, B., Nishiyama, M., and Watanabe, F. (2001), "New Approach for Modeling Confined Concrete: II-Rectangular Columns", Journal of Structural Engineering, ASCE, Vol. 127, No. 7, pp. 751-757.

Caccese, V. and Harris, H.G. (1986), "Seismic Behavior of Precast Concrete Shear Walls-Correlation of Experimental and Analytical Results" Proceedings of the 3rd US National Conference on EQ Engineering, Charleston, South Carolina, pp. 1347-1385.

Ciampi, V., Eligehausen, F., Popov, E.P., and Betero, V.V., (1982). "Analytical Model for Concrete Anchorages of Reinforcing Bars under Generalized Excitations", Earthquake

Engineering Research Center, Report No. UCB/EERC-82/23, University of California, Berkeley, California, USA.

Collins, M.P., and Mitchell, D., (1987) "Prestressed Concrete Basics" Canadian Prestressed Concrete Institute, Ottawa, Ontario, Canada.

Collins, M.P., Mitchell D., Adebar P., Vecchio FJ. (1996) "A General Shear Design Method" ACI Structural Journal, 93(1):36-47.

CSA A23.3 (2004), "Design of Concrete Structures", Canadian Standards Association, Rexdale, Ontario, Canada.

CSA S806 (2002), "Design and Construction of Building Components with Fibre-Reinforced Polymers", Canadian Standards Association, Rexdale, Ontario, Canada.

El-Amoury, T.A. (2004), "Seismic Rehabilitation of Concrete Frame Beam-Column Joints", Ph.D. Thesis, Department of Civil Engineering, McMaster University, Hamilton, Ontario, Canada.

Eligehausen, F., Popov, E.P., and Betero, V.V., (1983). "Local Bond Stress-Slip Relationship of deformed Bars under Generalized Excitations", Earthquake Engineering Research Center, Report No. UCB/EERC-83/23, University of California, Berkeley, California, USA.

Elnashai, A.S. and Pinho, R. (1997), "Repair and Strengthening of RC Walls Using Selective Techniques" Engineering Seismology and Earthquake Engineering, Civil engineering Department, Imperial College, London, ESEE Research Report No.97-1.

Elnashai, A.S., Pilakoutas, K., and Ambrayses, N.N., (1990), "Experimental Behavior of Reinforced Concrete Walls Under Earthquake Loading", Earthquake Engineering and Structural Dynamics, Vol. 19, pp. 387-407.

Fajfar, P., and Gaspersic, P., (1996). "The N2 method for the seismic damage analysis of RC buildings." Earthquake engineering and structural dynamics. Vol. 25, pp. 31-46.

Fam, A. and Rizkalla, S. (2001), "Confinement Model for Axially Loaded Concrete Confined by Circular Fiber-Reinforced polymer Tubes", ACI Structural Journal, Vol. 98, No.4, pp. 451-461.)

FEMA 273 (1997) "NEHRP Giudlines for the Seismic Rehabilitation of Buildings", Federal Emergency Management Agency, Washington, D.C., USA.

Filippou, F.C., Popov, E.P., and Betero, V.V., (1983). "Effect of Bond Deterioration on Hysteretic Behaviour of Reinforced Concrete Joints." Report No. UCB/EERC-83/19, Earthquake Engineering Research Center, University of California, Berkeley, California, USA.

Fintel, M. (1995), "Performance of Buildings with Shear Walls in Earthquakes of the Last Thirty Years", PCI Journal, Vol. 40, No.3, pp. 62-80.

Fiorato, A.E., Oesterle, R.G., and Corley, W.G. (1983), "Behavior of Earthquake Resistant Structural Walls Before and After Repair", ACI Journal, Vol. 80, pp. 403-413.

Fyfeco (2005), Product technical specification, http://www.fyfeco.com/ products/ compositesystems/ pdf/seh-51a.pdf , (Accessed January 2005).

Galal, K.E.M. (2002), "Modeling and Rehabilitation of non-ductile Spatial RC Columns", Ph.D. Thesis, Department of Civil Engineering, McMaster University, Hamilton, Ontario, Canada.

Ghobarah, A. and Youssef, M. (1999), "Modeling of Reinforced Concrete Structural Walls", Engineering Structures, Vol. 21, pp. 912-923.

Ghobarah, A., (2000) "Seismic Assessment of Existing RC Structures," Progress in Structural Engineering Matrial, No. 2, PP. 60-71.

http://www.hewett.norfolk.sch.uk/curric/NEWGEOG/Tectonic/Earth/Building.htm (accessed March 2006).

ICBO (2001). "Acceptance Criteria for Concrete and Reinforced and Unreinforced Masonry Strengthening Using Fiber-Reinforced Polymer (FRP), Composite Systems" Report AC 125, International Conference of Building Officials Evaluation Service, Inc., Whittier, California, USA.

Iso, M., Matsuzaki, Y., Sonobe Y., Nakamura H., and Watanabi M. (2000), "Experimental Study on Reinforced Concrete Columns Having Wing Walls Retrofitted with Continuous Fiber Sheets", 12th World Conference of Earthquake Engineering, New Zealand Society for Earthquake Engineering, Auckland, New Zealand, Paper No. 1865 .

Jennings, P.C. (1971) "Engineering Features of San Fernando Earthquake, February 9, 1971" California Institute of Technology, Report EERL 71-02 1971, Pasadena, June 1971.

Khalil, A. (2005), "Rehabilitation of Reinforced Concrete Structural Walls Using Fiber Composites", Ph.D. Thesis, Department of Civil Engineering, McMaster University, Hamilton, Ontario, Canada.

Khalil, A., and Ghobarah, A., (2005) "Behaviour of Rehabilitated Structural Walls," Journal of Earthquake Engineering, Vol. 9, No. 3, pp. 371-391.

Khatri, D. and Anderson, J.C., (1995) "Analysis of Reinforced Concrete Shear Wall Component Using ADINA Nonlinear Concrete Model", Computers& Structures, Vol. 56, No 2/3, pp. 485-504.

Kilar, V., and Fajfar, P., (1999). "Simple Pushover analysis of Asymmetric Buildingds." Earthquake engineering and structural dynamics, Vol. 26, pp.233-249.

Kim, S., and D'Amore, E., (1999). "Push-over Analysis Procedure in Earthquake Engineering." Earthquake Spectra, Vol. 15, pp. 417-434.

Kim, T.W, Foutch, D. A., and LaFive, J. M. (2005) "A Practical Model for Seismic Analysis of Reinforced Concrete Shear Wall Buildings", Journal of Earthquake Engineering, Vol. 9, No. 3, pp. 393-417.

Krawinkler, H. and Seneviratna, G. D. P. K. (1998), "Pros and Cons of a Pushover Analysis of Seismic Performance Evaluation" Engineering Structures 1998 pp. 452-464

Lefas, I.D. and Kotsovos, M. D. (1990) "Strength and Deformation Characteristics of Reinforced Concrete Walls Under Load Reversals", ACI Structural Journal, Vol. 87, No. 6, pp. 716-726.

Linde, P., Bachmann, H, (1994) "Dynamic Modelling and Design of Earthquike Resistant Walls", Earthquake Engineering and Structural Dynamic 23, 1331-1350.

Lombard J. C. (1999), "Seismic Strengthening and Repair of Reinforced Concrete Shear Walls Using Externally Bonded Carbon Fiber Tow Sheets", Master of Engineering Thesis, Carleton University, Ottawa, Ontario, Canada.

Lopes, M.S., (2001) "Experimental Shear-Dominated Response of RC Walls, Part I: Objectives, methodology and results", Engineering Structures 23, 229–239.

Lopes, M.S., (2001) "Experimental Shear-Dominated Response of RC Walls, Part II: Discussion of results and design implications", Engineering Structures 23, 564–574.

Mander, J.B., Priestly, M.J.N., and Park, R., (1988), "Theoretical Stress-Strain Model for Confined Concrete", Journal of Structural Engineering, ASCE, Vol. 114, No.8, pp. 1804-1826.

Marques, J.L.G., and Jirsa, J.O., 1975, "A Study of Hooked Bar Anchorages in Beam-Column Joints", ACI Structural Journal, Vol. 72, No. 5, pp. 198-209.

Mazzoni, S., McKenna, F., Scott, M.H., Fenves, G.L., and Jermic, B. (2007), OPENSEES, Open Source for Earthquake Engineering Simulation, Program Manual, from: http//peer.berkeley.edu/silvia/OpenSees/manual/html/, accessed July, 2007.

NBCC, 2005, "National Building Code of Canada", the National Research Council of Canada, Ottawa, Ontario, Canada.

Navidpour, N. (2000) "Finite Element Analysis of Low-Rise R/C Walls", Master of Applied Science in Civil Engineering Thesis, University of Ottawa, Ontario, Canada.

Oesterle, R. G. Aristizabal-Ochoa, J. D. Shiu, K. N., and Corley, W. G. (1984) "Web Crushing Of Reinforced Concrete Structural Walls", Journal of The American Concrete Institute, Vol. 81, No.3, pp. 231-241.

Orakcal, K., Wallace, J.W., and Conte, J.P. (2004) "Flexural Modeling of Reinforced Concrete Walls-Model Attributes", ACI Structural Journal, Vol. 101, No. 5, pp. 688-698.

Palermo, D., (2002) "Behaviour and Analysis of Reinforced Concrete Walls Subjected to Reversed Cyclic Loading", PhD Thesis, University of Toronto, Toronto, Ontario, Canada.

Park, Y.J., Ang, A.H-S., (1985) "Mechanistic Seismic Damage Model for Reinforced Concrete", Journal of structural engineering, ASCE, Vol. 111, No. ST4, 722-739.

Park, Y.J., Ang, A.H-S., and Wen Y.k. (1987) "Damage-Limiting Aseismic Design of Buildings", Earthquake spectra, Vol. 3, No. 1, 1-26.

Park, Y.J., Reinhorn, A.M. and Kunnath, S.K., (1987) "IDARC: Inelastic Damage Analysis of Reinforced Concrete Frame Shear-Wall Structures", National Centre for Earthquake Engineering, NCEER 87-008, State University of New York, Buffalo, NY.

Paterson, J. and Mitchell, D. (2003), "Seismic Retrofit of Shear Walls with Headed Bars and Carbon Fiber Wrap". Journal of Structural Engineering, ASCE, Vol. 129, No. 5, pp. 606-614.

Paulay, T. and Priestley, M.J.N., (1992), "Seismic Design of Reinforced Concrete and Masonry Buildings", John Wiley and Sons Inc., New York.

Paulay, T. and Priestley, M.J.N., (1993) "Stability of Ductile Structural Walls" ACI Structural Journal, Vol. 90, No.4, pp. 385-392.

Popovics, S. (1973), "Numerical Approach to the Complete Stress-Strain Curve of Concrete", Cement and Concrete Research, Vol. 3, No.5, 1973, pp. 583-599

Prakash, V., Powell, G.H., and Campbell, S., (1993) "DRAIN-2DX Base Program Description and User Guide, Version 1.10." University of California, Report No. UCB/SEMM-93/17, Berkeley, California.

Riva, P., Meda, A., and Giuriani, E. (2003), "Cyclic Behaviour of a Full Scale RC Structural Wall", Engineering Structures, Vol. 25, No.6, pp. 835-845.

Rodriguez-Gomez, S., and Cakmak, A.S., (1990) "Evaluation of Seismic Damage Indicies for Reinforced Concrete Structures", National Centre for Earthquake Engineering, NCEER 90-0022, State University of New York at Buffalo, NY.

Samaan, M., Mirmiran, A., and Shahawy, M. (1998), "Model of Concrete Confined by Fibre Composites", Journal of Structural Engineering, ASCE, Vol. 124, No.9, pp. 1025-1031.

Sanbis, G., Harris, H., White, R., and Mirza, S. (1983) "Structural Modeling and Experimental Techniques", Prentice Hall, Inc.

Soroushian, P., and Choi, K.B., 1989, "Local Bond of Deformed Bars with Different Diameters in Confined Concrete", ACI Structural Journal, Vol. 86, No. 2, pp. 217-222.

Soroushian, P., and Choi, K.B., 1991, "Analytical Evaluation of Straight Bar Anchorage Design in Exterior Joints", ACI Structural Journal, Vol. 88, No. 2, pp. 161-168.

Soroushian, P., Choi, K.B., Park, G.H., and Aslani, F., 1991a, "Bond of Deformed Bars to Concrete: Effects of Confinement Strength of Concrete", ACI Structural Journal, Vol. 88, No. 3, pp. 227-232.

Soroushian, P., Obasaki, K., and Marihunte, S., 1991b, "Analytical Modeling of Bonded Bars Under Cyclic Loads", Journal of Structural engineering, ASCE, Vol. 117, No. 1, pp. 48-60.

Soroushian, P., Obaseki, K., Nahi, M., and Rajas, M., 1988, "Pullout Behaviour of Hooked Bars in Exterior Beam-column Connections", ACI Structural Journal, Vol. 85, No. 3, pp. 269-276.

Spoelstra, M. and Monti, G. (1999), "FRP-Confined Concrete Model", Journal of Composites for Construction, Vol. 3, No.3, 1999, pp. 143-150.

Stevens, N.J., Uzumeri, M., and Collins, M.P., (1987) "Analytical Modeling of Reinforced Concrete Subjected to Monotonic and Reversed Loading", Report No 87-01, University of Toronto, Toronto, Canada .

Taghdi, M, Bruneau, M, Saatcioglu, M., (2000) "Seismic Retrofitting of Low-Rise Masonry And Concrete Walls Using Steel Strips", Journal of Structural Engineering, ASCE, Vol. 126, No. 9, pp. 1017-1025.

Taghdi, M., Bruneau, M. and Saatcioglu, M., (2000) "Analysis and Design of Low-Rise Masonry and Concrete Walls Retrofitted Using Steel Strips", Journal of Structural Engineering, Vol. 126, No. 9.

UBC (1964), Uniform Building Code, International Conference of Building Officials, Whittier, CA.

Vallenas, J.M., Bertero, V. V ., and Popov, E.P. (1979) "Hysteretic Behavior of Reinforced Concrete Structural Walls", Report No. UCB/EERC-79/20, Earthquake Engineering Research Center, University of California, Berkeley, California, USA.

Valles, R.E., Reinhorn, A.M. and Kunnath, S.K., Li, C., Madan, A., (1996) "IDARC2D Version 6.1: A Program for Inelastic Damage Analysis of Buildings", National Centre for Earthquake Engineering, NCEER 96-010, State University of New York at Buffalo, NY.

Vecchio, F.J. and Collins, M.P. (1986), "The Modified Compression Field Theory for Reinforced Concrete Elements Subjected to Shear", ACI Structural Journal, Vol. 83, No.2, pp. 219-231.

Viwathanatepa, S., Popov, E.P., and Betero, V.V., (1979) "Effects Of Generalized Loading On Bond Of Reinforcing Bars Embedded In Confined Concrete Blocks.", Earthquake Engineering Research Center, Report No. UCB/EERC-79/22, University of California, Berkeley, California, USA.

Vulcano, A., and V. V. Bertero. (1987) "Analytical Models for Predicting the Lateral Response of RC Shear Walls: Evaluation of their Reliability", Earthquake Engineering Research Center, EERC Report No. UCB/EERC–87/19, University of California, Berkeley, California, USA.

Wang, Y.C., and Restrpo, J.B., (2001) "Investigation of Concentrically Loaded Reinforced Concrete Columns Confined with Glass Fibre-Reinforced Polymer Jackets", ACI Structural Journal, Vol. 98, No 3, pp. 337-385.

Williams, M.S., and Blakeborough, A. (2001) "Laboratory Testing of Structures under Dynamic Loads: an Introductory Review" Philosophical Transactions: Mathematical, Physical and Engineering Sciences, Vol. 359, No. 1786, pp. 1651-1669.

Williams, M.S., and Sexsmith, R. (1995) "Seismic Damage Indecies for Concrete Structures: A State-of-the-Art Review" Earthquake Spectra, Vol. 11, No. 2, pp. 319-349.

Wiradinata S. and Saatcioglu M. (1986), "Tests of Squat Shear Walls Under Lateral Load Reversals", Proceedings of the 3rd US National Conference on Earthquake Engineering, Charleston, South Carolina, Earthquake Engineering Research Institute, California, US, pp. 1395-1406.

Wood S. (1991) "Performance of Reinforced concrete Buildings During the 1985 Chile Earthquake: Implication for the Design of Structural Walls", Earthquake Spectra, Vol. 7, N. 4, 607-638.

Wyllie, L. A., Abrahamson, N. Bolt, B., Castro, G., Durkin, M.E.(1986) "The Chile Earhquake of March 3, 1985-Performance of structures." Earthquake Spectra Vol. 2, No.2, pp. 293-371

Youssef, M., 2000, "Modeling Existing and Rehabilitated RC Buildings", Ph.D. Thesis, Department of Civil Engineering, McMaster University, Hamilton, Ontario, Canada, 143 pages.